ISSN 1881-7815 Online ISSN 1881-7823

BST BioScience Trends

Volume 20, Number 1
February 2026

IRCA BSSA
IACMHR

www.biosciencetrends.com

BST
BioScience Trends

ISSN: 1881-7815
Online ISSN: 1881-7823
CODEN: BTIRCZ
Issues/Year: 6
Language: English
Publisher: IACMHR Co., Ltd.

BioScience Trends is one of a series of peer-reviewed journals of the International Research and Cooperation Association for Bio & Socio-Sciences Advancement (IRCA-BSSA) Group. It is published bimonthly by the International Advancement Center for Medicine & Health Research Co., Ltd. (IACMHR Co., Ltd.) and supported by the IRCA-BSSA.

BioScience Trends devotes to publishing the latest and most exciting advances in scientific research. Articles cover fields of life science such as biochemistry, molecular biology, clinical research, public health, medical care system, and social science in order to encourage cooperation and exchange among scientists and clinical researchers.

BioScience Trends publishes Original Articles, Brief Reports, Reviews, Policy Forum articles, Communications, Editorials, News, and Letters on all aspects of the field of life science. All contributions should seek to promote international collaboration.

Editorial Board

Editorial and Head Office

Pearl City Koishikawa 603,
2-4-5 Kasuga, Bunkyo-ku, Tokyo 112-0003, Japan
E-mail: office@biosciencetrends.com

BioScience Trends

Editorial and Head Office

Pearl City Koishikawa 603, 2-4-5 Kasuga, Bunkyo-ku,
Tokyo 112-0003, Japan

E-mail: office@biosciencetrends.com
URL: www.biosciencetrends.com

Editorial Board Members

CONTENTS

Volume 20, Number 1, 2026

Editorial

Review

Original Article

Editorial

DOI: 10.5582/bst.2026.01055

Thoughts on dietary interventions for metabolic syndrome (MetS) in an era of metabolic heterogeneity

Wei Tang*

National Center for Global Health and Medicine, Japan Institute for Health Security, Tokyo, Japan.

SUMMARY: Metabolic syndrome (MetS) has long been used as a pragmatic tool for population-level cardiometabolic risk stratification, rather than as a mechanistically defined disease entity. However, mounting evidence suggests the existence of marked biological heterogeneity among individuals meeting identical MetS criteria, encompassing diverse metabolic phenotypes, disease trajectories, and responses to interventions. Such heterogeneity helps explain the limited and inconsistent effectiveness of uniform dietary strategies. In parallel, dietary research has shifted from a nutrient-centric approach to a food-based dietary pattern, emphasizing higher intakes of whole foods and reduced consumption of ultra-processed foods. In the context of metabolic heterogeneity, these shared food-level characteristics may confer relatively consistent metabolic benefits across diverse phenotypes. Future research may shift from uniform dietary recommendations to stratified strategies, grounded in dietary principles and informed by mechanistic insights, to better address metabolic heterogeneity.

Keywords: metabolic syndrome (MetS), metabolic heterogeneity, dietary patterns, ultra-processed foods, stratified strategies

Metabolic syndrome (MetS) was not originally conceived of as a precise clinical diagnosis but rather as a pragmatic framework for identifying individuals at elevated cardiometabolic risk. From the early observations of Kylin in the 1920s, through Haller's metabolic clustering hypothesis, to Reaven's landmark description of insulin resistance syndrome, the central aim of MetS has consistently been population-level risk stratification rather than mechanistic classification (*1-3*). Beginning with the World Health Organization's first formal definition in 1998, subsequent decades saw the development of additional diagnostic criteria by organizations such as the National Cholesterol Education Program Adult Treatment Panel III (ATP III) and the International Diabetes Federation (IDF) (*4-6*). The 2009 Joint Interim Statement sought to harmonize these definitions, acknowledging that no single threshold could fully capture the biological complexity underlying metabolic risk (*7*) (Figure 1).

Following the harmonization of diagnostic criteria in the 2009 Joint Interim Statement, subsequent advances have increasingly highlighted the limitations of threshold-based definitions in capturing the full spectrum of metabolic risk. These limitations, in turn, have driven the emergence of new conceptual frameworks. More recently, the American Heart Association introduced the concept of cardiovascular-kidney-metabolic (CKM) syndrome, framing MetS as an early upstream stage within a continuous cardiometabolic disease trajectory (*8*). In parallel, emerging phenotype-based approaches include metabolomic BMI (MetBMI) (*9*), a multiomic signature that captures metabolic dysfunction beyond measured BMI. By enabling risk stratification within conventional BMI categories, MetBMI reveals heterogeneity that is not apparent from anthropometric measures alone. One of the fundamental challenges underlying these developments is the pronounced biological heterogeneity of MetS. Even among individuals who meet identical diagnostic criteria, substantial differences may exist in metabolic phenotypes, disease trajectories, and responses to intervention (Table 1). For example, studies in African-American populations have shown that cardiometabolic risk may be underestimated at lower triglyceride levels, suggesting ethnic differences in lipid metabolism and limited generalizability of conventional triglyceride thresholds (*10*). Likewise, classic phenotypes, such as metabolically healthy obesity and metabolically unhealthy normal weight, provide clinically tangible examples of this heterogeneity, demonstrating that anthropometric measures alone do not reliably capture true metabolic risk (*11*). Beyond these observable phenotypic differences, age-related changes in body composition, chronic low-grade inflammation, declining insulin sensitivity, and sex-specific hormonal differences add further layers of metabolic complexity (*12-14*). Individuals with

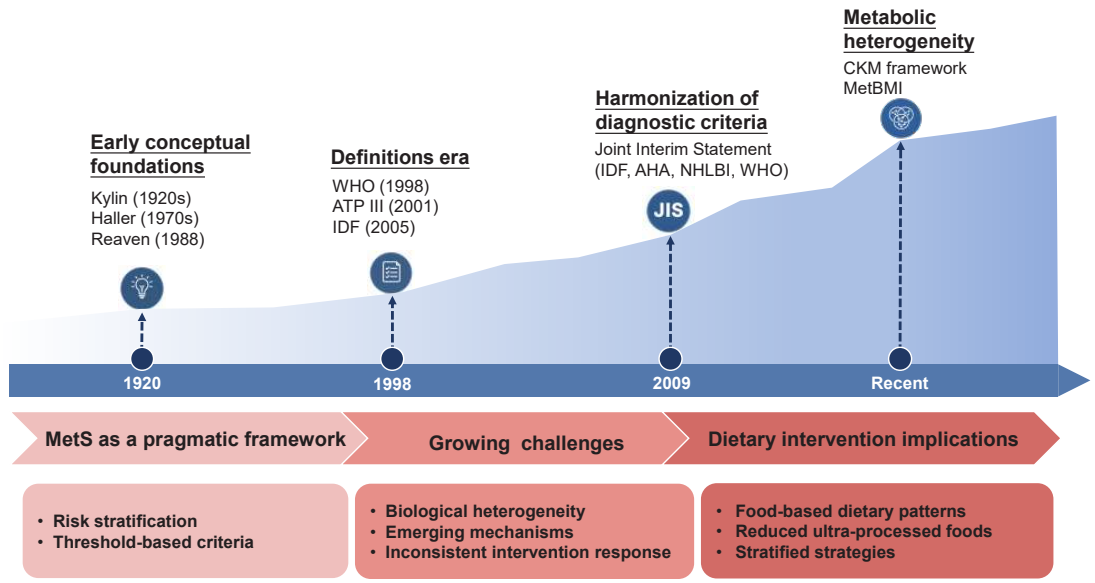

Figure 1. Conceptual evolution of metabolic syndrome and its impact on dietary intervention. The figure illustrates the historical development of MetS from early conceptual observations to the harmonization of diagnostic criteria, the emergence of new frameworks highlighting metabolic heterogeneity, and the resulting shift in the conceptual approach to dietary intervention. *Abbreviations*: MetS: metabolic syndrome; WHO: World Health Organization; ATP III: Adult Treatment Panel III of the National Cholesterol Education Program; IDF: International Diabetes Federation; JIS: Joint Interim Statement; AHA: American Heart Association; NHLBI: National Heart, Lung, and Blood Institute; CKM: cardiovascular–kidney–metabolic syndrome; MetBMI: metabolomic body mass index.

Table 1. Key sources of heterogeneity in MetS and their implications for dietary intervention

Heterogeneity	Core issue	Key manifestations	*Ref.*
Limited applicability of uniform diagnostic criteria	Insufficient cross-population applicability	In African-American populations, metabolic risk may be underestimated at lower triglyceride levels	(*10*)
Insensitivity of dichotomous thresholds	Phenotypic heterogeneity	Limited ability to identify metabolically unhealthy normal-weight individuals, potentially underestimating risk.	(*11*)
Limited applicability of standardized intervention strategies	Heterogeneous intervention responses	Age-related muscle loss reduces insulin sensitivity; sex-specific hormonal regulation of metabolism; interindividual differences in chronic low-grade inflammation	(*12-14*)
Challenges posed by emerging mechanisms	Conventional metabolic indicators inadequately reflect emerging mechanisms	Heterogeneous mechanisms (insulin resistance, adipose dysfunction, inflammation, gut microbiota) despite similar metabolic profiles.	(*15-17*)

similar fasting glucose or lipid profiles may exhibit fundamentally different underlying mechanisms, including insulin resistance, adipose dysfunction, inflammation, and alterations in gut microbiota (*15-17*). These mechanistic differences may influence individual responses to dietary interventions. For instance, interindividual differences in the capacity of gut microbial communities to ferment dietary fiber lead to variability in short-chain fatty acid (SCFA) production, which may influence insulin sensitivity and glucose homeostasis (*18-20*). As a whole, such heterogeneity poses a fundamental challenge to dietary intervention strategies, limiting the long-term efficacy of uniform dietary approaches (*21,22*).

Despite long-running debate regarding its clinical definition, the relevance of MetS is underscored by its sheer epidemiological scale. Recent global modeling studies estimate that more than 1.5 billion adults worldwide now meet diagnostic criteria for MetS, reflecting a dramatic rise over the past two decades (*23*). Importantly, MetS is not merely a descriptive label but a powerful predictor of adverse outcomes. Large prospective studies and meta-analyses have consistently shown that individuals with MetS face approximately a two-fold higher risk of cardiovascular events and a markedly elevated risk of developing type 2 diabetes, with estimates approaching a five-fold increase (*7,24*). Evidence from the Global Burden of Disease studies clearly indicates that core components of metabolic syndrome, including elevated systolic blood pressure, hyperglycemia, and obesity, now account for a substantial share of global mortality and DALYs. According to the GBD 2019 risk factor analysis, elevated fasting plasma glucose (≥ 5.4 mmol/L) contributes to approximately 6.5% of global DALYs and 2.4 million deaths, whereas

elevated systolic blood pressure (≥ 110-115 mmHg) is associated with around 10.8 million deaths and more than 200 million DALYs globally (*25*). Elevated low-density lipoprotein cholesterol (LDL) causes approximately 4.4 million deaths annually (*26*). In parallel, overweight and obesity (BMI ≥ 25 kg/m²) contribute to around 5 million deaths and 160 million disability-adjusted life years (DALYs) globally, with particularly pronounced increases observed in low- and middle-income countries (*27*). These observations explain why, despite its conceptual imperfections, MetS continues to serve as a pragmatic framework for population-level risk stratification.

Against the backdrop of growing metabolic heterogeneity and the limited capacity of uniform dietary interventions to deliver consistent and sustained benefits, dietary intervention research has increasingly shifted toward a pattern-based perspective in recent years. Attention has shifted to how foods are combined, processed, and embedded in daily eating patterns instead of a single nutrient. An increasing number of prospective studies and international dietary guidelines support a dietary pattern–based approach, advocating that public health strategies should prioritize improving food quality and dietary diversity rather than overly emphasizing upper limits on individual nutrient intake (*28-30*). Despite substantial differences in macronutrient composition, diverse healthy dietary patterns, including the Mediterranean, DASH, plant-based diets, and healthy eating indices importantly converge at the food level, consistently emphasizing higher intakes of whole foods, such as vegetables, fruits, legumes, and whole grains, while limiting ultra-processed foods and added sugars (*31-33*). This convergence at the food level is particularly relevant in the context of metabolic heterogeneity, as it suggests that food-based characteristics such as higher fiber intake and minimal processing may have relatively consistent metabolic effects across diverse metabolic phenotypes even when individuals differ in their responses to macronutrient composition (*21,34,35*). From this perspective, the growing focus on ultra-processed foods represents not merely a shift in nutritional trends but a pragmatic dietary strategy aimed at reducing overall metabolic risk at the population level in the context of pronounced metabolic heterogeneity. A substantial body of evidence consistently links a high intake of ultra-processed foods to adverse metabolic outcomes, including obesity, type 2 diabetes, and cardiovascular disease (*36-38*). Accordingly, recent scientific statements from the American Heart Association and the 2025-2030 Dietary Guidelines for Americans have explicitly called for limiting ultra-processed foods while prioritizing "eat real food" -based dietary patterns, underscoring a broader shift toward dietary interventions that are both metabolically relevant and feasible at the population level (*39*).

Overall, increasing metabolic heterogeneity challenges the notion of metabolic syndrome as a target for uniform dietary intervention. While MetS remains useful for population-level risk stratification, its biological diversity limits the effectiveness of standardized dietary strategies. A shift toward real food-based, pattern-oriented strategies may offer a more adaptable and scalable framework for reducing metabolic risk across biologically heterogeneous populations. Future research may move beyond universally optimal diets toward principle-based, mechanism-informed stratified approaches that retain shared food-level recommendations while incorporating metabolic and gut microbial features (*40,41*), thereby better accommodating metabolic heterogeneity while preserving population-level feasibility.

Funding: None.

Conflict of Interest: The author has no conflicts of interest to disclose.

References

1. Dabke K, Hendrick G, Devkota S. The gut microbiome and metabolic syndrome. J Clin Invest. 2019; 129:4050-4057.
2. Sarafidis PA, Nilsson PM. The metabolic syndrome: A glance at its history. J Hypertens. 2006; 24:621-626.
3. Okafor CI. The metabolic syndrome in Africa: Current trends. Indian J Endocrinol Metab. 2012; 16:56-66.
4. Huang PL. A comprehensive definition for metabolic syndrome. Dis Model Mech. 2009; 2:231-237.
5. Zimmet P, Magliano D, Matsuzawa Y, Alberti G, Shaw J. The metabolic syndrome: A global public health problem and a new definition. J Atheroscler Thromb. 2005; 12:295-300.
6. National Cholesterol Education Program (NCEP) Expert Panel on Detection, Evaluation, and Treatment of High Blood Cholesterol in Adults (Adult Treatment Panel III). Third Report of the National Cholesterol Education Program (NCEP) Expert Panel on Detection, Evaluation, and Treatment of High Blood Cholesterol in Adults (Adult Treatment Panel III) final report. Circulation. 2002; 106:3143-421.
7. Alberti KG, Eckel RH, Grundy SM, *et al*. Harmonizing the metabolic syndrome: A joint interim statement of the International Diabetes Federation Task Force on Epidemiology and Prevention; National Heart, Lung, and Blood Institute; American Heart Association; World Heart Federation; International Atherosclerosis Society; and International Association for the Study of Obesity. Circulation.2009; 120:1640-1645.
8. Ndumele CE, Rangaswami J, Chow SL, *et al*. Cardiovascular-kidney-metabolic health: A Presidential Advisory from the American Heart Association. Circulation. 2023; 148:1606-1635.
9. Watanabe K, Wilmanski T, Diener C, Earls JC, Zimmer A, Lincoln B, Hadlock JJ, Lovejoy JC, Gibbons SM, Magis AT, Hood L, Price ND, Rappaport N. Multiomic signatures of body mass index identify heterogeneous health phenotypes and responses to a lifestyle intervention. Nat Med.2023; 29:996-1008.
10. Madhusoodanan J. Searching for better biomarkers for metabolic syndrome. ACS Cent Sci. 2022; 8:682-685.
11. Stefan N. Metabolically healthy and unhealthy normal

weight and obesity. Endocrinol Metab (Seoul). 2020; 35:487-493.
12. Kalyani RR, Corriere M, Ferrucci L. Age-related and disease-related muscle loss: The effect of diabetes, obesity, and other diseases. Lancet Diabetes Endocrinol. 2014; 2:819-829.
13. Mauvais-Jarvis F. Sex differences in metabolic homeostasis, diabetes, and obesity. Biol Sex Differ. 2015; 6:14.
14. Grundy SM. Metabolic syndrome update. Trends Cardiovasc Med. 2016; 26:364-73.
15. Samuel VT, Shulman GI. The pathogenesis of insulin resistance: Integrating signaling pathways and substrate flux. J Clin Invest n.d.; 126:12-22.
16. Cani PD, Delzenne NM. The role of the gut microbiota in energy metabolism and metabolic disease. Curr Pharm Des. 2009; 15:1546-1558.
17. ONeill S, O'Driscoll L. Metabolic syndrome: A closer look at the growing epidemic and its associated pathologies. Obesity Reviews. 2015; 16:1-12.
18. Cronin P, Joyce SA, O'Toole PW, O'Connor EM. Dietary fibre modulates the gut microbiota. Nutrients. 2021; 13:1655.
19. Pham NHT, Joglekar MV, Wong WKM, Nassif NT, Simpson AM, Hardikar AA. Short-chain fatty acids and insulin sensitivity: A systematic review and meta-analysis. Nutr Rev. 2024; 82:193-209.
20 Zhao L, Zhang F, Ding X, *et al*. Gut bacteria selectively promoted by dietary fibers alleviate type 2 diabetes. Science. 2018; 359:1151-1156.
21. Zeevi D, Korem T, Zmora N, *et al*. Personalized nutrition by prediction of glycemic responses. Cell. 2015; 163.
22. Gardner CD, Trepanowski JF, Del Gobbo LC, Hauser ME, Rigdon J, Ioannidis JPA, Desai M, King AC. Effect of low-fat vs low-carbohydrate diet on 12-month weight loss in overweight adults and the association with genotype pattern or insulin secretion. JAMA. 2018; 319:667-679.
23. Noubiap JJ, Nansseu JR, Nyaga UF, Ndoadoumgue AL, Ngouo AT, Tounouga DN, Tianyi FL, Foka AJ, Lontchi-Yimagou E, Nkeck JR, Bigna JJ. Worldwide trends in metabolic syndrome from 2000 to 2023: A systematic review and modelling analysis. Nat Commun. 2025; 17:573.
24. Mottillo S, Filion KB, Genest J, Joseph L, Pilote L, Poirier P, Rinfret S, Schiffrin EL, Eisenberg MJ. The metabolic syndrome and cardiovascular risk A systematic review and meta-analysis. J Am Coll Cardiol .2010; 56:1113-1132.
25. GBD 2019 Risk Factors Collaborators. Global burden of 87 risk factors in 204 countries and territories, 1990-2019: A systematic analysis for the Global Burden of Disease Study 2019. Lancet. 2020; 396:1223-1249.
26. GBD 2017 Causes of Death Collaborators. Global, regional, and national age-sex-specific mortality for 282 causes of death in 195 countries and territories, 1980-2017: A systematic analysis for the Global Burden of Disease Study 2017. Lancet. 2018; 392:1736-1788.
27. GBD 2015 Obesity Collaborators; Afshin A, Forouzanfar MH, *et al*. Health effects of overweight and obesity in 195 countries over 25 years. N Engl J Med. 2017; 377:13-27.
28. Mozaffarian D. Dietary and policy priorities for cardiovascular disease, diabetes, and obesity: A comprehensive review. Circulation. 2016; 133:187-225.
29. Jacobs DR, Tapsell LC. Food, not nutrients, is the fundamental unit in nutrition. Nutr Rev. 2007; 65:439-450.
30. Monteiro CA, Cannon G, Levy RB, Moubarac JC, Louzada ML, Rauber F, Khandpur N, Cediel G, Neri D, Martinez-Steele E, Baraldi LG, Jaime PC. Ultra-processed foods: What they are and how to identify them. Public Health Nutr. 2019; 22:936-941.
31. Willett W, Rockström J, Loken B, *et al*. Food in the Anthropocene: The EAT-Lancet Commission on healthy diets from sustainable food systems. Lancet. 2019; 393:447-492.
32. Stewart RAH. Primary prevention of cardiovascular disease with a mediterranean diet supplemented with extra-virgin olive oil or nuts. N Engl J Med. 2018; 379:1388.
33. Mozaffarian D, Rosenberg I, Uauy R. History of modern nutrition science-Implications for current research, dietary guidelines, and food policy. BMJ. 2018; 361: k2392.
34. Reynolds A, Mann J, Cummings J, Winter N, Mete E, Te Morenga L. Carbohydrate quality and human health: A series of systematic reviews and meta-analyses. Lancet. 2019; 393:434-445.
35. Hu FB. Dietary pattern analysis: A new direction in nutritional epidemiology. Curr Opin Lipidol. 2002; 13:3-9.
36. Hall KD, Ayuketah A, Brychta R, *et al*. Ultra-processed diets cause excess calorie intake and weight gain: An inpatient randomized controlled trial of ad libitum food intake. Cell Metab. 2019; 30:67-77.
37. Srour B, Fezeu LK, Kesse-Guyot E, Allès B, Debras C, Druesne-Pecollo N, Chazelas E, Deschasaux M, Hercberg S, Galan P, Monteiro CA, Julia C, Touvier M. Ultraprocessed food consumption and risk of type 2 diabetes among participants of the NutriNet-Santé prospective cohort. JAMA Intern Med. 2020; 180:283-291.
38. Dai S, Wellens J, Yang N, *et al*. Ultra-processed foods and human health: An umbrella review and updated meta-analyses of observational evidence. Clin Nutr. 2024; 43:1386-1394.
39. U.S. Department of Agriculture; U.S. Department of Health and Human Services. Dietary Guidelines for Americans. *https://www.dietaryguidelines.gov* (accessed January 30, 2026).
40. Berry SE, Valdes AM, Drew DA, *et al*. Human postprandial responses to food and potential for precision nutrition. Nat Med. 2020; 26:964-973.
41. Muijsenberg A, Canfora EE, Blaak EE. Metabolic phenotypes, genotypes, and gut microbiome signatures in obesity: Implications for precision nutrition strategies in type 2 diabetes prevention. Nutr Rev. 2026; 84:158-188.

Received February 6, 2026; Accepted February 22, 2026.

**Address correspondence to:*
Wei Tang, National Center for Global Health and Medicine, Japan Institute for Health Security, 1-21-1 Toyama, Shinjukuku, Tokyo 162-8655, Japan.
E-mail: politang-tky@umin.ac.jp

Released online in J-STAGE as advance publication February 25, 2026.

Review

DOI: 10.5582/bst.2026.01003

Bacteriophage-derived depolymerases as antimicrobial synergists: A strategy to overcome resistance

Shuhong Han[1,2,3,§], David H Yang[4,§], Jiayin Shen[1,2,3,*], Hongzhou Lu[1,2,3,*]

[1] National Clinical Research Center for Infectious Diseases, The Third People's Hospital of Shenzhen and The Second Affiliated Hospital of Southern University of Science and Technology, Shenzhen, Guangdong, China;
[2] School of Medicine, Southern University of Science and Technology, Shenzhen, Guangdong, China;
[3] Guangdong Key Lab for Diagnosis and Treatment of Emerging Infectious Diseases, Shenzhen Third People's Hospital, Shenzhen, Guangdong, China;
[4] Department of Integrative Biology and Physiology, University of California, Los Angeles, CA, USA.

SUMMARY: Upon infection, bacteria form polysaccharides barriers, such as capsular polysaccharide (CPS), exopolysaccharide (EPS) and lipopolysaccharide (LPS). The barrier hinders antibiotic penetration and host immune clearance, exacerbating antimicrobial resistance crisis. Bacteriophages (phages), natural viruses that can specifically infect and kill bacteria, have evolved depolymerase to degrade the polysaccharides. This review evaluates the primary therapeutic value of depolymerases as synergists to existing therapies, systematically detailing their potential to enhance antibiotic efficacy, improve phage therapy, and augment host immunity. We further integrate an evolutionary perspective to analyze likely adaptive responses and potential strategies to eradicate resistance. Finally, the discussion addresses formulation challenges and future prospects for the clinical translation of depolymerase-based synergistic therapies.

Keywords: bacteriophages, depolymerase, biofilm dispersal, polysaccharide, antibacterial reagent, antibiotic resistance reversal, combination therapy, resistance evolution

1. Introduction

Bacteriophages (also known as phages) are viruses that infect microorganisms such as bacteria, fungi, algae, actinomycetes or spirochetes. With the largest number and highest genetic diversity in the earth's biosphere, phages can be found in every explored biome, and their number is estimated to be up to 10^{31} (*1*). Their proliferation strictly depends on the host: the process begins with injection of phage genomes into the host, and the genome destroys bacterial metabolism, eventually lysing the bacteria (*2*). Phages have become an effective alternative for antibiotics, especially with the increasing prevalence of multidrug-resistant (MDR) bacteria worldwide.

Phage infection begins with the critical step of the phage selectively attaching to the bacterial surface receptors, often mediated by tail fiber or tail spike proteins (TSPs) on the phage. Then adsorption is achieved through receptor binding protein (RBP), a prerequisite for cell wall degradation (*1,3*). This highly-specific process allows phages to inhibit bacterial growth with minimal effects on accompanying microflora of a target bacterium during infection (*4*). This precise targeting, however, is often hampered by the presence of polysaccharides, such as capsular polysaccharide (CPS), exopolysaccharide (EPS) and lipopolysaccharide (LPS), on the bacterial surface. Similarly, disruption of phage action occurs when the bacteria live as biofilms, a barrier preventing from the phage adsorption and penetration (*5*). The physical barrier also impedes drug penetration and masks bacterial surfaces, thereby conferring antibiotic resistance and impeding host immune recognition (*5,6*). Phage have evolved depolymerases that degrades bacterial polysaccharide to facilitate phage access (*4*).

There is increasing research attention that targets phage-derived depolymerase as a novel and powerful antimicrobial agent. Previous reviews have comprehensively cataloged their diversity (*4*), biochemical activities, and therapeutic efficacy (*7-9*), with particular emphasis on their potency in biofilm control (*10-13*). However, emerging evidence suggests that the most significant therapeutic value of depolymerases may not lie in their direct antibacterial activity, but in their ability to act as synergistic agents that enhance antibiotic efficacy and immune responses. While rarely inducing classic bacterial resistance problem (*14*), their therapeutic

application will inevitably exert evolutionary pressure, potentially driving bacterial adaptive strategies.

Therefore, this review expands from a functional summary of depolymerase to discuss a novel framework that integrates synergistic potentiation and evolutionary machinery. The discussion first establishes the role of depolymerases as antimicrobial synergists, detailing how their activity potentiates antibiotics, augments phage therapy, and empowers host immunity. Then, we address the related evolutionary dynamics, from potential bacterial resistance pathways to counterstrategies, such as protein engineering and combination therapies. By integrating the perspectives of synergistic therapy and evolutionary machinery, this article provides a next generation rationale for developing depolymerases into human therapeutics.

2. Overview of phage depolymerases

Phage depolymerases were partially purified from phage solutions by Hughes *et al.* in 1998 (*15*). As follows, the basic characteristics of phage depolymerases have been elaborated. These foundational understanding is critical for translating their function into practical application, such as synergistic therapeutics and engineered solutions.

2.1. Depolymerases play an important role in bacterial infection

CPS, EPS and LPS are decorative polysaccharides on the surface of bacterial cells. CPSs are found on the cell surface of a variety of bacterial species, binding tightly to the cell surface in a covalent attachment. As the protective component of pathogenic microorganisms, CPSs facilitate host colonization and physically prevent the action of bactericide by forming a barrier on bacterial surface (*16,17*). EPSs are the main matrix that enclose the bacteria cells in the biofilm mode of life (*18*). The significant difference between bacteria in biofilms and their planktonic counterparts is that biofilm protect bacteria from environmental stress conditions, such as chemicals, antibiotics, and immune cells attacks. Biofilms increase the resistance of some bacteria against the conventional antibiotics by around 1000-fold (*19,20*). Unlike CPSs, EPSs are not tightly bind to the cell and are often secreted into the extracellular matrix (*21*). LPS is usually considered as a ligand for phage tail fiber proteins during adsorption to the host bacteria (*4*). In addition, LPS also plays an important role in protecting bacteria from anti-bacterial peptides (*22*). Collectively, polysaccharides can reduce the absorption efficacy of some phages, and they also play a critical role in bacterial virulence and biofilm production. Another critical role of polysaccharides lies within their ability to act as a physical barrier against the penetration of conventional antibiotics and the host immune system (*23-25*). This simple but potent defensive role makes degrading the polysaccharides a strategic target for both phage infection and antimicrobial therapy.

Many phages produce depolymerase that specifically binds and degrades bacterial surface polysaccharides. Unlike lytic phages that destroy the cell, depolymerases act with high precision, stripping away these barriers to expose the underlying bacterial cell surface. The exposure sensitizes bacteria to external threats, such as antibiotics and immune effectors.

2.2. Common phenotype of depolymerases: The halo effect

When phages with depolymerases form plaque on bacterial lawn, the plaque is usually transparent in the center and surrounded by a translucent halo. The halo will continue to expand during incubation, while the size of the clear plaque does not change, constituting a typical phenomenon of depolymerase activity. It occurs phage replication slows down when bacteria are in stationary stage, while the excess depolymerases can still degrade the extracellular polysaccharide components of bacteria (*7*). This visual hallmark is a key indicator for identifying and isolating depolymerase-producing phages.

2.3. Diversity of depolymerases

With the ongoing exploration of phage-derived proteins, depolymerases have revealed remarkable diversity. According to the work of Pires DP *et al.* (*7*), most of phage depolymerases are considered structural proteins, as they are either encoded by or found in proximity to phage structural genes (such as tail fibers, base plates, and sometimes also in the neck). A small number of depolymerases are considered as soluble proteins since their coding genes are located far from any structural genes.

Based on the mechanisms of breaking cell barriers, phage depolymerases were distinguished into two classes: hydrolases and lyases (*7*). Both enzymes possess the ability to degrade carbohydrate barrier. Hydrolases catalyze the hydrolysis of glycosidic bonds in CPS and O-antigen on LPS chain (*26*), and there are six subtypes: sialidases, levanases, xylosidases, dextranases, rhamnosidases, and peptidases (*7*). The lyases cleave (1,4) glycosidic bonds by a β-elimination mechanism without using water molecule, and they are comprised of five groups: hyaluronate lyase, pectate lyase, alginate lyase, K5 lyase, and O-specific polysaccharide lyase (*8*). This mechanistic diversity supports their ability to target a wide spectrum of chemically distinct polysaccharides critical for bacterial defense.

The difference between the mechanism of hydrolysis and β-elimination results in differences in substrate specificity, so that therapy must be formulated with deliberations (*27*). Hydrolases, such as sialidases, dextranases, cleave glycosidic bonds via

hydrolysis, generating saccharides. Their actions are crucial for degrading neutral polysaccharides such as dextran and levan, commonly found in biofilms of *Lactobacillus* or *Bacillus* (*28*). In contrast, lyases, such as hyaluronidases and pectate lyases, act on acidic polysaccharides containing uronic acids [*e.g.*, alginate in *Pseudomonas aeruginosa* (*P. aeruginosa*), hyaluronan in *Streptococcus*] through β-elimination, producing unsaturated oligosaccharides with a double bond at the non-reducing end (*28,29*). The difference in catalytic mechanism and product chemistry suggests a divergence in their synergistic efficacy. For instance, alginate lyases degrade the viscous alginate matrix of *P. aeruginosa* biofilms to improve phage or antibiotic diffusion (*30*), but the unique unsaturated oligosaccharide produced have been reported to exhibit immunomodulatory or biofilm-dispersing activities (*31*). Conversely, the "cleaner" breakdown by hydrolases like dextranases may remove a physical barrier without significantly altering the chemical microenvironment. Therefore, combination therapy strategy should be optimized with regard to the selection of a depolymerase (hydrolase *vs*. lyase) based on the chemistry of biofilm maximize efficacy.

The mechanistic dichotomy also indicates differing biophysical requirements for optimal activity *in vivo*. Lyases often require specific cations (*e.g.*, Ca^{2+}) as cofactors for β-elimination, and the optimal activity is achieved under a narrower pH range with respect to the pKa of the uronic acid substrate(*32*). While also pH-dependent, hydrolases tend to manifest versatility through larger pH range, but susceptible to end product inhibition (*33*). Understanding these nuances is crucial for formulating stable, effective enzyme cocktails for specific infection microenvironments, such as the acidic wound bed or the cation-rich respiratory mucus.

2.4. Structure and function of depolymerases

Despite their great diversity, depolymerases share conserved structural features. The majority of depolymerases are present as elongated homotrimers within the tail fiber or tail spike of the phage baseplate (*26*). However, there are rare exceptions: depolymerase of *Escherichia coli* (*E. coli*) siphophage 63D is characterized as a homotetramer (*34*). Depolymerases are fibrous proteins with a parallel β-helix topology, which includes the active sites that facilitate the recognition and binding of specific sequences in the surface polysaccharides. The complex structure of depolymerase underlies their high chemical stability, allowing them to remain active across a wide range of temperature and pH (*26,35*).

A canonical trimeric depolymerase, such as that from the deep-sea thermophilic phage GVE2, comprises three domains: an N-terminal domain connects to receptor-binding protein and the phage baseplate, a central domain responsible for substrate recognition and enzymatic activity, and a C-terminal domain crucial for the formation of trimers (*36,37*). This modular architecture separates structural attachment, catalytic function, and oligomerization, constituting the key feature that facilitates natural evolution and enables protein engineering. Historically, trimerization was considered essential for function (*38*), while recent studies, such as Kp34gp57 capsular depolymerase of *Klebsiella* phage crystalize as a monomer, is largely due to the intra-subunit active site formed by beta-barrel insertion domains (*39*). This expands the structural understanding and suggests flexibility for engineering simplified, monomeric variants.

The structure of depolymerases can be modified to adapt to a wide array of polysaccharide receptors in vertical and horizontal transfers. Vertical transfer involves mutating the central domain at protruding loops of β-helix in the active site without altering its overall conformation. The alteration enables the peptide chain to adapt to different polysaccharide substrates (*26*). The horizontal transfer essentially replaces the existing central catalytic domain with a foreign one, allowing the immediate acquisition of new host specificities. According to Latka, *et al.*, such horizontal structural adaptation is supported by ample evidence from phages CUS-3, HK620, Sf6, and P22 (*26*). This evolutionary plasticity highlights their potential for engineering. The conserved N- and C-terminal domains can serve as a stable scaffold, allowing the grafting of novel catalytic domains to create depolymerases with tailored or broadened specificity. Such engineering strategies are key to developing evolutionarily robust therapies.

3. Applications and implications of depolymerases

The application of phage depolymerases has evolved from utilizing existing enzymes into strategically integrating enzymes into combination therapies and engineered platforms (*14*). This section moves beyond their standalone functions, focusing on their core value in synergistic combinations and addresses the evolutionary dynamics of their application.

3.1. Depolymerases precisely eradicate biofilm formation

Phage depolymerases degrade polysaccharides on the host bacterial surface, facilitating the subsequent adsorption, infection, and disintegration of host bacteria. Evidence from diverse animal models, including *Galleria mellonella* (*40,41*), zebrafish (*42*), chicken (*43,44*), and mice (*45*), confirms their potential to eradicate bacterial infection and improve survival rates. Their activity is particularly potent against biofilms, as they degrade the EPS matrix that encloses and protects bacterial communities. Ample reports indicate that depolymerases can disrupt biofilms *in vitro* and confer high levels of protection *in vivo*, such as depolymerase Dp42 from

Klebsiella pneumoniae (*K. pneumoniae*) phage vB_KpnP_IME409 (*45*), Dep-ORF8 from *Pasteurella multocida* (*P. multocida*) phage PHB02 (*46*), and Dp49 from *Acinetobacter baumannii* (*A.baumannii*) phage IME285 (*47*).

The high specificity of depolymerases enables targeted action, with certain enzymes active against only a single capsular type (*48*). While this specificity restricts the utility of mono-enzyme therapy to a narrow spectrum, it also makes depolymerases ideal tools for bacterial typing and precise diagnosis (*26,48*). Consequently, the full therapeutic potential of these enzymes is realized not in isolation, but in concert with other antibacterial agents and host immune defenses. This diagnostic precise can, in turn, inform subsequent targeted combination therapies.

3.2. Depolymerase acts as a synergist

Depolymerases have immense potential as powerful synergists for antibiotic treatments, and their synergistic actions manifest in multiple ways (Figure 1). A well-documented synergy is the enhancement of antibiotic efficacy. Depolymerases enhance antibiotic efficacy by degrading CPS and EPS matrix of biofilms to facilitate contact between bacteria and treatment. Hence, the simplest synergistic effect of depolymerase is to promote the effect of disinfectants. Chai, *et al*. reported that the combination of a *Klebsiella* depolymerase and chlorine dioxide removed approximately 92% of the biofilm bacteria (*49*).

Likewise, similar synergies can lower the minimum inhibitory concentration (MIC), even empowering antibiotics that are ineffective otherwise. Notably, the depolymerase from *K. pneumoniae* phage KPO1K2 significantly enhanced the efficacy of ciprofloxacin against biofilms. The effects extents to enabling gentamicin which was ineffective against biofilms alone. Data indicate potent effect of KPO1K2 synergy by reducing bacterial counts by 3.261 log, with a reduction of 5.373 log in young biofilms (*50*). Studies on depolymerase Dpo71 further strengthens the paradigm, indicating Dpo71's ability to remove the capsular barrier and facilitate binding of colistin to the bacterial surface. Another study in *Galleria mellonella* infection model indicate that the combination of Dpo71 and colistin achieved an 80% survival rate, significantly outperforming either agent alone (40% and 30% survival, respectively) (*51*). Considering the novel studies and the limitation of conventional antibiotics, depolymerase pre-treatment sensitizes resistant bacteria to provide a key strategy to revitalize existing agents.

Beyond antibiotics, depolymerases function as natural synergists for lytic phages. Their enzymatic activity pre-conditions the bacterial surface by cleaving receptor-masking polysaccharides, therefore contributing to phage absorption. Studies indicated that a recombinant depolymerase can extend the host range of phages to otherwise resistant bacteria. Specifically, the recombinant depolymerase targeting the KL51 capsule of *Klebsiella pneumoniae* expands the host range (*52*). Furthermore, a combined application of *Staphylococcus aureus* (*S. aureus*) phage *Kayvirus rodi* and the polysaccharide depolymerase Dpo7 (from a different phage) better eradicated *S. aureus* biofilms than either agent alone (*53*). With this regard, engineered phages expressing single/multiple recombinant depolymerases represent a promising strategy for enhanced killing efficacy and broader host range for phage therapies.

Depolymerase action also synergistically alter the dynamics of immune responses, potentially presenting as immunoadjuvant strategy. Ample reports indicate that depolymerases can reduce bacterial virulence and sensitize them to the immune system (*45,54,55*). Mechanistically, this involves the removal of immunosuppressive polysaccharide, therefore exposing pathogen-associated molecular patterns (PAMPs) such as peptidoglycan, lipoproteins, and unmasked LPS core components. These exposed PAMPs are recognized by specific host pattern recognition receptors (PRRs), such as Toll-like receptors (TLRs) and NOD-like receptors (NLRs), on innate immune cells. Immune

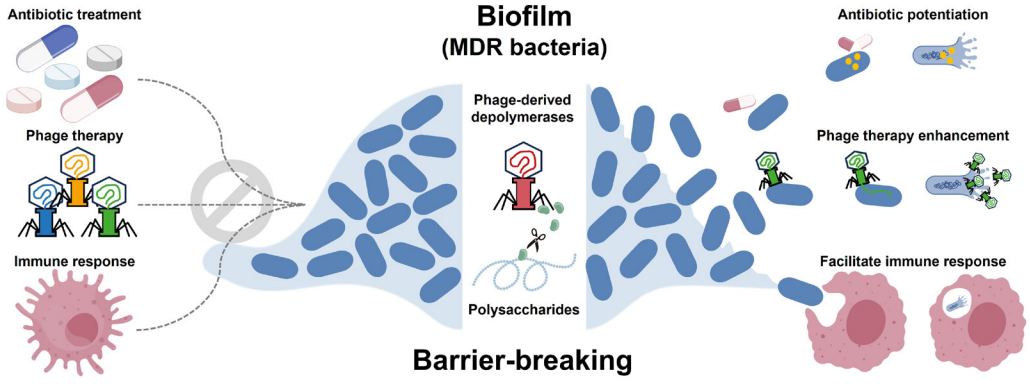

Figure 1. The potential of depolymerases as synergists. By enzymatically degrading key polysaccharide barriers (CPS, EPS and LPS), depolymerases remove a major obstacle to antimicrobial agents and immune effectors. Figure created with Biorender.

recognition triggers downstream pro-inflammatory signaling pathways (*e.g.*, NF-κB, MAPK), leading to the upregulated expression of cytokines, chemokines, and adhesion molecules. Consequently, depolymerase enhances opsonization and phagocytosis by macrophages and neutrophils (*56,57*), promoting a robust and coordinated recruitment of immune effectors to the infection site. In contrast with the antibiotic synergy, this synergy between depolymerase and host immune system presents an immunoadjuvant advantage of eliminating the bacteria without triggering widespread endotoxins release into the surrounding system, thereby reducing the scale of the infection and associated inflammatory events.

3.3. Bacterial resistance against depolymerase and potential counterstrategies

While depolymerases rarely induce classical resistance in the manner of antibiotics, their therapeutic use still exerts selective pressure that can drive adaptations. To design durable treatments, it is essential to anticipate these potential evolutionary routes. Key adaptations may include: a) Modification of the polysaccharide substrate (*e.g.*, altering acetylation (*58*)) to evade enzymatic recognition; b) Phase variation to express a different polysaccharide serotype resistant to the originally deployed depolymerase (*59,60*); and c) Upregulation of alternative EPS production to create a new, chemically distinct matrix (*61*).

These adaptive evolutions often emerge with exploitable fitness cost that jeopardizes the defensive integrity of bacteria and sensitize them to therapeutics. For instance, a point mutation and frameshift in the *wbaP* gene within the *cps* gene cluster of *K. pneumoniae* led to downregulated CPS production and upregulated production of smooth LPS. Though altering the glycocalyx profile, the evolutionary change attenuates virulence, enhances opsonization, and makes the bacteria more prone to immune clearance (*61*). This phenomenon reveals a strategic opportunity, in which depolymerase therapy can be designed not only to eliminate bacteria, but also to apply a selective pressure that actively steer bacterial populations towards a more vulnerable state to be exploited by a follow-up agent, such as antibiotic or the host immune system.

To preempt resistance, the application of depolymerase must be guided by evolutionary principles. Three main strategies can be employed to outmaneuver bacterial adaptation (Figure 2):

a. Cocktail Therapy: This approach utilizes mixtures of depolymerases that targets distinct polysaccharide antigens or epitopes on the same bacterium, making simultaneous escape mutations less probable. An example is phage ΦK64-1 which encodes 11 distinct depolymerase genes to counteract 11 different *Klebsiella* capsular types (*62*).

b. Genetic Engineering: Depolymerases can be engineered into multifunctional agents, such as depolymerase-lysin fusions, that attack independent, essential bacterial structures. Alternatively, protein engineering can broaden substrate specificity to target multiple variants.

c. Rational Combination Treatment: Depolymerases can be purposedly combined with antibiotics or phages in rotated or sequential therapy, with the depolymerase as a pioneer agent. This "depolymerase-first" approach aims to first strip away the polysaccharide shield, then immediately followed by a second agent (*e.g.*, a conventional antibiotic, phage, or other disinfectants) that exploits the newly exposed bacterial vulnerabilities. This creates a temporal elimination of two independent targets that sequentially takes out the external biofilm and the bacteria, making concurrent evolutionary escape difficult for the pathogen. This applies multifaceted selective pressures, reducing the chance that the pathogen evolves successful coping mechanism.

3.4. Delivery strategies and formulation of depolymerase-based therapies

Translating these synergistic and evolutionary concepts into antibacterial therapeutics requires novel delivery strategies and a thorough consideration of their biological fate as protein therapeutics. For topical treatments, delivery can be achieved by developing topical hydrogels or wound dressings for localized, sustained release of depolymerase into chronic wound infections resulted by bacterial biofilm. Infection in the respiratory system can be treated with direct delivery into the lungs with inhalable powders or spray drying (*63*). To further enhance stability and targeting, advanced formulation strategies such as microencapsulation within biodegradable polymers or encapsulation in liposomes (nanoliposomes) show great promise. These systems can protect the enzyme from premature degradation, control its release rate, and improve tissue-specific delivery while masking it from immune surveillance(*14,64,65*).

However, successful delivery hinges on addressing pharmacokinetic (PK) and safety of administered enzymes. These factors include *in vivo* stability, serum half-life, and immunogenicity upon administration. A critical aspect of immunogenicity is the risk of generating anti-drug antibodies (ADAs), which could intervene with the depolymerase activity and lead to hypersensitivity reactions that limits long-term therapeutic efficacy (*64,66*). While depolymerase action avoids the sudden endotoxin release associated with bacteriolysis, the rapid, large-scale degradation of structural polysaccharides could itself modulate local immune responses. The nature of this modulation remains an important area for preclinical safety assessment, as it could exacerbate inflammation. Their commercial viability is indicated by existing non-phage-derived EPS depolymerases,

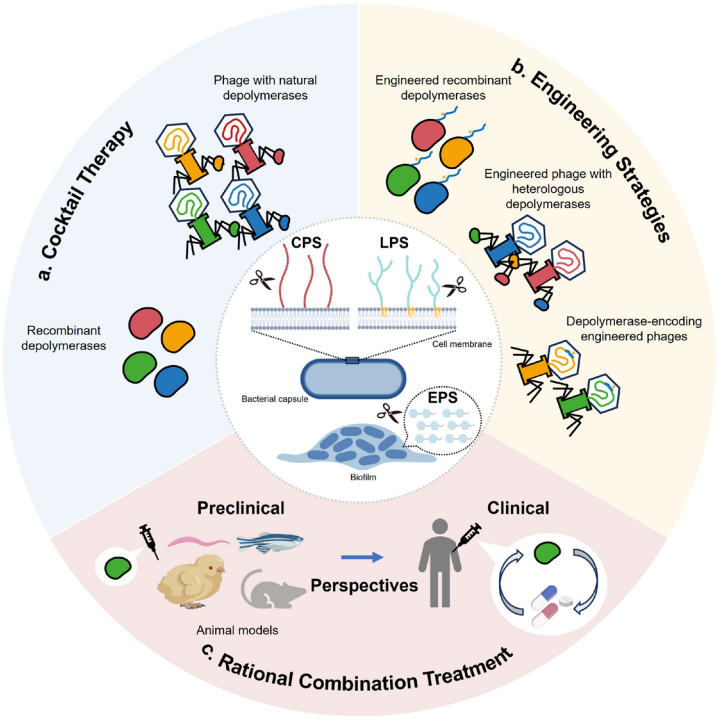

Figure 2. Schematic diagram of the counter-strategies of depolymerase as synergists. a) Cocktail Therapy: The foundational strategy employs mixtures of depolymerases targeting distinct polysaccharide antigens (*e.g.,* different capsule types) on the same pathogen. This multi-target approach increases the genetic barrier to resistance, making simultaneous escape mutations less probable. b) Engineering Strategies: A more advanced strategy involves direct protein engineering to create superior enzyme agents. This includes designing bifunctional fusion proteins (*e.g.*, depolymerase-lysin) that attack independent bacterial structures, or modifying the enzyme's active site to broaden its substrate specificity, thereby covering multiple pathogen variants with a single agent. c) Rational Combination Treatment: The most integrative strategy purposefully combines depolymerases with other antimicrobials (antibiotics or phages). Applying multifaceted selective pressures through rotation or sequence (*e.g.*, depolymerase first to strip the capsule, followed immediately by an antibiotic) hinders bacterial adaptation and prevents escape. Figure created with Biorender.

such as alginate lyase (Sigma-Aldrich) and dispersin B (Kane Biotech) (*7*), suggesting existing accessibility of enzyme-based biofilm control. Nevertheless, transitioning from commercial enzymes to human therapeutics demands rigorous evaluation under regulatory frameworks, requiring standardized assays for enzyme activity, potency, and stability in biologically relevant environments. Though developing existing enzyme-based products into clinically available products may require further research, existing evidence already indicate a clear path for future development. Therefore, the essence of future research lies within materializing the existing concept to develop an evolution-resistant combination therapy. With that regard, formulating depolymerase-based therapy is not a distant technical hurdle, but a critical breakthrough within reach.

4. Conclusion

As we approach a post-antibiotic era, finding sustainable alternatives to combat multidrug-resistant bacteria is at urgent need. The global threat of antibiotic resistance has led to tremendous interest in phage therapy (*67*). This review has synthesized current knowledge to propose that phage-derived depolymerases represent a unique class of antimicrobial adjuvants, manifesting potent synergistic functions. Our discussion elaborated on the depolymerases' ability to sensitize pathogens to conventional antibiotics and facilitate immune system eradication, therefore raising a concerted approach that mitigates the limitations of prior therapies.

While depolymerases rarely induce classic resistance (*67*), their use will exert selective pressure. Therefore, we believe future development of depolymerase-based therapies must focus on the evolutionary aspect of pathogens. Specifically, we proposed that cocktails therapies or other deliberate combinational treatments might manifest as effective counterstrategies. Although clinical application of depolymerases still require ample research, their proven efficacy in preclinical studies against biofilms and encapsulated bacteria is promising (*42,49,67,68*). A critical step towards the clinic will be navigating the unique regulatory pathway for depolymerases, which likely fall under the category of "antibiotic adjuvants" or novel enzymatic biology. This necessitates the development of consensus standards for defining and measuring enzymatic potency in therapeutic contexts, distinct from conventional antibiotics. In conclusion, depolymerases are likely ineffective as standalone replacements for antibiotics, rather as pivotal components of a synergistic and evolution driven strategy against bacterial infection. Further research

into the engineering, formulation, pharmacokinetics, immunogenicity, regulatory strategy, and integration of depolymerase into combination therapies is paramount to realizing their full potential in reducing our reliance on conventional antibiotics.

Funding: This work was supported by a grant from the National Natural Science Foundation of China (No. 82473753), National Key R&D Program of China (No. 2025YFC3408402), Prevention and Control of Emerging and Major Infectious Diseases-National Science and Technology Major Project (No. 2025ZD01908400), Shenzhen Clinical Research Center for Emerging Infectious Diseases (No. LCYSSQ20220823091203007), Shenzhen Key Laboratory for Diagnosis and Treatment Technology of Infectious Diseases, Shenzhen High-level Hospital Construction Fund, and Shanghai Science and Technology Innovation Action Plan in 2022 (No. 22N31900800).

Conflict of Interest: The authors have no conflicts of interest to disclose.

References

1. Dunne M, Hupfeld M, Klumpp J, Loessner MJ. Molecular Basis of Bacterial Host Interactions by Gram-Positive Targeting Bacteriophages. Viruses. 2018; 10:397.
2. Dion MB, Oechslin F, Moineau S. Phage diversity, genomics and phylogeny. Nat Rev Microbiol. 2020; 18:125-138.
3. Ge H, Hu M, Zhao G, Du Y, Xu N, Chen X, Jiao Xa. The "fighting wisdom and bravery" of tailed phage and host in the process of adsorption. Microbiol Res. 2020; 230:126344.
4. Knecht LE, Veljkovic M, Fieseler L. Diversity and Function of Phage Encoded Depolymerases. Front Microbiol. 2020; 10:2949.
5. Parasion S KM, Gryko R, Mizak L, Malm A. Bacteriophages as an alternative strategy for fighting biofilm development. Pol J Microbiol. 2014; 63:137-145.
6. Khadka S, Kinney EL, Ryan BE, Mike LA. Mechanisms governing bacterial capsular polysaccharide attachment and chain length. Ann N Y Acad Sci. 2025; 1548:80-98.
7. Pires DP, Oliveira H, Melo LD, Sillankorva S, Azeredo J. Bacteriophage-encoded depolymerases: their diversity and biotechnological applications. Appl Microbiol Biotechnol. 2016; 100:2141-2151.
8. Danis-Wlodarczyk KM, Wozniak DJ, Abedon ST. Treating Bacterial Infections with Bacteriophage-Based Enzybiotics: In Vitro, In Vivo and Clinical Application. Antibiotics. 2021; 10:1497.
9. Maciejewska B, Olszak T, Drulis-Kawa Z. Applications of bacteriophages versus phage enzymes to combat and cure bacterial infections: an ambitious and also a realistic application? Appl Microbiol Biotechnol. 2018; 102:2563-2581.
10. Chang C, Yu X, Guo W, Guo C, Guo X, Li Q, Zhu Y. Bacteriophage-Mediated Control of Biofilm: A Promising New Dawn for the Future. Front Microbiol. 2022; 13:825828.
11. Singh A, Padmesh S, Dwivedi M, Kostova I. How Good are Bacteriophages as an Alternative Therapy to Mitigate Biofilms of Nosocomial Infections. Infect Drug Resist. 2022; 15:503-532.
12. Chegini Z, Khoshbayan A, Vesal S, Moradabadi A, Hashemi A, Shariati A. Bacteriophage therapy for inhibition of multi drug-resistant uropathogenic bacteria: a narrative review. Ann Clin Microbiol Antimicrob. 2021; 20:30.
13. Topka-Bielecka G DA, Necel A, Bloch S, Nejman-Faleńczyk B, Węgrzyn G, Węgrzyn A. Bacteriophage-Derived Depolymerases against Bacterial Biofilm. Antibiotics (Basel). 2021; 10:175.
14. Wang H, Liu Y, Bai C, Leung SSY. Translating bacteriophage-derived depolymerases into antibacterial therapeutics: Challenges and prospects. Acta Pharm Sin B. 2024; 14:155-169.
15. Hughes KA, Sutherland IW, Clark J, MV. J. Bacteriophage and associated polysaccharide depolymerases-novel tools for study of bacterial biofilms. J Appl Microbiol. 1998; 85:583-590.
16. Li J, Feng S, Yu L, Zhao J, Tian F, Chen W, Zhai Q. Capsular polysaccarides of probiotics and their immunomodulatory roles. Food Sci Hum Wellness. 2022; 11:1111-1120.
17. Limoli DH, Jones CJ, Wozniak DJ, Ghannoum M, Parsek M, Whiteley M, Mukherjee P. Bacterial Extracellular Polysaccharides in Biofilm Formation and Function. Microbiol Spectr. 2015; 3:11.
18. Flemming H-C, Neu TR, Wozniak DJ. The EPS matrix: the "house of biofilm cells". J Bacteriol. 2007; 189:7945-7947.
19. Hoyle BD, Costerton JW. Bacterial resistance to antibiotics: the role of biofilms. Prog Drug Res. 1991; 37:91-105.
20. Ciofu O, Tolker-Nielsen T. Tolerance and Resistance of Pseudomonas aeruginosa Biofilms to Antimicrobial Agents-How P. aeruginosa Can Escape Antibiotics. Front Microbiol. 2019; 10:913.
21. Standish AJ, Morona R. The Role of Bacterial Protein Tyrosine Phosphatases in the Regulation of the Biosynthesis of Secreted Polysaccharides. Antioxid Redox Signal. 2014; 20:2274-2289.
22. Raetz CR, Whitfield C. Lipopolysaccharide endotoxins. Annu Rev Biochem. 2002; 71:635-700.
23. Skariyachan S, Sridhar VS, Packirisamy S, Kumargowda ST, Challapilli SB. Recent perspectives on the molecular basis of biofilm formation by Pseudomonas aeruginosa and approaches for treatment and biofilm dispersal. Folia Microbiol (Praha). 2018; 63:413-432.
24. Abrahams KA, Besra GS. Mycobacterial cell wall biosynthesis: a multifaceted antibiotic target. Parasitology. 2016; 145:116-133.
25. Ragupathi H, Pushparaj MM, Gopi SM, Govindarajan DK, Kandaswamy K. Biofilm matrix: a multifaceted layer of biomolecules and a defensive barrier against antimicrobials. Arch Microbiol. 2024; 206:432.
26. Latka A, Maciejewska B, Majkowska-Skrobek G, Briers Y, Drulis-Kawa Z. Bacteriophage-encoded virion-associated enzymes to overcome the carbohydrate barriers during the infection process. Appl Microbiol Biotechnol. 2017; 101:3103-3119.
27. Kim J, Liao X, Zhang S, Ding T, Ahn J. Application of phage-derived enzymes for enhancing food safety. Food Res Int. 2025; 209:116318.

28. Pires DP, Oliveira H, Melo LDR, Sillankorva S, Azeredo J. Bacteriophage-encoded depolymerases: their diversity and biotechnological applications. Appl Microbiol Biotechnol. 2016; 100:2141-2151.
29. Wang Y, Moradali MF, Goudarztalejerdi A, Sims IM, Rehm BHA. Biological function of a polysaccharide degrading enzyme in the periplasm. Sci Rep. 2016; 6:31249.
30. Blanco-Cabra N, Paetzold B, Ferrar T, Mazzolini R, Torrents E, Serrano L, Lluch-Senar M. Characterization of different alginate lyases for dissolving Pseudomonas aeruginosa biofilms. Sci Rep. 2020; 10:9390.
31. Chen YJ, Sui X, Wang Y, Zhao ZH, Han TH, Liu YJ, Zhang JN, Zhou P, Yang K, ZH Y. Preparation, structural characterization, biological activity, and nutritional applications of oligosaccharides. Food Chem X. 2024; 22:101289.
32. Chen C, Li X, Lu C, Zhou X, Chen L, Qiu C, Jin Z, Long J. Advances in alginate lyases and the potential application of enzymatic prepared alginate oligosaccharides: A mini review. Int J Biol Macromol. 2024; 260:129506.
33. Li S-F, Cheng F, Wang Y-J, Zheng Y-G. Strategies for tailoring pH performances of glycoside hydrolases. Crit Rev Biotechnol. 2023; 43:121-141.
34. Machida Y MK, Hattori K, Yamamoto S, Kawase M, Iijima S. Structure and function of a novel coliphage-associated sialidase. FEMS Microbiol Lett. 2000; 182:333-337.
35. Weigele PR, Scanlon E, King J. Homotrimeric, beta-stranded viral adhesins and tail proteins. J Bacteriol. 2003; 185:4022-4030.
36. Lin TL, Hsieh PF, Huang YT, Lee WC, Tsai YT, Su PA, Pan YJ, Hsu CR, Wu MC, Wang JT. Isolation of a bacteriophage and its depolymerase specific for K1 capsule of Klebsiella pneumoniae: implication in typing and treatment. J Infect Dis. 2014; 210:1734-1744.
37. Leiman PG, Battisti AJ, Bowman VD, Stummeyer K, Muhlenhoff M, Gerardy-Schahn R, Scholl D, Molineux IJ. The structures of bacteriophages K1E and K1-5 explain processive degradation of polysaccharide capsules and evolution of new host specificities. J Mol Biol. 2007; 371:836-849.
38. Guo Z, Liu M, Zhang D. Potential of phage depolymerase for the treatment of bacterial biofilms. Virulence. 2023; 14:2273567.
39. Maciejewska B SF, Latka A, Privitera M, Olejniczak S, Switala P, Ruggiero A, Marasco D, Kramarska E, Drulis-Kawa Z, Berisio R. Klebsiella phage KP34gp57 capsular depolymerase structure and function: from a serendipitous finding to the design of active mini-enzymes against K. pneumoniae. mBio. 2023; 14:e0132923.
40. Majkowska-Skrobek G, Latka A, Berisio R, Squeglia F, Maciejewska B, Briers Y, Drulis-Kawa Z. Phage-Borne Depolymerases Decrease Klebsiella pneumoniae Resistance to Innate Defense Mechanisms. Front Microbiol. 2018; 9:2517.
41. Majkowska-Skrobek G, Łątka A, Berisio R, Maciejewska B, Squeglia F, Romano M, Lavigne R, Struve C, Drulis-Kawa Z. Capsule-Targeting Depolymerase, Derived from Klebsiella KP36 Phage, as a Tool for the Development of Anti-Virulent Strategy. Viruses. 2016; 8:324.
42. Shahed-Al-Mahmud M, Roy R, Sugiokto FG, Islam MN, Lin M-D, Lin L-C, Lin N-T. Phage φAB6-Borne Depolymerase Combats Acinetobacter baumannii Biofilm Formation and Infection. Antibiotics (Basel). 2021; 10:279.
43. Miletic S, Simpson DJ, Szymanski CM, Deyholos MK, Menassa R. A Plant-Produced Bacteriophage Tailspike Protein for the Control of Salmonella. Front Plant Sci. 2015; 6:1221.
44. Waseh S, Hanifi-Moghaddam P, Coleman R, Masotti M, Ryan S, Foss M, MacKenzie R, Henry M, Szymanski CM, Tanha J. Orally administered P22 phage tailspike protein reduces salmonella colonization in chickens: prospects of a novel therapy against bacterial infections. PLoS One. 2010; 5:e13904.
45. Wang C, Li P, Niu W, et al. Protective and therapeutic application of the depolymerase derived from a novel KN1 genotype of Klebsiella pneumoniae bacteriophage in mice. Res Microbiol. 2019; 170:156-164.
46. Chen Y, Sun E, Yang L, Song J, Wu B. Therapeutic Application of Bacteriophage PHB02 and Its Putative Depolymerase Against Pasteurella multocida Capsular Type A in Mice. Front Microbiol. 2018; 9:1678.
47. Wang C, Li P, Zhu Y, Huang Y, Gao M, Yuan X, Niu W, Liu H, Fan H, Qin Y, Tong Y, Mi Z, Bai C. Identification of a Novel Acinetobacter baumannii Phage-Derived Depolymerase and Its Therapeutic Application in Mice. Front Microbiol. 2020; 11:1407.
48. Hsu CR, Lin TL, Pan YJ, Hsieh PF, Wang JT. Isolation of a bacteriophage specific for a new capsular type of Klebsiella pneumoniae and characterization of its polysaccharide depolymerase. PLoS One. 2013; 8:e70092.
49. Chai Z, Wang J, Tao S, Mou H. Application of bacteriophage-borne enzyme combined with chlorine dioxide on controlling bacterial biofilm. LWT-Food Sci Technol. 2014; 59:1159-1165.
50. Bansal S, Harjai K, S C. Aeromonas punctata derived depolymerase improves susceptibility of Klebsiella pneumoniae biofilm to gentamicin. BMC Microbiol. 2015; 15:119.
51. Chen X, Liu M, Zhang P, Xu M, Yuan W, Bian L, Liu Y, Xia J, Leung SSY. Phage-Derived Depolymerase as an Antibiotic Adjuvant Against Multidrug-Resistant Acinetobacter baumannii. Front Microbiol. 2022; 13:845500.
52. Roch M SR, Panis G, Martins WB, Andrey D. Synergistic activity of a KL51-depolymerase and a Sugarlandvirus bacteriophage against ST16 Klebsiella pneumoniae. Microbiol Spectr. 2025; 13:e0214225.
53. Duarte AC, Fernández L, Jurado A, Campelo AB, Shen Y, Rodríguez A, García P. Synergistic removal of Staphylococcus aureus biofilms by using a combination of phage Kayvirus rodi with the exopolysaccharide depolymerase Dpo7. Front Microbiol. 2024; 15:1438022.
54. Liu Y, Leung SSY, Huang Y, Guo Y, Jiang N, Li P, Chen J, Wang R, Bai C, Mi Z, Gao Z. Identification of Two Depolymerases From Phage IME205 and Their Antivirulent Functions on K47 Capsule of Klebsiella pneumoniae. Front Microbiol. 2020; 11:218.
55. Volozhantsev NV, Borzilov AI, Shpirt AM, Krasilnikova Valentina M, Verevkin VV, Denisenko EA, Kombarova Tatyana I, Shashkov AS, Knirel YA, Dyatlov IA. Comparison of the therapeutic potential of bacteriophage KpV74 and phage-derived depolymerase (β-glucosidase) against Klebsiella pneumoniae capsular type K2. Virus Res. 2022; 322:198951.
56. Jo E-K. Interplay between host and pathogen: immune defense and beyond. Exp Mol Med. 2019; 51:1-3.
57. Nam J, Kim A, Kim K, Moon JH, Baig J, Phoo M, Moon

JJ, Son S. Engineered polysaccharides for controlling innate and adaptive immune responses. Nat Rev Bioeng. 2024; 2:733-751.
58. Lee VT, Wang L, Wang Z, Zhang H, Jin Q, Fan S, Liu Y, Huang X, Guo J, Cai C, Zhang J-R, Wu H. A novel esterase regulates Klebsiella pneumoniae hypermucoviscosity and virulence. PLoS Pathog. 2024; 20:e1012675.
59. Zhang T, Ji S, Zhang M, Wu F, Li X, Luo X, Huang Q, Li M, Zhang Y, Lu R. Effect of capsular polysaccharide phase variation on biofilm formation, motility and gene expression in Vibrio vulnificus. Gut Pathog. 2024; 16:40.
60. Lukáčová M, Barák I, Kazár J. Role of structural variations of polysaccharide antigens in the pathogenicity of Gram-negative bacteria. Clin Microbiol Infect. 2008; 14:200-206.
61. Kaszowska M, Majkowska-Skrobek G, Markwitz P, Lood C, Jachymek W, Maciejewska A, Lukasiewicz J, Drulis-Kawa Z. The Mutation in wbaP cps Gene Cluster Selected by Phage-Borne Depolymerase Abolishes Capsule Production and Diminishes the Virulence of Klebsiella pneumoniae. Int J Mol Sci. 2021; 22:11562.
62. Pan Y-J, Lin T-L, Chen C-C, Tsai Y-T, Cheng Y-H, Chen Y-Y, Hsieh P-F, Lin Y-T, Wang J-T, Sandri-Goldin RM. Klebsiella Phage ΦK64-1 Encodes Multiple Depolymerases for Multiple Host Capsular Types. J Virol. 2017; 91:e02457-02416.
63. Bolsan AC, Sampaio GV, Rodrigues HC, Silva De Souza S, Edwiges T, Celant De Prá M, Gabiatti NC. Phage formulations and delivery strategies: Unleashing the potential against antibiotic-resistant bacteria. Microbiol Res. 2024; 282:127662.
64. Manzari MT, Shamay Y, Kiguchi H, Rosen N, Scaltriti M, Heller DA. Targeted drug delivery strategies for precision medicines. Nat Rev Mater. 2021; 6:351-370.
65. Pendam D, Tomake P, Debaje S, Guleria K, Saha A, Thakran P, Sangamwar AT. Advances in formulation strategies and stability considerations of amorphous solid dispersions. J Drug Deliv Sci Tec. 2025; 108:106922.
66. Howard EL, Goens MM, Susta L, Patel A, Wootton SK. Anti-Drug Antibody Response to Therapeutic Antibodies and Potential Mitigation Strategies. Biomedicines. 2025; 13:299.
67. Uyttebroek S CB, Onsea J, Ruythooren F, *et al*. Safety and efficacy of phage therapy in difficult-to-treat infections: a systematic review. Lancet Infect Dis. 2022; 22:e208-e220.
68. Li P, Ma W, Shen J, Zhou X. Characterization of Novel Bacteriophage vB_KpnP_ZX1 and Its Depolymerases with Therapeutic Potential for K57 Klebsiella pneumoniae Infection. Pharmaceutics. 2022; 14:1916.

Received January 6, 2026; Revised January 27, 2026; Accepted February 2, 2026.

[§]These authors contributed equally to this work.
**Address correspondence to:*
Hongzhou Lu and Jiayin Shen, National Clinical Research Center for Infectious Diseases, The Third People's Hospital of Shenzhen and The Second Affiliated Hospital of Southern University of Science and Technology, Shenzhen, Guangdong 518112, China.
E-mail: luhongzhou@szsy.sustech.edu.cn (HL), johnnie1111@hotmail.com (JS)

Released online in J-STAGE as advance publication February 6, 2026.

Review

DOI: 10.5582/bst.2026.01002

Implications of mitochondrial function in embryonic development

Jing Wang[1,2,§], Jing Zhou[3,§], Yanying Wang[4], Yun Li[5], Ling Wang[6,*], Lisha Li[1,*]

[1] Laboratory of Reproduction Immunology, Shanghai Key Laboratory of Female Reproductive Endocrine-related Diseases, Obstetrics and Gynecology Hospital, Fudan University Shanghai Medical College, Shanghai, China;
[2] Department of Gynecology, Yueyang Hospital of Integrated Traditional Chinese and Western Medicine, Shanghai University of Traditional Chinese Medicine, Shanghai, China;
[3] Department of Obstetrics and Gynecology, Nanfang Hospital, Southern Medical University, Guangzhou, Guangdong, China;
[4] Department of VIP Clinic, General Division, Shanghai East Hospital, Tongji University School of Medicine, Shanghai, China;
[5] Department of Oncology, Shanghai East Hospital, Tongji University School of Medicine, Shanghai, China;
[6] Department of Obstetrics, The First Affiliated Hospital, Guizhou University of Traditional Chinese Medicine, Guiyang, Guizhou, China.

SUMMARY: Mitochondria are organelles that play a crucial role in various physiological processes. They are particularly important during embryonic development, as their proper function is required for essential processes such as fertilization, implantation, and embryonic growth. In addition to their well-known role in adenosine triphosphate (ATP) synthesis and energy production, mitochondria serve multiple other functions during embryonic development. These include the synthesis of important metabolites, involvement in cell signaling pathways, regulation of reactive oxygen species, and facilitation of interactions between organelles. The mitochondrial genome, known as mitochondrial DNA (mtDNA), also plays a unique role in embryonic development. Dysfunction in mitochondria can lead to failures in fertilization, suboptimal embryo development, post-implantation failures, and mitochondrial-related diseases in adults. Advances in sequencing technology and experimental techniques have greatly improved our understanding of mitochondrial function. This paper reviews the roles of mitochondrial functions in embryonic development and the influence of mitochondrial technologies and it highlights the potential impact of understanding mitochondria's unique genetic and functional characteristics on embryonic development and offspring health.

Keywords: mitochondria, metabolism, mtDNA, embryonic development

1. Introduction

Mitochondria are known to have a highly functional structure and are found in eukaryotic cells. They play crucial roles in various cellular processes including material metabolism, energy metabolism, and signal transduction (*1*). Human embryonic development is a complex and fascinating process that involves various stages and cellular activities. Throughout preimplantation development, embryo implantation, and subsequent post-embryonic development, the embryo undergoes a series of energetic cellular processes that heavily rely on adenosine triphosphate (ATP) for energy (*2*). ATP is the primary energy currency of cells, and its production is critical for various cellular functions, including growth, division, and differentiation. Therefore, the maintenance of mitochondrial function is crucial to successful embryogenesis. However, mitochondria also serve other important roles beyond energy production.

2. Mitochondrial mechanisms governing early embryonic development

2.1. Mitochondrial energy metabolism and embryonic development

There is a huge heterogeneity in the number of mitochondria in human cells, and a large number of mitochondria are known to be distributed in the cytoplasm of oocytes (*3*). After fertilization, fertilized oocytes adjust the mitochondrial density in different intracellular regions, but their exact functional significance remains unknown (*4,5*). Mitochondria have also been reported to be disproportionately distributed in the formed blastomeres of developing embryos (*6*). The hypothesis is that mitochondrial aggregation may contribute to the direct and rapid supply of energy to the nucleus (*7*).

Early embryonic mitochondria appear spherical (≤ 1 μm) under electron microscopy, featuring sparse cristae and dense matrices (*8*). They retain this immature form

until the blastocyst stage, where they begin to elongate and form mature cristae (*9*). Despite the high energy demands of cleavage and blastocyst formation (*10*), pre-implantation embryos rely heavily on pyruvate oxidation rather than glucose. This strategy is thought to limit mitochondrial reactive oxygen species (ROS) generation (*11-13*). Pyruvate enters mitochondria directly for the tricarboxylic acid (TCA) cycle — bypassing cytosolic glycolysis — so it is a more efficient fuel source here. Indeed, removing pyruvate blocks development, whereas removing glucose or lactate does not (*14,15*). In the blastocyst stage, increased oxidative respiration coincides with mitochondrial cristae expansion (*16*). The molecular transition from anaerobic to aerobic respiration is orchestrally regulated by the stabilization of hypoxia-inducible factor 1-alpha (HIF-1α), a master regulator of oxygen homeostasis constitutively expressed in cleavage-stage embryos. HIF-1α upregulates pyruvate dehydrogenase (PDH) kinase 1 (PDK1) to shunt pyruvate away from the TCA cycle (*17,18*). HIF-1α also influences mitochondrial morphology to support anaerobic metabolism by upregulating dynamin-related protein 1 (DRP1) expression, resulting in fragmented mitochondria with limited cristae formation, which is characteristic of anaerobic metabolism (*19,20*). Notably, cristae maturation is related to an ROS balance by increasing expression of antioxidant enzymes and preventing oxidative damage despite higher oxygen consumption (*21*).

2.2. Mitochondrial substance metabolism and embryonic development

Mitochondrial metabolism is at the core of the cellular metabolic network, where the TCA, oxidative phosphorylation (OXPHOS), fatty acid oxidation, nucleotide synthesis, and amino acid metabolism all occur (*22*). Alterations in these activities may mediate changes in the oocyte and early embryo epigenetic landscape that affect subsequent developmental capacity (*23*). There is a complex relationship between mitochondrial activity and calcium signaling (*24*). Calcium is an activator of OXPHOS by activating dehydrogenases, respiratory chains, and ATP synthases required for cycling. There are several contact zones between the endoplasmic reticulum (ER) and mitochondria, known as mitochondrial-associated ER membranes (MAMs), that serve as the key physical and functional platform for calcium signaling crosstalk during embryonic development (*25*). This mechanism is known to play a role in fertilization, where calcium released from the ER activates the mitochondria and induces calcium oscillations necessary for oocyte activation (*26*). MAMs are enriched with core regulatory proteins including mitofusin 1/2 (MFN1/2), inositol 1,4,5-trisphosphate receptors on the ER, and voltage-dependent anion channels on the mitochondrial outer membrane, which together form a high-efficiency calcium transfer channel (*27*). Moreover, phosphatidylinositol metabolites in MAMs, such as

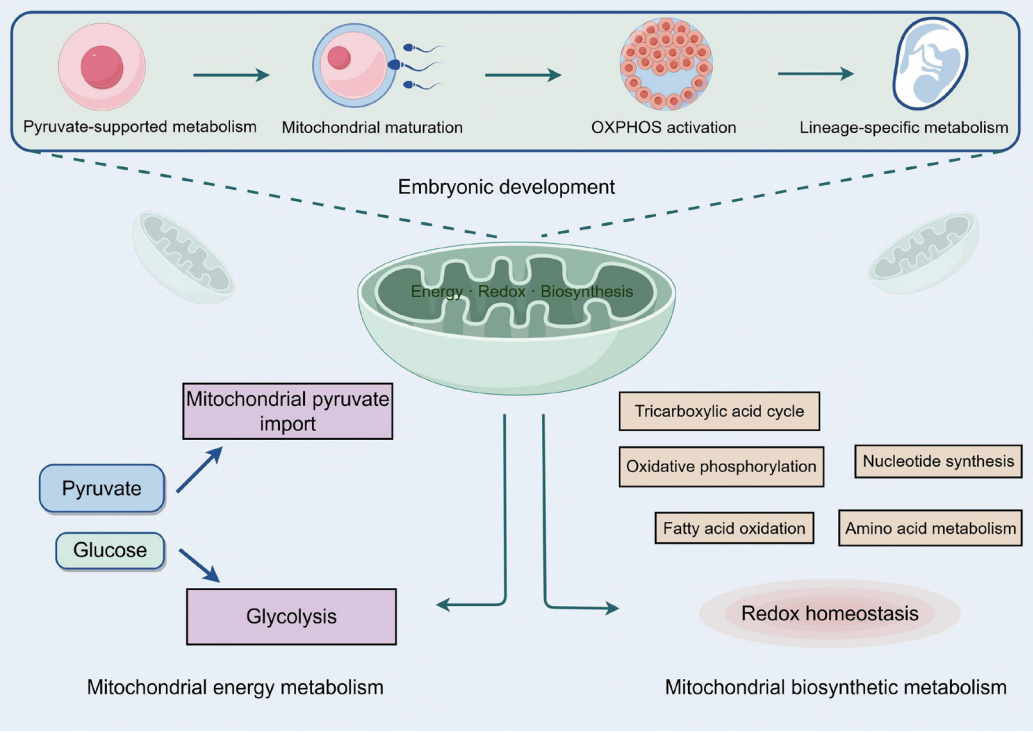

Figure 1. Metabolic transitions and mitochondrial maturation in early embryos. During early cleavage, metabolism relies primarily on pyruvate, while glucose utilization remains limited to the cytosol. As development progresses towards implantation, mitochondria undergo structural maturation and upregulate oxidative phosphorylation. Beyond ATP production, these organelles serve as hubs for the tricarboxylic acid cycle, fatty acid oxidation, and the synthesis of nucleotides and amino acids, thereby coordinating energy supply with redox homeostasis.

inositol 1,4,5-trisphosphate, can specifically bind to IP3Rs on the ER membrane to trigger calcium release, further amplifying calcium oscillation signals during fertilization (*28*). These findings collectively demonstrate that MAM-mediated precise regulation of calcium signaling is a prerequisite for normal oocyte-to-embryo transition.

Mitochondrial metabolites serve as critical substrates for epigenetic modifying enzymes and play pivotal regulatory roles in oocyte maturation and early embryonic development. α-Ketoglutarate functions as an essential cofactor for TET (ten-eleven translocation) family DNA demethylases and Jumonji C domain-containing histone demethylases, whereas acetyl-coenzyme A (acetyl-CoA) directly modulates histone acetylation levels as the obligate substrate for histone acetyltransferase. Notably, genetic ablation of *Drp1* results in pronounced reductions in both DNA methylation and H3K27me3 levels in oocytes, providing direct evidence for the indispensable role of mitochondrial functionality in the establishment of the maternal epigenome. The post-fertilization perinuclear redistribution of mitochondria surrounding the pronuclei may generate "localized metabolite microdomains," thereby establishing substrate concentration gradients that provide a spatially defined microenvironment for epigenetic modifying enzymes. This compartmentalized metabolic architecture is hypothesized to orchestrate the asymmetric epigenetic reprogramming of the paternal and maternal genomes during the earliest stages of embryogenesis (*29-31*).

In addition, there are interactions between the physical contacts of mitochondria and lipid droplets (LDs) (*32*). LDs staining of embryos from *in vitro* fertilization (IVF) and parthenogenetic activation (PA) sources in cattle and pigs, respectively, revealed possible dysregulation of lipid metabolism and mitochondrial dysfunction in PA embryos, suggesting significant differences in LD parameters between developmental stages and species studied (*33*). Research has demonstrated that LDs in mammalian eggs are utilized during embryonic diapause, revealing the functional role of LDs in embryonic development (*34*). A recent review highlighted the fact that LDs play essential roles in embryonic development across species by providing energy, supplying lipids for membrane formation, and protecting embryos against lipotoxicity, oxidative stress, and infection, with evidence showing that depletion of LDs in early embryos leads to developmental arrest and abnormalities (*35*).

Notably, mitochondrial fatty acid β-oxidation serves as a critical additional energy supply pathway for embryos transitioning to the blastocyst stage. As embryonic development progresses from the cleavage stage to the blastocyst, metabolic demands surge, and mitochondrial fatty acid β-oxidation is dynamically activated to complement pyruvate-dependent energy metabolism (*36,37*). This process involves a series of highly regulated steps: fatty acids stored in LDs are first activated to fatty acyl-CoA, then transported into the mitochondrial matrix *via* the carnitine palmitoyltransferase 1-mediated shuttle system, and subsequently degraded into acetyl-CoA. Acetyl-CoA then enters the tricarboxylic acid cycle to generate a large amount of ATP, meeting the high energy requirements for blastocyst expansion and lineage segregation (*38,39*). A recent study has confirmed that long-chain fatty acid β-oxidation is essential for preimplantation development. Inhibition of long-chain fatty acid β-oxidation results in downregulated expression of S phase-related genes and loss of H3K18ac modification. This finding provides evidence of the effect of fatty acid β-oxidation in metabolism-epigenetic crosstalk on early embryonic development (*40*).

A study found that the secretion of leptin increased in mothers with a high-fat diet by altering the mitochondrial function of mouse oocytes and fertilized eggs, activating nuclear PPAR-γ receptors, and stimulating the up-regulation of genes controlling fatty acid oxidation, resulting in abnormal development of fertilized eggs (*41*). As women age, lipid levels in the follicular fluid may disrupt the epigenetic landscape of the oocyte (*42*). Lipid-derived acetyl-CoA is more readily incorporated into histones than glucose-derived acetyl-CoA, suggesting plasticity in mitochondrial metabolism and a potential association with epigenetic remodeling (*43*). Culturing under atmospheric conditions (20% O_2) resulted in increased ROS levels in mouse embryos, abnormalities in mitochondrial morphology and function, and alterations in mitochondrial gene expression profiles compared to culturing under physiological conditions (5% O_2) (*44*). These studies suggest that the abnormal accumulation of ROS can seriously affect the normal development of embryos (*45*). Thus, maintaining mitochondrial metabolic function is vital for redox homeostasis and supports normal embryogenesis (Figure 2).

2.3. Mitochondrial dynamics in embryonic development

Mitochondria are the center of cell metabolism, and their size, density, and location are closely related to the status of cell metabolism (*46*). Mitochondria perform quality control through division and fusion to adjust their shape, length, and quantity. Mitochondrial dynamics allow for the exchange of lipid membrane and matrix contents, the repair of mitochondrial DNA (mtDNA) damage, and the regulation of mitochondrial biogenesis and apoptosis (*48*). In the context of reproductive biology, normal mitochondrial dynamics are indispensable for embryonic development, as evinced by gene-specific knockout models. Deficiencies in *Drp1*, mitochondrial fission factor (*Mff*), or *Mfn1/2* consistently result in developmental arrest, reduced embryo size, and impaired differentiation (*49*). The knockout of *Drp1* in mice

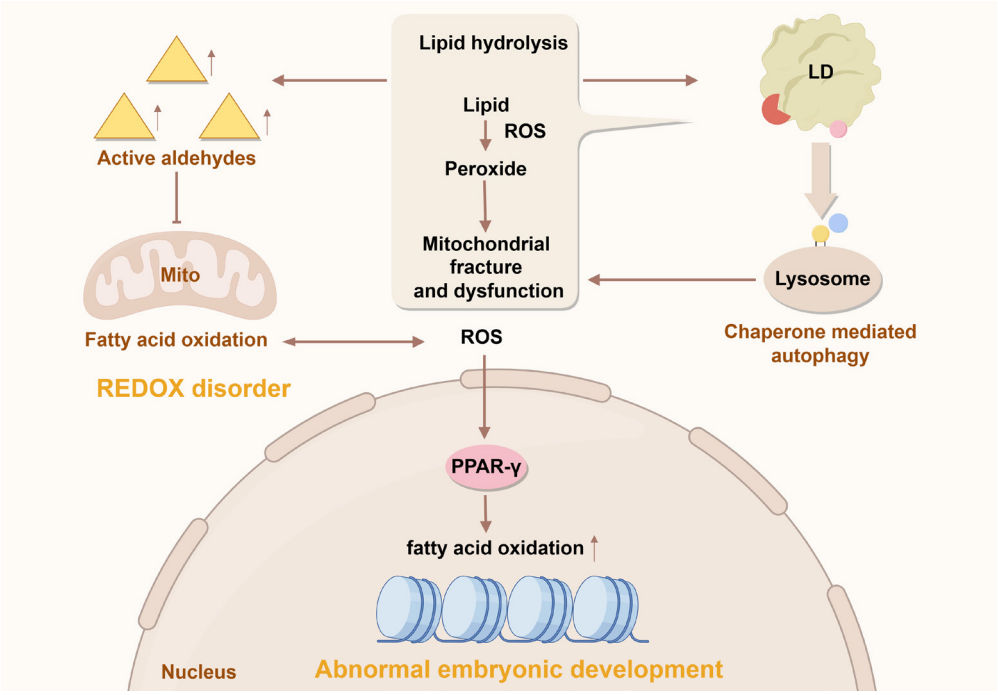

Figure 2. Redox imbalance drives lipid oxidation and mitochondrial dysfunction in embryonic cells. Elevated ROS levels trigger lipid peroxidation, generating active aldehydes and disrupting lipid homeostasis. Lipid droplets (LDs) undergo hydrolysis *via* lysosomal pathways, including chaperone-mediated autophagy, in response to stress. Under these oxidative conditions, mitochondria exhibit structural remodeling and altered fatty acid oxidation profiles. Mechanistically, ROS signaling activates nuclear PPAR-γ and downstream transcriptional programs regulating fatty acid metabolism. Cumulatively, these redox-induced metabolic and organelle defects predispose embryos to developmental abnormalities.

resulted in death of the embryo at E11.5, accompanied by a reduction in volume, which was associated with damage to placental giant cells (*30*). Disruption of mitochondrial fission by inhibiting DRP1 recruitment to the mitochondria leads to G2/M growth arrest in cells undergoing reprogramming and affects the early phase in reprogramming, suggesting that mitochondrial fission affects pluripotential reprogramming (*50,51*). A study suggested that MFNs play an important role in germ cell formation and embryonic development, including spermatogenesis, oocyte maturation, and embryonic development (*52*). MFNs are necessary for embryonic development and are involved by regulating mitochondrial fusion and homeostasis, thereby maintaining normal levels of ATP and a normal mitochondrial membrane potential (MMP) during embryonic development (*53*). During early embryonic development, low levels of MFN1 expression lead to the lethal fragmentation of the early embryo by destroying mitochondrial MMP and OXPHOS components, ultimately resulting in reduced embryo survival (*54*). Normal expression of MFN2 maintains blastocyst formation, while reduced expression of MFN2 leads to mitochondrial dysfunction and induces apoptosis through BCL2/BAX and $Ca2^{+}$, ultimately reducing blastocyst formation (*55*). These genes related to mitochondrial function are associated with various modes of cell death, and their roles in fertilization and embryonic development warrant further examination.

In addition to mitochondrial dynamics-associated genes, cell competition has emerged as a novel quality control mechanism capable of eliminating cells with compromised mitochondrial function during early embryonic development. Studies have demonstrated that approximately 35% of epiblast cells are eliminated prior to gastrulation in murine embryos, with single-cell transcriptomic analyses revealing that these eliminated cells exhibit pronounced signatures of mitochondrial dysfunction. This "purifying selection" mechanism ensures that cells harboring high-load mtDNA mutations or exhibiting suboptimal mitochondrial performance are culled through apoptotic pathways, thereby optimizing the overall mitochondrial fitness of the embryo prior to gastrulation. Notably, even non-pathogenic mtDNA sequence variants may be sufficient to trigger cell competition, suggesting that the behavior of mtDNA heteroplasmy may manifest along a continuum ranging from stochastic genetic drift to stringent selective pressure, contingent upon nuclear-cytoplasmic interactions and metabolic determinants (*56,57*).

Human embryos also rely on mitochondrial fission-fusion dynamics to regulate mtDNA heteroplasmy. Mutated mitochondria often exhibit reduced MMP and impaired OXPHOS, which are recognized as "damage signals". Mitochondrial fission prevents the spread of harmful mutations to the entire mitochondrial population and marks the mutated mitochondria for subsequent selective clearance *via* mitochondrial autophagy (*58*).

Mitochondrial fission-fusion imbalance impairs mtDNA quality control, leading to the accumulation of mutated mitochondria, which in turn disrupts NADH/NAD^+ redox homeostasis and reduces oocyte and embryo quality. Conversely, enhancing mitochondrial fusion *via* MFN activation or inhibiting USP30 to promote mitochondrial autophagy can improve the developmental competence of embryos with high mtDNA mutation loads (*59*). The crucial role of mtDNA mutation loads during embryonic development is described in further detail below. By screening out high-load mtDNA mutations and optimizing ATP production, mitochondrial dynamics ensure the metabolic homeostasis and genomic stability necessary for successful fertilization and embryogenesis.

2.4. mtDNA and embryonic development

In humans, like most mammals, mitochondria and mtDNA are entirely passed down maternally. Sperm contain very few mitochondria, which are destroyed after fertilization, while in oocytes, the mitochondrial reservoir is fully expanded, making an oocyte the cell with the most mitochondria in the organism (*60,61*). In human oocytes, the average number of copies of mtDNA is estimated to be about 250,000 (*62*). While most of the genes associated with mitochondrial biological activity are encoded by the nuclear genome, mtDNA encodes 13 proteins involved in the respiratory chain, as well as 22 transfer RNAs and two ribosomal RNAs (*63*). The mtDNA copy number grows exponentially during ovulation and peaks during fertilization (*64*). Failure of mature oocytes to increase the mtDNA copy number above the threshold may result in fertilization failure or early embryo arrest (*65*). During pre-implantation development, the number of mtDNA copies per cell gradually decreases. mtDNA is at a low level after fertilization and comparatively increases during embryo implantation (*66*). During the blastocyst stage, the final stage of pre-implantation development, mtDNA replication begins, but this is limited to the trophectoderm, where mtDNA replication is quiescent in the inner cell mass (*67*).

During gastrula formation, some pluripotent cells produce primordial germ cells, which contain copies of mitochondrial DNA that are passed to the next generation *via* metaphase II oocytes (*68*). These copies undergo a filtration or purification process that typically removes mutated copies of the mitochondrial genome to ensure that the maternal transmission of only certain genomes passes on minimal harmful effects to the next generation, also known as the mitochondrial genetic bottleneck (*69*). However, when the mutant load is high in these cells, mtDNA diseases occur (*70*). mtDNA copy number is generally considered to be an indicator of the number of mitochondria and is associated with oocyte fertilization potential (*71*). However, this is not consistent with the metabolic requirements of the blastocyst embryo, and this view is still a subject of debate (*72*). This controversy may be reconciled through the "compensatory biogenesis" hypothesis: when embryos are subjected to metabolic stress, they upregulate mitochondrial biogenesis to sustain ATP provision, consequently resulting in elevated mtDNA copy numbers. Accordingly, a heightened mtDNA copy number may reflect an overcompensatory response to adverse conditions rather than superior developmental competence. Supporting this notion, studies conducted in IVF patients with favorable prognoses have failed to demonstrate a significant correlation between the cumulus cell mtDNA copy number and implantation success rates, with no significant differences in mtDNA content observed between implanted and non-implanted embryos. Moreover, the mtDNA/gDNA ratio exhibits a negative correlation with patient age, underscoring the imperative of establishing "tissue-specific" and "age-dependent" threshold values rather than relying upon a singular universal numerical criterion (*73-75*). The advent of single-cell multi-omics technologies has afforded unprecedented opportunities to monitor how mtDNA mutations alter fateful decisions within specific cell lineages in real time. Integrating single-cell transcriptomic data with chromatin accessibility profiles enables the construction of regulatory networks governing early embryonic development and the identification of pivotal regulatory determinants orchestrating the differentiation of the inner cell mass and trophectoderm. Recent studies involving single-cell transcriptomic analyses have delineated mtDNA mutation-specific and lineage-specific compensatory mechanisms; these compensatory pathways are governed by transcription factors that promote organellar resilience and sustain mitochondrial functionality throughout critical developmental windows (*76,77*). Preimplantation embryo development is characterized by extensive reprogramming of the epigenetic landscape to support and regulate events in specific stages, including embryo genome activation and lineage norms (*78*). Perturbations of the nutritional environment around oocytes and preimplantation embryos may regulate the long-term health and viability of offspring by influencing metabolic changes in the programmed epigenome. In mouse and human oocytes, highly polarized mitochondria cluster around the oocyte cortex, and mitochondria with a low membrane potential are evenly distributed throughout the cytoplasm (*79*). After fertilization, mitochondria translocate and cluster around the two pronuclei to facilitate synthesis and ensure a uniform distribution of organelles between the resulting blastomeres, and mitochondria may be associated with mtDNA functioning (*80*). Mitochondrial repositioning occurs at the same time as differential regulation of the paternal and maternal epigenomes, so clustering may enable crosstalk between the nuclear and mitochondrial genomes and the establishment of local metabolite

domains to regulate epigenetic modifiers (*81*).

In order for cells to function effectively in different stages of development and maturation, the nuclear and mitochondrial genomes need to change in sync (*82*). During critical stages of development, cells strike a balance between their two genomes in order to be able to move on to the next stage of development (*83*). This process is mediated by the constant exchange of regulatory information between the nuclear and mitochondrial genomes (*84*). This ensures that the cell gets enough copies of mtDNA in any given stage so that the cell can use as much or as little OXPHOS-derived ATP as possible to perform certain functions (*85*). At the same time, nuclear genomes contribute to a genomic balance by altering epigenetic changes such as levels of DNA methylation that control gene expression (*86*). The mitochondrial genome contributes to a genomic balance through the mtDNA copy number, which affects cell metabolism, and metabolism is also influenced by the cell's mtDNA haplotype (*87*). These lineage-specific remodeling events are summarized in Figure 3.

2.5. Mitochondrial autophagy plays an important role in early embryonic development

The quality of mitochondria in the oocyte is widely recognized to determines the quality of the oocyte and, as a consequence, the developing embryo (*88*). The autophagy system targets damaged mitochondria and transports them to lysosomes for degradation (*89*). This catabolic process, called mitochondrial autophagy, helps maintain mitochondrial quality control in a variety of cell types (*90*). Autophagy occurs after conception and throughout embryogenesis. In addition to providing survival mechanisms in times of nutrient deficiency, autophagy also eliminates organelles and protein aggregates at specific points in time during development (*91*). Survival after a specific developmental stage also requires several autophagy genes (*92*).

Proteins of maternal origin that are present in oocytes after fertilization are widely believed to promote autophagy (*93*). After oocyte-specific ATG5 knockout, mice were fertilized with ATG5-deficient sperm; the embryos failed to survive and development stalled in the 4-cell to 8-cell stage (*94*). There is a lack of complete understanding of why embryos with defective autophagy die in the 4-to-8-cell stage, but protein synthesis decreases significantly. The autophagy-related gene Beclin1 plays an important role in early embryogenesis in mice (*95*). Homozygous mutations in Beclin1 led to early embryo death between days E7.5 and E8.5, and severe developmental delays were present in animals on day E7.5. Beclin1 may be involved in promoting amniotic duct closure and amniotic fold development (*96*).

In rodents, developmental programmed cell death is involved in embryonic development and usually occurs early in embryogenesis. The solid mass of ectodermal cells undergoes programmed cell death and forms a preamniotic cavity (*97*). Mouse ATG5−/− embryos feature a defect in apoptotic-corpse engulfment in the retina and lungs (*98*). Autophagy-dependent ATP production promotes PS-mediated apoptotic cell clearance in some developmental programmed cell death

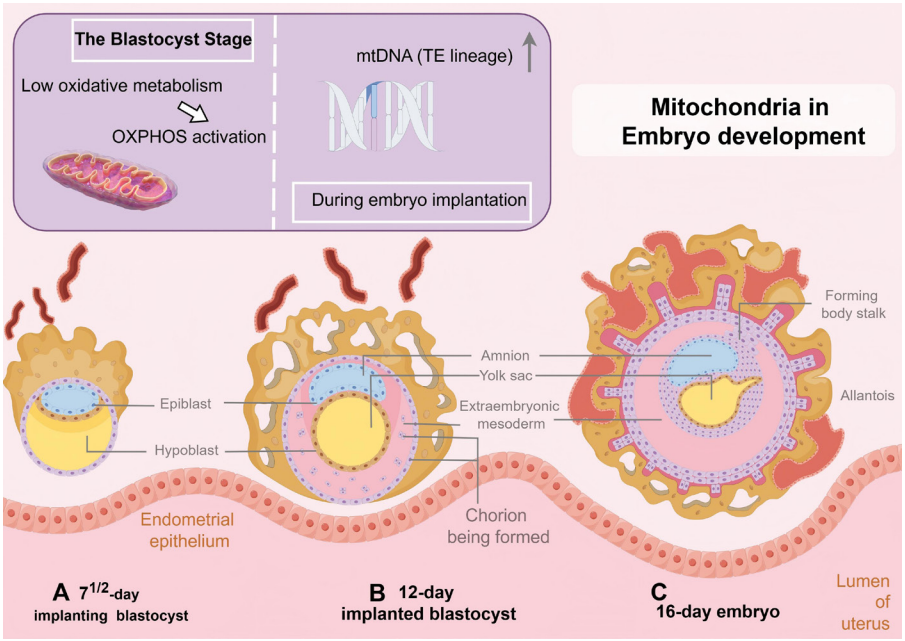

Figure 3. Mitochondrial dynamics during human implantation and early development. As the blastocyst implants, trophectoderm (TE) cells switch to a high-OXPHOS state with amplified mtDNA levels, supporting the metabolic demands of tissue invasion. In parallel, the spatial reorganization of mitochondria around pronuclei points to a direct role in nuclear reprogramming. These metabolic shifts provide the bioenergetic foundation required for embryonic genome activation and the epigenetic remodeling characteristic of early human embryogenesis.

contexts, but not all. The exact roles of mitochondrial autophagy and key genes in human embryonic development still need to be further studied and better understood.

2.6. Use of new techniques to study mitochondrial and embryonic development

A comprehensive analysis of age-related changes in gene expression profiles of mouse oocytes in the germinal vesicle (GV) stage was performed using single-cell RNA sequencing (scRNA-seq) (*99*). A study found that mitochondrial dysfunction, ER stress, and decreased antioxidant capacity may be involved in the process of oocyte senescence (*100*). In particular, downregulation of the mitochondrial coding subunit of the respiratory chain complex may play a key role in the relevant mechanisms. Mitochondria are not only organelles necessary for cell development but also play an important role in cell competition, eliminating unqualified cells during development. One study performed scRNA-seq on eliminated mouse epiblast cells and found that the eliminated cells not only displayed cellular competition characteristics but also impaired mitochondrial function (*101*). This finding suggests that differences in mitochondrial activity are key determinants of cellular competitiveness during early mammalian embryonic development.

Mitochondrial genome sequencing was used to study mtDNA heterogeneity, quantify single nucleotide variants and large structural variants, track heteroplasmy dynamics, and analyze the genetic linkage between variants at the individual mtDNA molecule level in single oocytes and human blastoids (*102*). A study observed the haplotype-resolved mitochondrial genomes from single human oocytes and single blastoids, revealing the linkage of rare heteroplasmic mutations and tracking heteroplasmy dynamics in the blastoid model of human early development (*103*). Several studies have showed that mtDNA content in cumulus cells does not predict development to a blastocyst or implantation (*104,105*). Another study has developed a new method of mtDNA sequencing, a cost-effective mtDNA targeted-sequencing protocol called single-cell sequencing that targets amplification of multiplex probes; this technique could be used to more economically ascertain the functional significance of mtDNA mutations in various stages of embryonic development (*106*). As these new technologies continue to be explored, they have continued to reveal the function of mitochondria and the role of mtDNA.

Mitochondrial replacement therapy (MRT) prevents the transmission of mtDNA-linked diseases by transferring nuclear DNA into enucleated donor oocytes—using pronuclear, spindle, or polar body transfer techniques (*107*). However, there are significant hurdles to its clinical use. Technologically, the carryover of even trace amounts of maternal mutant mtDNA poses a risk of "reversion," where mutant haplotypes proliferate and eventually overtake donor mtDNA, negating the therapy's benefit. Clinical trial data from children born following spindle transfer revealed a carryover of maternal mtDNA of a mere 0.8% in the blastocyst stage in one child; this subsequently increased to 30-60% at birth, demonstrating pronounced mtDNA reversion. Corroborating these findings, studies utilizing non-human primate models have similarly documented that in certain MRT-derived individuals, the proportion of maternal mtDNA in specific tissues increased from initial levels of <3% to levels as high as 17%. These observations indicate that trace quantities of carryover pathogenic mtDNA may confer a replicative advantage during development and undergo re-amplification. Studies indicate that this low-level heteroplasmy can undergo genetic drift or selective amplification during early embryonic development and after birth, potentially leading to the "reversal" of disease-causing mtDNA variants to clinically significant levels in tissues of offspring (*23*). Biological safety is also a major open question, particularly with regard to mito-nuclear compatibility. While recent single-cell data from spindle-transferred embryos have indicated seemingly normal development, these snapshots cannot rule out subtler disruptions arising from the mismatch between evolutionary co-adapted nuclear and mitochondrial genomes. Such mismatches could theoretically compromise metabolic fine-tuning or epigenetic stability in the long run. Beyond these biological risks, MRT sits at the center of heated ethical debates over germline modification and "three-parent" offspring. Therefore, despite its promise, MRT requires strict, long-term follow-up to validate its safety and efficacy before widespread adoption.

Non-invasive metabolic profiling represents another promising technological avenue. The analysis of metabolic fingerprints derived from spent embryo culture media has enabled the assessment of developmental competence and mitochondrial functional status without compromising embryo integrity. Nevertheless, precisely deducing mitochondrial homeostasis from culture medium metabolomics signatures is still technically challenging, owing to constraints in detection sensitivity and the inherent complexity of metabolite provenance. Future endeavors necessitate the integration of microfluidic platforms with high-throughput targeted metabolomics technologies to develop automated, non-invasive systems for the comprehensive evaluation of embryonic mitochondrial function (*108-110*).

3. Implications for embryo quality, developmental competence, and reproductive health

Mitochondria are now recognized as multifunctional organelles that extend far beyond ATP production. They are central to the dynamic regulation of

cellular metabolism, organelle interactions, signal transduction, and quality control systems. The stability of mitochondrial function plays an important role in all aspects of embryonic development.

Embryonic development is a key susceptibility window in the DOHaD framework, with mitochondrial dysfunction increasingly recognized as a link between early environmental stress and adult disease. Environmental toxicants like perfluorooctanoic acid (PFOA), for example, disrupt this bioenergetic balance by inducing oxidative stress and calcium dysregulation, which in turn leads to spindle defects and arrested development (*111*) Genetic factors are equally critical; mutations in maternal complex proteins such as OOEP and NLRP5 have been linked to mitochondrial insufficiency and early embryonic arrest (*112*). Importantly, these early defects may leave a lasting imprint. Studies in human iPSCs have found that mtDNA mutations can permanently shift metabolic profiles and alter differentiation trajectories (*113*). This suggests that early mitochondrial impairment could produce a form of "metabolic memory," potentially priming the individual for metabolic disorders later in life.

Research on mitochondria and embryonic development is expanding and promising. Mitochondria participate in the synthesis of several key metabolites such as amino acids, fatty acids, and nucleotides. These metabolites are necessary for the growth and development of embryos. Moreover, mitochondria are involved in the metabolism of glucose and fatty acids, which are important energy sources during embryogenesis. Dysfunctional mitochondria can lead to an insufficient supply of these metabolites, compromising embryonic development. Mitochondria also involved in calcium signaling, which regulates important cellular processes like cell division, gene expression, and apoptosis. Mitochondria can take up and release calcium ions, thereby influencing the activity of various proteins and enzymes. In addition, disruptions in mitochondrial reactive ROS homeostasis can have detrimental effects on embryonic development. Mitochondria interact with the ER, Golgi apparatus, and peroxisomes, facilitating processes like lipid metabolism, calcium signaling, and autophagy. Dysfunctional mitochondria can disrupt these interactions, leading to impaired embryonic development. The mitochondrial genome, mtDNA, also plays a unique role in embryonic development. Mutations in mtDNA can impair oxidative phosphorylation and ATP production, leading to mitochondrial diseases. These diseases can be transmitted from the mother to the offspring and have a significant impact on embryonic development and offspring health (Figure 4).

Advances in single-cell multi-omics now enable non-invasive assessment of mitochondrial function and mtDNA integrity in preimplantation embryos. Conventional methods of evaluating mitochondrial function in embryos often require invasive sampling, which compromises embryonic integrity and limits clinical applicability. Recent advances in single-cell multiomics technologies have revolutionized mitochondrial screening by enabling accurate, non-destructive assessment of mitochondrial status (*114*).

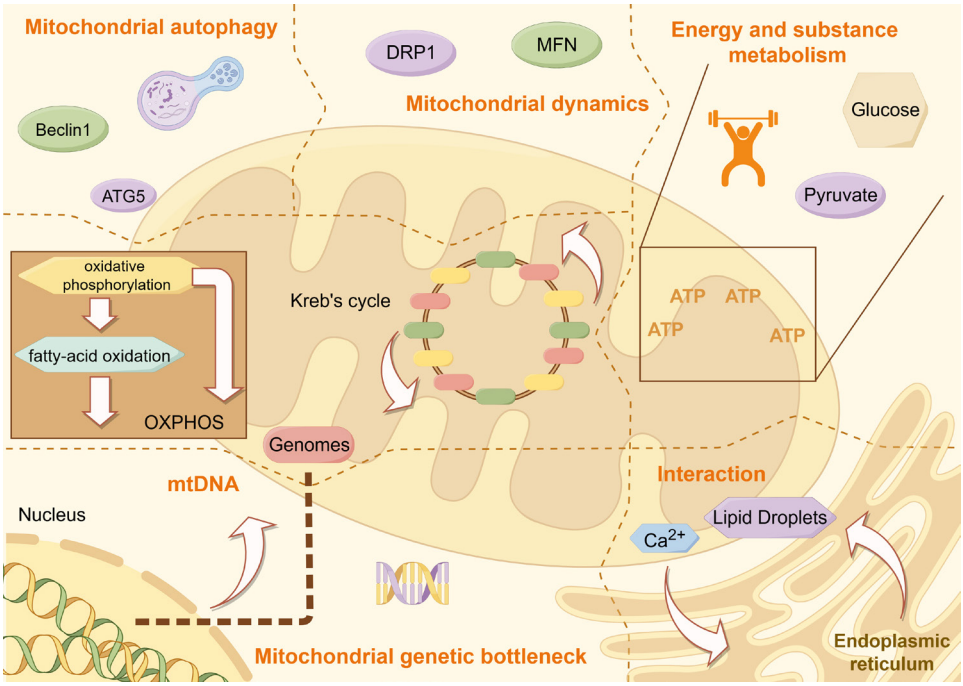

Figure 4. The role of mitochondria in embryonic cells. Mitochondria serve as central bioenergetic hubs, generating ATP *via* oxidative phosphorylation and fatty acid oxidation fueled by glucose and pyruvate metabolism. Organelle plasticity and quality control are governed by DRP1-mediated fission, MFN-dependent fusion, and ATG5/Beclin1-driven mitophagy. Beyond bioenergetics, mitochondria engage in extensive crosstalk with the endoplasmic reticulum and lipid droplets to coordinate Ca^{2+} signaling and lipid homeostasis. Moreover, the regulation of maternally inherited mtDNA involves a strict genetic bottleneck, ensuring the maintenance of mitochondrial genetic fidelity during embryogenesis.

Mounting evidence implicates mitochondrial metabolites as critical modulators of the epigenetic landscape in early embryos. Micro magnetic resonance spectroscopy (micro MRS) represents a breakthrough non-invasive technique for single-cell scale metabolic profiling of oocytes and preimplantation embryos (*109*). This method enables quantitative analysis of mitochondrial metabolites without compromising cellular integrity, generating metabolic fingerprints that correlate with oocyte maturity and embryonic developmental potential (*109*). Mitochondria are multifunctional regulators of embryonic development, integrating energy production, metabolic signaling, and epigenetic remodeling to ensure developmental success. MRT holds great promise for preventing mtDNA disorders and improving assisted reproductive technology (ART) outcomes, with ongoing technical refinements addressing key limitations such as residual mutations and mito-nuclear incompatibility. Future advances will likely focus on personalized MRT approaches, integration of non-invasive mitochondrial screening into routine ART workflows, and verification of long-term safety, ultimately expanding reproductive options for patients with a mitochondrial dysfunction and inherited mitochondrial diseases.

4. Future Perspectives

Despite substantial progress, the field still lacks a rigorous quantitative framework for defining "mitochondrial quality," with current assessments relying heavily on descriptive proxies such as the mtDNA copy number. A key unresolved question is how discrete mitochondrial features combine at the organelle level to influence developmental competence. In this context, recent evidence that oocytes actively suppress mitochondrial Complex I activity to limit ROS production challenges the prevailing assumption that elevated respiratory activity is inherently indicative of higher mitochondrial quality (*79*). These findings suggest that mitochondrial function must be evaluated in a developmental and context-dependent manner rather than through static measures of activity alone.

Current conceptual models also lack sufficient resolution in terms of lineage. The mechanisms governing mitochondrial fission, fusion, and mitophagy — and how these processes are differentially regulated between the inner cell mass and the trophectoderm — have yet to be fully understood. The increasing availability of single-cell multi-omics data has further exposed this limitation, raising the unresolved question of whether mitochondrial heterogeneity reflects stochastic variation or instead represents a regulated form of metabolic plasticity required for lineage commitment (*77,115*).

Finally, these uncertainties carry important implications for clinical translation. MRT shows therapeutic promise, but its broader implementation will require rigorous evaluation of potential mito-nuclear incompatibilities as well as the long-term stability of epigenetic states across generations (*116,117*). Addressing these challenges will require a shift from predominantly correlative studies towards mechanistic interventions that directly probe the functional limits of mitochondrial plasticity during early development.

Funding: This work was supported by the National Natural Science Foundation of China (grant no. 82304906 to LS Li, grant no. 82374243 to L Wang, and grant no. 82505643 to J Wang).

Conflict of Interest: The authors have no conflicts of interest to disclose.

References

1. Schorr S, van der Laan M. Integrative functions of the mitochondrial contact site and cristae organizing system. Semin Cell Dev Biol. 2018; 76:191-200.
2. Gu XW, Yang Y, Li T, Chen ZC, Fu T, Pan JM, Ou JP, Yang ZM. ATP mediates the interaction between human blastocyst and endometrium. Cell Proliferat. 2020; 53.
3. Kang X, Yan L, Wang J. Spatiotemporal distribution and function of mitochondria in oocytes. Reprod Sci. 2024; 31:332-340.
4. Bavister BD, Squirrell JM. Mitochondrial distribution and function in oocytes and early embryos. Hum Reprod. 2000; 15 Suppl 2:189-198.
5. Van Blerkom J, Davis P, Alexander S. Differential mitochondrial distribution in human pronuclear embryos leads to disproportionate inheritance between blastomeres: Relationship to microtubular organization, ATP content and competence. Hum Reprod. 2000; 15:2621-2633.
6. Podolak A, Woclawek-Potocka I, Lukaszuk K. The role of mitochondria in human fertility and early embryo development: What can we learn for clinical application of assessing and improving mitochondrial DNA? Cells-Basel. 2022; 11.
7. Lee IW, Tazehkand AP, Sha ZY, Adhikari D, Carroll J. An aggregated mitochondrial distribution in preimplantation embryos disrupts nuclear morphology, function, and developmental potential. Proc Natl Acad Sci U S A. 2024; 121:e2317316121.
8. Belli M, Palmerini MG, Bianchi S, Bernardi S, Khalili MA, Nottola SA, Macchiarelli G. Ultrastructure of mitochondria of human oocytes in different clinical conditions during assisted reproduction. Arch Biochem Biophys. 2021; 703:108854.
9. Zhang D, Deng W, Jiang T, Zhao Y, Bai D, Tian Y, Kong S, Zhang L, Wang H, Gao S, Lu Z. Maternal Ezh1/2 deficiency impairs the function of mitochondria in mouse oocytes and early embryos. J Cell Physiol. 2024; 239:e31244.
10. Boskovic N, Ivask M, Yazgeldi Gunaydin G, Yasar B, Katayama S, Salumets A, Org T, Kurg A, Lundin K, Tuuri T, Daub CO, Kere J. Oxygen level alters energy metabolism in bovine preimplantation embryos. Sci Rep. 2025; 15:11327.
11. Placidi M, Di Emidio G, Virmani A, D'Alfonso A, Artini PG, D'Alessandro AM, Tatone C. Carnitines

as mitochondrial modulators of oocyte and embryo bioenergetics. Antioxidants-Basel. 2022; 11.
12. Tiwari A, Myeong J, Hashemiaghdam A, Stunault MI, Zhang H, Niu X, Laramie MA, Sponagel J, Shriver LP, Patti GJ, Klyachko VA, Ashrafi G. Mitochondrial pyruvate transport regulates presynaptic metabolism and neurotransmission. Sci Adv. 2024; 10:eadp7423.
13. Wang L, Wang H, Luo J, Xie T, Mor G, Liao A. Decorin promotes decidual M1-like macrophage polarization *via* mitochondrial dysfunction resulting in recurrent pregnancy loss. Theranostics. 2022; 12:7216-7236.
14. Chinopoulos C. From glucose to lactate and transiting intermediates through mitochondria, bypassing pyruvate kinase: Considerations for cells exhibiting dimeric PKM2 or otherwise inhibited kinase activity. Front Physiol. 2020; 11.
15. Zhang H, Yan K, Sui L, Li P, Du Y, Hu J, Li M, Yang X, Liang X. Low-level pyruvate inhibits early embryonic development and maternal mRNA clearance in mice. Theriogenology. 2021; 166:104-111.
16. Chen C, Liu Q, Chen W, Gong Z, Kang B, Sui M, Huang L, Wang YJ. PRODH safeguards human naive pluripotency by limiting mitochondrial oxidative phosphorylation and reactive oxygen species production. EMBO Rep. 2024; 25:2015-2044.
17. Yao Q, Parvez-Khan M, Schipani E. *In vivo* survival strategies for cellular adaptation to hypoxia: HIF1alpha-dependent suppression of mitochondrial oxygen consumption and decrease of intracellular hypoxia are critical for survival of hypoxic chondrocytes. Bone. 2020; 140:115572.
18. Thomas LW, Ashcroft M. Exploring the molecular interface between hypoxia-inducible factor signalling and mitochondria. Cellular and Molecular Life Sciences. 2019; 76:1759-1777.
19. Kim H, Scimia MC, Wilkinson D, Trelles RD, Wood MR, Bowtell D, Dillin A, Mercola M, Ronai ZA. Fine-tuning of Drp1/Fis1 availability by AKAP121/Siah2 regulates mitochondrial adaptation to hypoxia. Mol Cell. 2011; 44:532-544.
20. Chiche J, Rouleau M, Gounon P, Brahimi-Horn MC, Pouyssegur J, Mazure NM. Hypoxic enlarged mitochondria protect cancer cells from apoptotic stimuli. J Cell Physiol. 2010; 222:648-657.
21. Chua YL, Dufour E, Dassa EP, Rustin P, Jacobs HT, Taylor CT, Hagen T. Stabilization of hypoxia-inducible factor-1alpha protein in hypoxia occurs independently of mitochondrial reactive oxygen species production. J Biol Chem. 2010; 285:31277-31284.
22. Boese AC, Kang S. Mitochondrial metabolism-mediated redox regulation in cancer progression. Redox Biol. 2021; 42:101870.
23. Yildirim RM, Seli E. The role of mitochondrial dynamics in oocyte and early embryo development. Semin Cell Dev Biol. 2024; 159-160:52-61.
24. Alevriadou BR, Patel A, Noble M, Ghosh S, Gohil VM, Stathopulos PB, Madesh M. Molecular nature and physiological role of the mitochondrial calcium uniporter channel. Am J Physiol Cell Physiol. 2021; 320:C465-C482.
25. Mao H, Chen W, Chen L, Li L. Potential role of mitochondria-associated endoplasmic reticulum membrane proteins in diseases. Biochem Pharmacol. 2022; 199:115011.
26. Yildirim RM, Seli E. Mitochondria as therapeutic targets in assisted reproduction. Human Reproduction. 2024; 39:2147-2159.
27. Wang N, Wang C, Zhao HY, He YC, Lan BW, Sun LK, Gao YF. The MAMs Structure and Its Role in Cell Death. Cells-Basel. 2021; 10.
28. Zhao WB, Sheng R. The correlation between mitochondria-associated endoplasmic reticulum membranes (MAMs) and Ca transport in the pathogenesis of diseases. Acta Pharmacol Sin. 2025; 46:271-291.
29. Xu Y, Xie W, Zhang J. Metabolic regulation of key developmental events during mammalian embryogenesis. Nat Cell Biol. 2025; 27:1219-1229.
30. Adhikari D, Lee IW, Al-Zubaidi U, Liu J, Zhang QH, Yuen WS, He LK, Winstanley Y, Sesaki H, Mann JR, Robker RL, Carroll J. Depletion of oocyte dynamin-related protein 1 shows maternal-effect abnormalities in embryonic development. Science Advances. 2022; 8.
31. Adhikari D, Lee IW, Yuen WS, Carroll J. Oocyte mitochondria-Key regulators of oocyte function and potential therapeutic targets for improving fertility. Biol Reprod. 2022; 106:366-377.
32. Hu L, Tang D, Qi B, Guo D, Wang Y, Geng J, Zhang X, Song L, Chang P, Chen W, Fu F, Li Y. Mfn2/Hsc70 complex mediates the formation of mitochondria-lipid droplets membrane contact and regulates myocardial lipid metabolism. Adv Sci (Weinh). 2024; 11:e2307749.
33. Arena R, Bisogno S, Gasior L, *et al*. Lipid droplets in mammalian eggs are utilized during embryonic diapause. Proc Natl Acad Sci U S A. 2021; 118.
34. Gao L, Zhang C, Zheng Y, Wu D, Chen X, Lan H, Zheng X, Wu H, Li S. Glycine regulates lipid peroxidation promoting porcine oocyte maturation and early embryonic development. J Anim Sci. 2023; 101.
35. Li T, Jin Y, Wu J, Ren Z. Beyond energy provider: Multifunction of lipid droplets in embryonic development. Biol Res. 2023; 56:38.
36. Shekhawat P, Bennett MJ, Sadovsky Y, Nelson DM, Rakheja D, Strauss AW. Human placenta metabolizes fatty acids: Implications for fetal fatty acid oxidation disorders and maternal liver diseases. Am J Physiol Endocrinol Metab. 2003; 284:E1098-1105.
37. Li J, Zhang J, Hou W, *et al*. Metabolic control of histone acetylation for precise and timely regulation of minor ZGA in early mammalian embryos. Cell Discov. 2022; 8:96.
38. Zhang L, Zhao J, Lam SM, *et al*. Low-input lipidomics reveals lipid metabolism remodelling during early mammalian embryo development. Nat Cell Biol. 2024; 26:278-293.
39. Dunning KR, Russell DL, Robker RL. Lipids and oocyte developmental competence: The role of fatty acids and beta-oxidation. Reproduction. 2014; 148:R15-27.
40. Zheng K, Cui H, Tang Z, Song E, Kong Q, Zhang J, Li H, Zhao Q. Long-chain fatty acid beta-oxidation regulates embryonic development by H3K18 acetylation in mice. Front Cell Dev Biol. 2025; 13:1683028.
41. Yu SY, Luan Y, Xu PC, Zhang Y, Dong R, Abazarikia A, Kim SY. Metabolic characteristics of granulosa cell tumor: Role of PPARgamma signalingdagger. Biol Reprod. 2024; 110:509-520.
42. Meulders B, Marei WFA, Loier L, Leroy J. Lipotoxicity and oocyte quality in mammals: Pathogenesis, consequences, and reversibility. Annu Rev Anim Biosci. 2025; 13:233-254.
43. Wu J, Singh K, Shing V, Gupta A, Arenberg BC,

Huffstutler RD, Lee DY, Sack MN. Mitochondrial fatty acid oxidation regulates monocytic type I interferon signaling *via* histone acetylation. Sci Adv. 2025; 11:eadq9301.
44. Belli M, Zhang L, Liu X, Donjacour A, Ruggeri E, Palmerini MG, Nottola SA, Macchiarelli G, Rinaudo P. Oxygen concentration alters mitochondrial structure and function in *in vitro* fertilized preimplantation mouse embryos. Hum Reprod. 2019; 34:601-611.
45. Sharma M, Punetha M, Saini S, Chaudhary S, Jinagal S, Thakur S, Kumar P, Kumar R, Sharma RK, Yadav PS, Kumar D. Mito-Q supplementation of *in vitro* maturation or *in vitro* culture medium improves maturation of buffalo oocytes and developmental competence of cloned embryos by reducing ROS production. Anim Reprod Sci. 2024; 260:107382.
46. Wang H, Liu C, Zhao YX, Gao G. Mitochondria regulation in ferroptosis. Eur J Cell Biol. 2020; 99.
47. Zhao S, Heng N, Wang H, Wang H, Zhang H, Gong J, Hu Z, Zhu H. Mitofusins: From mitochondria to fertility. Cell Mol Life Sci. 2022; 79:370.
48. Huynh DTN, Heo KS. Role of mitochondrial dynamics and mitophagy of vascular smooth muscle cell proliferation and migration in progression of atherosclerosis. Arch Pharm Res. 2021; 44:1051-1061.
49. Seo BJ, Yoon SH, Do JT. Mitochondrial dynamics in stem cells and differentiation. Int J Mol Sci. 2018; 19.
50. Li S, Zhang Y, Yuan R, Zhu S, Bai J, Miao Y, Ou X, Wang Q, Xiong B. ARHGAP26 deficiency drives the oocyte aneuploidy and early embryonic development failure. Cell Death Differ. 2025; 32:291-305.
51. Prieto J, Leon M, Ponsoda X, Garcia-Garcia F, Bort R, Serna E, Barneo-Munoz M, Palau F, Dopazo J, Lopez-Garcia C, Torres J. Dysfunctional mitochondrial fission impairs cell reprogramming. Cell Cycle. 2016; 15:3240-3250.
52. Shi XY, Tian Y, Wang YF, Zhang YR, Yin Y, Tian Q, Li L, Ma BX, He X, Zhou LQ. Mitofusin 1 drives preimplantation development by enhancing chromatin incorporation of histone H3.3. Adv Sci (Weinh). 2025; 12:e2414985.
53. Otasevic V, Surlan L, Vucetic M, Tulic I, Buzadzic B, Stancic A, Jankovic A, Velickovic K, Golic I, Markelic M, Korac A, Korac B. Expression patterns of mitochondrial OXPHOS components, mitofusin 1 and dynamin-related protein 1 are associated with human embryo fragmentation. Reprod Fertil Dev. 2016; 28:319-327.
54. Park MR, Hwang IS, Kwak TU, Lim JH, Hwang S, Cho SK. Low expression of mitofusin 1 is associated with mitochondrial dysfunction and apoptosis in porcine somatic cell nuclear transfer embryos. Anim Sci J. 2020; 91.
55. Wang L, Xu X, Kang L, Xiang W. Bone marrow mesenchymal stem cells attenuate mitochondria damage induced by hypoxia in mouse trophoblasts. PLoS One. 2016; 11:e0153729.
56. Lima A, Lubatti G, Burgstaller J, *et al*. Cell competition acts as a purifying selection to eliminate cells with mitochondrial defects during early mouse development. Nature Metabolism. 2021; 3:1091-+.
57. Latorre-Pellicer A, Lechuga-Vieco AV, Johnston IG, *et al*. Regulation of mother-to-offspring transmission of mtDNA heteroplasmy. Cell Metab. 2019; 30:1120-1130 e1125.
58. Tabara LC, Segawa M, Prudent J. Molecular mechanisms of mitochondrial dynamics. Nat Rev Mol Cell Biol. 2025; 26:123-146.
59. Yang L, Lin X, Tang H, *et al*. Mitochondrial DNA mutation exacerbates female reproductive aging *via* impairment of the NADH/NAD(+) redox. Aging Cell. 2020; 19:e13206.
60. Durairajanayagam D, Singh D, Agarwal A, Henkel R. Causes and consequences of sperm mitochondrial dysfunction. Andrologia. 2021; 53:e13666.
61. Vahedi Raad M, Firouzabadi AM, Tofighi Niaki M, Henkel R, Fesahat F. The impact of mitochondrial impairments on sperm function and male fertility: A systematic review. Reprod Biol Endocrinol. 2024; 22:83.
62. Sirard MA. Distribution and dynamics of mitochondrial DNA methylation in oocytes, embryos and granulosa cells. Sci Rep. 2019; 9:11937.
63. Gustafsson CM, Falkenberg M, Larsson NG. Maintenance and expression of mammalian mitochondrial DNA. Annu Rev Biochem. 2016; 85:133-160.
64. Long S, Zheng Y, Deng X, Guo J, Xu Z, Scharffetter-Kochanek K, Dou Y, Jiang M. Maintaining mitochondrial DNA copy number mitigates ROS-induced oocyte decline and female reproductive aging. Commun Biol. 2024; 7:1229.
65. Santos TA, El Shourbagy S, St John JC. Mitochondrial content reflects oocyte variability and fertilization outcome. Fertil Steril. 2006; 85:584-591.
66. Cecchino GN, Garcia-Velasco JA. Mitochondrial DNA copy number as a predictor of embryo viability. Fertility and Sterility. 2019; 111:205-211.
67. Lee SH, Rinaudo PF. Metabolic regulation of preimplantation embryo development *in vivo* and *in vitro*: Molecular mechanisms and insights. Biochem Biophys Res Commun. 2024; 726:150256.
68. Neupane J, Lubatti G, Gross-Thebing T, Ruiz Tejada Segura ML, Butler R, Gross-Thebing S, Dietmann S, Scialdone A, Surani MA. The emergence of human primordial germ cell-like cells in stem cell-derived gastruloids. Sci Adv. 2025; 11:eado1350.
69. Liao PC, Bergamini C, Fato R, Pon LA, Pallotti F. Isolation of mitochondria from cells and tissues. Methods Cell Biol. 2020; 155:3-31.
70. Lawless C, Greaves L, Reeve AK, Turnbull DM, Vincent AE. The rise and rise of mitochondrial DNA mutations. Open Biol. 2020; 10:200061.
71. Rai PK, Craven L, Hoogewijs K, Russell OM, Lightowlers RN. Advances in methods for reducing mitochondrial DNA disease by replacing or manipulating the mitochondrial genome. Essays Biochem. 2018; 62:455-465.
72. Zhao J, Yao K, Yu H, *et al*. Metabolic remodelling during early mouse embryo development. Nat Metab. 2021; 3:1372-1384.
73. Ji Y, Hu L. The mitochondrial DNA copy number of cumulus granulosa cells is associated with the symmetry of cleavage embryo but not blastocyst quality. Human Reproduction. 2021; 36:233-234.
74. Yang SC, Yu EJ, Park JK, Kim TH, Eum JH, Paek SK, Hwang JY, Lyu SW, Kim JY, Lee WS, Yoon TK, Song H, Lee HJ. The ratio of mitochondrial DNA to genomic DNA copy number in cumulus cell may serve as a biomarker of embryo quality in IVF cycles (Mar, 10.1007/s43032-021-00532-3, 2021). Reproductive Sciences. 2021; 28:2503-2503.
75. Desquiret-Dumas V, Clément A, Seegers V, Boucret L, Ferré-L'Hotellier V, Bouet PE, Descamps P, Procaccio

V, Reynier P, May-Panloup P. The mitochondrial DNA content of cumulus granulosa cells is linked to embryo quality. Human Reproduction. 2017; 32:607-614.
76. Burr SP, Klimm F, Glynos A, *et al*. Cell lineage-specific mitochondrial resilience during mammalian organogenesis. Cell. 2023; 186:1212-1229 e1221.
77. Nitsch L, Lareau CA, Ludwig LS. Mitochondrial genetics through the lens of single-cell multi-omics. Nature Genetics. 2024; 56:1355-1365.
78. Duranthon V, Watson AJ, Lonergan P. Preimplantation embryo programming: Transcription, epigenetics, and culture environment. Reproduction. 2008; 135:141-150.
79. Bahety D, Boke E, Rodriguez-Nuevo A. Mitochondrial morphology, distribution and activity during oocyte development. Trends Endocrinol Metab. 2024; 35:902-917.
80. Cummins JM. The role of maternal mitochondria during oogenesis, fertilization and embryogenesis. Reprod Biomed Online. 2002; 4:176-182.
81. Moura JP, Oliveira PJ, Urbano AM. Mitochondria: An overview of their origin, genome, architecture, and dynamics. Bba-Mol Basis Dis. 2025; 1871.
82. Alvarez-Dominguez JR, Melton DA. Cell maturation: Hallmarks, triggers, and manipulation. Cell. 2022; 185:235-249.
83. Rossmann MP, Dubois SM, Agarwal S, Zon LI. Mitochondrial function in development and disease. Dis Model Mech. 2021; 14.
84. Picard M. Mitochondrial synapses: Intracellular communication and signal integration. Trends Neurosci. 2015; 38:468-474.
85. Muthukumar G, Weissman JS. Shaping the composition of the mitochondrial outer membrane. Nat Cell Biol. 2025; 27:890-901.
86. Fitz-James MH, Cavalli G. Molecular mechanisms of transgenerational epigenetic inheritance. Nat Rev Genet. 2022; 23:325-341.
87. Lim K. Mitochondrial genome editing: Strategies, challenges, and applications. Bmb Rep. 2024; 57:19-29.
88. Shen QZ, Liu Y, Li HG, Zhang L. Effect of mitophagy in oocytes and granulosa cells on oocyte quality. Biology of Reproduction. 2021; 104:294-304.
89. Li AQ, Gao M, Liu BL, Qin Y, Chen L, Liu HY, Wu HY, Gong GH. Mitochondrial autophagy: Molecular mechanisms and implications for cardiovascular disease. Cell Death & Disease. 2022; 13.
90. Wang R, Wang GH. Autophagy in mitochondrial quality control. Adv Exp Med Biol. 2019; 1206:421-434.
91. Singh A, Perez ML, Kirsanov O, Padilla-Banks E, Guardia CM. Autophagy in reproduction and pregnancy-associated diseases. Iscience. 2024; 27.
92. Levine B, Kroemer G. Biological functions of autophagy genes: A disease perspective. Cell. 2019; 176:11-42.
93. Zhang P, Ni XJ, Guo Y, Guo XJ, Wang YF, Zhou ZM, Huo R, Sha JH. Proteomic-based identification of maternal proteins in mature mouse oocytes. Bmc Genomics. 2009; 10.
94. Tsukamoto S, Kuma A, Mizushima N. The role of autophagy during the oocyte-to-embryo transition. Autophagy. 2008; 4:1076-1078.
95. Ichimiya T, Yamakawa T, Hirano T, Yokoyama Y, Hayashi Y, Hirayama D, Wagatsuma K, Itoi T, Nakase H. Autophagy and autophagy-related diseases: A review. International Journal of Molecular Sciences. 2020; 21.
96. Noguchi S, Honda S, Saitoh T, Matsumura H, Nishimura E, Akira S, Shimizu S. Beclin 1 regulates recycling endosome and is required for skin development in mice. Communications Biology. 2019; 2.
97. D'Arcy MS. Cell death: A review of the major forms of apoptosis, necrosis and autophagy. Cell Biol Int. 2019; 43:582-592.
98. Morishita H, Eguchi S, Kimura H, Sasaki J, Sakamaki Y, Robinson ML, Sasaki T, Mizushima N. Deletion of autophagy-related 5 (Atg5) and Pik3c3 genes in the lens causes cataract independent of programmed organelle degradation. J Biol Chem. 2013; 288:11436-11447.
99. Ding Y, Zuo Y, Zhang B, *et al*. Comprehensive human proteome profiles across a 50-year lifespan reveal aging trajectories and signatures. Cell. 2025; 188:5763-5784 e5726.
100. Wang T, Xu P, Yuan J, Chen H, Guo X, Gao J, Wang Y, Yao D, Li X, Liu B, Liu Y. Mitochondrial dysfunction in oocytes: Implications for fertility and ageing. J Ovarian Res. 2025; 18:186.
101. Videla LA, Mariman A, Ramos B, Jose Silva M, Del Campo A. Standpoints in mitochondrial dysfunction: Underlying mechanisms in search of therapeutic strategies. Mitochondrion. 2022; 63:9-22.
102. Bi C, Wang L, Fan Y, *et al*. Single-cell individual full-length mtDNA sequencing by iMiGseq uncovers unexpected heteroplasmy shifts in mtDNA editing. Nucleic Acids Res. 2023; 51:e48.
103. Russo V, Ancora M, Gatta V, *et al*. Profiling of mitochondrial heteroplasmy in single human oocytes by next-generation sequencing. Mol Reprod Dev. 2022; 89:646-654.
104. Martinez-Moro A, Lamas-Toranzo I, Gonzalez-Brusi L, Perez-Gomez A, Padilla-Ruiz E, Garcia-Blanco J, Bermejo-Alvarez P. mtDNA content in cumulus cells does not predict development to blastocyst or implantation. Hum Reprod Open. 2022; 2022:hoac029.
105. Rahmawati P, Wiweko B, Boediono A. Mitochondrial DNA copy number in cumulus granulosa cells as a predictor for embryo morphokinetics and chromosome status. Syst Biol Reprod Med. 2023; 69:101-111.
106. Yao Y, Nishimura M, Murayama K, *et al*. A simple method for sequencing the whole human mitochondrial genome directly from samples and its application to genetic testing. Sci Rep. 2019; 9:17411.
107. Wolf DP, Mitalipov N, Mitalipov S. Mitochondrial replacement therapy in reproductive medicine. Trends Mol Med. 2015; 21:68-76.
108. Masouleh AAM, Eftekhari-Yazdi P, Sadrabadi AE, Esfehani RJ, Tobler M, Schuchardt S, Gianaroli L, Schmutzler A. Embryo metabolism as a novel non-invasive preimplantation test: Nutrients turn over and metabolomic analysis of human spent embryo culture media (SECM). Human Reproduction Update. 2025; 31:405-444.
109. Sivelli G, Barakat A, Marable KB, Gruet G, Bitetti SL, Behr B, Lodde V, Luciano AM, Herrera C, Blom M, Grisi M. Micro magnetic resonance spectroscopy for noninvasive metabolic screening of mammalian embryos and oocytes. Proc Natl Acad Sci U S A. 2025; 122:e2424459122.
110. Mancini V, McKeegan PJ, Schrimpe-Rutledge AC, Codreanu SG, Sherrod SD, McLean JA, Picton HM, Pensabene V. Probing morphological, genetic and metabolomic changes of *in vitro* embryo development in a microfluidic device. Biotechnol Prog. 2021; 37:e3194.
111. Zhou YT, Li R, Li SH, Ma X, Liu L, Niu D, Duan X.

Perfluorooctanoic acid (PFOA) exposure affects early embryonic development and offspring oocyte quality *via* inducing mitochondrial dysfunction. Environ Int. 2022; 167:107413.
112. Tong X, Jin J, Hu Z, Zhang Y, Fan HY, Zhang YL, Zhang S. Mutations in OOEP and NLRP5 identified in infertile patients with early embryonic arrest. Hum Mutat. 2022; 43:1909-1920.
113. Zhang C, Meng Y, Han J. Emerging roles of mitochondrial functions and epigenetic changes in the modulation of stem cell fate. Cell Mol Life Sci. 2024; 81:26.
114. Lareau CA, Dubois SM, Buquicchio FA, *et al*. Single-cell multi-omics of mitochondrial DNA disorders reveals dynamics of purifying selection across human immune cells. Nature Genetics. 2023; 55:1198-+.
115. Wang XM, Liu YX, Wang JZ, Lu XY, Guo ZP, Lv SM, Sun ZY, Gao T, Gao F, Yuan JX. Mitochondrial quality control in ovarian function: From mechanisms to therapeutic strategies. Reproductive Sciences. 2025; 32:1399-1413.
116. Braun E. Mitochondrial replacement techniques for treating infertility. J Med Ethics. 2024.
117. Noohi F, Ravitsky V, Knoppers BM, Joly Y. Mitochondrial replacement therapy: In whose interests? J Law Med Ethics. 2022; 50:597-602.

Received January 7, 2026; Revised February 3, 2026; Accepted February 6, 2026.

[§]These authors contributed equally to this work.

**Address correspondence to:*
Lisha Li, Laboratory of Reproduction Immunology, Shanghai Key Laboratory of Female Reproductive Endocrine-related Diseases, Obstetrics and Gynecology Hospital, Fudan University Shanghai Medical College, Shanghai, China.
E-mail: lishasmv@163.com

Ling Wang, Department of Obstetrics, The First Affiliated Hospital, Guizhou University of Traditional Chinese Medicine, No. 71 Baoshan North Road, Guiyang, China.
E-mail: dr.wangling@vip.163.com

Released online in J-STAGE as advance publication February 9, 2026.

Review

DOI: 10.5582/bst.2025.01279

The inflammation-aging axis: Shared and distinct mechanisms in physiological gut aging and IBD-associated accelerated gut aging

Lichao Yang[1,2], Zhixian Jiang[1], Qi Sun[1], Kenji Karako[3], Lianwen Yuan[1,*], Peipei Song[2,*]

[1] Department of General Surgery, The Second Xiangya Hospital of Central South University, Changsha, China;
[2] Center for Clinical Sciences, Japan Institute for Health Security, Tokyo, Japan;
[3] Department of Surgery, Graduate School of Medicine, The University of Tokyo, Tokyo, Japan.

SUMMARY: Inflammatory bowel disease (IBD) and physiological gut aging present with overlapping clinical features, including impaired barrier functioning, decreased nutrient absorption, and intestinal frailty. Emerging evidence indicates that even young IBD patients can exhibit gut phenotypes akin to those seen with aging. However, the two processes differ substantially in their underlying mechanisms. Gut aging is characterized by low-grade, chronic inflammation and gradual cellular senescence, whereas IBD involves persistent immune activation, cyclical tissue damage, and accelerated degenerative changes. This review systematically contrasts physiological gut aging and IBD-associated accelerated gut aging across several dimensions: cellular senescence and programmed cell death, immune cell remodeling, alterations in gut microbiota, changes in mesenteric adipose tissue, and the evolving role of the appendix. By integrating current advances in basic and translational research, this article highlights both the shared and distinct pathways driving gut dysfunction in aging and IBD, and underscores the importance of early recognition and targeted intervention for premature gut aging in clinical practice.

Keywords: gut aging, inflammatory bowel disease, cellular senescence, immune dysregulation, intestinal barrier

1. Introduction

As modern medicine has continued to advance, people's life expectancy has been increasing, and the gradual aging of various organs has brought about irreversible physiological changes (*1,2*). When the aging body cannot adapt to environmental changes, the excessive physiological burden may induce the onset and progression of diseases (*3*). Intestinal aging is a fundamental manifestation of organismal senescence. At the cellular and molecular levels, the aged gut epithelium undergoes structural remodeling, characterized by a reduced number of goblet cells, decreased expression of tight junction proteins, increased barrier permeability, and the maintenance of a chronic low-grade inflammatory microenvironment (*4-7*). Clinically, these alterations manifest as impaired nutrient absorption and intestinal dysmotility in the elderly population, highlighting the gut as a critical organ system vulnerable to aging (*8*).

Intriguingly, similar alterations are increasingly recognized in inflammatory bowel disease (IBD). Even in young patients and during clinical remission, impaired epithelial stem cell function, incomplete barrier repair, and sustained immune activation can be observed (*9-11*). Functionally, IBD patients continue to experience malabsorption, nutritional deficiencies, and delayed intestinal transit despite symptomatic remission (*12-14*). These parallels suggest that IBD represents a state of premature gut aging accelerated by chronic inflammation.

Mechanistically, both physiological gut aging and IBD involve epithelial stem cell exhaustion, immune senescence, and microbial dysbiosis. These converging processes support the concept of an "inflamm-aging axis," whereby chronic inflammation accelerates intestinal senescence and contributes to disease progression (*15,16*). Therefore, viewing IBD as "accelerated gut aging" may help emphasize the accelerated degenerative features of its disease course and provide a theoretical basis for introducing anti-aging interventions into treatment strategies (*17,18*).

Despite these similarities, existing reviews mainly emphasize inflammatory mechanisms in IBD and rarely provide a systematic comparison with physiological aging. To fill this gap, the present review offers the first multidimensional comparison of IBD-associated premature gut aging and physiological intestinal aging. By integrating evidence from cellular mechanisms, barrier functioning, immune remodeling, and clinical phenotypes, we aim to introduce the concept of the inflamm-aging axis and highlight its translational

potential in diagnosis and therapy.

2. Definition and basic characteristics of gut aging

Gut aging is an inevitable part of the organismal aging process and is primarily characterized by the gradual deterioration of cellular, tissue, and systemic functions within the intestine (*19*). Cellular senescence is one of the core mechanisms of gut aging, manifesting as the reduced proliferative capacity of epithelial cells, the accumulation of DNA damage, and the release of pro-inflammatory factors known as the senescence-associated secretory phenotype (SASP), all of which further contribute to a localized inflammatory state (*20-22*). In addition, increased oxidative stress and mitochondrial dysfunction lead to a redox imbalance and accelerate the degeneration of intestinal tissues (*23,24*). In addition, gut barrier dysfunction—such as decreased expression of tight junction proteins—renders the intestine more susceptible to invasion by external pathogens, further hastening the aging process (*25,26*). Gut microbiota dysbiosis is another key feature of gut aging, manifested as a reduction in beneficial bacteria, an increase in harmful bacteria, and abnormal levels of microbial metabolites such as short-chain fatty acids (SCFAs) (*27-29*). Finally, the impaired regenerative capacity of crypt stem cells (*30*), the decreased absorptive function of intestinal villi (*31*), progressive degeneration of the enteric nervous system (*6*), and disturbances in glucose and lipid metabolism within the gut and mesenteric fat (*32*) may all contribute, to varying degrees, to the progression of gut aging. These mechanisms do not occur in isolation; rather, their synergistic effects shape the biological changes that occur during gut aging. The multidimensional mechanisms of gut aging—including oxidative stress, chronic low-grade inflammation, stem cell exhaustion, barrier dysfunction, and microbial dysbiosis—are summarized in Figure 1, which provides an integrated overview of how these factors collectively impair intestinal homeostasis.

2.1. Active *vs.* passive patterns of immune responses

The intestinal immune system undergoes significant changes during aging, which are mainly characterized by low-grade chronic inflammation (inflammaging) and progressive immune dysfunction (immunosenescence) (*33*). During human aging, the overall number of various immune cells decreases to varying degrees, but some cell subsets increase with age, such as memory B cells, which become more abundant and exhibit increased production of pro-inflammatory cytokines (such as IL-1, IL-6, and TNF-α) (*34*). The activity of certain immune cells also declines with aging; for example, reduced dendritic cell activity weakens antigen-presenting capacity, resulting in diminished immune surveillance (*6,35*). Sustained aging leads to decreased expression of the transcription factor FoxO3 and drives macrophage polarization from the anti-inflammatory 'M2' phenotype to the pro-inflammatory 'M1' phenotype (*6*), resulting in reduced efficiency of clearing senescent cells (*36*), while phenotypic changes in muscularis macrophages may trigger disturbances in intestinal motility (*37*). In the intestines of aged mice, Dlc1+ Spock1+ intestinal macrophages decrease significantly, while Colq+ macrophages expand (*38*). Aging also reduces the deformability of T cells, leading to diminished migratory capacity (*39*). In addition, the reduction in regulatory T cells (Tregs) and the occurrence of abnormal T cell-driven cytokine and cytotoxic responses progressively impair the inhibition of pro-inflammatory responses, resulting in a mild but persistent inflammatory state in the local intestine (*40,41*).

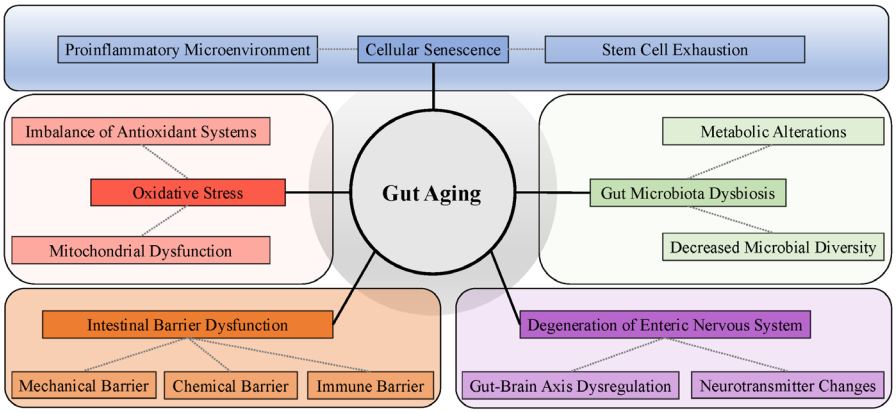

Figure 1. Multidimensional mechanisms underlying gut aging. This diagram summarizes the major pathological processes involved in gut aging, including oxidative stress driven by mitochondrial dysfunction and an antioxidant system imbalance, a chronic proinflammatory microenvironment, stem cell exhaustion, cellular senescence, and gut microbiota dysbiosis with decreased microbial diversity and metabolic alterations. Gut aging is also characterized by progressive intestinal barrier dysfunction affecting mechanical, chemical, and immune barriers and degeneration of the enteric nervous system, leading to gut-brain axis dysregulation and neurotransmitter changes. These interconnected mechanisms collectively contribute to impaired gut homeostasis and age-related vulnerability to gastrointestinal disorders.

This is accompanied by a weakening of the intestinal immune barrier, and such immune dysregulation not only exacerbates microbial imbalance but also facilitates invasion by external pathogens (*42*). Single-cell analyses show that in the intestines of aged mice, CD4+ naïve T cells decrease with age—a trend consistent with other organs—whereas the abundance of CD8+ T cells increases, mainly in the form of the CD8+ Gzmb+ T cell subset, uniquely in the gut, suggesting that the aging intestine possesses a distinct immune environment (*38*). Alongside age-related T cell expansion, various B cell and plasma cell subsets also expand significantly during gut aging. Notably, there is a marked increase in Mki67+ Mybl1+ germinal center B cells in the aging gut. IgA+ plasma cells and memory B cell subsets highly expressing Fcgbp are abundantly clustered in the aged intestinal mucosa, maintaining mucosal immune function (*38*). Although innate lymphoid cells have no significant regulatory effect on the aging process, marked enrichment of ILC3s can still be observed in the aging gut (*38*). Immune disorders linked to aging may also cause the translocation of intestinal bacteria, bacterial metabolites, and inflammatory mediators into mesenteric fat and even to distant organs *via* the systemic circulation (*43*). Due to age-related gut aging, a defective immune system accelerates the accumulation of unresolved inflammation in the intestine; however, this is not entirely irreversible. Time-restricted eating (TRE) can increase the abundance of anti-inflammatory bacteria and probiotics in the gut, elevate the proportion of Treg cells, and upregulate anti-aging serum metabolites, helping to reverse the aging state of the gut (*44*). A reasonable diet and eating habits can improve the inflammaging state associated with gut aging and even further reverse the decline of the immune system (*45,46*).

In contrast, intestinal immune changes in IBD are characterized by intense immune activation alternating with chronic inflammation, and these changes are difficult to reverse (*47*). Compared to gut aging, macrophages in the intestines of IBD patients are excessively activated, with significant increases in both M1 and M2 macrophage subsets, and widely infiltrate the tissue. An elevated M1/M2 macrophage ratio is associated with disease activity (*48,49*). Pro-inflammatory cell populations dominated by Th1 and Th17 cells are abnormally active in IBD patients, accompanied by high levels of pro-inflammatory cytokines such as IL-17 and IFN-γ (*50*). The proportion of Treg cells decreases significantly in IBD, and an increased Th17/Treg ratio predicts more severe colitis (*51,52*). This pathological hyperactivation of the immune system leads to severe damage to the intestinal barrier and massive colonization by pathogenic bacteria, resulting in a vicious cycle of inflammation, tissue destruction, and immune activation. In the early stages of IBD, there is a dysregulation of mucosal ILCs, manifesting as a reduction in ILC3s (*53*) and an increase in ILC2s (*54*). These lymphocyte changes are unable to suppress the chronic intestinal inflammation mediated by IL-23 in IBD (*55*). Activated dendritic cells accelerate antigen presentation, leading to the recruitment of large numbers of neutrophils to sites of intestinal injury (*56*). In the later stages of IBD, immunosenescence-like changes can also occur, with progressive decline in immune cell function and long-term damage caused by immune remodeling (*33*). Unlike the gradual immunosenescence of physiological gut aging, which mainly manifests as impaired absorption, immunosenescence in IBD progresses more rapidly, is accompanied by stronger inflammation and a more complex molecular network, and often leads to a restricted diet and more severe nutritional deficiency than in the elderly. Nutrition is a key determinant of immune function and the gut microbiota; micronutrients such as vitamins C, D, and E, as well as zinc and selenium, play important roles in supporting the function of many types of immune cells (*57*).

Although there are differences in their manifestations, there are still certain similarities in the fundamental features of the immune imbalance between physiological gut aging and IBD-associated accelerated gut aging. Both gut aging and IBD are characterized by disruption of immune homeostasis, such as the reduced function of Tregs, overexpression of pro-inflammatory factors, and weakening of the intestinal immune barrier. However, gut aging is more prone to low-grade chronic inflammation, mainly driven by immune cell exhaustion, stem cell decline, and endogenous metabolic alterations, and can be defined as "passive" immunosenescence. In contrast, IBD predominantly involves abnormally active pro-inflammatory cell populations, an excessively activated immune system, and high-grade inflammation driven by exogenous microbial dysbiosis, which can be regarded as "active" immunosenescence. Table 1 summarizes the phenotypic and functional changes in key intestinal immune cell subsets during physiological gut aging and IBD-associated accelerated gut aging, highlighting their distinct and overlapping roles. The immunological characteristics of both conditions not only provide important contrasts for disease research but also offer new insights for the development of specific therapeutic targets for different pathological states.

2.2. Similarities and differences in cellular mechanisms

2.2.1. Cell death

In both the aging gut and the IBD gut, cellular mechanisms are central drivers of tissue degeneration and disease progression. Telomere shortening and DNA damage serve as initiating factors. Oxidative stress and mitochondrial dysfunction are driving forces. In addition, restricted clearance of senescent cells and persistent SASP act as key maintenance factors. Cellular senescence is regarded as one of the hallmarks of aging and is defined as stable growth arrest mainly mediated by cell cycle

Table 1. Immune cell alterations in physiological gut aging *vs.* IBD-associated accelerated gut aging

Immune Cell	Subtype	Physiological Gut Aging	IBD-associated Accelerated Gut Aging	*Ref.*
T cell	Treg	↑ Quantity ↑ Proportion ↑ Suppression	↓ Stability or dysfunction ↓ Regulatory capacity	(*169,170*)
	CD4+	↓ Slight decrease ↓ Tends to result in functional exhaustion	↑ Th1/Th17 bias ↑ Activation	(*38,171*)
	CD8+	↓ Quantity ↑ Suppressive phenotype e.g., PD-1+	↑ Cytotoxicity ↑ Inflammatory function	(*38,147*)
B cell	-	↓ Antibody production ↓ Repertoire diversity	↑ IgA hypersecretion Altered Breg ratio	(*34,172*)
Macrophage	M1	↑ Mild activation ↑ Inflammatory signals	↑ Strong polarization ↑ Proinflammatory cytokines	(*6,36,38*)
	M2	↑ Reparative function	↓ Imbalance or suppressive dysfunction	(*36,38*)
	LLMs	↑ Number ↑ Anti-inflammatory bias	Unclear function Limited evidence	(*173,174*)
NK cell	-	↓ Total number ↓ Killing capacity	↑ Total number ↑ Pro-inflammatory activity	(*10,147*)
Dendritic cell	-	↓ Antigen presentation ↑ Tolerance induction	↑ CD83/CD86 expression ↑ Activation markers	(*6,35,175*)
Neutrophil	-	↓ Chemotaxis ↓ Inflammatory mediator release	↑ Aggregation ↑ NETs/ROS production	(*88,176*)
Innate Lymphoid Cells	ILC3	↓ Abundance ↓ IL-22 secretion ↓ Barrier support	↓ Number ↑ Aberrant activation ↑ ILC1-like shift	(*69*)

regulators such as p53, p21, and p16 (*58*). Under normal conditions, the clearance of senescent cells is often accompanied by the activation of programmed cell death (PCD) mechanisms, such as apoptosis and autophagy. In gut aging, however, dysregulation of intrinsic PCD can lead to restricted removal of senescent cells, and excessive accumulation of senescent cells further accelerates gut aging (*59*). Under physiological conditions, the shedding and renewal of intestinal epithelial cells (IECs) is closely related to the balance between cellular senescence and apoptosis. In the context of gut aging, genes regulating apoptosis are downregulated, while those regulating senescence are upregulated, indicating that senescent cells may not directly undergo apoptosis, but rather enter a SASP state to maintain chronic intestinal inflammation (*60*). Elevated levels of autophagy can induce cell death, whereas insufficient autophagy may trigger cellular senescence (*61*). The lysosome is the key regulator that maintains the balance between cellular senescence and cell death. Autophagic impairment due to lysosomal dysfunction is an important feature of oxidative stress-induced senescence (*62*). Senescent cells exhibit lysosomal amplification and dysfunction (*63*), and the age-dependent decline of lysosome processing and adaptation systems (LYPAS) may inevitably trigger senescence and/or cell death (*64*). In addition, senescent T cells in the gut of elderly individuals can activate the PAR1 signaling pathway, resulting in increased apoptosis of colonic epithelial cells, and also activate the PAR2 pathway, leading to the release of IL-8 by IECs and maintenance of a chronic inflammatory microenvironment (*65*).

Excessive activation of regulated cell death is a hallmark of IBD (*66*). Figure 2 integrates current evidence, highlighting the involvement of multiple modalities—including apoptosis, necroptosis, pyroptosis, ferroptosis, and autophagy—in IBD-associated intestinal injury. These interconnected pathways exacerbate epithelial barrier disruption, sustain chronic inflammation, and drive mucosal immune dysregulation, thereby linking cellular dysfunction with disease progression. Under normal circumstances, X-linked inhibitor of apoptosis protein (XIAP) suppresses TNF-driven intestinal inflammation and dysbiosis by promoting the innate immune responses of Paneth cells and dendritic cells (*67*). In IBD, an XIAP deficiency leads to increased expression of caspase-8, which not only activates extrinsic apoptosis but also promotes GSDMD processing and NLRP3 activation, thereby inducing pyroptosis (*68*). TNF is a key mediator of intestinal inflammation in IBD, and various TNF inhibitors are mainstream therapies for IBD (*69*). TNF drives cell death in the intestines of IBD patients through tumor necrosis factor receptor 1 (TNFR1)-mediated

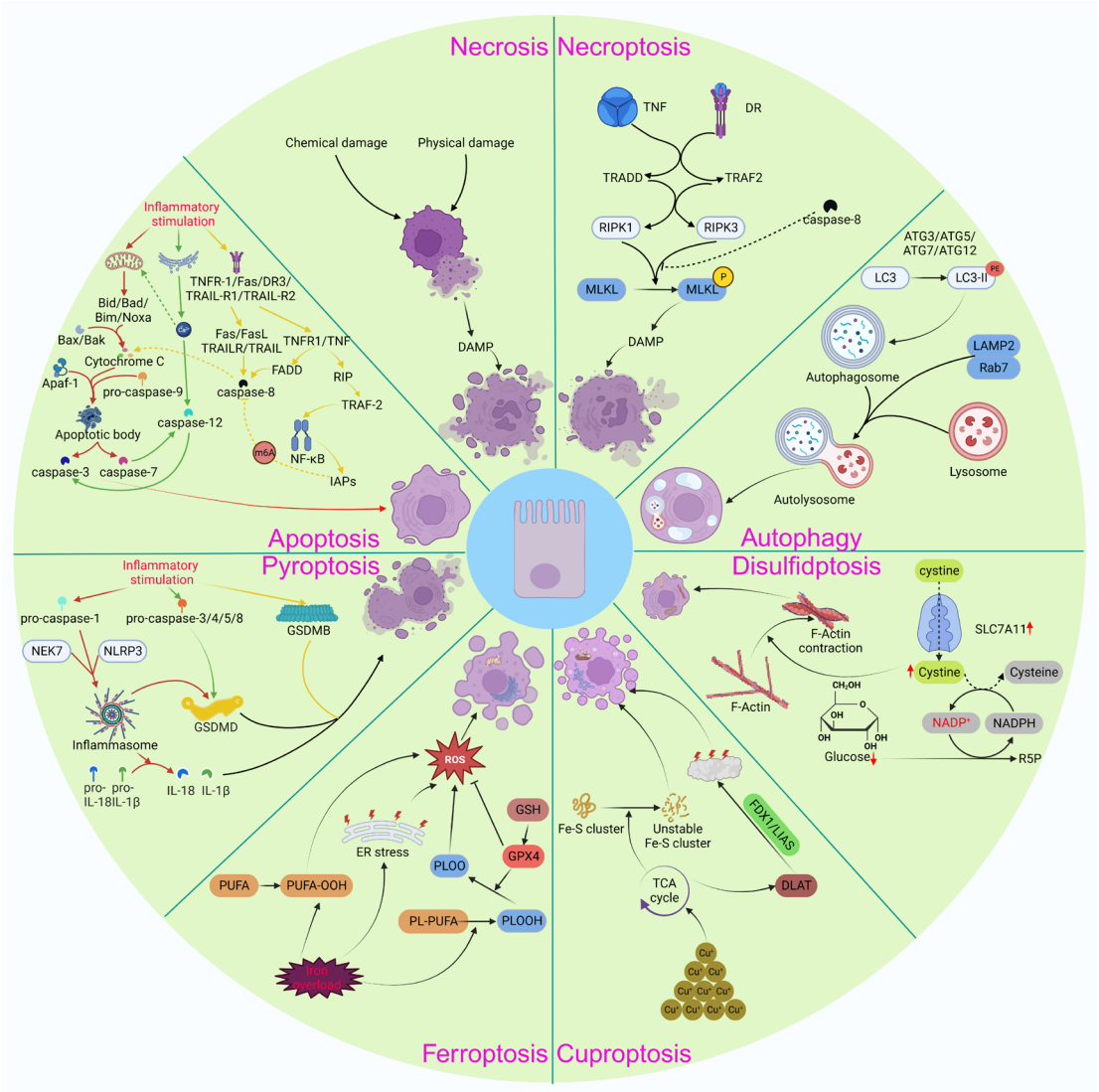

Figure 2. Roles and pathogenic mechanisms of various regulated cell death modalities in inflammatory bowel disease (IBD). This schematic illustrates the involvement and crosstalk of major forms of RCD — including apoptosis, necroptosis, pyroptosis, ferroptosis, and autophagy — in the pathogenesis of IBD. Key molecular pathways, such as caspase-dependent apoptosis, RIPK3/MLKL-mediated necroptosis, inflammasome- and gasdermin D–dependent pyroptosis, ferroptosis characterized by iron-driven lipid peroxidation, and impaired autophagy, contribute to epithelial barrier disruption, chronic inflammation, and mucosal immune dysregulation. Dysregulated cell death pathways may trigger excessive epithelial cell loss, release of damage-associated molecular patterns (DAMPs), and perpetuation of intestinal inflammation, thereby promoting disease progression in both ulcerative colitis and Crohn's disease.

activation of multiple signaling pathways; it can induce caspase-8- and caspase-3-mediated apoptosis as well as RIPK3-dependent necroptosis (*70,71*), and can also activate the NF-κB pathway, which promotes the binding of NEK7 to the NLRP3 inflammasome, leading to pyroptosis (*72*). Moreover, aberrant activation of the TNF/NF-κB signaling pathway in IBD not only regulates lipid peroxidation and GPX4 activity to induce ferroptosis (*73*) but also affects cellular metabolism and copper ion homeostasis to trigger cuproptosis (*74*) and can further enhance oxidative stress and metabolic disorders to promote disulfidptosis (*75*). In summary, unlike cell death in gut aging, cell death mechanisms in IBD patients are not simply single pathological processes but rather display diverse and interacting patterns—such as alternating activation of apoptotic and necrotic pathways or combined activation of autophagy and apoptosis—with distinct differences in the activation strength of common cell death modalities between IBD and gut aging (Figure 3). The diversity and frequent alternation of these mechanisms exacerbate immune system instability and make intestinal cells more susceptible to damage and clearance. Notably, the excessive activation of various forms of regulated cell death in the IBD gut does not appear to be aimed at clearing senescent cells, but rather represents an immune response by the body to cope with recurrent chronic inflammation.

2.2.2. Mitochondria

The SASP is a characteristic feature of cellular senescence, and the release of mitochondrial double-stranded RNA

(mt-dsRNA) into the cytosol is a common phenomenon in senescent cells. The mt-dsRNA/MAVS/MFN1 axis is a key driver of the SASP (*76*). Mitochondrial dysfunction inhibits the production of chylomicrons and the transport of dietary lipids in IECs, thereby impairing the gut's ability to absorb lipids (*77*). The pro-senescent effects of mitochondria are mainly mediated by inflammation and oxidative stress; the reactive oxygen species (ROS) they generate induce DNA damage response (DDR), accelerate telomere shortening, and trigger signaling networks that maintain the senescent phenotype, thus promoting the onset of senescence (*78*). Of course, the human body also has intrinsic anti-aging mechanisms — for example, Prohibitin 1 responds to mitochondrial ROS under oxidative stress by promoting Nix localization to mitochondria, thereby initiating mitophagy (*79*). These mechanisms influence gut health by promoting the decline of cellular function and weakening tissue functionality. Oxidative stress and mitochondrial dysfunction play critical roles in this process, leading to the accumulation of DNA damage, telomere shortening, and instability of cellular signaling pathways, thus exacerbating cellular senescence and the activation of PCD mechanisms.

Unlike the general process of gut aging, the loss of mitophagy in IBD not only disrupts the homeostasis of epithelial cells but can also lead to more severe pathological changes, such as Paneth cell dysfunction and mitochondrial accumulation (*79*). Recurrent chronic inflammation in the intestines of IBD patients can cause mitochondrial DNA damage (with mtDNA released extracellularly), activate the cGAS-STING pathway, and trigger innate immune responses, thereby further aggravating inflammation (*80,81*). Aberrant activation of the STING signaling pathway, by affecting mitochondrial stress and mitophagy, contributes to intestinal barrier disruption (*82*). High levels of ROS resulting from mitochondrial dysfunction exacerbate tissue injury in the IBD gut and lead to cell death, such as ferroptosis and necroptosis (*83,84*). Mitochondrial dysfunction in immune cells is also an important driver of inflammation in IBD. Dysregulated mitophagy in macrophages (such as disruption of the PINK1/Parkin pathway) results in excessive ROS production, drives pro-inflammatory responses of M1 macrophages, promotes the secretion of more TNF-α and IL-6, and worsens intestinal tissue damage (*85*). Mitochondrial metabolic disorders in T cells can disrupt immune homeostasis by causing an imbalance between effector T cells (Teff) and Tregs

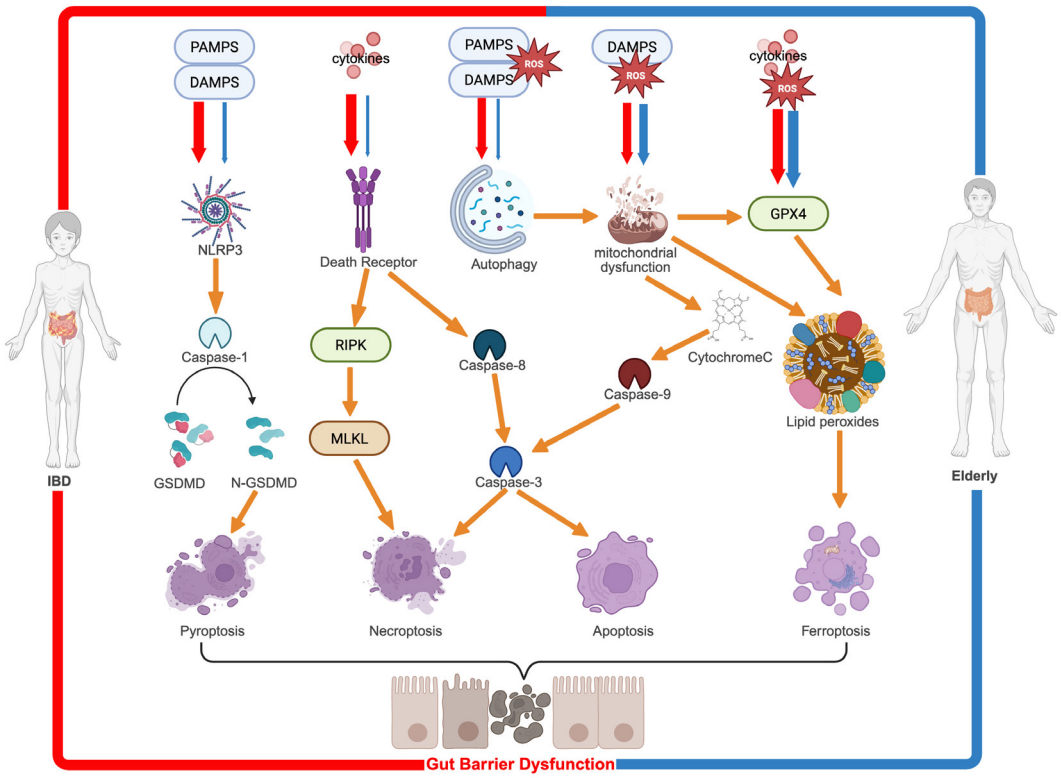

Figure 3. Schematic summary of regulated epithelial cell death pathways in the gut with inflammatory bowel disease (IBD), indicated by red arrows, versus aging, indicated by blue arrows, with arrow thickness indicating relative pathway strength. IBD prominently activates pyroptosis via the inflammasome–caspase-1–gasdermin D axis, promoting inflammation and barrier damage; necroptosis, driven by RIPK and MLKL, contributes to epithelial necrosis and leaky barrier integrity; and ferroptosis, characterized by iron accumulation, ROS-mediated lipid peroxidation, and GPX4 inactivation, plays a pivotal role in chronic IBD progression and mucosal erosion. Aging exacerbates mitochondrial dysfunction and oxidative stress, impairs autophagy/mitophagy, and diminishes GPX4 defense — thus potentiating apoptosis, necroptosis, and especially ferroptosis. The combined result of these distinct and overlapping death processes culminates in epithelial cell loss, tight junction disruption, mucosal thinning, and ultimately gut barrier dysfunction.

(*86,87*). In addition, the large amounts of ROS generated by neutrophils not only directly damage intestinal tissue but also promote cell death (such as ferroptosis and necroptosis) through ROS signaling, further aggravating inflammation (*88*). In addition, mitochondrial dysfunction is also associated with gut microbiota dysbiosis; for example, SCFAs, a class of gut microbial metabolites, can regulate mitochondrial function and thereby modulate cellular metabolism in intestinal epithelial and immune cells (*89*).

2.2.3. Intestinal stem cells (ISCs)

Stem cell exhaustion is a key mechanism in gut aging. As the function of crypt stem cells declines, the regenerative capacity of the tissue is significantly suppressed, impairing the ability of the gut to repair and renew itself; this may be closely related to age-dependent nonlinear DNA methylation (*90*). In the intestines of aged mice, mTORC1 drives ISC senescence through the p38 MAPK-p53 pathway, accelerating villus aging and resulting in defective intestinal nutrient absorption (*31*). The aging state of the intestine alters the structure of the small intestinal crypts and villi as well as crypt cell proliferation. Notum, produced by Paneth cells within the crypts, weakens the regenerative capacity of the aging intestinal epithelium *in vivo* by reducing Wnt activity in stem cells (*91,92*). Single-cell analysis has revealed that marker genes of specific ISC subpopulations in the aged small intestine are associated with negative regulation of the cell cycle and activation of apoptotic signaling pathways, further restricting the gut's repair capacity (*93*).

In IBD, the repeated chronic inflammatory environment has a unique impact on ISC function. Genetic factors, such as polymorphisms in autophagy-related genes (*e.g.*, ATG16L1), together with persistent inflammatory conditions, can lead to mitochondrial autophagy dysfunction in IECs, thereby affecting the homeostasis of ISCs (*79*). Dysregulation of ISC functioning may result in the reduced regenerative capacity of the crypts and trigger severe pathological changes, including Paneth cell dysfunction and cell death. Paneth cell dysfunction further exacerbates ISC depletion, while the interactions between ISCs and immune cells, as well as the pro-inflammatory signals (such as TNF-α and IL-6) they secrete, may further impair the reparative ability of stem cells *via* the inflammatory microenvironment (*94*). In addition, interactions between ISCs and gut microbiota have been found to be critical to ISC functioning. In IBD, the reduction in SCFAs further weakens the metabolic activity of ISCs, limiting their regenerative capacity (*81*).

2.3. Commonalities and divergences in barrier functioning and microbiota

Beyond cellular mechanisms such as cell death and stem cell exhaustion, alterations in the gut barrier and microbiota also represent pivotal points of divergence and convergence between physiological aging and IBD. The intestinal barrier and gut microbiota are the two core factors in maintaining gut health, and both are significantly affected in the pathological states of gut aging and IBD. The aging gut is characterized by a chronic, progressive decline in barrier functioning and dysbiosis, while IBD is marked by recurrent intestinal inflammation, accompanied by barrier damage and microbiota disturbances (*95*). Although the underlying mechanisms in these two conditions differ, there are certain similarities in the interactions between the barrier and the microbiota.

Both gut aging and IBD present with structural and functional damage to the intestinal barrier, resulting in increased intestinal permeability that allows microbes and their metabolic toxins to cross the barrier and trigger systemic inflammatory responses (*96*). In both conditions, there is a reduction in the expression of tight junction proteins (such as decreased levels of claudin and occludin), a decrease in mucus layer thickness, and reduced expression of antimicrobial peptides (such as β-defensins) (*97*). Excessive ROS in both gut aging and IBD directly impair barrier functioning by inducing the apoptosis or necroptosis of epithelial cells (*98,99*). Additionally, dysregulation of autophagy (such as ATG16L1 dysfunction) is also common in both settings, further weakening barrier repair capacity (*79*). Although the phenotypes of barrier dysfunction are similar in both conditions, there are differences in the driving factors of barrier damage and the mechanisms of barrier repair. In gut aging, barrier dysfunction is mainly driven by chronic oxidative stress, telomere shortening, and the decreased regenerative capacity of epithelial cells (*100*). In IBD, chronic inflammation induces the excessive release of pro-inflammatory cytokines, such as IL-17 and TNF-α, which activate the innate immune system of the gut, leading to epithelial injury and a rapid deterioration in barrier functioning (*101*). Dysregulation of intestinal mesenchymal cells further impairs the mechanical barrier by secreting pro-inflammatory cytokines and chemokines (*50*). As oxidative stress persists and the functioning of stem cells declines, this process is further exacerbated—not only affecting the physical and immune functions of the gut barrier but also limiting its self-repair capability. In the aging gut, the slower repair of the barrier is mainly due to the decreased proliferation and differentiation capacity of crypt stem cells (*16*). In IBD, repair may be characterized by immature or abnormal reconstruction due to excessive activation of inflammatory responses and may even lead to fibrosis (*102*).

The bidirectional relationship between barrier dysfunction and a microbiota imbalance forms a "vicious cycle" that jointly drives both gut aging and IBD (*103*). Barrier damage leads to increased translocation of microbes and their metabolic products (such as LPS) into the systemic circulation, triggering immune responses, while dysbiosis further impairs the barrier

by reducing beneficial metabolites (such as SCFAs) and increasing harmful ones (*104*). Both gut aging and IBD are characterized by the reduced diversity of gut microbiota and an increase in pathogenic bacteria (such as Escherichia coli), a dysbiosis that diminishes the protection of barrier functioning by the microbiota while enhancing pro-inflammatory properties (*105*). The patterns of a gut microbiota imbalance differ between the two pathological states: in gut aging, dysbiosis is mainly driven by host factors such as immunosenescence, dietary changes, and reduced gut motility (*106*), whereas in IBD, dysbiosis is usually induced by the inflammatory environment and long-term use of medications such as antibiotics and proton pump inhibitors (*107*). Additionally, in the aging gut, certain commensal bacteria (such as Bacteroides) may increase in abundance but display reduced metabolic capacity (*108*). In contrast, IBD is characterized by the excessive proliferation and colonization of mucosa-associated pathogens, such as adherent-invasive Escherichia coli (*109*). In IBD patients, chronic unhealed mucosal ulceration cannot be effectively repaired, and persistent tissue injury leads to ongoing epithelial damage and a significant reduction in intestinal absorptive function (*110,111*). The decline in absorptive function impairs both nutrient uptake and the elimination of bacterial metabolites, further aggravating the microbial imbalance, increasing the colonization of harmful strains, and reducing beneficial bacteria. In summary, this cycle of barrier weakening and microbiota dysbiosis progresses more slowly and cumulatively in gut aging but is far more intense in the IBD gut. Table 2 presents representative gut microbiota taxa altered in gut aging and IBD, along with their associations with inflammation, cellular senescence, and changes in relative abundance. Beyond cellular pathways, barrier dysfunction, and microbial imbalance, aging and IBD also induce organ-specific changes in the gut. These alterations, exemplified by mesenteric fat and the appendix, highlight how inflamm-aging manifests at the tissue level and extends beyond the mucosal interface.

3. Tissue and organ-specific changes in gut aging and IBD

3.1. Functional differences in mesenteric fat

Mesenteric adipose tissue (MAT) is a unique fat depot surrounding the intestines within the abdominal cavity and can be regarded as a special "organ" that is closely related to gut health, inflammation regulation, and immune responses. As the human body ages, there is an increase in and redistribution of adipose tissue, and NF-κB serves as an important regulatory factor in cellular senescence and the development of SASP within adipose tissue (*112*). Acute and dramatic changes in gene expression in MAT occur only in late life, but certain plasma proteins are highly correlated with gene expression in visceral MAT, including Postn, which is associated with lipid metabolism, and Thrombospondin-4, which promotes synapse formation (*113*). During gut aging, MAT reduces inflammatory responses and protects the intestinal barrier by secreting anti-inflammatory adipokines such as adiponectin (*114*). Decreased insulin sensitivity of adipose tissue may weaken its metabolic regulatory capacity and increase the risk of low-grade chronic inflammation (*115*). In aged MAT, immune cell infiltration increases, with M2 macrophages predominating. As gut aging progresses, however, macrophages gradually shift from the anti-inflammatory M2 phenotype to the pro-inflammatory M1 phenotype, which further exacerbates intestinal barrier dysfunction, manifesting as epithelial barrier impairment (*116*). In addition, fibrosis within adipose tissue and reduced local blood microcirculation further weaken its metabolic support (*117*). The latest UK Biobank study found that visceral adipose tissue progressively increases with age, rising by approximately 8.2% per decade in men and 5.3% in women (*118*). In elderly individuals, excessive accumulation of mesenteric fat may represent a potential driver of accelerated intestinal ageing.

Similarly, in IBD, excessive deposition of visceral fat—and particularly mesenteric fat—is commonly observed. Our study found that a higher ratio of visceral to subcutaneous fat (mesenteric fat index, or MFI) predicts an increased likelihood of requiring surgical intervention (*119*). In the early stages of IBD, MAT primarily plays a protective role (*120*). As intestinal barrier functioning

Table 2. Gut microbiota and associated functions in physiological gut aging and IBD-associated accelerated gut aging

Gut Microbiota	Metabolites	Inflammation	Cell Senescence	Abundance in Aging	Abundance in IBD	*Ref.*
Faecalibacterium prausnitzii	Butyrate	↓	↓	↓	↓	(*157,177,178*)
Akkermansia muciniphila	Mucin enzymes	→	↓	↑	↓	(*157,179*)
Roseburia spp.	Butyrate	↓	↓	↓	↓	(*180,181*)
Bilophila wadsworthia	Secondary bile acids	↑	↑	↑	↑	(*182,183*)
Bacteroides fragilis	Polysaccharides	↑	→	→	↑	(*184,185*)
Lactobacillus spp.	Lactate	↓	↓	↓	↓	(*186,187*)
Escherichia coli	Lipopolysaccharide	↑	↑	→	↑	(*178,188*)
Methanobrevibacter smithii	Methane	→	→	↑	→	(*189,190*)
Parabacteroides spp.	SCFAs	↓	↓	↓	↓	(*178,191*)

Note: The symbols ↑, ↓, and → respectively indicate an increase, a decrease, or no consistent or significant change in functional effects or abundance based on current evidence. Abbreviations: SCFAs, Short-chain fatty acids; ROS, Reactive oxygen species; IEC, Intestinal epithelial cell.

declines, adipocytes in MAT proliferate and secrete anti-inflammatory factors (such as adiponectin) to alleviate inflammation. Adipokines like adiponectin can inhibit the release of pro-inflammatory cytokines (such as TNF-α) and enhance the immune barrier functioning of the gut (*114*). Adipose tissue can also isolate damaged intestinal segments to reduce the spread of bacteria and their toxins, and proliferating adipocytes form "creeping fat" that covers the injured intestinal wall, providing a physical barrier (*121*). As IBD progresses, the role of MAT shifts from protective to pathological. An increasing mesenteric-to-abdominal fat ratio is associated with a worse prognosis in IBD (*122*). Persistent inflammation leads to further increases in intestinal permeability, resulting in the translocation of large numbers of intestinal bacteria into the MAT and excessive activation of the immune system (macrophages and T cells), which in turn promotes adipose tissue hyperplasia (*123*). Creeping fat secretes pro-inflammatory factors (such as IL-6 and CCL2) and fibrotic signaling molecules (such as TGF-β and fibroblast growth factors), thereby aggravating local inflammation, leading to intestinal fibrosis and strictures and ultimately causing intestinal obstruction (*124,125*). Additionally, the MAT exhibits insulin resistance and dysregulated secretion of adipokines (such as leptin and adiponectin) in IBD patients. These metabolic abnormalities may indirectly impair intestinal barrier functioning by enhancing immune cell activity (*126*). In summary, functioning of the MAT differs markedly between the aging gut and IBD: it can serve as a protector of the barrier but may also exacerbate pathological changes through abnormal adipose tissue proliferation.

3.2. Functional differences in the appendix

As a special immune organ within the gut, the appendix plays a potentially important role in both gut aging and IBD. First, the appendix is rich in gut-associated lymphoid tissue, which supports the differentiation and activation of immune cells and regulates the mucosal immune balance in the intestine (*127*). The appendix also provides a stable "refuge" for gut microbes, allowing the restoration of the intestinal ecosystem by releasing healthy microbiota, especially after disruptions such as antibiotic use (*128*). During gut aging, the reduction in lymphoid tissue in the appendix leads to a gradual weakening of its role in immune regulation of the gut (*129*). This immunosenescence-related change may decrease the appendix's support for gut microbiota homeostasis and increase the risk of a microbial imbalance. The levels of anti-inflammatory cytokines (such as IL-10) and Tregs in the appendix may also decrease, leading to the aggravation of chronic low-grade inflammation (*130*). The appendix's role as a sanctuary for commensal bacteria may diminish with aging, particularly as overall microbial diversity in the gut declines, further exacerbating dysbiosis (*131*).

The appendix has a dual role in IBD: in the early stages of IBD, it can assist in restoring gut microbial diversity and alleviate inflammation by secreting anti-inflammatory cytokines such as IL-10 (*132*). However, repeated episodes of IBD may lead to excessive activation of immune responses in the appendix, resulting in inflammatory cascades (*133*). Large numbers of Th17 cells in the appendix can aggravate intestinal inflammation by secreting pro-inflammatory cytokines such as IL-17 (*134,135*). Mendelian randomization studies have shown that simple appendicitis does not increase the risk of IBD, and IBD is associated with a reduced risk of simple appendicitis (*136*). Real-world studies indicate that appendectomy in adulthood may be associated with an increased risk of developing IBD, suggesting that the appendix has a protective role (*133*). Conversely, a nationwide cohort study from Sweden found that appendectomy due to appendicitis during adolescence was associated with a reduced risk of adult IBD, further indicating the dual role of the appendix (*137*). Crohn's disease (CD) patients who had undergone an appendectomy tend to have higher postoperative recurrence rates, which may be related to the higher incidence of penetrating disease (*138*). Unlike with CD, appendectomy has a positive effect on the clinical course of ulcerative colitis (UC), but it may increase the risk of colorectal tumors, suggesting that the appendix may play a greater role in pro-inflammatory responses and cancer linked to chronic inflammation in UC (*139*). The roles of the appendix differ in CD and UC, which can be attributed to the clinical characteristics of these diseases. In CD, intestinal inflammation is characterized by segmental, skip lesions, often involving the terminal ileum and the appendix; appendectomy may disrupt gut immune homeostasis and trigger systemic inflammation (*138*). In UC, inflammation is continuously distributed along the colonic mucosa, and appendectomy may reduce the source of pro-inflammatory factors from distal intestinal sites (such as the ileum and appendix), thereby providing some relief from colonic inflammation (*140*). In individuals with a higher genetic susceptibility, appendectomy may affect immune and microbial stability in the gut, potentially triggering CD (*141*). In UC, genetic background may result in a more pronounced pro-inflammatory role of the appendix, so appendectomy can protect against the risk of UC (*142*). Taken together, organ-specific changes such as those occurring in mesenteric fat and the appendix not only reflect premature aging features in IBD but also create a pro-inflammatory microenvironment. These alterations may ultimately converge on tumorigenic pathways, thereby bridging inflamm-aging and the transition to cancer.

4. Inflammation-to-cancer transition

The ultimate outcome of the inflammatory pathological states of gut aging and IBD is not intestinal fibrosis, but

rather malignant transformation of the inflamed tissue (*60*). In the aging gut, carcinogenesis typically results from the gradual accumulation of chronic low-grade inflammation that promotes tumor formation (*143*). Reduced telomerase activity in the aging gut renders cells more susceptible to DNA double-strand breaks and chromosomal instability (*144*). Telomere dysfunction not only mediates the release of various pro-inflammatory cytokines but also enhances tumorigenesis (*145*). In elderly patients with colorectal cancer, significant telomere shortening and dysfunction can be observed at the tumor sites (*146*). Additionally, as age increases, immunosenescence leads to the decreased cytotoxicity of NK cells and CD8+ T cells to tumor cells (*147*). Mitochondrial dysfunction and metabolic disorders also raise ROS levels, exacerbating DNA damage and abnormal cell proliferation (*148*). In summary, telomere dysfunction, immunosenescence, and mitochondrial impairment act synergistically to drive chronic inflammation, DNA damage, and loss of control over cell proliferation, ultimately promoting carcinogenesis in the aging gut.

Colitis-associated cancer (CAC) and sporadic colorectal cancer (sCRC) exhibit significant differences in epidemiology and molecular mechanisms. Epidemiological data show that the risk of CRC in patients with UC is 2%, 8%, and 18% after 10, 20, and 30 years, respectively, while the risk of CRC in patients with CD is about 4-6% after 20 years (*149*). Mechanistically, CAC is mainly driven by chronic inflammation, with sustained activation of the IL-6/STAT3 and NF-κB pathways in the inflammatory environment leading to COX-2 overexpression, inhibition of epithelial cell apoptosis, and the induction of early p53 mutations by ROS and RNS, thereby promoting carcinogenesis (*150*). In contrast, sCRC is primarily driven by an adenoma-carcinoma sequence mediated by APC mutations and is more likely to exhibit MSI-H-related DNA repair defects (*151*).

In clinical practice, patients with IBD-associated cancer often have a poorer prognosis and earlier distant metastasis, which may be related to the enhanced pro-carcinogenic effects of the gut microbiota and the inflammatory microenvironment. Studies have found that Fusobacterium nucleatum is significantly enriched in CAC tissues, and its FadA adhesin promotes epithelial proliferation by activating β-catenin and enhances the expression of genes driving the epithelial-mesenchymal transition (EMT), thereby increasing cancer cell invasiveness (*152,153*). In addition, certain toxic strains of Escherichia coli (pks^+ E. coli) produce colibactin, which can induce DNA breaks and increase the risk of carcinogenesis in IBD patients (*154*). Compared to sCRC, CAC is characterized by the absence of a typical adenoma stage, a high burden of inflammation-mediated mutations, a worse prognosis, and a higher risk of early metastasis, all of which may influence the screening and treatment strategies for IBD-associated cancer (*155*). As shown in Figure 4, IBD-associated colorectal cancer (shown on the left) arises from persistent NF-κB, STAT3, and COX-2 activation, which leads to DNA damage, early TP53 mutations, and rapid tumor progression. In contrast, aging-associated colorectal cancer (shown on the right) follows a slower trajectory characterized by telomere and mitochondrial dysfunction and the classical APC-KRAS-TP53 mutation sequence. This comparison highlights the mechanistic differences between carcinogenesis promoted by inflammation and that associated with aging. These findings underscore the clinical need to translate mechanistic insights into actionable biomarkers for improved disease management.

5. From biomarkers to clinical use

Given the complex interplay between chronic inflammation, aging-related tissue changes, and carcinogenesis, the identification of robust biomarkers has become essential. Gut aging is a natural process, and its diagnosis is based on the gradual decline in intestinal barrier functioning and alterations in cellular mechanisms. Researchers commonly assess gut aging by measuring biomarkers, including tight junction proteins (such as occludin and zonulin), mucus layer thickness, and the expression of antimicrobial peptides (such as β-defensins). Other indicators, such as telomere length, cell cycle assessment, and mitochondrial function assays, are also used to evaluate age-related decline in cellular functioning. Decreased gut microbiota diversity (such as a lower Shannon index) is closely associated with inflamm-aging, and changes in the abundance of specific bacteria — such as reduced levels of anti-inflammatory species like Faecalibacterium prausnitzii and increased abundance of potential pathogens like Eggerthella lenta — can serve as key biomarkers (*156,157*). In addition, measuring microbial metabolites (such as SCFAs) and using ecological indicators (such as the microbiome aging index) to quantify the aging state can provide precise biological evidence for gut aging (*157,158*). Imaging studies can also be used to detect gut aging; for example, intestinal MRI can be used to identify changes in intestinal wall thickness, decreased blood flow, and early signs of fibrosis (*159*). Functional tests, such as stool transit time and nutrient absorption efficiency, are used to assess intestinal physiological function (*160*).

Unlike gut aging, premature intestinal aging in IBD patients is caused by chronic inflammation and immune dysregulation, making its mechanisms more complex. In addition to the methods of detecting gut aging mentioned previously, significantly increased expression of pro-inflammatory cytokines and fecal calprotectin are also specific diagnostic markers for IBD-associated accelerated gut aging. A marked increase in pro-inflammatory bacteria such as adherent-invasive Escherichia coli (AIEC) and Enterococcus spp. also provides valuable guidance for diagnosing accelerated

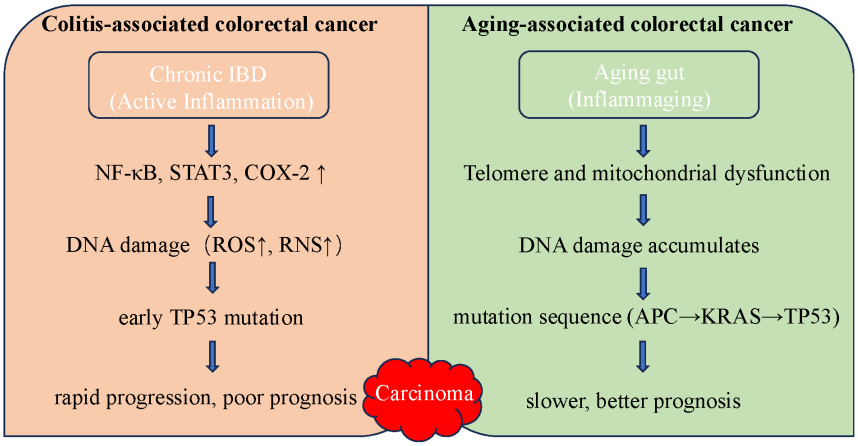

Figure 4. Distinct mechanistic pathways leading to colorectal cancer in IBD-associated and aging-associated contexts. The left side of the diagram shows the development of colitis-associated colorectal cancer, where chronic active inflammation in IBD drives persistent activation of the NF-κB, STAT3, and COX-2 pathways, leading to increased oxidative and nitrosative stress ROS↑, RNS↑, DNA damage, and early TP53 mutations. This results in rapid cancer progression and a poor prognosis. The right side depicts aging-associated colorectal cancer, in which the aging gut microenvironment inflammaging is characterized by telomere and mitochondrial dysfunction, gradual accumulation of DNA damage, and the classical sequence of the mutations APC→KRAS→TP53. This process is generally slower and associated with a better prognosis.

gut aging in IBD (*161*). Therefore, a future direction would be to develop comprehensive scoring tools (such as the Gut Aging Index) that combine biomarkers, functional assessments, and imaging technologies to diagnose accelerated gut aging (*162*). Current IBD assessment indices (such as CRP, fecal calprotectin, and endoscopy) primarily reflect the inflammatory burden and tissue injury but lack evaluation of long-term tissue degeneration, barrier dysfunction, and depletion of ISCs (*18*). When inflammation improves only in the short term, it may mask the progression of premature gut aging and ultimately result in a poor long-term prognosis for patients. Recurrent chronic inflammation leads to accelerated tissue degeneration (such as stem cell dysfunction and dysbiosis), and these "premature aging" features have significant effects on disease chronicity and treatment resistance but have not yet been incorporated into existing evaluation systems. Incorporating gut aging-related indicators into the assessment of IBD disease activity will help provide a more comprehensive understanding of disease biology and offer new directions for optimizing therapy. In addition, therapeutic strategies targeting premature gut aging may complement existing anti-inflammatory treatments, thereby improving long-term outcomes and reducing the risk of disease relapse in IBD patients.

The value of using anti-aging therapies to treat gut aging lies mainly in slowing functional decline and reducing the accumulation of inflammation, while these therapies are more auxiliary in IBD-associated accelerated gut aging, aiming to alleviate chronic damage and improve overall health. mTOR inhibitors (such as sirolimus) promote autophagy, protect ISC functioning, and reduce pro-inflammatory states, thus helping to delay the degeneration of crypt stem cells and barrier dysfunction (*31*). NAD^+ supplements (NMN or NR) restore NAD^+ levels, improve mitochondrial function, enhance cellular antioxidant capacity, and promote metabolic homeostasis (*163*). Spermidine (a natural polyamine) reduces inflammation by modulating autophagy pathways and repairing the intestinal barrier (*164*). Senolytics (senescent cell-clearing drugs) remove accumulated senescent cells, reducing functional decline caused by chronic inflammation (*165*). AMP activators (such as metformin and tedizolid) regulate cellular energy metabolism by activating AMPK signaling, reduce aging-related inflammation, and improve gut barrier functioning (*166*). IL-6/STAT3 inhibitors (such as tocilizumab) suppress pro-inflammatory signaling and reduce the inhibition of cellular regeneration by inflammation (*167*). In addition to these conventional anti-aging strategies, combining biologics with anti-aging therapies in clinical IBD management may help protect and restore prematurely aged intestinal function. Mesenchymal stem cells and fecal microbiota transplantation also have the potential for broad applicability in refractory IBD patients, especially due to their unique advantages in promoting tissue repair, restoring the microbiota balance, and modulating immune responses (*168*).

6. Conclusion

Aging of the intestine and IBD-associated premature gut aging share striking similarities at the cellular, molecular, and functional levels, including intestinal barrier dysfunction, immune dysregulation, and altered microbial homeostasis. These converging features support the concept of an "inflamm-aging axis," in which chronic inflammation accelerates tissue senescence and contributes to disease progression.

As a first step, future studies should determine

whether gut aging biomarkers — such as epithelial senescence signatures, tight junction protein decline, and microbiome aging indices — can be incorporated into IBD assessment systems to improve patient stratification and personalized therapy. Second, the possibility of using anti-aging interventions in IBD, including senolytics, autophagy modulators, and microbiome-targeted therapies, represents a promising adjunctive strategy beyond conventional anti-inflammatory treatments. Moreover, systematic comparisons of immune cell lineage remodeling between physiological aging and IBD are still lacking, and the contribution of organ-specific aging, such as the MAT and the appendix, to chronic inflammation and carcinogenesis needs to be explored further. Longitudinal and multi-omics studies need to be conducted to address these gaps.

In summary, by systematically contrasting IBD-associated premature gut aging with physiological intestinal aging, this review has introduced the concept of the inflamm-aging axis and highlighted its translational potential. Combining mechanistic insights with clinical use will not only deepen our understanding of intestinal pathophysiology but also inspire innovative diagnostic and therapeutic strategies for IBD.

Funding: This work was supported by Grants-in-Aid from the Ministry of Education, Science, Sports, and Culture of Japan (24K14216), the National Natural Science Foundation of China (82270590), the Hunan Provincial Natural Science Foundation (2025JJ50584), the Fundamental Research Funds for the Central Universities of Central South University (2024ZZTS0959 and CX20250428), and the China Scholarship Council program (202506370114).

Conflict of Interest: The authors have no conflicts of interest to disclose.

References

1. Partridge L, Deelen J, Slagboom PE. Facing up to the global challenges of ageing. Nature. 2018; 561:45-56.
2. López-Otín C, Blasco MA, Partridge L, Serrano M, Kroemer G. Hallmarks of aging: An expanding universe. Cell. 2023; 186:243-278.
3. Yousefzadeh MJ, Flores RR, Zhu Y, *et al.* An aged immune system drives senescence and ageing of solid organs. Nature. 2021; 594:100-105.
4. Sang Y, Ning X, Xu Q, Wang L, Yan Y, Zhang L, Bi X. Characterization of transcriptomics during aging and genes required for lifespan in Drosophila intestine. Sci Rep. 2025; 15:14692.
5. Tran L, Greenwood-Van Meerveld B. Age-associated remodeling of the intestinal epithelial barrier. J Gerontol A Biol Sci Med Sci. 2013; 68:1045-1056.
6. Becker L, Nguyen L, Gill J, Kulkarni S, Pasricha PJ, Habtezion A. Age-dependent shift in macrophage polarisation causes inflammation-mediated degeneration of enteric nervous system. Gut. 2018; 67:827-836.
7. Wang X, Luo Y, He S, *et al.* Age-, sex- and proximal-distal-resolved multi-omics identifies regulators of intestinal aging in non-human primates. Nat Aging. 2024; 4:414-433.
8. Salles N. Basic mechanisms of the aging gastrointestinal tract. Dig Dis Basel Switz. 2007; 25:112-117.
9. Guo Z, Wang G, Wu B, Chou WC, Cheng L, Zhou C, Lou J, Wu D, Su L, Zheng J, Ting JP, Wan YY. DCAF1 regulates Treg senescence *via* the ROS axis during immunological aging. J Clin Invest. 2020; 130:5893-5908.
10. Meng G, Monaghan TM, Duggal NA, Tighe P, Peerani F. Microbial-immune crosstalk in elderly-onset inflammatory bowel disease: Unchartered territory. J Crohns Colitis. 2023; 17:1309-1325.
11. Wei S, Wu X, Chen M, Xiang Z, Li X, Zhang J, Dong W. Exosomal-miR-129-2-3p derived from Fusobacterium nucleatum-infected intestinal epithelial cells promotes experimental colitis through regulating TIMELESS-mediated cellular senescence pathway. Gut Microbes. 2023; 15:2240035.
12. Rana SV, Sharma S, Malik A, Kaur J, Prasad KK, Sinha SK, Singh. Small intestinal bacterial overgrowth and orocecal transit time in patients of inflammatory bowel disease. Dig Dis Sci. 2013; 58:2594-2598.
13. Valvano M, Capannolo A, Cesaro N, Stefanelli G, Fabiani S, Frassino S, Monaco S, Magistroni M, Viscido A, Latella G. Nutrition, nutritional status, micronutrients deficiency, and disease course of inflammatory bowel disease. Nutrients. 2023; 15:3824.
14. Rana SV, Sharma S, Kaur J, Prasad KK, Sinha SK, Kochhar R, Malik A, Morya RK. Relationship of cytokines, oxidative stress and GI motility with bacterial overgrowth in ulcerative colitis patients. J Crohns Colitis. 2014; 8:859-865.
15. Funk MC, Zhou J, Boutros M. Ageing, metabolism and the intestine. EMBO Rep. 2020; 21:e50047.
16. Jasper H. Intestinal stem cell aging: Origins and interventions. Annu Rev Physiol. 2020; 82:203-226.
17. Sienkiewicz M, Sroka K, Binienda A, Jurk D, Fichna J. A new face of old cells: An overview about the role of senescence and telomeres in inflammatory bowel diseases. Ageing Res Rev. 2023; 91:102083.
18. Faye AS, Colombel JF. Aging and IBD: A new challenge for clinicians and researchers. Inflamm Bowel Dis. 2022; 28:126-132.
19. Hohman LS, Osborne LC. A gut-centric view of aging: Do intestinal epithelial cells contribute to age-associated microbiota changes, inflammaging, and immunosenescence? Aging Cell. 2022; 21:e13700.
20. Costa CM, Pedrosa SS, Kirkland JL, Reis F, Madureira AR. The senotherapeutic potential of phytochemicals for age-related intestinal disease. Ageing Res Rev. 2024; 104:102619.
21. Ferrucci L, Fabbri E. Inflammageing: chronic inflammation in ageing, cardiovascular disease, and frailty. Nat Rev Cardiol. 2018; 15:505-522.
22. Jang DH, Shin JW, Shim E, Ohtani N, Jeon OH. The connection between aging, cellular senescence and gut microbiome alterations: A comprehensive review. Aging Cell. 2024; 23:e14315.
23. Chen SY, Wang TY, Zhao C, Wang HJ. Oxidative stress bridges the gut microbiota and the occurrence of frailty syndrome. World J Gastroenterol. 2022; 28:5547-5556.
24. Wu M, Luo Q, Nie R, Yang X, Tang Z, Chen H. Potential implications of polyphenols on aging considering oxidative stress, inflammation, autophagy, and gut microbiota. Crit Rev Food Sci Nutr. 2021; 61:2175-2193.

25. Shemtov SJ, Emani R, Bielska O, Covarrubias AJ, Verdin E, Andersen JK, Winer DA. The intestinal immune system and gut barrier function in obesity and ageing. FEBS J. 2023; 290:4163-4186.
26. Shi L, Jin L, Huang W. Bile acids, intestinal barrier dysfunction, and related diseases. Cells. 2023;12:1888.
27. Zou Y, Yan H, Li C, Wen F, Jize X, Zhang C, Liu S, Zhao Y, Fu Y, Li L, Liu F, Chen J, Li R, Chen X, Tian M. A pectic polysaccharide from Codonopsis pilosula alleviates inflammatory response and oxidative stress of aging mice *via* modulating intestinal microbiota-related gut-liver axis. Antioxid Basel Switz. 2023; 12:1781.
28. Gurumayum N, Devi MB, Khound P, Bhattacharya A, Sarma H, Khan MR, Devi. Bioactive fraction of Musa balbisiana seed mitigates D-galactose-induced brain aging *via* SIRT1/PGC-1α/FoxO3a activation and intestinal barrier dysfunction by modulating gut microbiota and core metabolites. Free Radic Biol Med. 2025; 226:43-55.
29. Singh R, Chandrashekharappa S, Bodduluri SR, *et al.* Enhancement of the gut barrier integrity by a microbial metabolite through the Nrf2 pathway. Nat Commun. 2019; 10:89.
30. Abankwah JK, Wang Y, Wang J, Ogbe SE, Pozzo LD, Chu X, Bian Y. Gut aging: A wane from the normal to repercussion and gerotherapeutic strategies. Heliyon. 2024; 10:e37883.
31. He D, Wu H, Xiang J, Ruan X, Peng P, Ruan Y, Chen YG, Wang Y, Yu Q, Zhang H, Habib SL, De Pinho RA, Liu H, Li B. Gut stem cell aging is driven by mTORC1 *via* a p38 MAPK-p53 pathway. Nat Commun. 2020; 11:37.
32. Chen Y, Hao Z, Zhao H, Duan X, Jia D, Li K, Yang Y, Cui H, Gao M, Zhao D. Berberine alleviates intestinal barrier dysfunction in glucolipid metabolism disorder hamsters by modulating gut microbiota and gut-microbiota-related tryptophan metabolites. J Sci Food Agric. 2023; 103:1464-1473.
33. Santoro A, Bientinesi E, Monti D. Immunosenescence and inflammaging in the aging process: Age-related diseases or longevity? Ageing Res Rev. 2021; 71:101422.
34. Agrawal S, Gupta S. TLR1/2, TLR7, and TLR9 signals directly activate human peripheral blood naive and memory B cell subsets to produce cytokines, chemokines, and hematopoietic growth factors. J Clin Immunol. 2011; 31:89-98.
35. Bashir H, Singh S, Singh RP, Agrewala JN, Kumar R. Age-mediated gut microbiota dysbiosis promotes the loss of dendritic cells tolerance. Aging Cell. 2023; 22:e13838.
36. Delfini M, Stakenborg N, Viola MF, Boeckxstaens G. Macrophages in the gut: Masters in multitasking. Immunity. 2022; 55:1530-1548.
37. Becker L, Spear ET, Sinha SR, Haileselassie Y, Habtezion A. Age-related changes in gut microbiota alter phenotype of muscularis macrophages and disrupt gastrointestinal motility. Cell Mol Gastroenterol Hepatol. 2019; 7:243-245. e2.
38. Zhang Z, Schaefer C, Jiang W, Lu Z, Lee J, Sziraki A, Abdulraouf A, Wick B, Haeussler M, Li Z, Molla G, Satija R, Zhou W, Cao J. A panoramic view of cell population dynamics in mammalian aging. Science. 2024; eadn3949.
39. Gao H, Nepovimova E, Adam V, Heger Z, Valko M, Wu Q, Kuca K. Age-associated changes in innate and adaptive immunity: Role of the gut microbiota. Front Immunol. 2024; 15:1421062.
40. Møller SH, Hsueh PC, Yu YR, Zhang L, Ho PC. Metabolic programs tailor T cell immunity in viral infection, cancer, and aging. Cell Metab. 2022; 34:378-395.
41. Carrasco E, Gómez de Las Heras MM, Gabandé-Rodríguez E, Desdín-Micó G, Aranda JF, Mittelbrunn M. The role of T cells in age-related diseases. Nat Rev Immunol. 2022; 22:97-111.
42. Branca JJV, Gulisano M, Nicoletti C. Intestinal epithelial barrier functions in ageing. Ageing Res Rev. 2019; 54:100938.
43. Kociszewska D, Vlajkovic S. Age-related hearing loss: The link between inflammaging, immunosenescence, and gut dysbiosis. Int J Mol Sci. 2022; 23:7348.
44. Chen Y, Li X, Yang M, *et al.* Time-restricted eating reveals a 'younger' immune system and reshapes the intestinal microbiome in human. Redox Biol. 2024; 78:103422.
45. Ghosh TS, Rampelli S, Jeffery IB, *et al.* Mediterranean diet intervention alters the gut microbiome in older people reducing frailty and improving health status: The NU-AGE 1-year dietary intervention across five European countries. Gut. 2020; 69:1218-1228.
46. Di Giosia P, Stamerra CA, Giorgini P, Jamialahamdi T, Butler AE, Sahebkar A. The role of nutrition in inflammaging. Ageing Res Rev. 2022; 77:101596.
47. Geremia A, Biancheri P, Allan P, Corazza GR, Di Sabatino A. Innate and adaptive immunity in inflammatory bowel disease. Autoimmun Rev. 2014; 13:3-10.
48. Zhang K, Guo J, Yan W, Xu L. Macrophage polarization in inflammatory bowel disease. Cell Commun Signal CCS. 2023; 21:367.
49. Zhuang H, Lv Q, Zhong C, Cui Y, He L, Zhang C, Yu J. Tiliroside ameliorates ulcerative colitis by restoring the M1/M2 macrophage balance *via* the HIF-1α/glycolysis pathway. Front Immunol. 2021; 12:649463.
50. Liu L, Davidorf B, Dong P, Peng A, Song Q, He Z. Decoding the mosaic of inflammatory bowel disease: Illuminating insights with single-cell RNA technology. Comput Struct Biotechnol J. 2024; 23:2911-23.
51. Zhang Y, Chen J, Fu H, Kuang S, He F, Zhang M, Shen Z, Qin W, Lin Z, Huang S. Exosomes derived from 3D-cultured MSCs improve therapeutic effects in periodontitis and experimental colitis and restore the Th17 cell/Treg balance in inflamed periodontium. Int J Oral Sci. 2021; 13:43.
52. Jia L, Jiang Y, Wu L, Fu J, Du J, Luo Z, Guo L, Xu J, Liu Y. Porphyromonas gingivalis aggravates colitis *via* a gut microbiota-linoleic acid metabolism-Th17/Treg cell balance axis. Nat Commun. 2024; 15:1617.
53. Joseph AM, Ahmed A, Goc J, Horn V, Fiedler B, Garone D, Grigg JB, Uddin J, Teng F, Fritsch M, Vivier E, Sonnenberg GF. RIPK3 and caspase-8 interpret cytokine signals to regulate ILC3 survival in the gut. Mucosal Immunol. 2024; 17:1212-1221.
54. Kokkinou E, Soini T, Pandey RV, *et al.* The single-cell transcriptional landscape of innate and adaptive lymphocytes in pediatric-onset colitis. Cell Rep Med. 2023; 4:101038.
55. Ahmed A, Joseph AM, Zhou J, Horn V, Uddin J, Lyu M, Goc J; JRI Live Cell Bank; Sockolow RE, Wing JB, Vivier E, Sakaguchi S, Sonnenberg GF. CTLA-4-expressing ILC3s restrain interleukin-23-mediated inflammation. Nature. 2024; 630:976-983.
56. Saez A, Herrero-Fernandez B, Gomez-Bris R, Sánchez-Martinez H, Gonzalez-Granado JM. Pathophysiology of inflammatory bowel disease: Innate immune system. Int J Mol Sci. 2023; 24:1526.
57. Calder PC, Ortega EF, Meydani SN, Adkins Y,

Stephensen CB, Thompson B, Zwickey H. Nutrition, immunosenescence, and infectious disease: An overview of the scientific evidence on micronutrients and on modulation of the gut microbiota. Adv Nutr Bethesda Md. 2022; 13:S1-S26.
58. Guan L, Crasta KC, Maier AB. Assessment of cell cycle regulators in human peripheral blood cells as markers of cellular senescence. Ageing Res Rev. 2022; 78:101634.
59. Sender R, Milo R. The distribution of cellular turnover in the human body. Nat Med. 2021; 27:45-48.
60. in P, Duan X, Li L, Zhou P, Zou CG, Xie K. Cellular senescence in cancer: Molecular mechanisms and therapeutic targets. MedComm. 2024; 5:e542.
61. Rajendran P, Alzahrani AM, Hanieh HN, Kumar SA, Ben Ammar R, Rengarajan T, Alhoot MA. Autophagy and senescence: A new insight in selected human diseases. J Cell Physiol. 2019; 234:21485-21492.
62. Tai H, Wang Z, Gong H, *et al.* Autophagy impairment with lysosomal and mitochondrial dysfunction is an important characteristic of oxidative stress-induced senescence. Autophagy. 2017; 13:99-113.
63. Moreno-Blas D, Gorostieta-Salas E, Castro-Obregón S. Connecting chaperone-mediated autophagy dysfunction to cellular senescence. Ageing Res Rev. 2018; 41:34-41.
64. Tan JX, Finkel T. Lysosomes in senescence and aging. EMBO Rep. 2023; 24:e57265.
65. Park SS, Lee YK, Kim YH, Park SH, Kang HY, Kim JC, Kim DJ, Lim SB, Yoon G, Kim JH, Choi YW, Park TJ. Distribution and impact of p16INK4A+ senescent cells in elderly tissues: A focus on senescent immune cell and epithelial dysfunction. Exp Mol Med. 2024; 56:2631-41.
66. Blander JM. On cell death in the intestinal epithelium and its impact on gut homeostasis. Curr Opin Gastroenterol. 2018; 34:413-419.
67. Wahida A, Müller M, Hiergeist A, *et al.* XIAP restrains TNF-driven intestinal inflammation and dysbiosis by promoting innate immune responses of Paneth and dendritic cells. Sci Immunol. 2021; 6:eabf7235.
68. Hughes SA, Lin M, Weir A, *et al.* Caspase-8-driven apoptotic and pyroptotic crosstalk causes cell death and IL-1β release in X-linked inhibitor of apoptosis (XIAP) deficiency. EMBO J. 2023; 42:e110468.
69. Zhou L, Zhou W, Joseph AM, Chu C, Putzel GG, Fang B, Teng F, Lyu M, Yano H, Andreasson KI, Mekada E, Eberl G, Sonnenberg G. Group 3 innate lymphoid cells produce the growth factor HB-EGF to protect the intestine from TNF-mediated inflammation. Nat Immunol. 2022; 23:251-261.
70. Kuo WT, Shen L, Zuo L, Shashikanth N, Ong MLDM, Wu L, Zha J, Edelblum KL, Wang Y, Wang Y, Nilsen SP, Turner JR. Inflammation-induced occludin downregulation limits epithelial apoptosis by suppressing caspase-3 expression. Gastroenterology. 2019; 157:1323-1337.
71. Blander JM. Death in the intestinal epithelium-basic biology and implications for inflammatory bowel disease. FEBS J. 2016; 283:2720-2730.
72. Chen X, Liu G, Yuan Y, Wu G, Wang S, Yuan L. NEK7 interacts with NLRP3 to modulate the pyroptosis in inflammatory bowel disease *via* NF-κB signaling. Cell Death Dis. 2019; 10:906.
73. Fontes A, Jauch AT, Sailer J, Engler J, Azul AM, Zischka H. Metabolic derangement of essential transition metals and potential antioxidant therapies. Int J Mol Sci. 2024; 25:7880.
74. Li H, Chan L, Bartuzi P, *et al.* Copper metabolism domain-containing 1 represses genes that promote inflammation and protects mice from colitis and colitis-associated cancer. Gastroenterology. 2014; 147:184-195.e3.
75. Liu X, Nie L, Zhang Y, *et al.* Actin cytoskeleton vulnerability to disulfide stress mediates disulfidptosis. Nat Cell Biol. 2023; 25:404-414.
76. López-Polo V, Maus M, Zacharioudakis E, Lafarga M, Attolini CS, Marques FDM, Kovatcheva M, Gavathiotis E, Serrano M. Release of mitochondrial dsRNA into the cytosol is a key driver of the inflammatory phenotype of senescent cells. Nat Commun. 2024; 15:7378.
77. Moschandrea C, Kondylis V, Evangelakos I, *et al.* Mitochondrial dysfunction abrogates dietary lipid processing in enterocytes. Nature. 2024; 625:385-392.
78. Correia-Melo C, Marques FD, Anderson R, *et al.* Mitochondria are required for pro-ageing features of the senescent phenotype. EMBO J. 2016; 35:724-742.
79. Alula KM, Delgado-Deida Y, Callahan R, Till A, Underwood L, Thompson WE, Souza RF, Dassopoulos T, Onyiah J, Venuprasad K, Theiss AL. Inner mitochondrial membrane protein Prohibitin 1 mediates Nix-induced, Parkin-independent mitophagy. Sci Rep. 2023; 13:18.
80. Wands D, Lau SY, Chuah CS, *et al.* P0065 Circulating cell-free DNA and mitochondrial DNA differentiate disease activity in paediatric-onset inflammatory bowel disease: Interim analysis from Scotland-wide Mini-MUSIC study (2020-26). J Crohns Colitis. 2025; 19(Supp 1):i427.
81. Dimitrov G, Ryffel B, Togbe D, Quesniaux V. cGAS-STING DNA-sensing in inflammatory bowel diseases. Trends Mol Med. 2025; 31:165-180.
82. Springer E, Bornhäuser J, Bakr M, *et al.* P0078 The role of epithelial STING in a genetic IBD Model of autophagy deficiency and its interplay with the Integrated stress response. J Crohns Colitis. 2025; 19(Supp 1):i443-444.
83. Ho GT, Theiss AL. Mitochondria and inflammatory bowel diseases: Toward a stratified therapeutic intervention. Annu Rev Physiol. 2022; 84:435-459.
84. Liu J. Aged garlic therapeutic intervention targeting inflammatory pathways in pathogenesis of bowel disorders. Heliyon. 2024; 10:e33986.
85. Wen X, Tang L, Zhong R, Liu L, Chen L, Zhang H. Role of mitophagy in regulating intestinal oxidative damage. Antioxid Basel Switz. 2023; 12:480.
86. Zhang J, Jiang Y, Fan D, Qiu Z, He X, Liu S, Li L, Dai Z, Zhang L, Shu Z, Li L, Zhang H, Yang T, Luo Y. Chemical activation of mitochondrial ClpP to modulate energy metabolism of CD4+ T cell for inflammatory bowel diseases treatment. Cell Rep Med. 2024; 5:101840.
87. Lin L, Ren R, Xiong Q, Zheng C, Yang B, Wang H. Remodeling of T-cell mitochondrial metabolism to treat autoimmune diseases. Autoimmun Rev. 2024;23:103583.
88. Danne C, Michaudel C, Skerniskyte J, *et al.* CARD9 in neutrophils protects from colitis and controls mitochondrial metabolism and cell survival. Gut. 2023; 72:1081-1092.
89. Hirose M, Sekar P, Eladham MWA, Albataineh MT, Rahmani M, Ibrahim SM. Interaction between mitochondria and microbiota modulating cellular metabolism in inflammatory bowel disease. J Mol Med Berl Ger. 2023; 101:1513-1526.
90. Olecka M, van Bömmel A, Best L, Haase M, Foerste S, Riege K, Dost T, Flor S, Witte OW, Franzenburg S, Groth M, von Eyss B, Kaleta C, Frahm C, Hoffmann S. Nonlinear DNA methylation trajectories in aging male mice. Nat Commun. 2024; 15:3074.
91. Pentinmikko N, Iqbal S, Mana M, *et al.* Paneth cell produced Notum attenuates regeneration of aged intestinal

epithelium. Nature. 2019; 571:398-402.
92. Nalapareddy K, Nattamai KJ, Kumar RS, Karns R, Wikenheiser-Brokamp KA, Sampson LL, Mahe MM, Sundaram N, Yacyshyn MB, Yacyshyn B, Helmrath MA, Zheng Y, Geiger H. Canonical Wnt signaling ameliorates aging of intestinal stem cells. Cell Rep. 2017; 18:2608-2621.
93. Cai Y, Xiong M, Xin Z, *et al.* Decoding aging-dependent regenerative decline across tissues at single-cell resolution. Cell Stem Cell. 2023; 30:1674-1691.e8.
94. Chopra Y, Acevedo K, Muise A, Frost K, Schechter T, Krueger J, Ali M, Chiang KY, Kim VH, Grunebaum E, Wall D. Gut immunomodulation with vedolizumab prior to allogeneic hematopoietic stem cell transplantation in pediatric patients with inflammatory bowel disease. Transplant Cell Ther. 2024; 30:546.e1-546.e7.
95. Liu A, Lv H, Wang H, Yang H, Li Y, Qian J. Aging increases the severity of colitis and the related changes to the gut barrier and gut microbiota in humans and mice. J Gerontol A Biol Sci Med Sci. 2020; 75:1284-1292.
96. Liu X, Ma Y, Guan K, Liu R, Mao K, Xu X, Li Q, Wang R. Intestinal barrier, immunity and gut microbiota-based protective effects of Lactococcus lactis HF08 and its postbiotic derivative on aging and aging colitis mice. Food Res Int Ott Ont. 2024; 197:115164.
97. Dambroise E, Monnier L, Ruisheng L, Aguilaniu H, Joly JS, Tricoire H, Rera M. Two phases of aging separated by the Smurf transition as a public path to death. Sci Rep. 2016; 6:23523.
98. Xu T, Ning X, Wu J, Wang Q, Wang Z, Chen Z, Tang X, Bai P, Pu K, Li L, Zhang R. Metabolic nanoregulator remodels gut microenvironment for treatment of inflammatory bowel disease. ACS Nano. 2024; 18:7123-7135.
99. Duan C, Kuang L, Xiang X, Zhang J, Zhu Y, Wu Y, Yan Q, Liu L, Li T. Activated Drp1-mediated mitochondrial ROS influence the gut microbiome and intestinal barrier after hemorrhagic shock. Aging. 2020; 12:1397-1416.
100. Homolak J. Gastrointestinal redox homeostasis in ageing. Biogerontology. 2023; 24:741-752.
101. Chen Y, Cui W, Li X, Yang H. Interaction between commensal bacteria, immune response and the intestinal barrier in inflammatory bowel disease. Front Immunol. 2021; 12:761981.
102. Macias-Ceja DC, Mendoza-Ballesteros MT, Ortega-Albiach M, *et al.* Role of the epithelial barrier in intestinal fibrosis associated with inflammatory bowel disease: Relevance of the epithelial-to mesenchymal transition. Front Cell Dev Biol. 2023; 11:1258843.
103. Parikh K, Antanaviciute A, Fawkner-Corbett D, *et al.* Colonic epithelial cell diversity in health and inflammatory bowel disease. Nature. 2019; 567:49-55.
104. Loh JS, Mak WQ, Tan LKS, Ng CX, Chan HH, Yeow SH, Foo JB, Ong YS, How CW, Khaw KY. Microbiota-gut-brain axis and its therapeutic applications in neurodegenerative diseases. Signal Transduct Target Ther. 2024; 9:37.
105. Arnauts K, Sudhakar P, Verstockt S, Lapierre C, Potche S, Caenepeel C, Verstockt B, Raes J, Vermeire S, Sabino J, Verfaillie C, Ferrante M. Microbiota, not host origin drives ex vivo intestinal epithelial responses. Gut Microbes. 2022; 14:2089003.
106. Zheng H, Zhang C, Wang Q, Feng S, Fang Y, Zhang S. The impact of aging on intestinal mucosal immune function and clinical applications. Front Immunol. 2022; 13:1029948.
107. Mehandru S, Colombel JF. The intestinal barrier, an arbitrator turned provocateur in IBD. Nat Rev Gastroenterol Hepatol. 2021; 18:83-4.
108. Arnold JW, Roach J, Fabela S, Moorfield E, Ding S, Blue E, Dagher S, Magness S, Tamayo R, Bruno-Barcena JM, Azcarate-Peril MA. The pleiotropic effects of prebiotic galacto-oligosaccharides on the aging gut. Microbiome. 2021; 9:31.
109. Gong H, Gan X, Qin B, Chen J, Zhao Y, Qiu B, Chen W, Yu Y, Shi S, Li T, Liu D, Li B, Wang S, Wang H. Structural characteristics of steamed Polygonatum cyrtonema polysaccharide and its bioactivity on colitis *via* improving the intestinal barrier and modifying the gut microbiota. Carbohydr Polym. 2024; 327:121669.
110. Rath T, Atreya R, Neurath MF. A spotlight on intestinal permeability and inflammatory bowel diseases. Expert Rev Gastroenterol Hepatol. 2023; 17:893-902.
111. Vancamelbeke M, Vanuytsel T, Farré R, Verstockt S, Ferrante M, Van Assche G, Rutgeerts P, Schuit F, Vermeire S, Arijs I, Cleynen I. Genetic and transcriptomic bases of intestinal epithelial barrier dysfunction in inflammatory bowel disease. Inflamm Bowel Dis. 2017; 23:1718-29.
112. Santos TWD, Pereira QC, Fortunato IM, Oliveira FS, Alvarez MC, Ribeiro ML. Body composition and senescence: Impact of polyphenols on aging-associated events. Nutrients. 2024; 16:3621.
113. Schaum N, Lehallier B, Hahn O, *et al.* Aging hallmarks exhibit organ-specific temporal signatures. Nature. 2020; 583:596-602.
114. Sideri A, Stavrakis D, Bowe C, Shih DQ, Fleshner P, Arsenescu V, Arsenescu R, Turner JR, Pothoulakis C, Karagiannides I. Effects of obesity on severity of colitis and cytokine expression in mouse mesenteric fat. Potential role of adiponectin receptor 1. Am J Physiol Gastrointest Liver Physiol. 2015; 308:G591-G604.
115. Kredel LI, Siegmund B. Adipose-tissue and intestinal inflammation - Visceral obesity and creeping fat. Front Immunol. 2014; 5:462.
116. Ruggiero AD, Key CCC, Kavanagh K. Adipose tissue macrophage polarization in healthy and unhealthy obesity. Front Nutr. 2021; 8:625331.
117. Khan S, Chan YT, Revelo XS, Winer DA. The immune landscape of visceral adipose tissue during obesity and aging. Front Endocrinol. 2020; 11:267.
118. Losev V, Lu C, Tahasildar S, Senevirathne DS, Inglese P, Bai W, King AP, Shah M, de Marvao A, O'Regan DP. Sex-specific body fat distribution predicts cardiovascular ageing. Eur Heart J. 2025; ehaf553.
119. Yang L, Liu G, Zhang Y, Yao B, Wu Q, Peng L, Wang X, Yuan L. Quantitative analysis of adipose tissue for predicting Crohn's disease postoperative endoscopic recurrence and anastomotic ulcer. Int J Colorectal Dis. 2023; 38:170.
120. Hwang N, Kang D, Shin SJ, Yoon BK, Chun J, Kim JW, Fang S. Creeping fat exhibits distinct Inflammation-specific adipogenic preadipocytes in Crohn's disease. Front Immunol. 2023; 14:1198905.
121. Ha CWY, Martin A, Sepich-Poore GD, *et al.* Translocation of viable gut microbiota to mesenteric adipose drives formation of creeping fat in humans. Cell. 2020; 183:666-683.e17.
122. Dowling L, Jakeman P, Norton C, Skelly MM, Yousuf H, Kiernan MG, Toomey M, Bowers S, Dunne SS, Coffey JC, Dunne CP. Adults with Crohn's disease exhibit elevated gynoid fat and reduced android fat irrespective of disease relapse or remission. Sci Rep. 2021; 11:19258.

123. Caprara G, Allavena P, Erreni M. Intestinal macrophages at the crossroad between diet, inflammation, and cancer. Int J Mol Sci. 2020; 21:4825.
124. Xiong Z, Wu P, Zhang Y, Chen J, Shen Y, Kamel I, Wu B, Zheng X, Li Z. Radiological biomarkers reflecting visceral fat distribution help distinguish inflammatory bowel disease subtypes: A multicenter cross-sectional study. Insights Imaging. 2024; 15:70.
125. Wu F, Wu F, Zhou Q, Liu X, Fei J, Zhang D, Wang W, Tao Y, Lin Y, Lin Q, Pan X, Sun K, Xie F, Bai L. A CCL2+DPP4+ subset of mesenchymal stem cells expedites aberrant formation of creeping fat in humans. Nat Commun. 2023; 14:5830.
126. Valentini L, Wirth EK, Schweizer U, Hengstermann S, Schaper L, Koernicke T, Dietz E, Norman K, Buning C, Winklhofer-Roob BM, Lochs H, Ockenga J. Circulating adipokines and the protective effects of hyperinsulinemia in inflammatory bowel disease. Nutr Burbank Los Angel Cty Calif. 2009; 25:172-181.
127. Niu C, Xu W, Xiong S. Appendectomy mitigates Coxsackievirus B3-induced viral myocarditis. Viruses. 2023; 15:1974.
128. Mahmud MR, Akter S, Tamanna SK, Mazumder L, Esti IZ, Banerjee S, Akter S, Hasan MR, Acharjee M, Hossain MS, Pirttilä AM. Impact of gut microbiome on skin health: Gut-skin axis observed through the lenses of therapeutics and skin diseases. Gut Microbes. 2022; 14:2096995.
129. Collard MK, Bardin J, Laurin M, Ogier-Denis E. The cecal appendix is correlated with greater maximal longevity in mammals. J Anat. 2021; 239:1157-69.
130. Girard-Madoux MJH, Gomez de Agüero M, Ganal-Vonarburg SC, Mooser C, Belz GT, Macpherson AJ, Vivier E. The immunological functions of the appendix: An example of redundancy? Semin Immunol. 2018; 36:31-44.
131. Senda T, Dogra P, Granot T, Furuhashi K, Snyder ME, Carpenter DJ, Szabo PA, Thapa P, Miron M, Farber DL. Microanatomical dissection of human intestinal T-cell immunity reveals site-specific changes in gut-associated lymphoid tissues over life. Mucosal Immunol. 2019; 12:378-389.
132. Demyashkin G, Gorokhov K, Shchekin V, Vadyukhin M, Matevosyan A, Rudavina A, Pilipchuk A, Pilipchuk A, Kochetkova S, Atiakshin D, Shegay P, Kaprin A. Features of appendix and the characteristics of appendicitis development in children with COVID-19. Biomedicines. 2024; 12:312.
133. Chung WS, Chung S, Hsu CY, Lin CL. Risk of inflammatory bowel disease following appendectomy in adulthood. Front Med. 2021; 8:661752.
134. Cheluvappa R, Luo AS, Grimm MC. T helper type 17 pathway suppression by appendicitis and appendectomy protects against colitis. Clin Exp Immunol. 2014; 175:316-322.
135. Cheluvappa R. Identification of new potential therapies for colitis amelioration using an appendicitis-appendectomy model. Inflamm Bowel Dis. 2019; 25:436-444.
136. Zhang Y, Yang L, Yuan L. Investigating the causal relationship between inflammatory bowel disease and simple appendicitis using Mendelian randomization. Sci Rep. 2024; 14:23617.
137. Kiasat A, Ekström LD, Marsk R, Löf-Granström A, Gustafsson UO. Childhood appendicitis and future risk of inflammatory bowel disease - A nationwide cohort study in Sweden 1973-2017. Colorectal Dis Off J Assoc Coloproctology G B Irel. 2022; 24:975-983.
138. van der Does de Willebois EML, Sari C, Mookhoek A, Joustra V, van Dieren S, D'Haens GR, Bemelman WA, Buskens CJ. The clinical relevance of an inflamed appendix in Crohn's disease. J Crohns Colitis. 2024; 18:812-817.
139. Mark-Christensen A, Kristiansen EB, Myrelid P, Laurberg S, Erichsen R. Appendectomy and Risk of advanced colorectal neoplasia in inflammatory bowel disease: A nationwide population-based cohort study. Inflamm Bowel Dis. 2024; 30:877-883.
140. Nyboe Andersen N, Gørtz S, Frisch M, Jess T. Reduced risk of UC in families affected by appendicitis: A Danish national cohort study. Gut. 2017; 66:1398-402.
141. Roderburg C, Loosen SH, May P, Yaqubi K, Luedde T, Kostev K. The nexus between appendicitis and chronic inflammatory bowel diseases: Unraveling an intriguing association. Medicine (Baltimore). 2024; 103:e38859.
142. Deng P, Wu J. Meta-analysis of the association between appendiceal orifice inflammation and appendectomy and ulcerative colitis. Rev Esp Enferm Dig. 2016; 108:401-10.
143. Calcinotto A, Kohli J, Zagato E, Pellegrini L, Demaria M, Alimonti A. Cellular senescence: Aging, cancer, and injury. Physiol Rev. 2019; 99:1047-1078.
144. Shay JW. Role of telomeres and telomerase in aging and cancer. Cancer Discov. 2016; 6:584-593.
145. Chakravarti D, LaBella KA, DePinho RA. Telomeres: History, health, and hallmarks of aging. Cell. 2021; 184:306-322.
146. Hastie ND, Dempster M, Dunlop MG, Thompson AM, Green DK, Allshire RC. Telomere reduction in human colorectal carcinoma and with ageing. Nature. 1990; 346:866-868.
147. Lian J, Yue Y, Yu W, Zhang Y. Immunosenescence: A key player in cancer development. J Hematol OncolJ Hematol Oncol. 2020; 13:151.
148. Ziegler DV, Vindrieux D, Goehrig D, *et al.* Calcium channel ITPR2 and mitochondria-ER contacts promote cellular senescence and aging. Nat Commun. 2021; 12:720.
149. Shah SC, Itzkowitz SH. Colorectal cancer in inflammatory bowel disease: mechanisms and management. Gastroenterology. 2022; 162:715-730.e3.
150. Lasry A, Zinger A, Ben-Neriah Y. Inflammatory networks underlying colorectal cancer. Nat Immunol. 2016; 17:230-240.
151. Becker WR, Nevins SA, Chen DC, *et al.* Single-cell analyses define a continuum of cell state and composition changes in the malignant transformation of polyps to colorectal cancer. Nat Genet. 2022; 54:985-995.
152. Wu M, Li J, An Y, Li P, Xiong W, Li J, Yan D, Wang M, Zhong G. Chitooligosaccharides prevents the development of colitis-associated colorectal cancer by modulating the intestinal microbiota and mycobiota. Front Microbiol. 2019; 10:2101.
153. Wieczorska K, Stolarek M, Stec R. The role of the gut microbiome in colorectal cancer: Where are we? Where are we going? Clin Colorectal Cancer. 2020; 19:5-12.
154. Arthur JC, Perez-Chanona E, Mühlbauer M, *et al.* Intestinal inflammation targets cancer-inducing activity of the microbiota. Science. 2012; 338:120-123.
155. Rajamäki K, Taira A, Katainen R, *et al.* Genetic and epigenetic characteristics of inflammatory bowel disease-associated colorectal cancer. Gastroenterology. 2021; 161:592-607.
156. Jackson MA, Jeffery IB, Beaumont M, Bell JT, Clark AG, Ley RE, O'Toole PW, Spector TD, Steves CJ. Signatures of early frailty in the gut microbiota. Genome Med. 2016; 8:8.

157. O'Toole PW, Jeffery IB. Gut microbiota and aging. Science. 2015; 350:1214-1215.
158. Zhang L, Liao J, Chen Q, Chen M, Kuang Y, Chen L, He W. Characterization of the gut microbiota in frail elderly patients. Aging Clin Exp Res. 2020; 32:2001-2011.
159. Hinssen F, Mensink M, Huppertz T, van der Wielen N. Impact of aging on the digestive system related to protein digestion in vivo. Crit Rev Food Sci Nutr. 2025; 65:5871-5887
160. McKay LF, Smith RG, Eastwood MA, Walsh SD, Cruikshank JG. An investigation of colonic function in the elderly. Age Ageing. 1983; 12:105-110.
161. Palmela C, Chevarin C, Xu Z, Torres J, Sevrin G, Hirten R, Barnich N, Ng SC, Colombel JF. Adherent-invasive Escherichia coli in inflammatory bowel disease. Gut. 2018; 67:574-587.
162. Vieujean S, Gillard R, Delanaye P, Seidel L, Bequet E, Salée C, Meuwis MA, Massot C, Pierre N, Meunier P, Cavalier E, Louis E. Matrix gla protein, a potential marker of tissue remodelling and physiological ageing of the gut in Crohn's disease. Scand J Gastroenterol. 2024; 59:296-303.
163. Zhang H, Ryu D, Wu Y, Gariani K, Wang X, Luan P, D'Amico D, Ropelle ER, Lutolf MP, Aebersold R, Schoonjans K, Menzies KJ, Auwerx J. NAD^+ repletion improves mitochondrial and stem cell function and enhances life span in mice. Science. 2016; 352:1436-1443.
164. Ma L, Ni Y, Wang Z, Tu W, Ni L, Zhuge F, Zheng A, Hu L, Zhao Y, Zheng L, Fu Z. Spermidine improves gut barrier integrity and gut microbiota function in diet-induced obese mice. Gut Microbes. 2020; 12:1-19.
165. Zhang L, Pitcher LE, Prahalad V, Niedernhofer LJ, Robbins PD. Targeting cellular senescence with senotherapeutics: Senolytics and senomorphics. FEBS J. 2023; 290:1362-1383.
166. Sun Q, Bravo Iniguez A, Tian Q, Du M, Zhu MJ. Dietary cannabidiol activates PKA/AMPK signaling and attenuates chronic inflammation and leaky gut in DSS-induced colitis mice. Mol Nutr Food Res. 2024; 68:e2300446.
167. Serrano C, Galán S, Rubio JF, Candelario-Martínez A, Montes-Gómez AE, Chánez-Paredes S, Cedillo-Barrón L, Schnoor M, Meraz-Ríos MA, Villegas-Sepúlveda N, Ortiz-Navarrete V, Nava P. Compartmentalized Response of IL-6/STAT3 Signaling in the Colonic Mucosa Mediates Colitis Development. J Immunol. 2019; 202:1239-1249
168. Ocansey DKW, Wang L, Wang J, *et al.* Mesenchymal stem cell-gut microbiota interaction in the repair of inflammatory bowel disease: An enhanced therapeutic effect. Clin Transl Med. 2019; 8:31.
169. Kim ME, Lee JS. Immune diseases associated with aging: Molecular mechanisms and treatment strategies. Int J Mol Sci. 2023; 24:15584.
170. Ou Q, Power R, Griffin MD. Revisiting regulatory T cells as modulators of innate immune response and inflammatory diseases. Front Immunol. 2023;14:1287465.
171. Salminen A. Activation of immunosuppressive network in the aging process. Ageing Res Rev. 2020; 57:100998.
172. Rybtsova N, Berezina TN, Rybtsov S. Molecular markers of blood cell populations can help estimate aging of the immune system. Int J Mol Sci. 2023; 24:5708.
173. Angelovich TA, Shi MD, Zhou J, Maisa A, Hearps AC, Jaworowski A. *Ex vivo* foam cell formation is enhanced in monocytes from older individuals by both extrinsic and intrinsic mechanisms. Exp Gerontol. 2016; 80:17-26.
174. Liu B, Zhu L, Lei L, Li H, Cong R, Hou J, Zhao J, Li P, Tang Y, Su Z, Tu J, Jiang L. Lesional Macrophage-Targeted Nanomedicine Regulating Cholesterol Homeostasis for the Treatment of Atherosclerosis. Adv Mater. 2025; 37:e2502581.
175. Islam SMS, Ryu HM, Sohn S. Tetragenococcus halophilus alleviates intestinal inflammation in mice by altering gut microbiota and regulating dendritic cell activation *via* CD83. Cells. 2022; 11:1903.
176. Kiilerich KF, Andresen T, Darbani B, Gregersen LHK, Liljensøe A, Bennike TB, Holm R, Moeller JB, Andersen V. Advancing inflammatory bowel disease treatment by targeting the innate immune system and precision drug delivery. Int J Mol Sci. 2025; 26:575.
177. Krueger ME, Boles JS, Simon ZD, Alvarez SD, McFarland NR, Okun MS, Zimmermann EM, Forsmark CE, Tansey MG. Comparative analysis of Parkinson's and inflammatory bowel disease gut microbiomes reveals shared butyrate-producing bacteria depletion. NPJ Park Dis. 2025; 11:50.
178. Yan H, Qin Q, Yan S, Chen J, Yang Y, Li T, Gao X, Ding S. Comparison of the gut microbiota in different age groups in China. Front Cell Infect Microbiol. 2022; 12:877914.
179. Zhang K, Dong Y, Ding Y, Wang X, Liu T, Zhong W, Cao H. Illuminating prospects of probiotic Akkermansia muciniphila in intestinal inflammation and carcinogenesis. Microbiol Res. 2025; 299:128240.
180. Zhu L, Xu LZ, Zhao S, Shen ZF, Shen H, Zhan LB. Protective effect of baicalin on the regulation of Treg/Th17 balance, gut microbiota and short-chain fatty acids in rats with ulcerative colitis. Appl Microbiol Biotechnol. 2020; 104:5449-5460.
181. Konstanti P, Gómez-Martínez C, Muralidharan J, *et al.* Faecal microbiota composition and impulsivity in a cohort of older adults with metabolic syndrome. Sci Rep. 2024; 14:28075.
182. Lázár B, László SB, Hutka B, *et al.* A comprehensive time course and correlation analysis of indomethacin-induced inflammation, bile acid alterations and dysbiosis in the rat small intestine. Biochem Pharmacol. 2021; 190:114590.
183. Chen W, Wei Y, Xiong A, *et al.* Comprehensive analysis of serum and fecal bile acid profiles and interaction with gut microbiota in primary biliary cholangitis. Clin Rev Allergy Immunol. 2020; 58:25-38.
184. Zhong Y, Chang X, Zhao Z, Zheng L, Kuang G, Li P, Liu C, Fan Y, Liang Z, Zhuang K, Xie Q, Liu Y. *Bacteroides fragilis* capsular polysaccharide A ameliorates ulcerative colitis in rat by recovering intestinal barrier integrity and restoring gut microbiota. Front Pharmacol. 2024; 15:1402465.
185. Yan Y, Tian L, Zhao Y, *et al.* Bacteroides fragilis toxin suppresses METTL3-mediated m6A modification in macrophage to promote inflammatory bowel disease. J Crohns Colitis. 2025; 19:jjae179.
186. Abdi M, Lohrasbi V, Asadi A, Esghaei M, Jazi FM, Rohani M, Talebi M. Interesting probiotic traits of mother's milk Lactobacillus isolates; From bacteriocin to inflammatory bowel disease improvement. Microb Pathog. 2021; 158:104998.
187. Lakshminarayanan B, Guinane CM, O'Connor PM, Coakley M, Hill C, Stanton C, O'Toole PW, Ross RP. Isolation and characterization of bacteriocin-producing bacteria from the intestinal microbiota of elderly Irish subjects. J Appl Microbiol. 2013; 114:886-898.
188. Jacobsen GE, Gonzalez EE, Mendygral P, *et al.* Deep sequencing of Crohn's disease lamina propria phagocytes identifies pathobionts and correlates with pro-inflammatory gene expression. Inflamm Bowel Dis. 2025;

31:1203-1219.
189. Kumpitsch C, Fischmeister FPS, Mahnert A, Lackner S, Wilding M, Sturm C, Springer A, Madl T, Holasek S, Högenauer C, Berg IA, Schoepf V, Moissl-Eichinger C. Reduced B12 uptake and increased gastrointestinal formate are associated with archaeome-mediated breath methane emission in humans. Microbiome. 2021; 9:193.
190. Mohammadzadeh R, Mahnert A, Shinde T, Kumpitsch C, Weinberger V, Schmidt H, Moissl-Eichinger C. Age-related dynamics of predominant methanogenic archaea in the human gut microbiome. BMC Microbiol. 2025; 25:193.
191. Deleu S, Machiels K, Raes J, Verbeke K, Vermeire S. Short chain fatty acids and its producing organisms: An overlooked therapy for IBD? EBioMedicine. 2021; 66:103293.

Received September 12, 2025; Revised November 6, 2025; Accepted November 16, 2025.

Address correspondence to:
Lianwen Yuan, Department of General Surgery, The Second Xiangya Hospital of Central South University. 139 Renmin Middle Road, Changsha, Hunan, China.
E-mail: yuanlianwen@csu.edu.cn

Peipei Song, Center for Clinical Sciences, Japan Institute for Health Security, Tokyo, 1-21-1 Toyama Shinjuku-ku, Tokyo 162-8655, Japan.
E-mail: psong@jihs.go.jp

Released online in J-STAGE as advance publication November 20, 2025.

Review

DOI: 10.5582/bst.2025.01271

Research on precision treatment of pancreatic cancer targeted by antibody-drug conjugates

Xinyue Liu[1,§], Weishuai Liu[2,§,*], Chao Wu[3], Yudong Yuan[3], Antao Chang[1,*], Jihui Hao[1,*]

[1] Department of Pancreatic Cancer, Tianjin Medical University Cancer Institute and Hospital, National Clinical Research Center for Cancer, State Key Laboratory of Draggability Evaluation and Systematic Translational Medicine, Tianjin Key Laboratory of Digestive Cancer, Tianjin's Clinical Research Center for Cancer, Tianjin, China;
[2] Department of Pain Management, Tianjin Medical University Cancer Institute and Hospital, National Clinical Research Center for Cancer, Tianjin Key Laboratory of Digestive Cancer, Tianjin's Clinical Research Center for Cancer, Tianjin, China;
[3] Department of Lung Cancer, Tianjin Medical University Cancer Institute and Hospital, National Clinical Research Center for Cancer, Tianjin Key Laboratory of Digestive Cancer, Tianjin's Clinical Research Center for Cancer, Tianjin, China.

SUMMARY: Pancreatic cancer, and especially pancreatic ductal adenocarcinoma (PDAC), is extremely difficult to treat due to early asymptomatic stage, molecular heterogeneity, and resistance to conventional treatments, with a 5-year survival rate of less than 10%. Antibody-drug conjugates (ADCs), as an emerging precision therapy, show the potential to treat PDAC through the synergy of antibody targeting and cytotoxic drugs. Multiple targets (such as uPAR, Mesothelin, CLDN18.2, and TROP2) are highly expressed in PDAC, which has become the key direction of ADC development. However, the matrix barrier restricts drug delivery, heterogeneous expression leads to efficacy differentiation, and drug resistance mechanisms further limit the role of ADCs. To overcome these challenges, researchers are exploring high-stability single domain antibodies, more potent payloads and linkers, bystander effect mechanisms, and combined treatment strategies with immune, autophagy, DNA damage repair, and other pathways. Bispecific ADC, conditionally activated ADC, and penetration enhancement design have also been used to improve efficacy. On the whole, ADCs offer hope for the treatment of PDAC. Future research and development should focus on improving delivery efficiency, alleviating drug resistance, and individualized design.

Keywords: antibody-drug conjugates, pancreatic cancer, precision treatment

1. Introduction

1.1. Current status of and challenges in the treatment of pancreatic cancer

Pancreatic cancer is one of the most lethal malignancies worldwide. It is a heterogeneous disease consisting of multiple subtypes, the most common of which is pancreatic ductal adenocarcinoma (PDAC), which accounts for nearly 90% of all cases. Other types include pancreatic neuroendocrine tumors and intraductal papillary mucinous tumors (*1*). PDAC, the focus of this review, is notorious for its asymptomatic early stages, complex molecular profiles, and resistance to conventional therapies. Over the past few decades, significant advances in molecular biology and imaging technology have greatly enhanced the understanding of PDAC, revealing the complex interactions between genetic predisposition and external environmental risk factors in particular (*2*). Nevertheless, PDAC remains the leading cause of cancer-related death, with a 5-year survival rate of approximately 10%, highlighting the need for more effective treatments (*3*). Recent studies have increasingly focused on elucidating the complex mechanisms behind pancreatic tumorigenesis, which involve key gene variations (such as KRAS, TP53, SMAD4, and CDKN2A gene mutations), the dynamic role of the tumor microenvironment, and the strategies adopted by tumors to evade immune surveillance (*4-8*). At the clinical level, the advent of new therapeutic modalities, including targeted therapy and immunotherapy, has shown their potential. However, there are still major challenges. An example is chemotherapy resistance: the median progression-free survival (PFS) for the FOLFIRINOX/mFOLFIRINOX regimen is only 6.4 months (PRODIGE-24 trial) (*9*). Moreover, immunotherapy is ineffective: the objective response rate (ORR) to a programmed death receptor 1 inhibitor single agent is less than 3% (KEYNOT-158 subgroup analysis) (*10*). Furthermore, the tumor matrix is a barrier: a dense fibrous matrix accounts for more than 70% of the tumor volume, hindering drug

penetration (*7*).

Despite these advances, PDAC treatment remains severely hampered by its inherent complexities, and especially the difficulty of effectively targeting both the tumor and its microenvironment, underscoring the urgent need for novel therapeutic strategies.

1.2. Mechanism of action and advantages of ADC drugs

ADCs represent an innovative class of targeted cancer therapy that chemically links monoclonal antibodies (mAbs) to potent small-molecule cytotoxic payloads *via* a specialized linker. ADCs are designed to precisely deliver cytotoxic agents to malignant cells while sparing healthy tissues. This strategy ingeniously combines the cytotoxic potency of chemotherapeutic drugs with the specificity of mAbs, thereby improving targeting accuracy, minimizing damage to normal tissues, reducing systemic toxicity, and enhancing therapeutic efficacy (*11*). The core structure of an ADC consists of three components: the cytotoxic payload, the linker, and the mAb (Figure 1). The stability and efficacy of these components collectively determine the specificity of each ADC drug (*12*).

Compared to standard chemotherapy or immune checkpoint inhibitors, ADCs exhibit superior targeting precision and enhanced cytotoxicity against tumors that clearly express specific surface antigens. However, their efficacy might be suboptimal in poorly vascularized tumors or those with low antigen density (*12*). The mechanism of action of ADCs initiates when the mAb component specifically recognizes and binds to the target antigen on the surface of cancer cells. Subsequently, through internalization, the ADC is taken up into the cancer cell. Following internalization, lysosomal proteases cleave cleavable linkers to release the payload; if the linker is non-cleavable, the entire ADC molecule is degraded to release the payload (*13*). The released cytotoxic agents then kill the targeted cancer cells by inhibiting critical cellular functions such as microtubule assembly and DNA replication.

Notably, the bystander effect can significantly influence treatment outcomes under certain circumstances (*14*). When the released payload is membrane-permeable, it can diffuse into neighboring cells – even those that do not express the target antigen (*14*). This phenomenon is particularly crucial in tumors exhibiting heterogeneous antigen expression, where complete eradication solely through direct targeting is challenging. However, the bystander effect is a double-edged sword: the ability of cytotoxic payloads to diffuse into the tumor microenvironment can also cause various complications affecting the safety and efficacy of ADC therapy (*15*). Therefore, the magnitude of this effect largely depends on parameters such as payload properties, linker stability, and tumor architecture (*15*).

Selecting appropriate surface target proteins is paramount for ADC safety and efficacy. An ideal target antigen should possess the following characteristics: *i*) Expression is exclusive or predominant in tumor cells, with minimal to no expression in normal tissues; *ii*) It should be non-secreted, because a circulating antigen can cause off-target binding of ADC outside the tumor site, reducing tumor targeting and causing safety concerns; *iii*) It should efficiently internalize upon binding to its corresponding antibody, enabling the ADC-antigen complex to enter the cell and release the cytotoxic payload (*16,17*).

In summary, ADCs function by binding target antigens, undergoing internalization, releasing cytotoxic payloads, and killing cancer cells. While the bystander effect can overcome antigen heterogeneity, it also

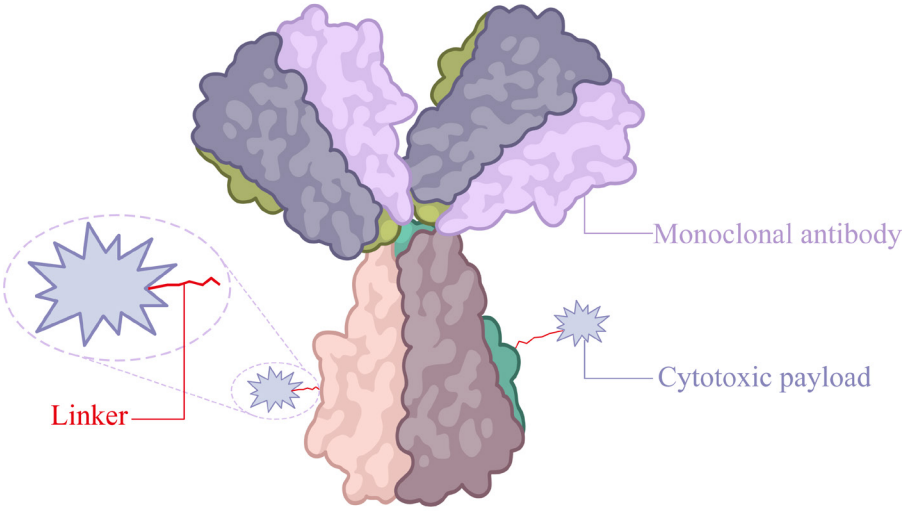

Figure 1. Schematic diagram of antibody drug conjugates. The core structure of an ADC consists of three components: the cytotoxic payload, the linker, and the monoclonal antibody.

introduces potential risks. Optimizing the three core ADC components - the antibody, linker, and cytotoxic payload - remains key to enhancing their safety profile and therapeutic efficacy (*18*). The purpose of this review is to comprehensively summarize the current status of and challenges with the treatment of PDAC and the progress of research on ADC drugs in PDAC. Finally, this review summarizes the challenges faced by ADC treatment for PDAC, it proposes strategies to overcome these challenges, and it suggests directions for future research in this area.

2. Progress of research on ADC targets in PDAC

In PDAC, several targets are under active investigation for ADC development. Urokinase plasminogen activator receptor (uPAR) is overexpressed in approximately 80% of PDAC and is abundantly present in both tumor and stromal cells, enabling dual tumor-stroma cytotoxicity in desmoplastic tumors. Mesothelin, expressed in about 50% of PDAC, shows limited physiological function in normal tissues; while clinical antibody therapies have yielded modest benefits, next-generation ADCs may exhibit enhanced efficacy by inducing pyroptosis and stimulating antitumor immunity. Claudin-18 isoform 2 (CLDN18.2) is highly expressed in roughly 40% of PDAC, and early trials of ADCs and bispecific antibodies have resulted in encouraging response and disease control rate (DCR) (Table 1).

2.1. uPAR

The uPAR is highly expressed in 80% of PDAC, promoting its invasion and metastasis. A point worth noting is that PDAC exhibits the highest levels of uPAR mRNA among all other tumor types and displays significant differences in expression compared to the normal pancreas and chronic pancreatitis (*19-21*). uPAR is also widely present in various non-cancer cells in activated tumor-associated stroma, including cancer-associated fibroblasts, macrophages, neutrophils, and endothelial cells (*19*). The simultaneous expression of tumors and stroma may provide better therapeutic gains in PDAC and stromal-rich tumors by promoting targeted and orthogonal anti-tumor activity (*22*). The difficulty in research on ADC drugs in PDAC lies in its fibrogenic tumor matrix microenvironment. The dense extracellular matrix forms a physical barrier that blocks the penetration of chemotherapy drugs, which is also a key reason for its poor response to different types of chemotherapy (*10*). Therefore, by taking advantage of the extensive expression of uPAR in both tumor cells and the surrounding stroma of dense tumors, a site-specific ADC can be developed using the high-affinity, cross-species reactive, and efficiently internalizing anti-uPAR mAb FL1 (*23*), conjugated with the potent anthracycline derivative PNU-158692.

Table 1. Comparison of main targets in PDAC ADC development

Target	Expression rate	Clinical trial phase	Representative drug	Preliminary efficacy data	Main advantages	Main limitations
uPAR	High expression in PDAC	Preclinical/Early Phase	Example: ABT-414	No publicly available clinical efficacy data	Highly specific targeting of tumor cells, potential for low toxicity	High expression heterogeneity, potentially leading to unstable efficacy; lack of extensive clinical validation data
Mesothelin	Moderate to high expression	Phase I/II	Example: Anetumab ravtansine	No publicly available clinical efficacy data	Expressed in various solid tumors, potentially applicable to multiple cancer types; some efficacy in other cancer types	Expression in normal tissues may cause off-target toxicity; expression and efficacy in PDAC still need further validation
CLDN18.2	High expression in PDAC	Phase I/II	Example: IBI343	ORR: 23.3%, DCR: 81.4%, PFS: 5.3 months	High expression in PDAC, likely applicable to most patients; some efficacy in other cancer types	Expression in normal gastric mucosa may cause off-target toxicity; expression and efficacy in PDAC still need further validation

2.2. Mesothelin

Mesothelin is positive in 50% of PDAC, and its high expression is mainly confined to pericardium, pleura, peritoneum, and vaginal membrane. Mesothelin does not seem to have significant biological functions in normal adult tissues. Mesothelin is highly expressed in mesothelioma, serous ovarian cancer, PDAC, and some gastric cancer and lung adenocarcinoma, and it is involved in tumor proliferation, metastasis, resistance to chemotherapy or radiotherapy, and immune escape (*24*). So far, antibodies, ADCs, and bispecific antibodies with immune checkpoints have been studied in malignant tumors expressing mesothelin. In clinical studies targeting antibodies against mesothelin, the therapeutic benefits are relatively small. The use of novel mesothelin targeted delivery, ADCs, and more effective payloads in immune checkpoint inhibitors could improve therapeutic efficacy (*25,26*). An anti-mesothelin targeted ADC induced pyroptosis and stimulated anti-tumor immune response in a mouse cancer model. Microtubule lytic enzymes and ADCs containing microtubule lytic enzymes can induce pyroptosis, which is crucial for anti-tumor immune and therapeutic responses due to thermogenic cell death (*27*). Anetumab ravtansine is an ADC of the anti-mesothelin antibody linked to the maytansinoid N2′-deacetyl-N2′-(3-mercapto-1-oxopropyl)-maytansine, and it has been studied in 45 patients across 10 dose escalation cohorts. The most common drug-related adverse events include fatigue, nausea, diarrhea, anorexia, vomiting, peripheral sensory neuropathy, and keratitis/corneal disease. There were no drug-related deaths. The pharmacokinetics of anetumab ravtansine are directly proportional to its dosage; its average half-life is 5.5 days. Among 148 cases of mesothelioma, ovarian cancer, PDAC, non-small cell lung cancer and breast cancer, complete remission occurred in 1 case, partial remission occurred in 11, and stable disease occurred in 66 cases. Anetumab ravtansine has shown controllable safety and favorable pharmacokinetic characteristics in patients with mesothelin-expressing solid tumors who have undergone severe pretreatment, and it has demonstrated encouraging preliminary anti-tumor activity (*28*).

2.3. CLDN18.2

CLDN18.2, a tight junction protein selectively expressed in cancer cells with lower levels in normal tissues, is an attractive target for therapy (*29*). It is highly expressed in 40% of PDAC cases and is associated with cancer progression, metastasis, and prognosis, making it a potential therapeutic target (*30,31*). mAbs, bispecific antibodies, and ADCs have shown promise in improving clinical outcomes. Early clinical trials have confirmed its strong anti-tumor activity, and especially when combined with chemotherapy and immunotherapy (*31,32*).

CMG901 is a novel ADC that links humanized anti-CLDN18.2 antibodies to the microtubule disruptor monomethyl auristatin (MMA) E (*33,34*). Additionally, several early-phase trials presented at American Society of Clinical Oncology 2024 explored other CLDN18.2-targeting strategies, including ADCs like LM-302 and IBI343, bispecific anti-CLDN18.2/CD3 antibodies (IBI389), and chimeric antigen receptor (CAR) T-cell therapy (CT041) for CLDN18.2-positive refractory advanced solid tumors (*35*). In patients treated with IBI343, 80% experienced treatment-related adverse events (TRAEs), with 25.7% experiencing grade ≥ 3 TRAEs. Common adverse events included anemia (42.9%), nausea (25.7%), and vomiting (25.7%). As of January 15, 2024, 25 of 89 evaluable patients showed partial response, resulting in an ORR of 28% and DCR of 80%. In the 6-mg/kg group with ≥ 60% CLDN18.2 expression, the ORR was 38.5% and DCR 84.6%, with a 40% ORR in PDAC patients (*36*). In a study of IBI389 involving 64 patients with CLDN18.2-positive PDAC (84.4% of whom were stage IV), TRAEs occurred in 96.9% of patients, with 54.7% experiencing grade ≥ 3 events. Common grade ≥ 3 TRAEs included elevated gamma-glutamyl transferase (20.3%) and a decreased lymphocyte count (9.4%). Cytokine release syndrome occurred in 51.6% of patients, though no grade ≥ 3 cytokine release syndrome was observed. As of January 31, 2024, among 23 evaluable patients, 7 had partial response and 9 had stable disease, with an ORR of 30.4% and DCR of 69.6% (*37*). These innovative approaches could extend CLDN18.2-targeted therapy to more tumor types, benefiting those with lower CLDN18.2 expression.

2.4. Other targets

In addition to the aforementioned studies, ADC development for multiple targets such as TROP2, HER2, B7-H3, and EGFR in PDAC has also been studied, as shown in Table 2, and each target has different expression rates, clinical stages, and treatment challenges.

In addition to the well-studied targets, recent research has identified several other promising molecules for PDAC ADC therapy. One such example is ozuriftamab vedotin (BA3021), a novel conditionally active biologic ADC directed against receptor tyrosine kinase-like orphan receptor 2 (ROR2). Importantly, this agent is designed to selectively bind ROR2 only under the acidic conditions of the tumor microenvironment, thereby improving tumor specificity and minimizing off-target toxicity. Preclinical studies demonstrated that this conditionally active construct is both effective and well tolerated, suggesting that ROR2-targeted ADCs may offer a viable treatment strategy for patients with ROR2-expressing tumors (*52*).

Another potential target is transforming growth factor alpha (TGF-α), which is markedly overexpressed in pancreatic adenocarcinoma relative to normal pancreatic tissues. When mAbs against TGF-α are conjugated to

Table 2. Pancreatic cancer-associated targets in ADC development

Target	Expression rate	Furthest clinical trial stage	Representative drugs	Present situation
TROP2	50–70%	Phase II/ III	Sacituzumab govitecan	● Bone marrow toxicity (≥ grade 3 neutropenia 35%) (*38-40*) ● The cytoprotective role of autophagy in the combination of TROP2-targeted antibody-driven drugs in the treatment of PDAC provides a new perspective for exploration of the mechanism of and formulation of a treatment strategy for PDAC (*41*). The Phase III ASCENT clinical study showed that the total survival time of triple negative breast cancer was nearly doubled. The median OS was 11.8 months (sacituzumab govitecan group) *vs.* 6.9 months (monotherapy group) (*42*). ● HuNb (TROP2-HSA) - MMAE (characterized by the use of nanobodies to counteract TROP2 and human serum albumin (HSA)) has good affinity, internalization efficiency, and anti-tumor activity (*43*).
HER2	5–10%	Phase III	Trastuzumab deruxtecan (T-DXd)	● Trastuzumab deruxtecan (T-DXd) is an antibody drug conjugate targeting human epidermal growth factor receptor 2 (HER2) (*44-47*) ● Among 267 patients receiving T-DXd treatment, the ORR was 37.1% (n=99; [95% CI, 31.3 to 43.2]), with responses observed in all cohorts. The median DOR was 11.3 months (95% CI, 9.6-17.8), the median PFS was 6.9 months (95% CI, 5.6-8.0), and the median OS was 13.4 months (95% CI, 11.9-15.5). In patients with HER2 IHC 3+expression in the central nervous system (n=75), the ORR was 61.3% (95% CI, 49.4 to 72.4), the median DOR was 22.1 months (95% CI, not reaching 9.6), the median PFS was 11.9 months (95% CI, 8.2 to 13.0), and the median OS was 21.1 months (95% CI, 15.3 to 29.6). ≥ grade 3 drug-related adverse events were observed in 40.8% of patients; 10.5% of patients experienced drug-related interstitial lung disease (ILD), with three deaths (*48*).
B7-H3	50–60%	Phase I	Vobramitamab Duocarmazine	● Immune checkpoint functions are complex, and multiple drug developments have failed (*49,50*)
EGFR	70–90%	Development terminated	Depatuxizumab mafodotin	● Overexpression of EGFR is a potential mechanism of resistance to T-DXd, which can be overcome through combination therapy strategies targeting EGFR (*45,51*)

cytotoxic payloads such as MMAF, the resulting ADCs exhibit significant anti-proliferative effects, effectively reducing the viability of TGF-α-expressing PDAC cells. These findings highlight TGF-α as a promising candidate for further preclinical exploration and clinical development in ADC therapy (*53*).

HER3 has also emerged as an attractive target. In December 2024, the U.S. Food and Drug Administration granted accelerated approval for the bispecific antibody zenocutuzumab, which simultaneously targets HER3 and HER2, for the treatment of non-small cell lung cancer and PDAC harboring NRG1 fusions. NRG1 encodes neuregulin-1, a high-affinity ligand of HER3 that drives oncogenic signaling. Parallel to this, AMT-562, a next-generation HER3-targeted ADC, is being investigated for its potential to expand therapeutic options across HER3-expressing tumors (*54,55*).

Nectin-4 is another target of increasing interest. A Nectin-4-directed ADC, Nectin-4-MMAE, was shown to induce apoptosis and cell death in Nectin-4-positive PDAC cell lines (BxPC-3 and YAPC). Mechanistic studies further revealed that Nectin-4-MMAE inactivates the AKT/mTOR pathway, thereby inducing autophagy. In xenograft models, Nectin-4-MMAE alone displayed potent anti-tumor activity, and its efficacy was enhanced when combined with autophagy inhibitors, leading to greater tumor regression than either agent alone. These results suggest that both monotherapy and combination approaches targeting Nectin-4 could provide promising therapeutic avenues in PDAC (*56,57*). Moreover, clinical data from the Phase I EV-101 trial of enfortumab vedotin, an FDA-approved Nectin-4-targeted ADC, showed an ORR of 43%, with a median overall survival (OS) of 12.3 months and a one-year OS rate of 51.8% (*58*).

Carcinoembryonic antigen-related cell adhesion molecules (CEACAMs) represent another important family of targets. CEACAM5, a glycosylated surface protein rarely expressed in normal adult tissues but frequently overexpressed in multiple cancers, has been implicated in tumor progression and metastasis. A novel human single-domain ADC targeting CEACAM5 demonstrated potent anti-tumor activity in both *in vitro* and *in vivo* models (*59*). While CAR-T therapies against CEACAM5 remain in the preclinical stage, they may offer an alternative or complementary strategy for patients resistant to ADCs (*60*). Similarly, CEACAM6 has been investigated as a potential target, with strategies such as delivering BET protein degraders *via* CEACAM6-targeted ADCs showing promise preclinically (*61,62*). Dual-targeting approaches have also been developed: CT109-SN-38, an ADC with specificity for both CEACAM5 and CEACAM6, has shown efficacy in selectively killing PDAC cells (*31,63*). More recently, EBC-129, an ADC designed to selectively bind tumor-specific N-glycosylation epitopes on CEACAM5/6, demonstrated encouraging preliminary results in a Phase I expansion cohort of PDAC. At doses

of 1.8 mg/kg and 2.2 mg/kg, the ORR was 25% and 20%, respectively, while the DCR reached 87.5% and 63.6%. The median PFS was 19 and 12 weeks, respectively, and notably, 82% of patients exhibited antigen expression levels considered suitable for EBC-129 therapy (*64*).

In addition, several other tumor-associated antigens have been investigated as potential ADC targets. hSD5-vedotin, an auristatin-based ADC directed against EphA2, exploits the tumor-specific expression of EphA2 in PDAC cells to drive endocytosis, release its MMAE payload, and exhibit potent anti-tumor action even at low antibody concentrations (*65*). SGN-B6A, another vedotin-based ADC, targets integrin β6 and has shown promise in preclinical PDAC studies (*66*). Oba01 has been developed to target death receptor 5, providing a novel biological rationale for future clinical evaluation in PDAC (*67*). SGN-CD228A is an investigational vedotin ADC directed at melanotransferrin (CD228/MELTF/p97), a glycoprotein associated with tumor progression (*68*).

Other notable targets include MUC1, intercellular adhesion molecule-1 (ICAM1), and related surface proteins. HzMUC1-ADC represents a new approach to exploit the overexpression of MUC1 in pancreatic and other solid tumors (*69*). ICAM1 is differentially upregulated on PDAC cells but minimally expressed in normal tissues, enabling selective tumor recognition. ICAM1-targeted ADCs, developed with optimized linkers and cytotoxic payloads, have shown potent anti-tumor activity, and their efficacy can be further evaluated using molecular imaging techniques such as magnetic resonance imaging-based non-invasive monitoring of therapeutic response (*70,71*).

In addition to established targets, several novel candidates are under active investigation for ADC development. Plectin, also referred to as cell surface reticulin when localized on the plasma membrane of malignant cells, is highly expressed and readily accessible, making it an attractive molecular target for ADC-based strategies (*2*). Another promising molecule is prostate stem cell antigen (PSCA), which is consistently expressed across all stages of prostate cancer, including advanced androgen-independent disease and bone metastases. Preclinical studies have shown that the ADC F12-MMAE, consisting of the anti-mitotic agent MMAE conjugated to IgG1 F12, exhibits dose-dependent efficacy and specificity in a PSCA-positive PC-3 xenograft model in NOD/SCID gamma mice. Beyond prostate cancer, PSCA has also been proposed as a valuable diagnostic and therapeutic marker in PDAC (*72*).

Fibroblast activation protein, a membrane-associated protein, is another noteworthy target. Its multifaceted interactions with both tumor cells and the surrounding tumor microenvironment highlight its potential relevance in both diagnostic applications and therapeutic intervention (*73*). Likewise, glypican family member phosphatidylinositol proteoglycan-1 has been identified as a potential target that could facilitate the design of innovative therapeutic strategies for PDAC (*74*).

While these findings expand the pool of potential targets and highlight novel avenues for ADC-based therapy, their successful translation into clinical practice remains uncertain.

3. Challenges in ADC development for PDAC

The development of ADCs for PDAC faces several significant barriers, limiting their clinical success. A major challenge is the lack of high-density tumor-specific antigens, as PDAC exhibits low expression of highly specific antigens that are essential for effective targeting by ADCs. Additionally, stromal barriers surrounding PDAC tumors impede the penetration of ADCs into the tumor cells, reducing therapeutic efficacy. Antigen heterogeneity within the tumor further complicates treatment, as varying levels of antigen expression, coupled with resistance mechanisms such as drug efflux and target loss, contribute to suboptimal therapeutic outcomes. Moreover, ADCs often induce dose-limiting toxicities, such as myelosuppression and corneal toxicity, particularly in PDAC patients, which severely impact the therapeutic index. Finally, despite promising preclinical data, low clinical translation rates pose a critical issue, with many ADCs failing to progress beyond Phase I trials due to limited efficacy or unexpected safety concerns. These factors collectively underscore the complex challenges in advancing ADCs for PDAC treatment, necessitating further research and innovation to overcome these obstacles (Figure 2).

4. Promoting the multi-dimensional progress of ADC therapy for PDAC

One of the main scientific challenges facing the development of PDAC ADC is the extremely low drug delivery efficiency. Pancreatic cancer has a highly fibrotic tumor matrix, which constitutes a dense physical barrier, that greatly hampers drug penetration and severely limits the therapeutic effect of a drug. To address this issue, researchers have developed human universal domain antibodies (UdAb) with smaller structures and higher stability. The n501 UdAb targeting carcinoembryonic antigen 5T4 exhibits extremely high stability, and its conjugate n501-SN38 demonstrates the ability to penetrate deeper tumor tissue, a higher rate of tumor uptake, and a faster rate of tumor accumulation in a mouse model, thereby displaying significantly enhanced anti-tumor action. This result shows that an ADC based on UdAb has good therapeutic prospects and is especially suitable for tumor types with significant tissue barriers such as solid tumors (*75*).

That said, the design strategy of bispecific ADCs also offers new ideas for improving targeting accuracy and efficacy. For example, BL-B01D1 is an EGFR-HER3

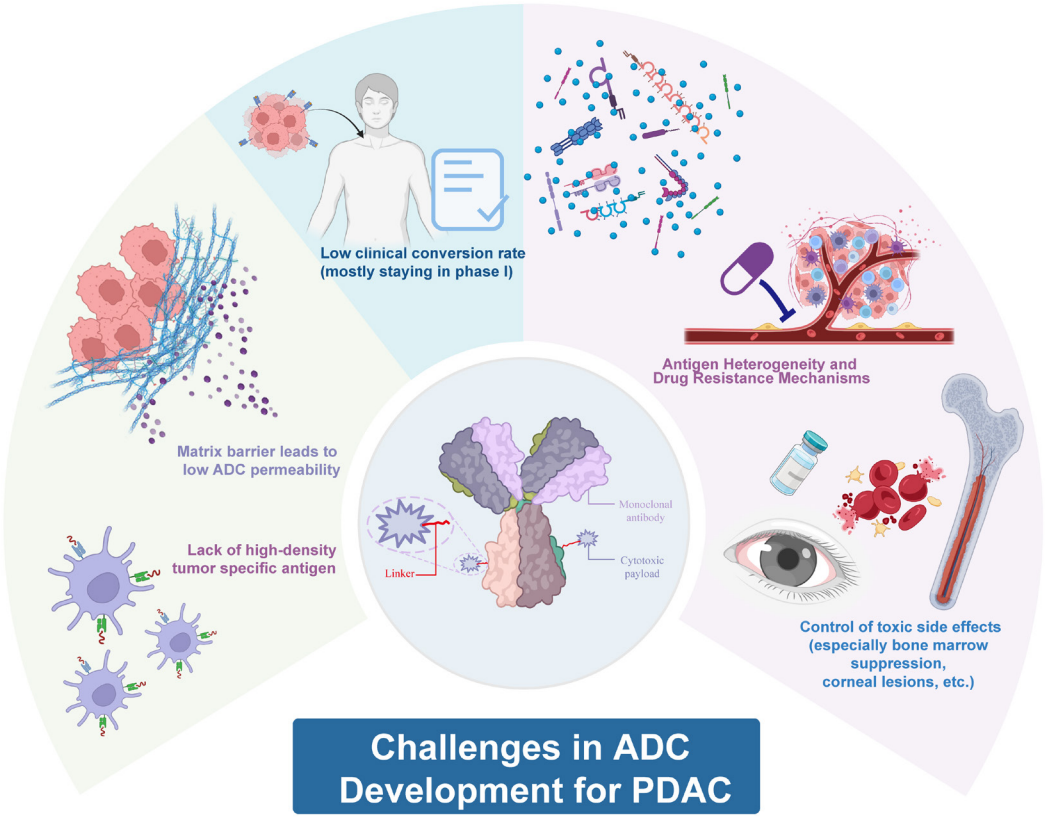

Figure 2. Challenges in developing ADCs for PDAC. Key barriers include the low expression of tumor-specific antigens, stromal barriers limiting ADC penetration, antigen heterogeneity, resistance mechanisms such as drug efflux and target loss, and dose-limiting toxicities like myelosuppression and corneal toxicity. Despite promising preclinical data, low clinical translation rates hinder progress beyond Phase I trials. These challenges highlight the need for continued research and innovation in ADC development for PDAC.

bispecific ADC developed specifically for patients with locally advanced or metastatic solid tumors, and it has shown excellent targeting efficiency and toxicity control in clinical studies (*76*) as well as being a dual-targeted ADC that can simultaneously counteract mesenchymal epithelial transition (MET) and origin receptor (RON) for the treatment of cancers with high phenotypic heterogeneity. A dual-targeted approach in the form of an ADC is highly effective and has long-lasting therapeutic effects on tumors exhibiting MET/RON heterogeneous phenotypes, indicating that ADCs dually targeting MET and RON can serve as a new strategy for treating tumors with expression phenotype heterogeneity (*77*). The bispecific antibody IMV-M is designed to selectively bind to and aggregate death receptor 5 by a novel mechanism of aggregating multiple IMV-M molecules onto a single MUC16 molecule and binding to the tumor antigen MUC16. MUC16 is overexpressed in most subtypes of ovarian cancer, PDAC, and lung cancer and is minimally expressed in normal tissues, indicating that this bispecific antibody has wide applicability (*78*). With advances in modern biotechnology, new carefully designed antibodies have ultimately paved the way for the successful clinical treatment of various cancers, which includes precise tumor immunotherapy (*79*).

Advances in platform technology have also provided key support tools for ADC therapy. Electron microscopy can study the interactions between tumor microbiota and cancer cell migration and also assist in the development of targeted therapies such as ADCs and aptamer-drug conjugates (*80*). In addition, innovative biological delivery strategies are also being developed. For example, the system that combines genetically modified Salmonella typhimurium VNP20009 with aptamer drug conjugate utilizes the natural chemotaxis of bacteria towards the hypoxic microenvironment in tumor areas to achieve targeted drug delivery and local release of the drug. A study found that this strategy can prolong the serum stability of aptamer drug conjugate to 48 hours, significantly increase the drug concentration at the tumor site, and promote bacterial colonization, tumor cell death, and enhanced T-cell infiltration (*81*).

The introduction of synthetic lethal mechanisms also provides a new therapeutic approach for ADC therapy. By combining drugs targeting the DNA repair pathway such as ADC and ataxia telangiectasia and rad3-related kinase (ATR) inhibitors, treatment selectivity can be enhanced without increasing toxicity and adverse reactions, providing a more strategic therapeutic breakthrough for PDAC, the "silent killer" (*82*).

5. Current breakthroughs in and the future design blueprint for ADC treatment for PDAC

Due to the matrix-rich microenvironment and the lack of a high-density tumor-specific antigen in PDAC, PDAC is still a disease that is difficult to target. The next generation of ADCs needs to integrate penetration-enhancing antibodies + immune regulatory payloads + intelligent linkers. Research has found that targeting proteoglycan-1 (GPC1) on cancer associated fibroblasts using GPC1 ADCs conjugated with phosphatidylinositol GPC1 and MMAE in matrix-rich tumors such as PDAC is a useful method (*83,84*). Thus, the necessity of customized ADC design to enhance the outcomes of various types of cancer needs to be recognized (*13*). A humanized anti- tissue factor (TF) Ab (clone. 1084), coupled with MMAE or deruxtecan (DXd), showed more potent anti-tumor activity in tumors with strong and uniform TF expression, while a DXd-coupled anti-TF ADC was more effective in tumors with weak and heterogeneous TF expression. An analysis of a PDAC tissue array showed that TF expression was weak and uneven in most TF-positive specimens, which suggests that DXd's response rate to cancer might be higher than an MMAE-coupled anti-TF ADC. However, findings have indicated that optimizing the ADC payload separately in each patient can maximize the potential of ADC therapy (*85,86*). Extending the half-life of single domain ADCs through albumin binding enhances anti-tumor efficacy (*87*).

6. Strategies to overcome barriers in ADC development

6.1. Penetration enhancement

Improving the penetration of ADCs into tumors is a critical challenge. Tumors, and particularly those with dense extracellular matrices, often prevent effective drug delivery. Studies are exploring methods to enhance drug penetration, such as modifying the physical properties of ADCs or utilizing targeted agents to break down tumor barriers (*7,10*).

6.2. Novel linkers and payloads

Several studies have focused on developing more efficient payloads (*e.g.*, exatecan, MMAE, and muscarine alkaloids) and optimized linkers (*e.g.*, cleavable or stable linkers) to improve ADC internalization and cytotoxicity. For instance, a study using triptolide as a payload for PDAC employed silyl ether as a cleavable linker. This linker offers easy synthesis and controllable drug release rates by modifying the silyl ether group (*88*). Additionally, a second-generation amanitin-based ADC (ATAC) targeting TROP2, with Trodelvy's humanized RS7 antibody (hRS7), showed superior efficacy to Trodelvy in treating refractory PDAC and triple negative breast cancer, completely eradicating the tumors (*89*). Similarly, a BET protein degradation product that was delivered *via* a CEACAM6-targeted ADC demonstrated inhibition of tumor growth in PDAC models (*90*).

6.3. Bispecific and conditionally activated ADCs

To address tumor heterogeneity and improve specificity, bispecific ADCs and conditionally activated ADCs are being explored. For instance, ADCs with bystander effects can overcome antigen heterogeneity by enabling the cytotoxic payload to kill tumor cells of different phenotypes. This approach is particularly useful for tumors that exhibit diverse antigen expression profiles. By optimizing adapters and conjugation methods, a novel ADC has been developed, and it displays excellent anti-tumor efficacy and a strong bystander killing effect both *in vivo* and *in vitro* (*91*). Moreover, ADCs can be conditionally activated in the tumor microenvironment through enzymatic hydrolysis, reducing toxicity to normal tissues while enhancing tumor-specific activity.

6.4. Combination therapies

Combining ADCs with other therapeutic agents, such as immune checkpoint inhibitors, autophagy inhibitors, and ATR inhibitors, can enhance ADC efficacy by leveraging multi-target and multi-mechanism synergism. This approach is particularly beneficial in overcoming the challenges posed by the "immune desert" microenvironment of PDAC. For example, combining Nectin-4-targeted ADCs with autophagy inhibitors has demonstrated more potent anti-tumor action (*56*).

7. Conclusions and future directions

PDAC, one of the most invasive and drug-resistant solid tumors, remains a significant challenge in clinical oncology. The efficacy of traditional therapies, including chemotherapy, radiotherapy, targeted therapy, and immunotherapy, is limited in PDAC, particularly due to the complex tumor microenvironment, significant antigen heterogeneity, and the dense fibrotic matrix that severely impedes the efficient delivery of therapeutic drugs. In this context, ADCs have emerged as a promising therapeutic approach, combining the specificity of mAbs with the potent cytotoxicity of payloads, demonstrating significant progress across multiple solid tumors and showing potential in PDAC.

However, the clinical use of ADCs in PDAC still faces several challenges. The first major hurdle is the accessibility and specificity of suitable targets. PDAC lacks highly dense, tumor-specific antigens, and although targets like uPAR, Mesothelin, and CLDN18.2 show promise, their significant heterogeneity leads to inconsistent ADC efficacy. Moreover, the dense tumor matrix not only restricts drug penetration but also

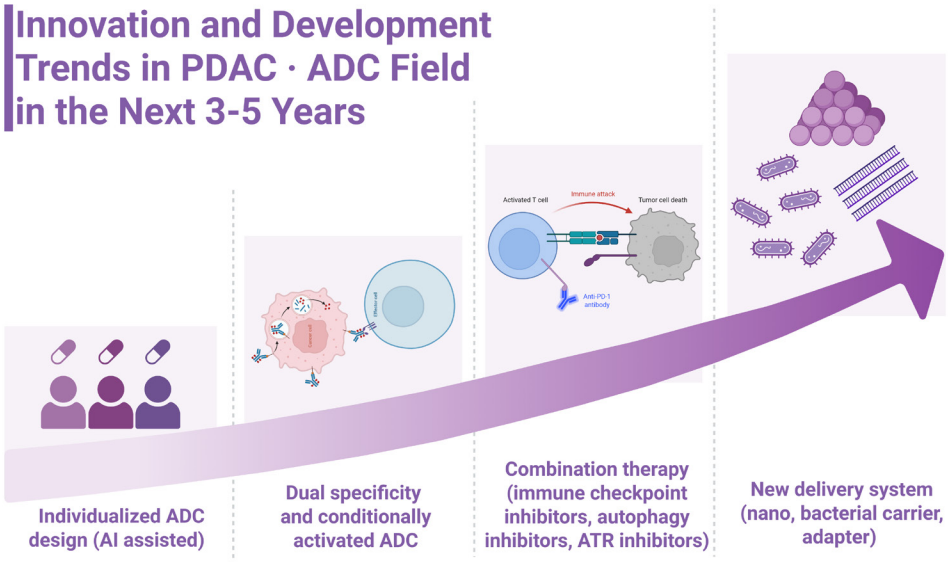

Figure 3. Innovation and development trends in the area of PDAC·ADC over the next 3-5 years. Future directions in antibody-drug conjugate development. Bispecific and conditionally activated ADCs will enhance precision targeting and release by responding to tumor-specific conditions. AI-assisted personalized ADC design, leveraging multi-omics and machine learning, will enable customized anti-cancer strategies. Combination therapies with immune checkpoint inhibitors, autophagy inhibitors, and ATR inhibitors are expected to improve efficacy and overcome drug resistance. Advanced delivery systems, such as nanoparticles, engineered bacterial carriers, and adapter platforms, will enhance tissue penetration, improve drug stability, and offer novel solutions for treating refractory solid tumors.

contributes to immune evasion and the development of drug resistance, preventing therapeutic drugs from reaching effective concentrations at the tumor site. Emerging resistance mechanisms, such as lysosomal dysfunction and exosome-mediated drug efflux, further limit ADC efficacy.

To overcome these challenges, future research must focus on optimizing ADCs at multiple levels. Over the next 3-5 years, the area of ADCs is poised for multidimensional innovation and integrated development. First, bispecific and conditionally activated ADCs will offer more precise targeting and release, recognizing two different tumor-associated antigens or responding to specific conditions in the tumor microenvironment (such as a low pH or specific enzyme activity). This approach is expected to significantly improve the therapeutic window and reduce toxicity risks. Second, artificial intelligence-assisted personalized ADC design will leverage multi-omics data and machine learning models to select the most suitable antibodies, linkers, and drug-loading regimens for individual patients, leading to a truly "customized" anti-cancer strategy. The combination therapy model is poised to significantly expand the therapeutic potential of ADCs. When paired with immune checkpoint inhibitors, autophagy inhibitors, and DNA damage repair pathway inhibitors, ADCs are expected to produce synergistic anti-tumor effects and help overcome drug resistance. These combinations may prove particularly effective in addressing the "immune desert" state often seen in PDAC, enabling more comprehensive tumor targeting and enhancing immune-mediated responses. Additionally, innovative drug delivery systems, including nanoparticles, engineered bacterial carriers, and adapter platforms, can circumvent the delivery challenges faced by traditional ADCs. These advanced delivery mechanisms will improve tissue penetration, enhance drug stability, and provide novel therapeutic avenues for treating refractory solid tumors (Figure 3).

An important point to emphasize is that ADCs are not a "universal key" but rather a "customized weapon" that requires precise tumor typing, personalized design, and dynamic monitoring during treatment. As interdisciplinary tools such as nanotechnology, artificial intelligence, and bioinformatics continue to develop, future ADCs will likely become more intelligent, accurate, and efficient. The integration of emerging delivery systems, like bacterial vectors and aptamer platforms, along with synthetic lethal strategies, holds great promise in enhancing the scope of ADC treatment for refractory solid tumors such as PDAC.

This review has sought to provide a comprehensive reference for the future development of PDAC precision therapies, highlighting the critical research directions that will guide the next phase of ADC innovation. It also calls for increased clinical-translational research to bridge the gap between preclinical advances and clinical use, ultimately driving breakthroughs in PDAC treatment. ADCs offer a glimmer of hope for PDAC patients, and through collaboration, mechanistic research, and clinical validation, they may become an effective weapon in improving survival outcomes for this challenging cancer.

Funding: This work was supported by grants from

the Tianjin Project to Build Key Medical Disciplines (Specialties) (TJYXZDXK-009A), the Tianjin Health Research Project (TJWJ2023QN012), and the National Natural Science Foundation of China (82303718, 82473460).

Conflict of Interest: The authors have no conflicts of interest to disclose.

References

1. Mizrahi JD, Surana R, Valle JW, Shroff RT. Pancreatic cancer. Lancet. 2020; 395:2008-2020.
2. Dimastromatteo J, He J, Adams RB, Kelly KA. Imaging cell surface plectin in PDAC patients - A first-in-human phase 0 study report. Mol Imaging Biol. 2025; 27:389-399.
3. Hu JX, Zhao CF, Chen WB, Liu QC, Li QW, Lin YY, Gao F. Pancreatic cancer: A review of epidemiology, trend, and risk factors. World J Gastroenterol. 2021; 27:4298-4321.
4. Martinez-Bosch N, Vinaixa J, Navarro P. Immune evasion in pancreatic cancer: From mechanisms to therapy. Cancers. 2018; 10:6.
5. Cancer Genome Atlas Research Network. Integrated genomic characterization of pancreatic ductal adenocarcinoma. Cancer Cell. 2017; 32:185-203.e13.
6. Sherman MH, Beatty GL. Tumor microenvironment in pancreatic cancer pathogenesis and therapeutic resistance. Annu Rev Pathol. 2023; 18:123-148.
7. Tirpe A, Streianu C, Isachesku E, Simon I, Berindan-Neagoe I. The road to overcome pancreatic cancer: Where are we? Heliyon. 2024; 10:e38196.
8. Zhen DB, Safyan RA, Konick EQ, Nguyen R, Prichard CC, Chiorean EG. The role of molecular testing in pancreatic cancer. Ther Adv Gastroenterol. 2023; 16:17562848231171456.
9. Nagaraju GP, Farran B, Luong T, El-Rayes BF. Understanding the molecular mechanisms that regulate pancreatic cancer stem cell formation, stemness and chemoresistance: A brief overview. Semin Cancer Biol. 2023; 88:67-80.
10. Zhan T, Betge J, Schulte N, Dreikhausen L, Hirth M, Li M, Weidner P, Leipertz A, Teufel A, Ebert MP. Digestive cancers: Mechanisms, therapeutics and management. Signal Transduct Target Ther. 2025; 10:24.
11. Theocharopoulos C, Ziogas IA, Douligeris CC, Efstathiou A, Kolorizos E, Ziogas DC, Kontis E. Antibody-drug conjugates for hepato-pancreato-biliary malignancies: "Magic bullets" to the rescue? Cancer Treat Rev. 2024; 129:102806.
12. Nguyen TD, Bordeau BM, Balthasar JP. Mechanisms of ADC toxicity and strategies to increase ADC tolerability. Cancers. 2023; 15:713.
13. Yajaman DR, Oh Y, Trevino JG, Harrell JC. Advancing antibody-drug conjugates: Precision oncology approaches for breast and pancreatic cancers. Cancers. 2025; 17:1792.
14. Giugliano F, Corti C, Tarantino P, Michelini F, Curigliano G. Bystander effect of antibody-drug conjugates: Fact or fiction? Curr Oncol Rep. 2022; 24:809-817.
15. Tang H, Liu Y, Yu Z, Sun M, Lin L, Liu W, Han Q, Wei M, Jin Y. The analysis of key factors related to ADCs structural design. Front Pharmacol. 2019; 10:373.
16. Xing L, Lv L, Ren J, Yu H, Zhao X, Kong X, Xiang H, Tao X, Dong D. Advances in targeted therapy for pancreatic cancer. Biomed Pharmacother. 2023; 168:115717.
17. Fu Z, Li S, Han S, Shi C, Zhang Y. Antibody drug conjugate: The "biological missile" for targeted cancer therapy. Signal Transduct Target Ther. 2022; 7:93.
18. Wittwer NL, Brown MP, Liapis V, Staudacher AH. Antibody drug conjugates: Hitting the mark in pancreatic cancer? J Exp Clin Cancer Res. 2023; 42:280.
19. Metrangolo V, Ploug M, Engelholm LH. The urokinase receptor (uPAR) as a "Trojan horse" in targeted cancer therapy: Challenges and opportunities. Cancers (Basel). 2021; 13:5376.
20. Peng L, Li Y, Yao S, Gaedcke J, Baart VM, Sier CFM, Neesse A, Ellenrieder V, Bohnenberger H, Fuchs F, Kitz J, Ströbel P, Küffer S. Urokinase-type plasminogen activator receptor (uPAR) cooperates with mutated KRAS in regulating cellular plasticity and gemcitabine response in pancreatic adenocarcinomas. Cancers. 2023; 15:1587.
21. Kumar AA, Buckley BJ, Ranson M. The urokinase plasminogen activation system in pancreatic cancer: Prospective diagnostic and therapeutic targets. Biomolecules. 2022; 12:152.
22. Hessmann E, Buchholz SM, Demir IE, Singh SK, Gress TM, Ellenrieder V, Neesse A. Microenvironmental determinants of pancreatic cancer. Physiol Rev. 2020; 100:1707-1751.
23. Metrangolo V, Blomquist MH, Dutta A, Gårdsvoll H, Krigslund O, Nørregaard KS, Jürgensen HJ, Ploug M, Flick MJ, Behrendt N, Engelholm LH. Targeting uPAR with an antibody-drug conjugate suppresses tumor growth and reshapes the immune landscape in pancreatic cancer models. Sci Adv. 2025; 11:eadq0513.
24. Lv J, Li P. Mesothelin as a biomarker for targeted therapy. Biomark Res. 2019; 7:18.
25. Chu GJ, Linton A, Kao S, Klebe S, Adelstein S, Yeo D, Rasko JEJ, Cooper WA. High mesothelin expression by immunohistochemistry predicts improved survival in pleural mesothelioma. Histopath. 2023; 83:202-210.
26. Chu Q. Targeting Mesothelin in Solid Tumours: Anti-mesothelin antibody and drug conjugates. Curr Oncol Rep. 2023; 25:309-323.
27. Wittwer N, Staudacher A, Liapis V, Cardarelli P, Warren H, Brown M. An anti-mesothelin targeting antibody drug conjugate induces pyroptosis and ignites antitumor immunity in mouse models of cancer. J Immunother Cancer. 2023; 11:e006274.
28. Hassan R, Blumenschein GR, Moore KN, *et al.* First-in-human, multicenter, phase I dose-escalation and expansion study of anti-mesothelin antibody-drug conjugate anetumab ravtansine in advanced or metastatic solid tumors. J Clin Oncol. 2020; 38:1824-1835.
29. Katoh M, Katoh M. Claudin 1, 4, 6 and 18 isoform 2 as targets for the treatment of cancer (Review). Int J Mol Med. 2024; 54:100.
30. Xu Q, Jia C, Ou Y, Zeng C, Jia Y. Dark horse target Claudin18.2 opens new battlefield for pancreatic cancer. Front Oncol. 2024; 14:1371421.
31. O'Brien NA, McDermott MSJ, Zhang J, *et al.* Development of a novel CLDN18.2-directed monoclonal antibody and antibody-drug conjugate for treatment of CLDN18.2-positive cancers. Mol Cancer Ther. 2023; 22:1365-1375.
32. Lu Z, Shi M, Zheng X, Liang Y, Wang J, Zou Z, Luo R, Feng M, Yang X, Zhou Y, Li X. Preclinical evaluation of ^{89}Zr/^{177}Lu-labeled amatuximab for theranostic application

in pancreatic ductal adenocarcinoma. Int J Pharm. 2024; 667:124946.
33. Ruan DY, Liu FR, Wei XL, *et al.* Claudin 18.2-targeting antibody-drug conjugate CMG901 in patients with advanced gastric or gastro-oesophageal junction cancer (KYM901): A multicentre, open-label, single-arm, phase 1 trial. Lancet Oncol. 2025; 26:227-238.
34. Xu G, Liu W, Wang Y, Wei X, Liu F, He Y, Zhang L, Song Q, Li Z, Wang C, Xu R, Chen B. CMG901, a Claudin18.2-specific antibody-drug conjugate, for the treatment of solid tumors. Cell Rep Med. 2024; 5:101710.
35. Zhou KI, Strickler JH, Chen H. Targeting Claudin-18.2 for cancer therapy: Updates from 2024 ASCO annual meeting. J Hematol Oncol. 2024; 17:73.
36. Yu X, Zhang J, Tazbirkova A, *et al.* Safety and efficacy of IBI343 (anti-claudin18.2 antibody-drug conjugate) in patients with advanced pancreatic ductal adenocarcinoma or biliary tract cancer: Preliminary results from a phase 1 study. J Clin Oncol. 2024; 42:3037-3037.
37. Hao J, Zheng L, Ruihong D, *et al.* Safety and efficacy of IBI389, an anti-CLDN18.2/CD3 bispecific antibody, in patients with advanced pancreatic ductal adenocarcinoma: Preliminary results from a phase 1 study. J Clin Oncol. 2024; 42:4011-4011.
38. Pratt EC, Mandleywala K, Bauer D, Bolaender A, Chao G, Castanares MA, Collins EC, Lewis JS. Pretargeted Trop-2 immunoPET for rapid, selective detection of pancreatic tumors. Clin Cancer Res. 2025; 31:2719-2726.
39. Liu Y, Huang W, Saladin RJ, Hsu JC, Cai W, Kang L. Trop2-targeted molecular imaging in solid tumors: Current advances and future outlook. Mol Pharm. 2024; 21:5909-5928.
40. Sun LP, Bai WQ, Zhou DD, Wu XF, Zhang LW, Cui AL, Xie ZH, Gao RJ, Zhen YS, Li ZR, Miao QF. hIMB1636-MMAE, a novel TROP2-targeting antibody-drug conjugate exerting potent antitumor efficacy in pancreatic cancer. J Med Chem. 2023; 66:14700-14715.
41. Xu C, Huang X, Hu Q, Xue W, Zhou K, Li X, Nan Y, Ju D, Wang Z, Zhang X. Modulating autophagy to boost the antitumor efficacy of TROP2-directed antibody-drug conjugate in pancreatic cancer. Biomed Pharmacother. 2024; 180:117550.
42. Bardia A, Tolaney SM, Loirat D, *et al.* Sacituzumab govitecan (SG) versus treatment of physician's choice (TPC) in patients (pts) with previously treated, metastatic triple-negative breast cancer (mTNBC): Final results from the phase 3 ASCENT study. J Clin Oncol. 2022; 40:1071-1071.
43. Xu C, Zhu M, Wang Q, Cui J, Huang Y, Huang X, Huang J, Gai J, Li G, Qiao P, Zeng X, Ju D, Wan Y, Zhang X. TROP2-directed nanobody-drug conjugate elicited potent antitumor effect in pancreatic cancer. J Nanobiotech. 2023; 21:410.
44. Oaknin A, Lee JY, Makker V, *et al.* Efficacy of trastuzumab deruxtecan in HER2-expressing solid tumors by enrollment HER2 IHC status: Post hoc analysis of DESTINY-PanTumor02. Adv Ther. 2024; 41:4125-4139.
45. Gupta A, Michelini F, Shao H, *et al.* EGFR-directed antibodies promote HER2 ADC internalization and efficacy. Cell Rep Med. 2024; 5:101792.
46. Yao H, Yan M, Tong Z, *et al.* Safety, efficacy, and pharmacokinetics of SHR-A1811, a human epidermal growth factor receptor 2-directed antibody-drug conjugate, in human epidermal growth factor receptor 2-expressing or mutated advanced solid tumors: A global phase I trial. J Clin Oncol. 2024; 42:3453-3465.
47. Jones L, Cunningham D, Starling N. HER-2 directed therapies across gastrointestinal tract cancers - A new frontier. Cancer Treat Rev. 2024; 129:102789.
48. Meric-Bernstam F, Makker V, Oaknin A, *et al.* Efficacy and safety of trastuzumab deruxtecan in patients with HER2-expressing solid tumors: Primary results from the DESTINY-PanTumor02 phase II trial. J Clin Oncol. 2024; 42:47-58.
49. Perovic D, Dusanovic Pjevic M, Perovic V, Grk M, Rasic M, Milickovic M, Mijovic T, Rasic P. B7 homolog 3 in pancreatic cancer. World J Gastroenterol. 2024; 30:3654-3667.
50. Brignole C, Calarco E, Bensa V, Giusto E, Perri P, Ciampi E, Corrias MV, Astigiano S, Cilli M, Loo D, Bonvini E, Pastorino F, Ponzoni M. Antitumor activity of the investigational B7-H3 antibody-drug conjugate, vobramitamab duocarmazine, in preclinical models of neuroblastoma. J Immunother Cancer. 2023; 11:e007174.
51. Zhu M, Zhou L, Hu S, Miao Q, Gong J, Zhang N, Zhang G, Wang M, Wang J, He H, Wang Y. Rational design and systemic appraisal of an EGFR-targeting antibody-drug conjugate LR-DM1 for pancreatic cancer. J Med Chem. 2022; 65:7141-7153.
52. Chang HW, Frey G, Wang J, Liu H, Xing C, Chen J, Boyle WJ, Short JM. Preclinical development of ozuriftamab vedotin (BA3021), a novel ROR2-specific conditionally active biologic antibody-drug conjugate. MAbs. 2025; 17:2490078.
53. Romero-Pérez I, Montero JC, Redondo-Puente M, Del Carmen Gómez-García M, Morell-Ginestà M, Capellá G, Pandiella A. An antibody-drug conjugate targeting soluble and membrane-bound TGFα is effective against pancreatic tumors. J Exp Clin Cancer Res. 2025; 44:158.
54. Garrett JT, Tendler S, Feroz W, Kilroy MK, Yu H. Emerging importance of HER3 in tumorigenesis and cancer therapy. Nat Rev Clin Oncol. 2025; 22:348-370.
55. Weng W, Meng T, Pu J, *et al.* AMT-562, a novel HER3-targeting antibody-drug conjugate, demonstrates a potential to broaden therapeutic opportunities for HER3-expressing tumors. Mol Cancer Ther. 2023; 22:1013-1027.
56. Fu R, Wang C, Yin T, Zhang X, Xu Y, Shi Y, Xu J, Zhang W, Ding Z. A novel and promising therapeutic approach for treating pancreatic cancer: Nectin-4-targeted antibody-drug conjugates alone or combined with autophagy inhibitors. Int J Mol Med. 2025; 55:66.
57. Zhang J, Liu R, Wang S, *et al.* Bulumtatug Fuvedotin (BFv, 9MW2821), a next-generation Nectin-4 targeting antibody-drug conjugate, in patients with advanced solid tumors: A first-in-human, open-label, multicenter, phase I/II study. Ann Oncol. 2025; 36:934-943.
58. Fukuokaya W, Koike Y, Yata Y, *et al.* Real world evidence of enfortumab vedotin in patients with advanced urothelial cancer: A multicenter observational study. Int J Urol. 2024; 31:342-347.
59. Zhu XY, Li QX, Kong Y, Huang KK, Wang G, Wang YJ, Lu J, Hua GQ, Wu YL, Ying TL. A novel human single-domain antibody-drug conjugate targeting CEACAM5 exhibits potent *in vitro* and *in vivo* antitumor activity. Acta Pharmacol Sin. 2024; 45:609-618.
60. Kim YJ, Li W, Zhelev DV, Mellors JW, Dimitrov DS, Baek DS. Chimeric antigen receptor-T cells are effective against CEACAM5 expressing non-small cell lung cancer cells resistant to antibody-drug conjugates. Front Oncol. 2023; 13:1124039.

61. Kogai H, Tsukamoto S, Koga M, Miyano M, Akagi T, Yamaguchi A, Mori K, Gotoh K, Nakazawa Y. Broad-spectrum efficacy of CEACAM6-targeted antibody-drug conjugate with BET protein degrader in colorectal, lung, and breast cancer mouse models. Mol Cancer Ther. 2025; 24:392-405.
62. Kong Y, Xie F, Zhang Z, *et al.* Evaluation of novel anti-CEACAM6 antibody-based conjugates for radioimmunotheranostics of pancreatic ductal adenocarcinoma. Eur Radiol. 2023; 33:7077-7088.
63. Cardenas KCA, Enos CW, Spear MR, Austin DE, Almofeez R, Kortchak S, Pincus L, Guo H-B, Dolezal S, Pierce JM, Furth E, Gineste C, Kwon Y, Gelber C. CT109-SN-38, a Novel antibody-drug conjugate with dual specificity for CEACAM5 and 6, elicits potent killing of pancreatic cancer cells. Curr Cancer Drug Targets. 2024; 24:720-732.
64. ecancer. ASCO 2025: Experimental Drug Development Centre announces the presentation of updated data from the phase 1 study of antibody-drug conjugate EBC-129 at the 2025 Annual Meeting of the American Society of Clinical Oncology. (ASCO) *http://ecancer.org/en/news/26567-asco-2025-experimental-drug-development-centre-announces-the-presentation-of-updated-data-from-the-phase-1-study-of-antibody-drug-conjugate-ebc-129-at-the-2025-annual-meeting-of-the-american-society-of-clinical-oncology-asco* (accessed August 1, 2025).
65. Chang FL, Lee CC, Tsai KC, Lin TY, Chiang CW, Pan SL, Lee YC. An auristatin-based antibody-drug conjugate targeting EphA2 in pancreatic cancer treatment. Biochem Biophys Res Commun. 2023; 688:149214.
66. Lyon RP, Jonas M, Frantz C, Trueblood ES, Yumul R, Westendorf L, Hale CJ, Stilwell JL, Yeddula N, Snead KM, Kumar V, Patilea-Vrana GI, Klussman K, Ryan MC. SGN-B6A: A new vedotin antibody-drug conjugate directed to integrin beta-6 for multiple carcinoma indications. Mol Cancer Ther. 2023; 22:1444-1453.
67. Zheng C, Zhou D, Li W, Duan Y, Xu M, Liu J, Cheng J, Xiao Y, Xiao H, Gan T, Liang J, Zheng D, Wang L, Zhang S. Therapeutic efficacy of a MMAE-based anti-DR5 drug conjugate Oba01 in preclinical models of pancreatic cancer. Cell Death Dis. 2023; 14:295.
68. Mazahreh R, Mason ML, Gosink JJ, *et al.* SGN-CD228A is an investigational CD228-directed antibody-drug conjugate with potent antitumor activity across a wide spectrum of preclinical solid tumor models. Mol Cancer Ther. 2023; 22:421-434.
69. Wu G, Li L, Liu M, Chen C, Wang G, Jiang Z, Qin Y, He L, Li H, Cao J, Gu H. Therapeutic effect of a MUC1-specific monoclonal antibody-drug conjugates against pancreatic cancer model. Cancer Cell Int. 2022; 22:417.
70. Huang J, Agoston AT, Guo P, Moses MA. A rationally designed ICAM1 antibody drug conjugate for pancreatic cancer. Adv Sci (Weinh). 2020; 7:2002852.
71. Mosley M, Baguña Torres J, Allen D, Cornelissen B. Immuno-imaging of ICAM-1 in tumours by SPECT. Nucl Med Biol. 2020; 84-85:73-79.
72. Chu X, Shin S, Baek DS, *et al.* Discovery of a novel highly specific, fully human PSCA antibody and its application as an antibody-drug conjugate in prostate cancer. MAbs. 2024; 16:2387240.
73. Zhang Z, Tao J, Qiu J, Cao Z, Huang H, Xiao J, Zhang T. From basic research to clinical application: Targeting fibroblast activation protein for cancer diagnosis and treatment. Cell Oncol (Dordr). 2024; 47:361-381.
74. Busato D, Mossenta M, Dal Bo M, Macor P, Toffoli G. The proteoglycan glypican-1 as a possible candidate for innovative targeted therapeutic strategies for pancreatic ductal adenocarcinoma. Int J Mol Sci. 2022; 23:10279.
75. Wu Y, Li Q, Kong Y, *et al.* A highly stable human single-domain antibody-drug conjugate exhibits superior penetration and treatment of solid tumors. Mol Ther. 2022; 30:2785-2799.
76. Ma Y, Huang Y, Zhao Y, *et al.* BL-B01D1, a first-in-class EGFR-HER3 bispecific antibody-drug conjugate, in patients with locally advanced or metastatic solid tumours: A first-in-human, open-label, multicentre, phase 1 study. Lancet Oncol. 2024; 25:901-911.
77. Wang M, Ma Q, Suthe SR, Hudson RE, Pan JY, Mikelis C, Zhu MJ, Wu ZG, Shi DR, Yao HP. Humanized dual-targeting antibody-drug conjugates specific to MET and RON receptors as a pharmaceutical strategy for the treatment of cancers exhibiting phenotypic heterogeneity. Acta Pharmacol Sin. 2025; 46:1375-1389.
78. Goldmacher VS, Gershteyn I, Chari R, Kovtun Y. A bispecific anti-MUC16/anti-death receptor 5 antibody achieves effective and tumor-selective death receptor 5-mediated tumor regression. Sci Rep. 2025; 15:9909.
79. Jin S, Sun Y, Liang X, Gu X, Ning J, Xu Y, Chen S, Pan L. Emerging new therapeutic antibody derivatives for cancer treatment. Signal Transduct Target Ther. 2022; 7:39.
80. Dai H, Chen X, Yang J, Wang Y, Loiola RA, Lu A, Cheung KCP. Insights and therapeutic advances in pancreatic cancer: The role of electron microscopy in decoding the tumor microenvironment. Front Cell Dev Biol. 2024; 12:1460544.
81. Xiao Y, Pan T, Da W, Liu Y, Chen S, Chen D, Liu K, Zheng Y, Xie D, Gao Y, Xu H, Sun Y, Tan W. Aptamer-drug conjugates-loaded bacteria for pancreatic cancer synergistic therapy. Signal Transduct Target Ther. 2024; 9:272.
82. Li T, Yu X, Wan X, Liu J, Zheng J, Sun Z, Zhao Y, Chen J, Chen H, Yang Y, Jiang B. Exploiting synthetic lethality in PDAC with antibody drug conjugates and ATR inhibition. Eur J Med Chem. 2025; 286:117305.
83. Tsujii S, Serada S, Fujimoto M, Uemura S, Namikawa T, Nomura T, Murakami I, Hanazaki K, Naka T. Glypican-1 is a novel target for stroma and tumor cell dual-targeting antibody-drug conjugates in pancreatic cancer. Mol Cancer Ther. 2021; 20:2495-2505.
84. Munekage E, Serada S, Tsujii S, Yokota K, Kiuchi K, Tominaga K, Fujimoto M, Kanda M, Uemura S, Namikawa T, Nomura T, Murakami I, Hanazaki K, Naka T. A glypican-1-targeted antibody-drug conjugate exhibits potent tumor growth inhibition in glypican-1-positive pancreatic cancer and esophageal squamous cell carcinoma. Neoplasia. 2021; 23:939-950.
85. Tsumura R, Anzai T, Koga Y, Takashima H, Matsumura Y, Yasunaga M. Anti-tissue factor antibody conjugated with monomethyl auristatin E or deruxtecan in pancreatic cancer models. Cancer Sci. 2024; 115:3986-3996.
86. Nieto-Jiménez C, Sanvicente A, Díaz-Tejeiro C, Moreno V, Lopez de Sá A, Calvo E, Martínez-López J, Pérez-Segura P, Ocaña A. Uncovering therapeutic opportunities in the clinical development of antibody-drug conjugates. Clin Transl Med. 2023; 13:e1329.
87. Li Q, Kong Y, Zhong Y, Huang A, Ying T, Wu Y. Half-life extension of single-domain antibody-drug conjugates by albumin binding moiety enhances antitumor efficacy. MedComm. 2024; 5:e557.

88. Wang H, Huangfu S, Wei D, Sun Z, Wu Y, Yu X, Jiang B, Chen H. Triptolide-based cleavable antibody-drug conjugates for pancreatic cancer. Eur J Med Chem. 2025; 295:117798.
89. Papacharisi E, Braun AC, Vranic M, Pahl AM, Hechler T. Novel amanitin-based antibody-drug conjugates targeting TROP2 for the treatment of pancreatic cancer. Mol Cancer Ther. 2025; 24:485-496.
90. Nakazawa Y, Miyano M, Tsukamoto S, *et al.* Delivery of a BET protein degrader *via* a CEACAM6-targeted antibody-drug conjugate inhibits tumour growth in pancreatic cancer models. Nat Commun. 2024; 15:2192.
91. Guo Y, Shen Z, Zhao W, *et al.* Rational identification of novel antibody-drug conjugate with high bystander killing effect against heterogeneous tumors. Adv Sci (Weinh). 2024; 11:e2306309.

Received September 3, 2025; Revised November 11, 2025; Accepted November 17, 2025.

[§]These authors contributed equally to this work.
**Address correspondence to:*
Jihui Hao, Department of Pancreatic Cancer, Tianjin Medical University Cancer Institute and Hospital, Hexi District, Huanhuxi Road, Tianjin 300060, China.
E-mail: haojihui@tjmuch.com

Antao Chang, Department of Pancreatic Cancer, Tianjin Medical University Cancer Institute and Hospital, Hexi District, Huanhuxi Road, Tianjin 300060, China.
E-mail: changantao@tjmuch.com

Weishuai Liu, Department of Pain Management, Tianjin Medical University Cancer Institute and Hospital, Hexi District, Huanhuxi Road, Tianjin 300060, China.
E-mail: liuweishuai@tjmuch.com

Released online in J-STAGE as advance publication November 19, 2025.

Original Article

DOI: 10.5582/bst.2026.01030

Dietary patterns and metabolic syndrome in a population living at a high altitude and consuming a halal diet: A cross-sectional study combining Dietary Approaches to Stop Hypertension (DASH) principles and locally derived patterns

Yuanzheng Liu[1,§], Tiemei Li[2,§], Wen Peng[3], Peipei Song[4,*], Yanming Ren[1,*]

[1] Department of Traditional Chinese Medicine, Qinghai University Medical College, Xining, Qinghai, China;
[2] Department of Maternal, Child and Adolescent Health, School of Public Health, Anhui Medical University, Hefei, Anhui, China;
[3] Department of Public Health, Qinghai University Medical College, Xining, Qinghai, China;
[4] Center for Clinical Sciences, Japan Institute for Health Security, Tokyo, Japan.

SUMMARY: Metabolic syndrome (MetS), characterized by the clustering of metabolic risk factors, substantially increases the risk of cardiovascular disease and type 2 diabetes. Although dietary patterns (DPs) are known to influence MetS, evidence remains limited regarding the applicability of established dietary principles in populations living at a high altitude in an environment with a halal diet. This study examined the associations between both a priori and locally derived DPs and MetS and its components, with particular emphasis on low high-density lipoprotein cholesterol (HDL-C). A cross-sectional analysis was performed among 1,133 adults ages 18–80 using data from an ongoing pilot cohort study (2024–2025). DPs were identified using a modified Dietary Approaches to Stop Hypertension (DASH) score and factor analysis. Associations with MetS and its components were assessed using inverse probability of exposure-weighted logistic regression. Subgroup and interaction analyses evaluated effect modification, and mediation analysis examined the mediating role of being overweight. The prevalence of MetS was 54.81%. Three major DPs were identified: the Sugary Drinks and Fast-Food Pattern, the Halal Protein-Rich Pattern, and the Traditional Grain and Tonic Pattern. The DASH score was moderately correlated with the Halal Protein-Rich Pattern (Spearman's $r = 0.37$). Participants in the highest tertile of the Halal Protein-Rich Pattern had a significantly lower risk of MetS compared to those in the lowest tertile (OR = 0.64, 95% CI: 0.45–0.92; p for trend < 0.05), as well as a 35% lower risk of low HDL-C. In contrast, higher adherence to the Sugary Drinks and Fast-Food Pattern was associated with an increased risk of low HDL-C. Similar protective associations were observed for higher DASH scores. Subgroup analyses showed that the Halal Protein-Rich Pattern was inversely associated with MetS among overweight participants (OR = 0.80, 95% CI: 0.66–0.96). Mediation analysis indicated that being overweight mediated 19.84% of the association between the Halal Protein-Rich Pattern and MetS. In conclusion, in a high-altitude environment with a halal diet, both DASH and a culturally adapted Halal Protein-Rich Pattern were inversely associated with MetS and low HDL-C in particular. DASH offers an evidence-based guideline, while the Halal Protein-Rich Pattern reflects a culturally appropriate and locally practical diet. Longitudinal studies are warranted to confirm these findings.

Keywords: metabolic syndrome (MetS), populations living at a high altitude, dietary pattern, cross-sectional study

1. Introduction

Metabolic syndrome (MetS), defined as the clustering of abdominal obesity, dyslipidemia, hypertension, and impaired glucose regulation, is a major risk factor for type 2 diabetes, cardiovascular disease, and premature mortality (*1,2*). Over the past two decades, the global burden of MetS has continued to rise. A comprehensive analysis of data from 2000 to 2023 shows that the prevalence of MetS increased from 14.7% to 31.0% among women and from 9.0% to 25.7% among men. By 2023, approximately 1.54 billion adults worldwide were estimated to have MetS, including 846 million women and 692 million men (*3*). These metabolic abnormalities substantially elevate the risk of type 2 diabetes and cardiovascular disease (*4,5*), positioning MetS as a major and growing public health challenge globally. Based on surveillance data from 2015 to 2017 covering 31 Chinese

provinces and individuals age 20 and older, the burden of metabolic abnormalities associated with MetS remains substantial and increases significantly with age. The standardized prevalence was 39.0% among individuals ages 45–59, 43.9% among those ages 60–74, and 44.2% among those age 75 and older. Among obese individuals, the prevalence can be as high as 70% (*6*). Given the aging population and rising obesity rates in China (*7,8*), these findings emphasize that MetS prevention and control efforts should particularly focus on older populations and those who are overweight or obese. Among Asian populations, low high-density lipoprotein cholesterol (HDL-C) is a common dyslipidemic phenotype and is associated with cardiometabolic risk (*9,10*). In underdeveloped and rural areas of China, low HDL-C is a substantial contributor to dyslipidemia and remains prevalent (*11-13*), underscoring the practical significance of jointly investigating MetS and low HDL-C in populations of interest.

The unique characteristics of high-altitude environments result in more complex patterns of MetS prevalence. Several studies at high altitudes suggested that the prevalence of MetS may be lower than in some low-altitude areas (*14-16*), but variations in lifestyle, socioeconomic status, and diagnostic criteria across regions can lead to significant fluctuations in results (with prevalence ranging from 6.2% to 32.8%) (*17-19*). In the high-altitude regions of Qinghai Province (1900–3710 meters), the prevalence of MetS, as measured by the guidelines of the Chinese Diabetes Society, was 21.1% (*20*). Qinghai Province is part of the Qinghai–Tibet Plateau and is a region settled by multiple ethnic groups. In addition to Han and Tibetan populations, long-established ethnic minorities such as Hui, Salar, and Tu also reside in Qinghai (*21*).

The prevalence of MetS varies significantly between different ethnic groups (*22-25*). Several studies have shown that the prevalence of MetS in the Hui population is higher compared to other ethnic groups, such as the Han (*17,26,27*). In a nationwide cross-sectional survey, the prevalence of MetS was 22.82% in the Hui population, 19.80% in the Han population, and 6.17% in the Tibetan population (*17*). However, the prevalence of MetS in areas with plateaus, including those inhabited by the Hui, Salar, and Han populations consuming halal food, remains unclear due to considerable variation in results, and this needs to be clarified through empirical research rather than relying on past experience.

In global chronic disease prevention, diet is widely recognized as one of the most critical modifiable factors, and international guidelines are increasingly shifting toward optimizing overall dietary patterns (DPs) with a food-based emphasis (*28,29*). The updated 2025-2030 Dietary Guidelines for Americans notably reinforce an "Eat real food" orientation, prioritizing whole and minimally processed foods while reducing the intake of highly processed foods and added sugars to enhance real-world feasibility (*30*). Compared to individual nutrients, DPs provide a more stable reflection of food combinations and real-life eating behaviors (*1,31-33*). International guidelines and authoritative institutions emphasize the importance of healthy diets in cardiovascular metabolic risk management, including dietary frameworks such as the Dietary Approaches to Stop Hypertension (DASH) (*34,35*). However, the evidence supporting DASH primarily originates from Western dietary contexts, where the foundational food composition, nutrient ratios, and cooking methods differ significantly from those in the Northwestern plateau regions of China. Directly extrapolating this framework to populations living at a high altitude and consuming a halal diet may overlook the multidimensional influences of ethnic culture, environmental adaptation, and metabolic exposure.

The aim of this study was to explore the relationship between DPs and MetS and its components in the context of a halal dietary culture on the Qinghai Plateau. Although research on the influence of different dietary cultures on MetS is available, studies on the metabolic burden and protective effects of halal DPs in high-altitude areas remain scarce. This study's aim was to assess the impact of DPs on MetS and key components, such as low HDL-C, in the context of a halal diet in plateau regions by combining a priori DP (DASH) with a posteriori DP (principal component analysis, PCA), providing a theoretical basis for future dietary interventions in high-altitude regions.

2. Materials and Methods

2.1. Study population

This study was a cross-sectional analysis of an ongoing pilot cohort study of natural populations on the Qinghai-Tibet Plateau (2024-0204-SFC-0019). Multistage, stratified, cluster-randomized sampling was used to select participants in a halal dietary culture in eastern Qinghai Province between August 2024 and July 2025, yielding a total of 1,307 individuals. Inclusion criteria were residents ages 18–80 who had lived in plateau regions for at least 12 months (*36,37*). Exclusion criteria were pregnant or breastfeeding women, individuals with severe mental or cognitive impairments, and individuals unable to complete the survey due to illness. Demographic, socioeconomic, dietary, medication, and lifestyle information were collected through standardized face-to-face interviews. In the absence of reliable prior estimates of MetS prevalence in specific populations in this region, the minimum required sample size was calculated using a single-sample proportion formula. Based on previous research indicating a prevalence of MetS of 21.10% among populations in high-altitude areas of Qinghai Province (*20*), with a *p*-value of 0.05, a 95% confidence level (Z = 1.96), and

an allowable error of d = 0.05, the minimum sample size was determined to be approximately 256 individuals. Considering the potential design effect and non-response rate associated with multistage cluster sampling, a design effect of 2.0 was applied, and a non-response rate of 20% was assumed. This resulted in a target minimum sample size of 640 individuals. Individuals from ethnic groups with small sample sizes, including the Tu (n = 20), Mongolians (n = 8), and Tibetans (n = 9), were excluded. In addition, 137 participants were excluded due to missing key variables or extreme values. Ultimately, 1,133 adults were included in the final analysis. All investigators received standardized training before the formal survey, and written informed consent was obtained from all participants before data collection. The study was approved by the Medical Ethics Committee of the School of Medicine, Qinghai University (Approval No. 2023-027).

2.2. Dietary assessment

Dietary intake was assessed using a semi-quantitative food frequency questionnaire (FFQ). This questionnaire asked about the usual frequency of consumption and portion size of 47 food items over the past year. This list of foods was developed based on local dietary habits, as determined by market surveys, and was then reviewed by nutrition experts. The dietary questionnaire used in this cohort study was adapted from the survey tool used in the Chronic Diseases and Their Risk Factors Surveillance among Adult Residents at Disease Surveillance Sites in Qinghai Province study (*38*). To ensure the questionnaire was suitable for this research context, its reliability and validity were assessed. Cronbach's alpha was 0.768, indicating acceptable internal consistency (*39*). The Kaiser–Meyer–Olkin (KMO) value was 0.752, and Bartlett's test of sphericity yielded a significant result ($p < 0.001$), confirming that the data are suitable for factor analysis.

For each food category, participants reported intake (converted to average grams per meal using standard portion templates) and consumption frequency (ranging from multiple times daily to several times monthly). Beverage and salt-related exposure independently impact metabolic outcomes but is often overlooked in conventional food group aggregations, participants were asked separately about tea and sugar-sweetened beverage consumption. In addition, the data were supplemented with information on high-salt foods and primary sources of salt, such as pickled foods, to better characterize local DPs and modifiable exposure. To accommodate cultural and religious sensitivities among the primary population, the questionnaire did not include questions about individual smoking and drinking habits. However, given the significant health implications of environmental exposure, a question on passive smoking was retained. Using the aforementioned FFQ, total daily energy intake was estimated based on the Chinese Food Exchange List and the 2018 Chinese Food Composition Table (*40,41*) (Supplementary Table S1, *https://www.biosciencetrends.com/action/getSupplementalData.php?ID=288*).

2.3. Assessment of DPs

To better ascertain the dietary characteristics of the study population, all participants were scored for adherence to specific DPs, including the predefined DASH diet and three posterior DPs derived from baseline cohort data. Adherence to the DASH diet was evaluated using a modified DASH score, in which low-fat and fat-free dairy products were substituted with full-fat dairy products because of their very low consumption in the study population (*42,43*). Processed soy products, such as bean flour dough, are excluded from the DASH diet, which emphasizes low-sodium intake and unprocessed legumes and nuts (*44*). In addition, nuts were excluded due to their extremely limited consumption and lack of a distinct food group in the FFQ. For each food component of the DASH diet, food groups were classified into quintiles, and participants were assigned scores from 1 to 5 based on their intake rank. The total score was then calculated by summing the individual component scores (*45*) (Supplementary Table S2, *https://www.biosciencetrends.com/action/getSupplementalData.php?ID=288*).

A posteriori DPs were identified *via* factor analysis of each variable's correlation matrix, using PCA with maximum variance rotation. The KMO sampling adequacy measure (KMO = 0.762) and Bartlett's sphericity test ($p < 0.001$) indicated that the data were suitable for factor analysis. To determine the number of factors to retain, a comprehensive approach was adopted, considering eigenvalues, scree plots, and interpretability (Supplementary Figure S1, *https://www.biosciencetrends.com/action/getSupplementalData.php?ID=288*). Food groups contributing significantly to specific DPs were identified by selecting factor loadings greater than 0.30 (*18*) for the three rotated factors. The final three DPs were identified, accounting for 21.64% of the total cumulative variance. Subsequently, DP scores (factor scores) were calculated, and each pattern was divided into three tertile groups (T1–T3). T1 represents the low-score group, while T2 and T3 represent the medium and high-score groups, respectively.

2.4. Outcome variable

Participants were diagnosed with MetS if they met at least three of the following five criteria (*46*): *i*) Elevated waist circumference (WC): WC ≥ 90 cm in men or ≥ 80 cm in women; *ii*) elevated blood pressure (BP): systolic BP ≥ 130 mmHg or diastolic BP ≥ 85 mmHg, or self-reported hypertension; *iii*) Reduced HDL-C: HDL-C

< 1.03 mmol/L in men or < 1.30 mmol/L in women, or receiving lipid-lowering treatment; *iv*) elevated triglycerides (TG): TG ≥ 1.7 mmol/L, or on medication for elevated TG; and *v*) Impaired fasting glucose (IFG): IFG ≥ 5.6 mmol/L, or self-reported diabetes.

2.5. Covariates

In this study, covariates were selected using the directed acyclic graph (*47*) method within a causal inference framework (Supplementary Figure S2, *https://www.biosciencetrends.com/action/getSupplementalData.php?ID=288*). Potential confounding factors that could affect the association between DPs and MetS were identified. Crude was an unadjusted model. Model 1 was adjusted for age and sex. Model 2 was further adjusted for level of education, ethnicity, physical activity, passive smoking, household income, family history of diabetes, family history of hypertension, and marital status.

2.6. Statistical analysis

Continuous variables are expressed as the mean ± SD and were compared using the Student's *t*-test. Categorical variables are expressed as frequencies (percentages) and were compared using the χ^2 test or Fisher's exact test. DPs were identified using PCA, and food items with factor loadings ≥ 0.30 were considered meaningful contributors. Factor scores were used to categorize DPs into tertiles of low (T1), medium (T2), and high (T3), with the lowest tertile serving as the reference group.

Marginal structural models, which combined logistic regression with the inverse probability of exposure weighting (IPEW), were used to estimate associations between the four DP score tertiles and MetS, as well as its components separately. The lowest tertile of the DP score served as the reference group. To determine the preferred weighting method, six weighting methods were used in the primary analysis, with the tertiles of DP scores serving as the dependent variable and confounders identified by DAGs serving as the independent variables. The balance of confounders across different exposure groups was then assessed. In the final model, entropy balancing weighting due to the optimal balance of confounders (Supplementary Figure S3, *https://www.biosciencetrends.com/action/getSupplementalData.php?ID=288*) was used. The results of the effect were expressed as odds ratios (ORs) and 95% confidence intervals (CIs).

Stratified analyses by predefined subgroups (including sex, age, ethnicity, level of education, employment status, income, and BMI) are also presented for MetS and its components. In addition, logistic regression was used to explore the associations between each food group in the FFQ and MetS, as well as its components. Then, to further illustrate the associations between DPs and MetS and low HDL-C, the mediating effects of overweight status, the neutrophil-to-lymphocyte ratio (NLR), and the systemic immune-inflammation index (SII) were explored. All statistical analyses were performed using R version 4.5.1 and Stata version 18.

3. Results

3.1. Characteristics of DPs

The DASH score ranged from 10 to 34. Participants were categorized into tertiles (T1–T3) of DASH adherence (Supplementary Table S3, *https://www.biosciencetrends.com/action/getSupplementalData.php?ID=288*). Compared to participants in the lowest tertiles (T1), those in the highest tertiles (T3) reported higher intakes of fruits, vegetables, whole grains, and legumes/nuts, and low intakes of sodium, red/processed meat, and sugar-sweetened beverages.

Using factor analysis, three distinct DPs were identified (Table 1, Supplementary Figure S1, *https://www.biosciencetrends.com/action/getSupplementalData.php?ID=288*). The Sugary Drinks and Fast-Food Pattern was characterized by frequent consumption of barbecued foods, instant rice noodles, functional beverages, carbonated beverages, instant noodles, other sugary beverages, pure fruit juices, processed meats, fried foods, sugar-sweetened tea beverages, and desserts. The Halal Protein-Rich Pattern was characterized by a high consumption of mushrooms, dried bean curd sticks, tofu, edible fungi, algae, chicken, cow and sheep milk, yogurt, fresh fruit, bean flour dough, corn, mutton, animal offal, dried vegetables, and millet. The Traditional Grain and Tonic Pattern was characterized by frequent consumption of wolfberries, red dates, eight treasure tea, beef, vermicelli, dried fruits, potatoes, and sweet potatoes, as well as fried flour-based foods.

3.2. Baseline characteristics according to the lowest and highest tertiles of the various dietary scores

This study enrolled 1,133 participants in 2025. The mean age was 54.58 ± 12.11 years. The prevalence of MetS was 54.81% (56.73% in males and 53.23% in females). Among overweight individuals, the prevalence of MetS was 55.49%, and the prevalence of low HDL-C was 51.10%. The study population predominantly consisted of Hui (45.45%) and Salar (43.78%) participants, with Han participants accounting for 10.77%. Compared to participants without MetS, those with MetS were significantly older, had a greater WC, and higher BMI, had a lower level of education and lower levels of physical activity (Supplementary Table S3, *https://www.biosciencetrends.com/action/getSupplementalData.php?ID=288*; $p < 0.05$).

Table 1. Dietary patterns identified by principal component analysis in an environment with halal food in Qinghai

Variable	Sugary Drinks and Fast-Food Pattern	Halal Protein-Rich Pattern	Traditional Grain and Tonic Pattern
	Factor1	Factor2	Factor3
Barbecued Foods	0.6206	0.0434	0.2133
Instant Rice Noodles	0.6165	-0.008	-0.015
Functional Beverages	0.6124	0.1553	-0.0429
Carbonated Beverages	0.6053	0.0562	0.0395
Instant Noodles	0.5969	0.0117	0.0542
Other Sugary Beverages	0.5765	0.1218	0.0033
Pure Fruit Juice	0.5751	0.1979	-0.0382
Processed Meat	0.5636	0.1098	-0.0634
Fried Food	0.5273	-0.0276	0.3017
Sugar-sweetened Tea Beverages	0.5067	0.2454	-0.0504
Desserts	0.4433	0.1087	0.1078
Mushrooms	0.1159	0.5547	0.0431
Dried Bean Curd Sticks	0.1773	0.5418	0.1513
Fresh Tofu	0.057	0.5278	0.146
Edible Fungi	0.0928	0.5199	0.0677
Algae	0.2021	0.4689	-0.0565
Chicken	0.0913	0.4516	0.2225
Cow and Sheep Milk	0.0828	0.4308	0.1183
Yogurt	0.231	0.4279	0.2563
Fresh Fruits	0.0872	0.4119	0.3245
Bean Flour Dough	0.1278	0.3719	0.0536
Corn	0.0026	0.3588	0.0068
Mutton	0.1023	0.3522	0.303
Animal Offal	0.0477	0.3423	0.023
Dried Vegetables	0.2263	0.3297	0.0329
Millet	0	0.3224	-0.0664
Wolfberries	-0.0297	0.1384	0.7082
Red Dates	-0.0152	0.0921	0.7074
Eight Treasure Tea	0.2477	-0.0747	0.5269
Beef	0.0295	0.1705	0.4519
Vermicelli	0.1288	0.1331	0.4009
Dried Fruits	0.1575	0.2262	0.355
Potatoes And Sweet Potatoes	0.0125	-0.0553	0.3155
Fried Flour-Based Foods	0.2692	-0.0629	0.3011
Variances explained (%)	7.57%	7.07%	7.01%
Cumulative variance explained (%)	7.57%	14.64%	21.64%

Method of extraction: Principal component analysis with varimax rotation. Tables in bold indicate absolute factor loadings are higher than 0.30 and considered to belong to the corresponding dimension in the column. Red: positive scores; blue: negative scores; darker colors indicate higher DP scores.

Demographic and lifestyle characteristics of 1,133 participants are shown based on tertiles of four DP scores (Table 2). Participants in the T3 for the Sugary Drinks and Fast-Food Pattern were the youngest (51.81 ± 12.82 years), had a median household income between 10,000–50,000 CNY, a higher level of education, and more moderate-to-vigorous physical activity. Compared to participants in T1, those in T3 of the Halal Protein-Rich Pattern were younger, had a lower level of education, engaged more frequently in moderate-to-vigorous physical activity, and were more likely to be exposed to passive smoking. Participants in the high-scoring Traditional Grain and Tonic Pattern (T3) reported higher exposure to passive smoking, included

Table 2. Demographic and lifestyle characteristics of participants by tertiles of major dietary patterns scores in Qinghai (n = 1133)

		Sugary Drink and Fast-Food Pattern				Halal Protein-Rich Pattern			
	All (n = 1,133)	T1 (n = 397)	T2 (n = 373)	T3 (n = 363)	p	T1 (n = 377)	T2 (n = 378)	T3 (n = 378)	p
Sex, n (%)									
Male	513 (45.28%)	172 (43.32%)	148 (39.68%)	193 (53.17%)	< 0.001	168 (44.56%)	163 (43.12%)	182 (48.15%)	0.237
Female	620 (54.72%)	225 (56.68%)	225 (60.32%)	170 (46.83%)		209 (55.44%)	215 (56.88%)	196 (51.85%)	
Age, years	54.58 ± 12.11	56.43 ± 10.64	56.74 ± 10.97	50.34 ± 13.59	< 0.001	56.05 ± 11.32	55.06 ± 11.71	52.65 ± 13.02	0.001
Weight, kg	68.98 ± 12.11	68.84 ± 12.17	67.70 ± 12.17	70.53 ± 11.86	0.044	68.06 ± 12.12	68.81 ± 12.09	70.31 ± 12.06	0.139
BMI, kg/m^2	26.44 ± 3.12	26.52 ± 3.35	26.35 ± 2.98	26.44 ± 3.00	0.753	26.46 ± 3.16	26.45 ± 3.04	26.41 ± 3.17	0.966
Waist, cm	93.44 ± 8.51	93.86 ± 8.13	93.66 ± 8.12	92.74 ± 9.26	0.184	93.08 ± 8.53	93.62 ± 9.13	93.62 ± 7.84	0.601
SBP, mmHg	132.82 ± 35.09	132.25 ± 18.60	136.46 ± 54.83	129.71 ± 18.95	0.033	136.27 ± 54.61	132.17 ± 19.54	130.02 ± 17.92	0.056
DBP, mmHg	81.19 ± 11.59	81.70 ± 11.63	81.27 ± 10.68	80.55 ± 12.41	0.420	81.31 ± 11.20	80.75 ± 11.78	81.52 ± 11.78	0.646
HDL, mmol/L	1.16 ± 0.22	1.19 ± 0.23	1.16 ± 0.21	1.13 ± 0.23	0.009	1.13 ± 0.22	1.17 ± 0.23	1.18 ± 0.22	0.002
LDL, mmol/L	3.31 ± 0.78	3.35 ± 0.74	3.30 ± 0.82	3.28 ± 0.79	0.641	3.28 ± 0.81	3.36 ± 0.79	3.30 ± 0.73	0.527
GLU, mmol/L	5.15 ± 2.00	5.39 ± 2.45	5.03 ± 1.70	5.02 ± 1.70	0.030	4.92 ± 1.83	5.11 ± 2.09	5.44 ± 2.04	0.001
TG, mmol/L	1.78 ± 1.17	1.80 ± 1.34	1.71 ± 0.87	1.84 ± 1.24	0.224	1.86 ± 1.23	1.75 ± 1.02	1.74 ± 1.24	0.339
CH, mmol/L	4.83 ± 0.76	4.87 ± 0.74	4.84 ± 0.78	4.77 ± 0.76	0.149	4.79 ± 0.81	4.87 ± 0.77	4.82 ± 0.69	0.381
SII	396.35 ± 189.68	382.76 ± 164.88	403.31 ± 216.94	404.05 ± 184.64	0.167	373.04 ± 193.13	412.42 ± 208.69	403.52 ± 162.56	0.015
NLR	2.07 ± 0.88	2.06 ± 0.83	2.13 ± 1.06	2.02 ± 0.71	0.229	2.01 ± 0.91	2.10 ± 0.92	2.10 ± 0.80	0.279
Passive smoking, n (%)	143 (12.62%)	44 (11.08%)	54 (14.48%)	45 (12.40%)	0.362	57 (15.12%)	51 (13.49%)	35 (9.26%)	0.044
Income (ten thousand/year), n (%)					0.097				0.413
≤1	382 (33.72%)	139 (35.01%)	135 (36.19%)	108 (29.75%)		137 (36.34%)	126 (33.33%)	119 (31.48%)	
1-5	568 (50.13%)	194 (48.87%)	190 (50.94%)	184 (50.69%)		182 (48.28%)	197 (52.12%)	189 (50.00%)	
≥5	183 (16.15%)	64 (16.12%)	48 (12.87%)	71 (19.56%)		58 (15.38%)	55 (14.55%)	70 (18.52%)	
Ethnicity, n (%)					0.001				< 0.001
Hui	515 (45.45%)	160 (40.30%)	186 (49.87%)	169 (46.56%)		268 (71.09%)	166 (43.92%)	81 (21.43%)	
Salar	496 (43.78%)	197 (49.62%)	135 (36.19%)	164 (45.18%)		70 (18.57%)	163 (43.12%)	263 (69.58%)	
Han	122 (10.77%)	40 (10.08%)	52 (13.94%)	30 (8.26%)		39 (10.34%)	49 (12.96%)	34 (8.99%)	
Job, n (%)					< 0.001				< 0.001
Agri-forestry worker	901 (79.52%)	319 (80.35%)	325 (87.13%)	257 (70.80%)		325 (86.21%)	311 (82.28%)	265 (70.11%)	
Public employee	121 (10.68%)	30 (7.56%)	21 (5.63%)	70 (19.28%)		29 (7.69%)	34 (8.99%)	58 (15.34%)	
Other	111 (9.80%)	48 (12.09%)	27 (7.24%)	36 (9.92%)		23 (6.10%)	33 (8.73%)	55 (14.55%)	
Level of education, n (%)					< 0.001				< 0.001
Below primary school	664 (65.68%)	263 (73.67%)	235 (73.21%)	166 (49.85%)		248 (73.37%)	211 (64.13%)	205 (59.59%)	
Primary school	188 (18.60%)	54 (15.13%)	50 (15.58%)	84 (25.23%)		41 (12.13%)	77 (23.40%)	70 (20.35%)	
Junior high school and above	159 (15.73%)	40 (11.20%)	36 (11.21%)	83 (24.92%)		49 (14.50%)	41 (12.46%)	69 (20.06%)	

DP scores were stratified into equal tertiles, T1-T3, representing the lowest to highest tertiles of dietary pattern scores. *Abbreviations*: MetS, metabolic syndrome; WC, waist circumference; BP, blood pressure; HDL-C, high-density lipoprotein cholesterol; TAG, triacylglycerol; SII, systemic immune-inflammation index; NLR, neutrophil-to-lymphocyte ratio; BMI, body mass index; SBP, systolic blood pressure; DBP, diastolic blood pressure; HDL, high-density lipoprotein cholesterol; LDL, low-density lipoprotein cholesterol; GLU, fasting plasma glucose; TG, triglycerides; CH, total cholesterol; IFG, impaired fasting glucose.

Table 2. Demographic and lifestyle characteristics of participants by tertiles of major dietary patterns scores in Qinghai (*n* = 1133) (continued)

	Sugary Drink and Fast-Food Pattern					Halal Protein-Rich Pattern			
	All (*n* = 1,133)	T1 (*n* = 397)	T2 (*n* = 373)	T3 (*n* = 363)	*p*	T1 (*n* = 377)	T2 (*n* = 378)	T3 (*n* = 378)	*p*
Marital , *n* (%)					0.344				0.452
Married	1005 (88.70%)	354 (89.17%)	336 (90.08%)	315 (86.78%)		337 (89.39%)	339 (89.68%)	329 (87.04%)	
Unmarried/widowed/ divorced/separated	128 (11.30%)	43 (10.83%)	37 (9.92%)	48 (13.22%)		40 (10.61%)	39 (10.32%)	49 (12.96%)	
Physical activity , *n* (%)					0.111				< 0.001
Light	935 (82.52%)	324 (81.61%)	320 (85.79%)	291 (80.17%)		336 (89.12%)	308 (81.48%)	291 (76.98%)	
Moderate/Heavy	198 (17.48%)	73 (18.39%)	53 (14.21%)	72 (19.83%)		41 (10.88%)	70 (18.52%)	87 (23.02%)	
Mets	621 (54.81%)	222 (55.92%)	219 (58.71%)	180 (49.59%)	0.039	225 (59.68%)	206 (54.50%)	190 (50.26%)	0.034
Hypertension	510 (45.01%)	186 (46.85%)	183 (49.06%)	141 (38.84%)	0.014	176 (46.68%)	176 (46.56%)	158 (41.80%)	0.306
Central obesity	931 (82.17%)	332 (83.63%)	321 (86.06%)	278 (76.58%)	0.002	307 (81.43%)	311 (82.28%)	313 (82.80%)	0.884
Obesity	274 (24.18%)	100 (25.19%)	83 (22.25%)	91 (25.07%)	0.568	96 (25.46%)	97 (25.66%)	81 (21.43%)	0.308
Elevated BP	702 (61.96%)	254 (63.98%)	245 (65.68%)	203 (55.92%)	0.014	246 (65.25%)	239 (63.23%)	217 (57.41%)	0.070
Elevated WC	993 (87.64%)	354 (89.17%)	340 (91.15%)	299 (82.37%)	0.001	328 (87.00%)	329 (87.04%)	336 (88.89%)	0.666
IFG	260 (22.95%)	114 (28.72%)	77 (20.64%)	69 (19.01%)	0.003	66 (17.51%)	86 (22.75%)	108 (28.57%)	0.001
Low HDL-C	579 (51.10%)	184 (46.35%)	197 (52.82%)	198 (54.55%)	0.056	223 (59.15%)	191 (50.53%)	165 (43.65%)	< 0.001
Elevated TAG	468 (41.31%)	163 (41.06%)	154 (41.29%)	151 (41.60%)	0.989	177 (46.95%)	153 (40.48%)	138 (36.51%)	0.013

DP scores were stratified into equal tertiles, T1-T3, representing the lowest to highest tertiles of dietary pattern scores. *Abbreviations*: MetS, metabolic syndrome; WC, waist circumference; BP, blood pressure; HDL-C, high-density lipoprotein cholesterol; TAG, triacylglycerol; SII, systemic immune-inflammation index; NLR, neutrophil-to-lymphocyte ratio; BMI, body mass index; SBP, systolic blood pressure; DBP, diastolic blood pressure; HDL, high-density lipoprotein cholesterol; LDL, low-density lipoprotein cholesterol; GLU, fasting plasma glucose; TG, triglycerides; CH, total cholesterol; IFG, impaired fasting glucose.

Table 2. Demographic and lifestyle characteristics of participants by tertiles of major dietary patterns scores in Qinghai (n = 1133) (continued)

	Traditional Grain and Tonic Pattern				DASH			
	T1 (n = 340)	T2 (n = 391)	T3 (n = 402)	p	T1 (n = 397)	T2 (n = 412)	T3 (n = 324)	p
Sex, n (%)								
Male	148 (43.53%)	163 (41.69%)	202 (50.25%)	0.044	195 (49.12%)	182 (44.17%)	136 (41.98%)	0.136
Female	192 (56.47%)	228 (58.31%)	200 (49.75%)		202 (50.88%)	230 (55.83%)	188 (58.02%)	
Age, years	56.64 ± 12.43	54.00 ± 12.71	53.42 ± 11.01	0.001	53.70 ± 12.43	55.08 ± 11.33	55.04 ± 12.65	0.204
Weight, kg	66.50 ± 12.09	69.67 ± 11.87	70.06 ± 12.15	0.005	70.38 ± 12.29	68.56 ± 12.52	67.66 ± 11.29	0.040
BMI, kg/m^2	26.15 ± 3.00	26.70 ± 3.02	26.44 ± 3.29	0.045	26.79 ± 3.20	26.30 ± 3.15	26.20 ± 2.95	0.021
Waist, cm	93.53 ± 7.97	93.89 ± 8.16	92.92 ± 9.26	0.291	93.60 ± 9.33	93.24 ± 8.08	93.49 ± 8.01	0.827
SBP, mmHg	135.95 ± 56.96	132.34 ± 18.94	130.63 ± 19.26	0.168	133.81 ± 20.10	133.36 ± 51.76	130.91 ± 20.14	0.150
DBP, mmHg	80.93 ± 10.36	81.86 ± 11.97	80.76 ± 12.17	0.377	81.68 ± 12.43	80.47 ± 10.38	81.50 ± 11.95	0.254
HDL, mmol/L	1.17 ± 0.22	1.16 ± 0.22	1.16 ± 0.23	0.763	1.11 ± 0.22	1.19 ± 0.22	1.19 ± 0.21	< 0.001
LDL, mmol/L	3.35 ± 0.79	3.28 ± 0.78	3.32 ± 0.78	0.634	3.28 ± 0.78	3.31 ± 0.76	3.35 ± 0.81	0.667
GLU, mmol/L	5.37 ± 2.24	5.04 ± 1.69	5.09 ± 2.05	0.075	5.01 ± 1.81	4.88 ± 1.38	5.68 ± 2.68	< 0.001
TG, mmol/L	1.78 ± 0.92	1.76 ± 1.37	1.81 ± 1.14	0.824	1.88 ± 1.27	1.66 ± 0.78	1.83 ± 1.42	0.008
CH, mmol/L	4.87 ± 0.71	4.80 ± 0.76	4.82 ± 0.80	0.325	4.76 ± 0.78	4.85 ± 0.70	4.89 ± 0.80	0.076
SII	406.74 ± 180.98	394.89 ± 207.71	388.97 ± 178.23	0.401	378.07 ± 161.67	401.88 ± 208.59	411.70 ± 194.92	0.029
NLR	2.11 ± 0.83	2.08 ± 1.05	2.02 ± 0.71	0.261	2.05 ± 0.79	2.05 ± 0.88	2.13 ± 0.97	0.435
Passive smoking, n (%)	33 (9.71%)	51 (13.04%)	59 (14.68%)	0.121	49 (12.34%)	81 (19.66%)	13 (4.01%)	< 0.001
Income (ten thousand/year), n (%)				0.038				0.464
≤1	129 (37.94%)	131 (33.50%)	122 (30.35%)		127 (31.99%)	134 (32.52%)	121 (37.35%)	
1-5	163 (47.94%)	184 (47.06%)	221 (54.98%)		199 (50.13%)	214 (51.94%)	155 (47.84%)	
≥5	48 (14.12%)	76 (19.44%)	59 (14.68%)		71 (17.88%)	64 (15.53%)	48 (14.81%)	
Ethnicity, n (%)				< 0.001				< 0.001
Hui	126 (37.06%)	172 (43.99%)	217 (53.98%)		265 (66.75%)	152 (36.89%)	98 (30.25%)	
Salar	161 (47.35%)	176 (45.01%)	159 (39.55%)		122 (30.73%)	152 (36.89%)	222 (68.52%)	
Han	53 (15.59%)	43 (11.00%)	26 (6.47%)		10 (2.52%)	108 (26.21%)	4 (1.23%)	
Job, n (%)				0.009				0.011
Agri-forestry worker	269 (79.12%)	301 (76.98%)	331 (82.34%)		318 (80.10%)	335 (81.31%)	248 (76.54%)	
Public employee	29 (8.53%)	44 (11.25%)	48 (11.94%)		51 (12.85%)	40 (9.71%)	30 (9.26%)	
Other	42 (12.35%)	46 (11.76%)	23 (5.72%)		28 (7.05%)	37 (8.98%)	46 (14.20%)	
Level of education, n (%)				0.001				0.788
Below primary school	213 (74.22%)	226 (64.94%)	225 (59.84%)		250 (64.60%)	202 (66.45%)	212 (66.25%)	
Primary school	48 (16.72%)	60 (17.24%)	80 (21.28%)		69 (17.83%)	57 (18.75%)	62 (19.38%)	
Junior high school and above	26 (9.06%)	62 (17.82%)	71 (18.88%)		68 (17.57%)	45 (14.80%)	46 (14.37%)	

DP scores were stratified into equal tertiles, T1-T3, representing the lowest to highest tertiles of dietary pattern scores. *Abbreviations*: MetS, metabolic syndrome; WC, waist circumference; BP, blood pressure; HDL-C, high-density lipoprotein cholesterol; TAG, triacylglycerol; SII, systemic immune-inflammation index; NLR, neutrophil-to-lymphocyte ratio; BMI, body mass index; SBP, systolic blood pressure; DBP, diastolic blood pressure; HDL, high-density lipoprotein cholesterol; LDL, low-density lipoprotein cholesterol; GLU, fasting plasma glucose; TG, triglycerides; CH, total cholesterol; IFG, impaired fasting glucose.

Table 2. Demographic and lifestyle characteristics of participants by tertiles of major dietary patterns scores in Qinghai (*n* = 1133) (continued)

	Traditional Grain and Tonic Pattern				DASH			
	T1 (*n* = 340)	T2 (*n* = 391)	T3 (*n* = 402)	*p*	T1 (*n* = 397)	T2 (*n* = 412)	T3 (*n* = 324)	*p*
Marital , *n* (%)				0.010				0.792
Married	289 (85.00%)	346 (88.49%)	370 (92.04%)		349 (87.91%)	366 (88.83%)	290 (89.51%)	
Unmarried/widowed/divorced/separated	51 (15.00%)	45 (11.51%)	32 (7.96%)		48 (12.09%)	46 (11.17%)	34 (10.49%)	
Physical activity , *n* (%)				0.290				0.045
Light	288 (84.71%)	324 (82.86%)	323 (80.35%)		335 (84.38%)	347 (84.22%)	253 (78.09%)	
Moderate/Heavy	52 (15.29%)	67 (17.14%)	79 (19.65%)		62 (15.62%)	65 (15.78%)	71 (21.91%)	
Mets	195 (57.35%)	215 (54.99%)	211 (52.49%)	0.413	249 (62.72%)	200 (48.54%)	172 (53.09%)	< 0.001
Hypertension	162 (47.65%)	184 (47.06%)	164 (40.80%)	0.105	187 (47.10%)	177 (42.96%)	146 (45.06%)	0.496
Central obesity	287 (84.41%)	331 (84.65%)	313 (77.86%)	0.019	316 (79.60%)	344 (83.50%)	271 (83.64%)	0.251
Obesity	68 (20.00%)	104 (26.60%)	102 (25.37%)	0.091	119 (29.97%)	84 (20.39%)	71 (21.91%)	0.003
Elevated BP	224 (65.88%)	247 (63.17%)	231 (57.46%)	0.052	258 (64.99%)	252 (61.17%)	192 (59.26%)	0.265
Elevated WC	301 (88.53%)	349 (89.26%)	343 (85.32%)	0.203	339 (85.39%)	365 (88.59%)	289 (89.20%)	0.232
IFG	77 (22.65%)	90 (23.02%)	93 (23.13%)	0.987	81 (20.40%)	78 (18.93%)	101 (31.17%)	< 0.001
Low HDL-C	172 (50.59%)	209 (53.45%)	198 (49.25%)	0.484	239 (60.20%)	193 (46.84%)	147 (45.37%)	< 0.001
Elevated TAG	146 (42.94%)	149 (38.11%)	173 (43.03%)	0.284	190 (47.86%)	151 (36.65%)	127 (39.20%)	0.004

DP scores were stratified into equal tertiles, T1-T3, representing the lowest to highest tertiles of dietary pattern scores. *Abbreviations*: MetS, metabolic syndrome; WC, waist circumference; BP, blood pressure; HDL-C, high-density lipoprotein cholesterol; TAG, triacylglycerol; SII, systemic immune-inflammation index; NLR, neutrophil-to-lymphocyte ratio; BMI, body mass index; SBP, systolic blood pressure; DBP, diastolic blood pressure; HDL, high-density lipoprotein cholesterol; LDL, low-density lipoprotein cholesterol; GLU, fasting plasma glucose; TG, triglycerides; CH, total cholesterol; IFG, impaired fasting glucose.

more members of the Hui group, and were younger. The DASH high-scoring group (T3) had a higher proportion of members of the Salar group, a relatively lower BMI, engaged in moderate to vigorous physical activity, and were exposed to passive smoking at a lower frequency.

3.3. Association between DP tertiles and MetS and its components

Figure 1 shows the associations between tertiles of the DASH and Halal Protein-Rich Pattern scores and MetS and some of its components. After sequential adjustment for covariates from the crude Model to Model 2, higher scores on the Halal Protein-Rich Pattern were associated with a lower risk of MetS [Model 2 OR (95% CI): 0.74 (0.52–1.05) for T2 and 0.64 (0.45–0.92) for T3 *vs.* T1; *p* for trend < 0.05]. For low HDL-C, higher scores for the Sugary Drinks and Fast-Food Pattern were associated with increased disease risk [Model 2 OR (95% CI): 1.69 (1.20–2.39) for T2 and 1.75 (1.22–2.49) for T3; *p* for trend < 0.05]. In contrast, the Halal Protein-Rich Pattern was inversely associated with low HDL-C [Model 2 OR (95% CI): 0.52 (0.37–0.75) for T2 and 0.35 (0.24–0.51) for T3; *p* for trend < 0.05]. For elevated TG, higher Halal Protein-Rich Pattern scores were also associated with reduced disease risk [Model 2 OR (95% CI): 0.66 (0.47–0.94) for T2 and 0.49 (0.34–0.70) for T3, respectively; *p* for trend < 0.05]. However, for IFG, a higher score on the Sugary Drinks and Fast-Food Pattern was inversely associated with IFG in Model 2 [OR (95% CI): 0.63 (0.43–0.94) for T2 and 0.58 (0.38–0.87) for T3, respectively; *p* for trend < 0.05]. Conversely, higher Halal Protein-Rich Pattern scores were associated with increased risk of IFG, with OR (95% CI) values of 1.00, 1.59 (1.03–2.45), and 2.37 (1.55–3.62), respectively. Similarly, the DASH score displayed associations with these outcomes that were similar to those displayed by the Halal Protein-Rich Pattern.

In addition, the associations between individual food items and MetS, as well as HDL-C, are shown in Supplementary Table S4 (*https://www.biosciencetrends.com/action/getSupplementalData.php?ID=288)*. Chicken, fresh fruits, mutton, and bean flour dough were positively associated with the Halal Protein-Rich Pattern, which remained significantly associated with a reduced risk of low HDL-C after FDR correction.

3.4. Subgroup analysis

For simplicity, we report only the associations of two DPs (DASH and the Halal Protein-Rich Pattern) with MetS and low HDL-C (Figure 2). In individuals with a Halal Protein-Rich Pattern, a significant association with MetS was observed in the overweight subgroup. Among overweight participants, a higher Halal Protein-Rich Pattern score was associated with a lower risk of MetS (OR = 0.80, 95% CI: 0.66–0.96), but there was no significant interaction between overweight and non-overweight groups. In contrast, a significant interaction by sex was observed for the Halal Protein-Rich Pattern (*p* for interaction = 0.024) (Figure 2A). Among individuals with a higher DASH score, the risk of MetS decreased significantly in females (OR = 0.93, 95% CI: 0.88–0.98) and in the Salar subgroup (OR = 0.89, 95% CI: 0.88–0.98). A significant interaction between ethnicity and the DASH score was observed (*p* for interaction = 0.004), suggesting heterogeneity of the association across ethnic groups (Figure 2A). There were no significant differences across the remaining subgroups, and no additional interaction effects were detected. Among individuals consuming the Halal Protein-Rich Pattern, a significantly reduced risk of low HDL-C was observed in participants > the age of 60 (OR = 0.38, 95% CI: 0.24–0.57), with a significant interaction by age group (*p* for interaction < 0.001). In addition, participants engaged in agriculture, forestry, animal husbandry, and fisheries exhibited a significantly lower risk of low HDL-C (OR = 0.61, 95% CI: 0.50–0.74), with a significant interaction across occupational groups (*p* for interaction = 0.044) (Figure 2B). In contrast, there were no significant interaction effects between the DASH score and the risk of low HDL-C for any subgroup. Overall, the Halal Protein-Rich Pattern was associated with a reduced risk of low HDL-C in individuals > the age of 60 (Figure 2B).

The Halal Protein-Rich Pattern was associated with an increased risk of elevated WC and elevated IFG among participants with a primary school education or below (Supplementary Table S5, Table S6, *https://www.biosciencetrends.com/action/getSupplementalData.php?ID=288*). A significant interaction between DASH score and elevated BP was observed across age groups (Supplementary Table S7, *https://www.biosciencetrends.com/action/getSupplementalData.php?ID=288*). However, the Halal Protein-Rich Pattern was associated with a reduced risk of elevated TG among participants with primary school education or below (Supplementary Table S8, *https://www.biosciencetrends.com/action/getSupplementalData.php?ID=288*). In the remaining subgroups, the Halal Protein-Rich Pattern did not interact with DASH in terms of elevated BP, elevated TG, or IFG (Supplementary Tables S5-S8, *https://www.biosciencetrends.com/action/getSupplementalData.php?ID=288*).

3.5. Mediation analysis

To further elucidate whether being overweight mediates the associations between the Halal Protein-Rich Pattern and MetS as well as low HDL-C, a mediation analysis was performed with being overweight specified as the mediator. The same mediation analysis was performed for DASH. After adjusting for confounding factors, the total effect of the Halal Protein-Rich Pattern on

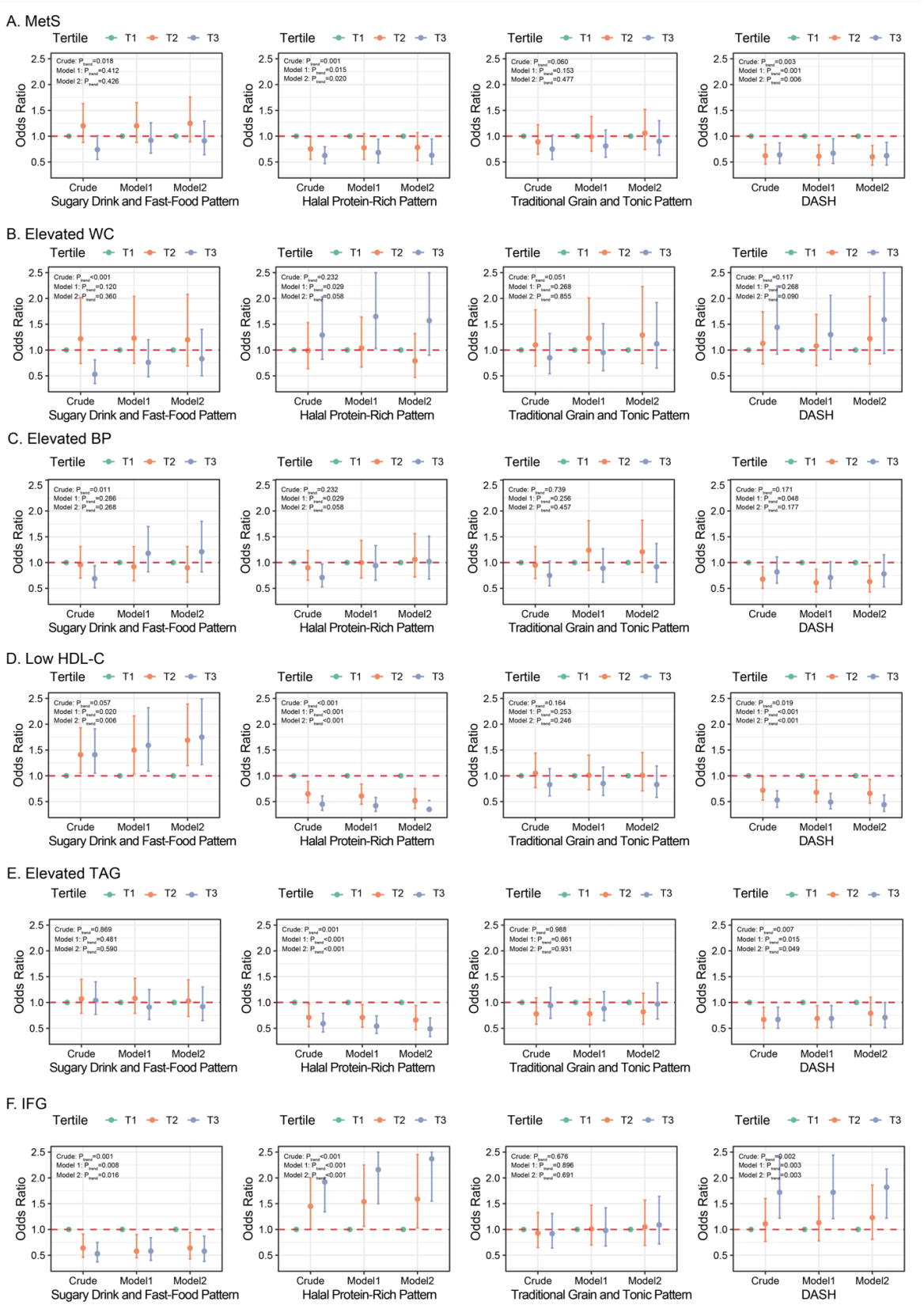

Figure 1. Associations between tertiles of three dietary pattern scores and DASH with Mets and its components in Qinghai. Crude was an unadjusted model. Model 1 was adjusted for age and sex. Model 2 was further adjusted for level of education, physical activity, passive smoking, household income, family history of diabetes, family history of hypertension, and marital status. Total energy intake was an additional adjustment variable in Model 2 for the DASH dietary pattern (not included in Model 2 of the other three DPs). DP scores were stratified into equal tertiles (T1-T3, representing the lowest to highest tertiles of DP scores, with T1 in green, T2 in orange, and T3 in blue). The filled dots represent adjusted odds ratios, and the vertical lines represent 95% confidence intervals. *Abbreviations*: DASH, Dietary Approaches to Stop Hypertension; DP, dietary pattern; MetS, metabolic syndrome; WC, waist circumference; BP, blood pressure; HDL-C, high-density lipoprotein cholesterol; TAG, triacylglycerol; IFG, impaired fasting glucose.

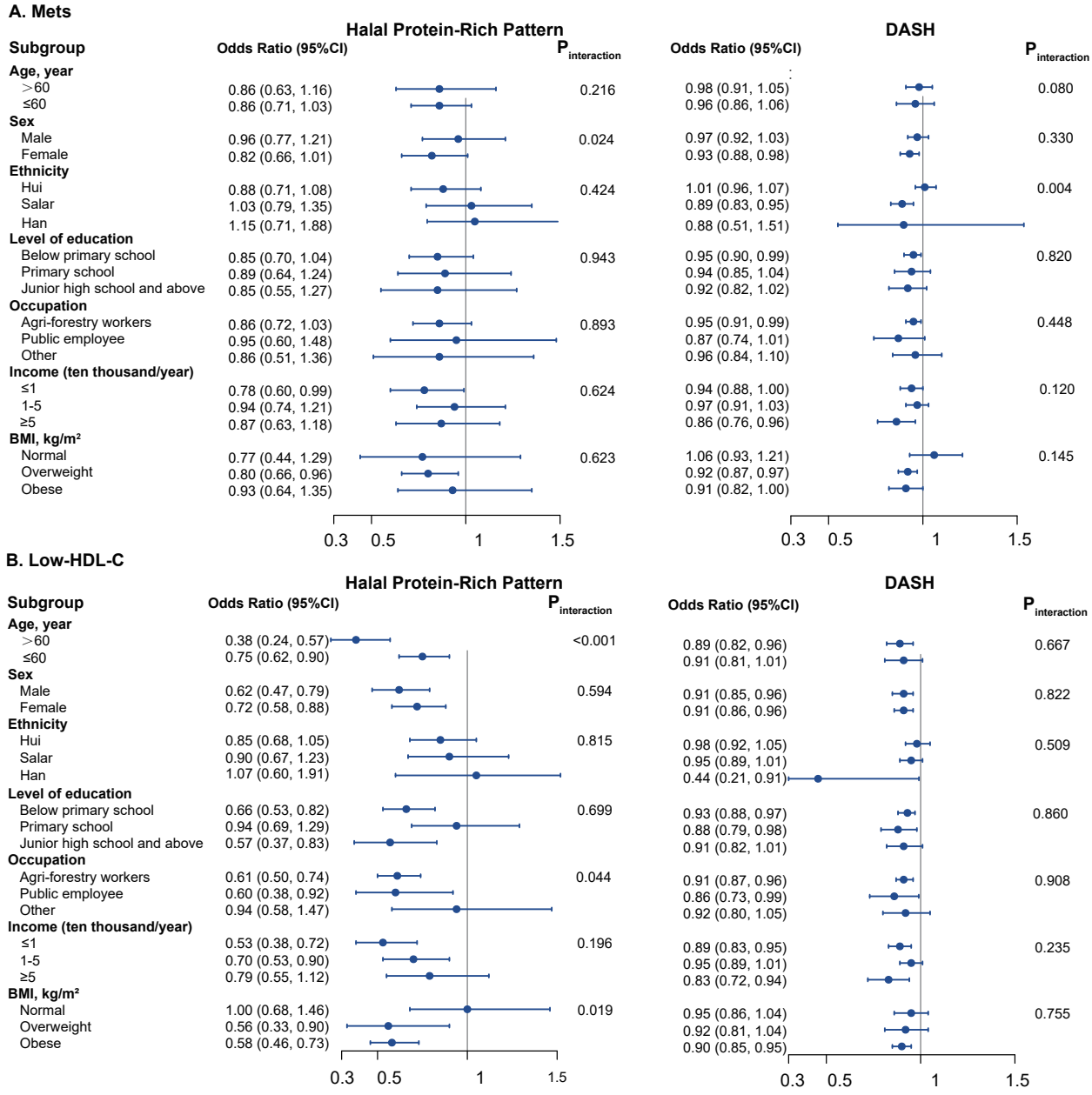

Figure 2. Stratified analysis of estimated associations between various dietary patterns and MetS risks and low HDL-C. Crude was an unadjusted model. Model 1 was adjusted for age and sex. Model 2 was further adjusted for level of education, physical activity, passive smoking, household income, family history of diabetes, family history of hypertension, and marital status. Total energy intake was an additional adjustment variable in Model 2 for the DASH DP (not included in Model 2 of the other three DPs). P-interaction was determined to examine the interaction among different subgroups. The filled blue dots represent adjusted odds ratios, and the blue lines represent 95% confidence intervals. Abbreviations: DASH, Dietary Approaches to Stop Hypertension; DP, dietary pattern; MetS, metabolic syndrome; HDL-C, high-density lipoprotein cholesterol.

MetS displayed a marginally protective association (OR = 0.87, $p = 0.084$). After additionally accounting for being overweight, the direct effect was significant (OR = 0.81, $p = 0.015$). The indirect effect, *via* being overweight, was $\beta = 0.012$ ($p = 0.020$), corresponding to 19.84% of the total effect mediated (Figure 3A). DASH displayed no significant overall effect on MetS ($p > 0.05$); nevertheless, the direct effect was significant after accounting for being overweight (OR = 0.94, $p = 0.016$). The indirect effect *via* being overweight was $\beta = 0.002$ ($p = 0.040$), accounting for 9.44% of the mediating proportion (Figure 3C).

Similarly, both DPs displayed protective associations with a low HDL-C outcome. The association with the Halal Protein-Rich Pattern remained robust after accounting for being overweight, with a strong direct effect (OR = 0.58, $p < 0.001$) and only a modest change from the total effect (OR = 0.68); the mediation effect accounted for 4.18% (Figure 3B). For DASH, the direct effect of being overweight was OR = 0.91 ($p < 0.001$), whereas the indirect effect *via* being overweight was not significant (Figure 3D). To further

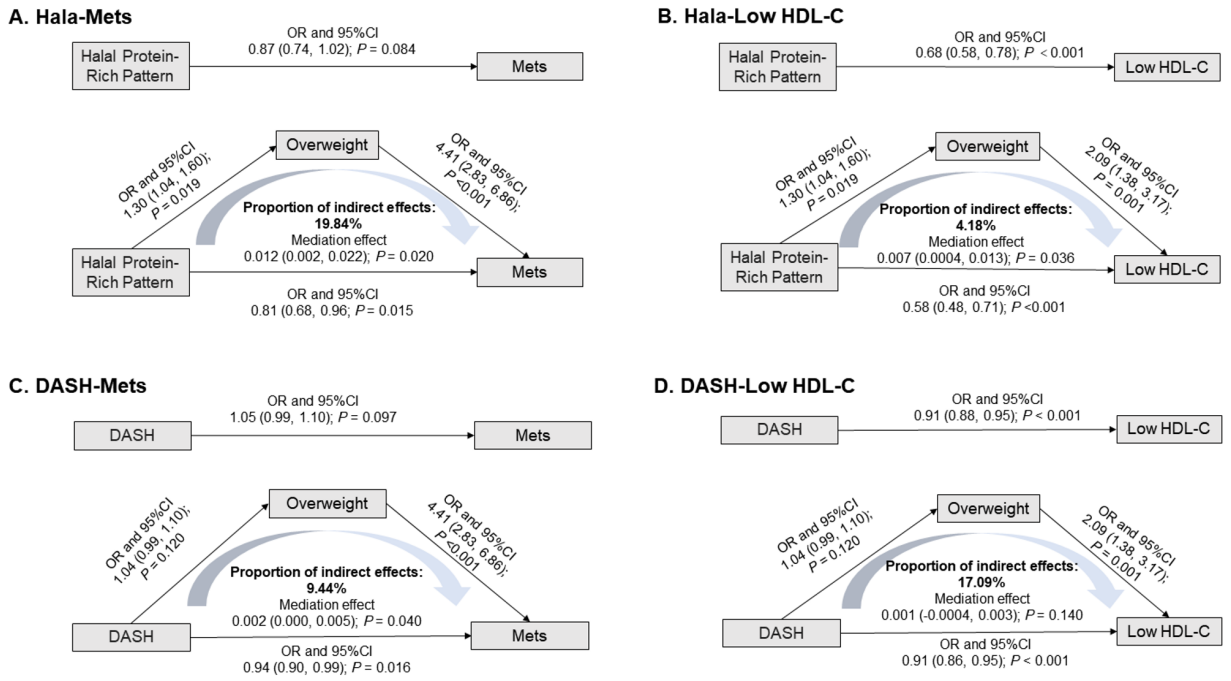

Figure 3. Mediation analysis of the associations between dietary patterns and Mets and its components mediated by being overweight. Abbreviations: DASH, Dietary Approaches to Stop Hypertension; MetS, metabolic syndrome; HDL-C, high-density lipoprotein cholesterol.

assess whether inflammatory pathways mediate the associations between DASH and the Halal Protein-Rich Pattern and MetS and low HDL-C, mediation analyses were performed using the SII and NLR as mediators. Neither SII nor NLR displayed significant indirect effects (Supplementary Figures S4 and S5, *https://www.biosciencetrends.com/action/getSupplementalData.php?ID=288*; $p > 0.05$).

4. Discussion

4.1. The key drivers: Older age and central obesity

The overall prevalence of MetS in this study was 54.81%, which is higher than that reported in some previous studies of plateau-dwelling populations. This elevated prevalence is likely driven primarily by an older age (54.58 ± 12.11) and the high burden of central obesity (82.17%) in the study population. Previous evidence consistently indicates that the prevalence of MetS increases markedly with age, reaching over 58% among individuals ≥ the age of 60 (*48,49*), suggesting that age may partly increase the overall estimate. Central obesity is recognized as one of the core pathogenic factors for MetS. Evidence from diverse populations consistently indicates that the prevalence of MetS among individuals with central obesity is generally high (> 60%) (*50,51*), with rates reaching up to 78.5% among men (*52*), based on estimates derived from published data.

In addition, shifts in lifestyle patterns may also be contributing to the growing burden of disease. As urbanization has accelerated in recent years, mounting evidence from northwestern and plateau regions has indicated am increased clustering of metabolic abnormalities and cardiovascular risk factors. For instance, a 2025 survey conducted in rural northwestern China reported a MetS prevalence of 53.6% among women ≥the age of 50 (*53*). Among Tibetan adults living at a high altitude, the prevalence of hypertension has been reported to exceed 60%, with the clustering of two or more cardiovascular risk factors approaching 50% (*54*). Long-term outcomes also suggest an increasing burden in plateau regions. In Qinghai, the age-standardized diabetes mortality increased from 1.74/100,000 (1975) to 20.44/100,000 (2020) (≈10-fold) (*55*). Using the same standardization approach, the National Mortality Surveillance System estimate was 13.62/100,000 in 2020 (*56*). Overall, plateau regions may experience a chronic disease burden comparable to that in low-altitude areas when unfavorable age and lifestyle factors accumulate, with more rapid increases in some indicators.

4.2. DASH principles and the Halal Protein-Rich Pattern in practice

This study identified four DPs, among which both DASH and the Halal Protein-Rich Pattern displayed a consistent protective association with MetS, with a correlation of approximately 0.37 (Figure 4A) that suggested a moderate association. Components shared between the two patterns mainly include vegetables, fruits, whole grains, and dairy products (Figure 4B).

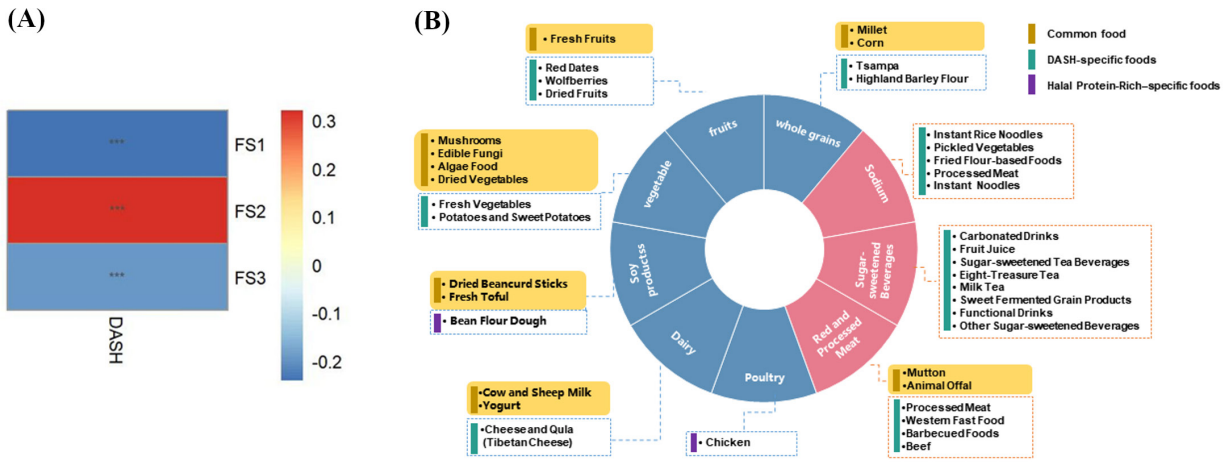

Figure 4 Correlations between PCA-derived dietary patterns and the DASH diet, and shared and unique food components of the Halal Protein-Rich Pattern and DASH. (A) Heatmap showing Spearman rank correlation coefficients between the DASH dietary score and three dietary patterns identified by principal component analysis (PCA). FS1: Sugary Drink and Fast-Food Pattern, FS2: Halal Protein-Rich Pattern, and FS3: Traditional Grain and Tonic Pattern. Correlation coefficients for FS1, FS2, and FS3 were −0.28086, 0.37391, and −0.18196, respectively, with *P* values < 0.001 for all. **(B)** Food composition of the Halal Protein-Rich dietary pattern in relation to the DASH diet. Portions of the circle in blue represent food groups recommended for higher intake in the DASH diet, while portions of the circle in red indicate food groups recommended for moderate intake. Foods are further classified by color: yellow indicates foods common to both dietary patterns, green indicates DASH-specific foods, and purple indicates Halal Protein-Rich Patterns-specific foods.

The DASH diet emphasizes a high intake of vegetables and fruits, fiber-rich staple foods, and limited red meat, all of which have been shown by multiple studies to be beneficial for cardiometabolic health. These findings are consistent with research results from populations in the US, Europe, and Asia *(57–59)*. Unlike the beans recommended in the traditional DASH diet, a wide variety of soy products are a key component of traditional diets in East Asian countries, including China, South Korea, and Japan. In Chinese adult populations, higher soy product intake is associated with a lower prevalence of MetS and better metabolic components (*60*). Intervention evidence from systematic reviews and meta-analyses also suggests that soy product consumption helps improve lipid and glucose metabolism markers (*61*). In the Halal Protein-Rich Pattern, the bean flour dough (a local specialty) is typically made by mixing pea flour with refined wheat flour. In China, where dietary energy intake has long been predominantly derived from carbohydrate-rich staple grains (*62*), this food meets the local carbohydrate needs while aligning as closely as possible with the DASH principles. In traditional Chinese dairy consumption, whole milk and whole-fat yogurt are more common, with a higher proportion than low-fat dairy products. While earlier guidelines recommended reducing saturated fat intake, the latest US dietary guidelines have affirmed the nutritional value of whole-fat dairy products (*30*). Studies show that dairy consumption, and especially whole-fat dairy, is also associated with a reduced risk of MetS (*63-65*). The matrix of dairy products may have a combined effect on lipid metabolism, energy metabolism, and insulin sensitivity, which cannot be simply equated with saturated fat intake (*66-68*). High dietary salt intake is recognized as a key risk factor for hypertension. There is consistent evidence demonstrating its clear association with elevated BP (*69,70*). Reducing salt intake effectively lowers BP and reduces the risk of cardiovascular disease (*71,72*). Among the plateau population in this study, sodium intake was significantly higher than the daily intake recommended by China's Dietary Reference Intakes. However, there was no significant correlation between salt intake and BP or the components of MetS. This finding is consistent with the recent report by Xiao *et al.* (*73*), which indicated that in high-altitude areas of Tibet where there is a higher intake of fats and sodium, this pattern of higher intake did not directly translate into a higher burden of hypertension. Whether this phenomenon is directly related to altitude itself warrants further investigation.

Overall, these findings suggest that the Halal Protein-Rich Pattern largely incorporates DASH-consistent healthy food components within the local halal diet, supporting its potential cultural adaptability and practical feasibility for MetS prevention at high altitudes.

4.3. Diet improves low HDL-C

Low HDL-C is one of the most common types of dyslipidemia in Asian populations (*74-77*). In the current study, a high prevalence of low HDL-C (53.8%) was observed. This is consistent with previous studies of rural populations in Northwestern China, where the prevalence of low HDL-C was 55–68% (*78*).

Current lipid management strategies focus more on reducing LDL-C to lower cardiovascular risk, and simply increasing HDL-C through medication may not necessarily lead to improved cardiovascular outcomes (*79,80*). Therefore, management of low HDL-C is focused more on lifestyle changes and optimization of overall diet composition. In the current study, both DASH and the Halal Protein-Rich Pattern were associated with a reduced risk of low HDL-C. However, the protective association for low HDL-C was not observed with equal strength across all populations. Stratified and interaction analyses revealed that the protective effect of the Halal Protein-Rich Pattern was more pronounced in subgroups with greater metabolic vulnerability. The association was stronger in the population ≥ the age of 60 compared to the population <the age of 60. In addition, the effect was more significant in overweight/obese individuals. Aging and obesity are often accompanied by chronic low-grade inflammation, immune activation in adipose tissue, and exacerbated insulin resistance (*81,82*). Insulin resistance is commonly associated with a characteristic lipid profile of high TG and low HDL cholesterol (*83,84*). Given these circumstances, more beneficial DPs are more likely to demonstrate significant marginal benefits in these populations. In a further exploration of the analysis of individual foods, several items that were positively associated with the Halal Protein-Rich Pattern (such as chicken, fresh fruits, and bean flour dough) remained significantly associated with a reduced risk of low HDL-C after FDR correction. This provides compositional-level support for the effect of the Halal Protein-Rich Pattern on low HDL-C.

4.4. Dietary changes trump weight loss

Being overweight is not only a risk factor for MetS but also potentially serves as a mediating pathway through which diet influences MetS, by affecting fat accumulation, insulin sensitivity, and inflammation (*85,86*). The current study found that being overweight mediates only a small portion (less than 20%) of the association between DPs and MetS, with most of the risk still attributed to the direct effects of the DPs. For low HDL-C, both DASH and the Halal Protein-Rich Pattern maintained significant protective associations even after adjusting for BMI, with a minor mediating effect. These findings are consistent with existing research and further support the direct regulatory role of diet quality in lipoprotein metabolism (*87*). The above results suggest that the effect of dietary composition on metabolic health may extend beyond the energy balance. For example, the Sugary Drinks and Fast-Food Pattern, characterized by a high consumption of barbecued foods, instant noodles, and carbonated beverages, is negatively correlated with HDL-C levels. This is consistent with mechanisms described in the literature, in which high-sugar, high-fat diets exacerbate oxidative stress and inflammation, thereby disrupting lipid metabolism (*88,89*). In addition, the population in the current study was relatively older on average (54.58 years), and with aging, there is often a decrease in muscle mass and an increase in fat proportion, leading to changes in body composition. BMI has limitations in accurately reflecting true obesity and related metabolic risks in these populations (*90*). This further supports the notion that focusing solely on weight loss or BMI reduction may be insufficient for preventing and controlling MetS.

4.5. Potential inflammatory mechanisms linking DPs to MetS

Several dietary interventions and reviews have indicated that healthy diets can reduce chronic low-grade inflammation, thereby influencing MetS (*31,91,92*). In the current study, inflammation markers (SII and NLR) were not significantly associated with MetS or its components, but this does not negate the role of inflammation. Both SII and NLR are composite indices derived from peripheral blood cell counts and are susceptible to influence by acute infections, hematological conditions, and other systemic factors, which may limit their specificity in capturing diet-related chronic metabolic inflammation. Therefore, in this study population, the associations between DPs and metabolic outcomes may not be fully reflected by these blood count-based inflammatory indicators. In addition, DPs can directly modulate the composition and function of the gut microbiota, which may play an important role in the dietary regulation of MetS (*93,94*). Importantly, metabolic and inflammatory processes relevant to MetS may also be shaped by the unique hypoxic and climatic conditions at high altitudes, which are discussed in the following section.

4.6. Impact of high altitudes on metabolism

Regions at high altitudes exhibit a complex environmental profile characterized by a low atmospheric pressure, a low oxygen partial pressure, low temperatures, and a low humidity. Prolonged exposure to this hypoxic and hypobaric environment triggers compensatory adaptations across multiple physiological systems, including key pathways such as glucose and lipid metabolism, the regulation of oxidative stress, and the control of inflammation.

In terms of glucose metabolism, central obesity is a significant risk factor for type 2 diabetes due to its effect on insulin resistance (*95*). According to ADA criteria, diabetes has an overall prevalence of approximately 12.8% among Chinese adults, reaching 21.1% in the 50–59 age group (*96*). In representative samples from multiple provinces, the prevalence of diabetes among

centrally obese individuals was around 15–16% (*97*). In contrast, the overall prevalence of diabetes in this study population was 12.89%, and 13.96% among participants with central obesity (Supplementary Tables S3, *https://www.biosciencetrends.com/action/getSupplementalData.php?ID=288*). This population was older on average and had a high prevalence of central obesity (>80%), and yet the prevalence of diabetes remained lower than national estimates reported for comparable age groups and obesity status. This discrepancy may be related to metabolic adaptations developed through long-term exposure to hypoxic conditions among populations living at a high altitude. Previous studies have shown that, compared to populations living at lower altitudes, those living at higher altitudes generally have lower fasting blood glucose levels and improved glucose tolerance (*98,99*). Animal experiments have shown that simulated high-altitude hypoxia can enhance the mitochondrial function of skeletal muscles and improve insulin sensitivity by activating the AMPK pathway (*100*). Mechanistically, exposure to hypoxic conditions at high altitudes can induce hypoxia-inducible factors and related molecular pathways that promote anaerobic glycolytic glucose metabolism, enabling more efficient glucose utilization and, to some extent, reducing the risk of type 2 diabetes (*101*). In addition, the cold and low humidity in regions at high altitudes have also been associated with a risk of type 2 diabetes. One study reported that for every 1°C increase in ambient temperature, the age-adjusted incidence of diabetes increases by 0.0314% (*102*), and another reported that each 1% increase in relative humidity is associated with a 12% higher likelihood of diabetes (*103*).

The effects of high-altitude hypoxia on lipid metabolism are inconclusive. Some studies suggest that higher altitudes are associated with a lower BMI, smaller WC, and reduced serum TG and low-density lipoprotein cholesterol (LDL-C) levels (*104-106*). A study of the Jiarong Tibetan population in Western Sichuan found that the contribution of dietary fat to energy increased to over 50% at higher altitudes. However, residents consuming these high-fat, high-energy diets did not have significantly elevated total cholesterol levels. In fact, LDL-C displayed a negative correlation with fat intake (*107*). At the same time, studies have also identified abnormalities in the lipid profiles of populations living at high altitudes. For example, some studies have reported elevated levels of total cholesterol and LDL-C among Tibetan residents who primarily consume high-fat diets. Conversely, hypertriglyceridemia is more prevalent among Han residents, whose staple diet consists mainly of carbohydrates, in plateau regions (*108*). Therefore, the effects of high-altitude hypoxia on lipid metabolism do not follow a uniform pattern and may be influenced by energy expenditure levels and dietary composition, resulting in heterogeneous lipid metabolic profiles across different populations.

In addition to glucose and lipid metabolism, oxidative stress and inflammatory responses also undergo complex changes at high altitudes. Hypoxia is widely recognized as an important trigger of oxidative stress, and acute exposure is often accompanied by transient elevations in circulating inflammatory mediators (*109,110*). However, with prolonged exposure at moderate altitudes, the body gradually makes adaptive adjustments, such as increased adiponectin levels and decreased leptin levels (*111*), indicating adaptive regulation that favors metabolic homeostasis under chronic hypoxic conditions (*112,113*). As adipose tissue is prone to chronic, low-grade inflammation induced by local hypoxia, the lean body phenotype commonly observed in populations living at high altitudes may alleviate the inflammatory burden associated with obesity to some extent.

4.7. Dietary recommendations for populations living at a high altitude

Evidence suggests that adults living in pastoral regions at high altitudes typically have energy and protein intakes close to the levels recommended by the Chinese Dietary Reference Intakes, while consuming excessive fat and sodium and not consuming sufficient vitamin C and other micronutrients (*73*). From a public health perspective, the value of this study lies not only in identifying DPs, but also in proposing a transferable framework for translating evidence-based DASH principles into locally feasible dietary strategies for high altitudes.

Specifically, maintaining traditional carbohydrate-based staple foods while prioritizing whole grains and legume-based products (*e.g.*, bean flour dough, highland barley products, and tsampa) may improve dietary fiber and plant protein intake and align with the metabolic preference for glucose utilization under chronic hypoxic conditions. Previous studies have indicated that oxygen-limited environments are associated with reduced reliance on lipid oxidation and increased glucose utilization (*99,114,115*). Therefore, carbohydrate-based DPs may be more consistent with metabolic adaptations.

For individuals with low HDL-C, dietary recommendations should emphasize optimization of fat quality rather than indiscriminate fat restriction. In pastoral regions with large ethnic populations, this may involve retaining ruminant meat and dairy products as key protein sources while reducing the intake of highly processed high-fat meats and increasing the consumption of plant-based fat sources rich in unsaturated fatty acids, such as legumes and nuts. Vitamin C insufficiency also warrants attention. Although traditional dried vegetables provide dietary fiber and minerals, vitamin C is highly susceptible to loss during drying and storage. Without substantially altering traditional DPs, increasing intake

of storable fresh vegetables (*e.g.*, cabbage, Chinese cabbage, and radish) and seasonal fruits, alongside improved cooking practices, may help address this gap.

Finally, given the widespread excess sodium intake in these regions relative to the Chinese Dietary Reference Intakes, culturally acceptable sodium reduction strategies, such as limiting preserved foods, reducing salt and salty condiments, and increasing potassium-rich vegetables (particularly potatoes, a staple crop in northwestern China) and fruits, may contribute to the gradual attainment of an appropriate sodium intake in populations living at a high altitude.

4.8. Strengths and limitations

This study is the first to assess DPs in a population living at a high altitude and consuming a halal diet in Qinghai Province, combining a priori DASH DP with posteriori factor analysis to provide a more comprehensive evaluation. The consistency between the two approaches further supports the positive impact of DPs on metabolic health. Factor analysis also identified culturally specific healthy DPs, providing contextually relevant evidence for precision nutrition interventions in plateau regions with large ethnic populations, with strong practical and regional significance. From a global public health perspective on populations living at high altitudes, this study provides a significant reference. At least 5.7% of the global population is estimated to reside in regions at high altitudes. In China, plateau areas account for approximately 16.7% of the national land area and are inhabited by nearly 60 million people (*116,117*). These populations face environmental challenges such as chronic hypoxia, cold temperatures, and limited dietary diversity, resulting in unique metabolic adaptations. In this context, this study has analyzed characteristics of metabolic adaptation and DPs, proposing an approach to improving metabolism by optimizing dietary composition and fat quality in low-oxygen environments. This provides a referential framework for developing evidence-based dietary intervention strategies that are tailored to different high-altitude regions while respecting local diets.

This study had several limitations. First, the cross-sectional design prevented the identification of causal relationships between DPs and MetS components. Reverse causation cannot be excluded, particularly for IFG, as individuals with abnormal glucose levels may have already adopted healthier dietary behaviors before the dietary assessment, potentially resulting in an apparent inverse association. In other words, people who have already been diagnosed with metabolic abnormalities might alter their diets, which could affect the results of this study and give the appearance that healthier DPs are associated with better outcomes. Given that this study is part of an ongoing study of a natural population cohort living at a high altitude, the next step will be to perform a longitudinal analysis based on follow-up data. To address the potential reverse causality in the results related to IFG in this study, the cohort follow-up will exclude individuals with known metabolic abnormalities at the baseline to enhance causal inference. Second, there may be recall bias in the food frequency survey, as individuals may struggle to accurately recall or report their dietary intake. Due to some participants' low levels of literacy and language differences, the use of simple tools and translation assistance was the only feasible way to collect dietary information. DP analysis captures only part of changes in food consumption and may not fully represent diet quality (*118*).

Third, due to the influence of a halal diet and religious factors, information on smoking and drinking among individuals was not collected, which may lead to residual confounding. However, exposure to passive smoking was included as a covariate in this study to partially control for tobacco-related effects. In addition, the drinking behavior of the study population is culturally restricted, and its potential impact as a major confounding factor on the relationship between DPs and MetS is relatively limited. Fourth, in China, the estimation of salt intake may be biased by the common practice of mixed dishes and shared meals, potentially leading to inaccuracies in the salt intake estimates in this study. Lastly, future longitudinal studies should prioritize stable inflammatory markers such as CRP and IL-6, along with gut microbiome analysis, to provide a more comprehensive assessment of the diet's impact on low-grade inflammation and MetS, thereby improving mechanistic understanding and comparability. Given the environmental characteristics of chronic hypoxia in regions at high altitudes, subsequent analyses will incorporate an altitude gradient.

5. Conclusion

In conclusion, this study has demonstrated that evidence-based dietary guidelines can be effectively translated into culturally appropriate DPs at high altitudes where a halal diet is consumed. The DASH diet provides a robust scientific foundation, while the Halal Protein-Rich Pattern illustrates its practical and culturally relevant application. These findings support the use of localized DPs as feasible strategies for nutritional intervention. Moreover, for middle-aged and older adults, optimizing dietary composition and nutrient density should be a key focus of future nutritional strategies.

Funding: This work was supported by a grant from the Qinghai Provincial Department of Science and Technology (Grant No. 2024-0204-SFC-0019).

Conflict of Interest: The authors have no conflicts of interest to disclose.

References

1. Ahluwalia N, Andreeva VA, Kesse-Guyot E, Hercberg S. Dietary patterns, inflammation and the metabolic syndrome. Diabetes Metab. 2013; 39:99-110.
2. Neeland IJ, Lim S, Tchernof A, Gastaldelli A, Rangaswami J, Ndumele CE, Powell-Wiley TM, Després JP. Metabolic syndrome. Nat Rev, Dis Primers .2024; 10:77.
3. Noubiap JJ, Nansseu JR, Nyaga UF, Ndoadoumgue AL, Ngouo AT, Tounouga DN, Tianyi FL, Foka AJ, Lontchi-Yimagou E, Nkeck JR, Bigna JJ. Worldwide trends in metabolic syndrome from 2000 to 2023: A systematic review and modelling analysis. Nat Commun. 2025; 17:573.
4. Wang Y, Fouret G, Bonafos B, Blachnio-Zabielska A, Leroy T, Crouzier D, Barea B, Gaillet S, Moro C, Lecomte J, Coudray C, Feillet-Coudray C. Long-term follow-up of muscle lipid accumulation, mitochondrial activity and oxidative stress and their relationship with impaired glucose homeostasis in high fat high fructose diet-fed rats. J Nutr Biochem. 2019; 64:182-97.
5. Unwin N, Shaw J, Zimmet P, Alberti KGMM. Impaired glucose tolerance and impaired fasting glycaemia: The current status on definition and intervention. Diabet Med. 2002; 19:708-23.
6. Yao F, Bo Y, Zhao L, Li Y, Ju L, Fang H, Piao W, Yu D, Lao X. Prevalence and influencing factors of metabolic syndrome among adults in China from 2015 to 2017. Nutrients. 2021; 13:4475.
7. The State Council of the People's Republic of China. Over one-fifth of Chinese population older than 60, says official report. *https://english.www.gov.cn/news/202410/12/content_WS6709cb9ac6d0868f4e8ebbda.html* (accessed January 2, 2026)
8. The State Council of the People's Republic of China. China launches initiative to tackle obesity surge. *https://english.www.gov.cn/news/202409/24/content_WS66f29ab3c6d0868f4e8eb349.htm* (accessed January 3, 2026)
9. Huxley RR, Barzi F, Lam TH, Czernichow S, Fang X, Welborn T, Shaw J, Ueshima H, Zimmet P, Jee SH, Patel JV, Caterson I, Perkovic V, Woodward M; Asia Pacific Cohort Studies Collaboration and the Obesity in Asia Collaboration. Isolated low levels of high-density lipoprotein cholesterol are associated with an increased risk of coronary heart disease: An individual participant data meta-analysis of 23 studies in the Asia-Pacific region. Circulation. 2011; 124:2056-64.
10. Xia Q, Chen Y, Yu Z, Huang Z, Yang Y, Mao A, Qiu W. Prevalence, awareness, treatment, and control of dyslipidemia in Chinese adults: A systematic review and meta-analysis. Front Cardiovasc Med. 2023; 10:1186330.
11. Yu S, Guo X, Li GX, Yang H, Zheng L, Sun Y. Lower or higher HDL-C levels are associated with cardiovascular events in the general population in rural China. Lipids Health Dis. 2020; 19:152.
12. Liu X, Yu S, Mao Z, Li Y, Zhang H, Yang K, Zhang H, Liu R, Qian X, Li L, Bie R, Wang C. Dyslipidemia prevalence, awareness, treatment, control, and risk factors in Chinese rural population: The Henan rural cohort study. Lipids Health Dis. 2018; 17:119.
13. Sun G-Z, Li Z, Guo L, Zhou Y, Yang H-M, Sun Y-X. High prevalence of dyslipidemia and associated risk factors among rural Chinese adults. Lipids Health Dis. 2014; 13:189.
14. Zila-Velasque JP, Grados-Espinoza P, Challapa-Mamani MR, Sánchez-Alcántara F, Cedillo-Balcázar J, Cs AD, Hernandez-Bustamante EA, Tejada-Flores J, Piano Suárez A, Pacheco-Mendoza J, Benites-Zapata VA. Prevalence of metabolic syndrome and its components according to altitude levels: A systematic review and meta-analysis. Sci Rep. 2024; 14:27581.
15. Huang X, Hu Y, Du L, Lin X, Wu W, Fan L, Li L, Zhong X, Gong Q, Gao L, Kuang W. Metabolic syndrome in native populations living at high altitude: A cross-sectional survey in Derong, China. BMJ Open. 2020; 10:e032840.
16. Zhou J, He R, Shen Z, *et al*. Altitude and metabolic syndrome in China: Beneficial effects of healthy diet and physical activity. J Glob Health. 2023; 13:04061.
17. Qin X, Qiu L, Tang G, Tsoi MF, Xu T, Zhang L, Qi Z, Zhu G, Cheung BMY. Prevalence of metabolic syndrome among ethnic groups in China. BMC Public Health. 2020; 20:297.
18. Wang H, Wang Y, Shi Z, Zhao L, Jian W, Li K, Xu R, Wu Y, Xu F, Wang Y, Peng W. Association between dietary patterns and metabolic syndrome and modification effect of altitude: A cohort study of Tibetan adults in China. Nutrients. 2023; 15:2226.
19. Sherpa LY, Deji, Stigum H, Chongsuvivatwong V, Nafstad P, Bjertness E. Prevalence of metabolic syndrome and common metabolic components in high altitude farmers and herdsmen at 3700 m in Tibet. High Alt Med Biol. 2013; 14:37-44.
20. Ma Y, Li Y, Zhang Z, Du G, Huang T, Zhao ZZ, Liu S, Dang Z. Establishment of a risk prediction model for metabolic syndrome in high altitude areas in Qinghai Province, China: A cross-sectional study. Diabetes Metab Syndr Obes. 2024; 17:2041-52.
21. Jia X, Lee HF, Cui M, Liu C, Zeng L, Yue RPH, Zhao Y, Lu H. Habitat variability and ethnic diversity in Northern Tibetan Plateau. Sci Rep. 2017; 7:918.
22. Rampal S, Mahadeva S, Guallar E, Bulgiba A, Mohamed R, Rahmat R, Arif MT, Rampal L. Ethnic differences in the prevalence of metabolic syndrome: Results from a multi-ethnic population-based survey in Malaysia. PLoS One. 2012; 7:e46365.
23. Krishnadath ISK, Toelsie JR, Hofman A, Jaddoe VWV. Ethnic disparities in the prevalence of metabolic syndrome and its risk factors in the Suriname Health Study: A cross-sectional population study. BMJ Open. 2016; 6:e013183.
24. Zhang R, Sun J, Wang C, Wang X, Zhao P, Yuan Y, Ai H, Zhou Q. The racial disparities in the epidemic of metabolic syndrome with increased age: A study from 28,049 Chinese and American Adults. Front Public Health. 2021; 9:797183.
25. Sigit FS, Tahapary DL, Trompet S, Sartono E, Willems van Dijk K, Rosendaal FR, de Mutsert R. The prevalence of metabolic syndrome and its association with body fat distribution in middle-aged individuals from Indonesia and the Netherlands: A cross-sectional analysis of two population-based studies. Diabetol Metab Syndr. 2020; 12:2.
26. Su Y, Lu Y, Li W, Xue M, Chen C, Haireti M, Li Y, Liu Z, Liu Y, Wang S, Yao H. Prevalence and Correlation of Metabolic Syndrome: A cross-sectional study of nearly 10 million multi-ethnic Chinese adults. Diabetes Metab Syndr Obes. 2020; 13:4869-83.
27. Yi Z, Jing J, Xiu-ying L, Hongxia X, Jianjun Y, Yuhong

Z. Prevalence of the metabolic syndrome among rural original adults in NingXia, China. BMC Public Health. 2010; 10:140.
28. World Health Organization (WHO). Healthy diet. *https://www.who.int/news-room/fact-sheets/detail/healthy-diet* (accessed January 3, 2026).
29. Lichtenstein AH, Appel LJ, Vadiveloo M, Hu FB, Kris-Etherton PM, Rebholz CM, Sacks FM, Thorndike AN, Van Horn L, Wylie-Rosett J. 2021 Dietary Guidance to Improve Cardiovascular Health: A Scientific Statement from the American Heart Association. Circulation. 2021; 144:e472-87.
30. U.S. Department of Agriculture; U.S. Department of Health and Human Services. Dietary Guidelines for Americans. *https://www.dietaryguidelines.gov/*(accessed January 3, 2026).
31. Fabiani R, Naldini G, Chiavarini M. Dietary patterns and metabolic syndrome in adult subjects: A systematic review and meta-analysis. Nutrients. 2019; 11:2056.
32. Sonnenberg L, Pencina M, Kimokoti R, Quatromoni P, Nam BH, D'Agostino R, Meigs JB, Ordovas J, Cobain M, Millen B. Dietary patterns and the metabolic syndrome in obese and non-obese Framingham women. Obes Res. 2005; 13:153-62.
33. Aekplakorn W, Satheannoppakao W, Putwatana P, Taneepanichskul S, Kessomboon P, Chongsuvivatwong V, Chariyalertsak S. Dietary pattern and metabolic syndrome in Thai adults. J Nutr Metab. 2015; 2015:468759.
34. National Heart, Lung, and Blood Institute (NHLBI), National Institutes of Health (NIH). Metabolic Syndrome - Treatment. *https://www.nhlbi.nih.gov/health/metabolic-syndrome/treatment* (accessed January 2, 2026).
35. American Heart Association. Diet change may return bigger heart health rewards than other lifestyle changes. *https://www.heart.org/en/news/2022/09/07/diet* (accessed January 2, 2026).
36. Tinoco-Solórzano A, Avila-Hilari A, Avellanas-Chavala ML, *et al*. Definitions and consensus recommendations on critical care medicine at altitude from the Expert Committee on Critical Care Medicine at Altitude of the Pan-American and Iberian Federation of Critical Care Medicine and Intensive Care. Med Intensiva (Engl Ed). 2025; 49:502256.
37. Leng R, Guo A, Qian G, Mao S. Influence of sedentary behavior on sleep quality in postmenopausal women in high-altitude regions of China: A cross-sectional study. Front Neurol. 2024; 15:1476010.
38. Ma FC, Zhou MR, Yue JN, *et al*. Analysis of dietary patterns and dietary characteristics among adults in surveillance sites in Qinghai Province. Acta Nutrimenta Sinica. 2016, 38: 402-404. (in Chinese)
39. Tavakol M, Dennick R. Making sense of Cronbach's alpha. Int J Med Educ. 2011; 2:53-55.
40. National Health Commission of the People's Republic of China. Dietary guideline of obesity in adult (2024). J Hygiene Res. 2024; 53:347-351. (in Chinese)
41. National Institute for Nurtition and Health. China Food Composition Tables. 6ed. Beijing: Peking University Medical Press; 2018. (in Chinese)
42. Chiu S, Bergeron N, Williams PT, Bray GA, Sutherland B, Krauss RM. Comparison of the DASH (Dietary Approaches to Stop Hypertension) diet and a higher-fat DASH diet on blood pressure and lipids and lipoproteins: A randomized controlled trial. Am J Clin Nutr. 2016; 103:341-7.
43. Xiao ML, Lin JS, Li YH, Liu M, Deng YY, Wang CY, Chen YM. Adherence to the Dietary Approaches to Stop Hypertension (DASH) diet is associated with lower presence of non-alcoholic fatty liver disease in middle-aged and elderly adults. Public Health Nutr. 2020; 23:674-82.
44. Lin PH, Aickin M, Champagne C, Craddick S, Sacks FM, McCarron P, Most-Windhauser MM, Rukenbrod F, Haworth L; Dash-Sodium Collaborative Research Group. Food group sources of nutrients in the dietary patterns of the DASH-Sodium trial. J Am Diet Assoc. 2003; 103:488-96.
45. Xiao X, Qin Z, Lv X, *et al*. Dietary patterns and cardiometabolic risks in diverse less-developed ethnic minority regions: results from the China Multi-Ethnic Cohort (CMEC) Study. Lancet Reg Health West Pac. 2021; 15:100252.
46. Alberti KG, Eckel RH, Grundy SM, *et al*. Harmonizing the metabolic syndrome: A joint interim statement of the International Diabetes Federation Task Force on Epidemiology and Prevention; National Heart, Lung, and Blood Institute; American Heart Association; World Heart Federation; International Atherosclerosis Society; and International Association for the Study of Obesity. Circulation. 2009; 120:1640-5.
47. Tennant PWG, Murray EJ, Arnold KF, Berrie L, Fox MP, Gadd SC, Harrison WJ, Keeble C, Ranker LR, Textor J, Tomova GD, Gilthorpe MS, Ellison GTH. Use of directed acyclic graphs (DAGs) to identify confounders in applied health research: Review and recommendations. Int J Epidemiol. 2021; 50:620-32.
48. Chen D, Zhang H, Shao J, Tang L, Wu J, Ye Z. Summary of the best evidence of diet and physical activity management in patients with metabolic syndrome. Zhejiang Da Xue Xue Bao Yi Xue Ban. 2022; 51:27-37.
49. Hildrum B, Mykletun A, Hole T, Midthjell K, Dahl AA. Age-specific prevalence of the metabolic syndrome defined by the International Diabetes Federation and the National Cholesterol Education Program: The Norwegian HUNT 2 study. BMC Public Health. 2007; 7:220.
50. He Y, Li Y, Bai G, Zhang J, Fang Y, Zhao L, Zhao W, Yang X, Ding G. Prevalence of metabolic syndrome and individual metabolic abnormalities in China, 2002-2012. Asia Pac J Clin Nutr. 2019; 28:621-33.
51. Zhu L, Spence C, Yang JW, Ma GX. The IDF definition is better suited for screening metabolic syndrome and estimating risks of diabetes in Asian American adults: Evidence from NHANES 2011-2016. J Clin Med. 2020; 9:3871.
52. Sy RG, Llanes EJ, Reganit PF, Castillo-Carandang N, Punzalan FE, Sison OT, Khaing NE, Poulton R, Woodward M, Tai ES. Socio-demographic factors and the prevalence of metabolic syndrome among Filipinos from the LIFECARE cohort. J Atheroscler Thromb. 2014; 21: S9-17.
53. Jiao Y, Zhang C, Ming J, *et al*. Rural, urban and suburban differences in the prevalence of metabolic syndrome in individuals aged ≥50 years in Northwest China. Front Public Health. 2025; 13:1589196.
54. Xu S, Jiayong Z, Li B, Zhu H, Chang H, Shi W, Gao Z, Ning X, Wang J. Prevalence and clustering of cardiovascular disease risk factors among Tibetan adults in China: A population-based study. PLoS One. 2015; 10:e0129966.

55. Xu LL, Duan R, Sha QY, *et al*. Trend analysis of mortality of diabetes mellitus among residents in Qinghai Province, China, 1975-2020. J Environmental Hygiene. 2023, 13: 629-634. (in Chinese)
56. Wang F, Wang W, Yin P, Liu Y, Liu J, Wang L, Qi J, You J, Lin L, Zhou M. Mortality and years of life lost in diabetes mellitus and its subcategories in China and its provinces, 2005–2020. J Diabetes Res. 2022; 2022:1609267.
57. Mozaffarian D. Dietary and policy priorities for cardiovascular disease, diabetes, and obesity: A comprehensive review. Circulation. 2016; 133:187-225.
58. Song Y, Lobene AJ, Wang Y, Hill Gallant KM. The DASH diet and cardiometabolic health and chronic kidney disease: A narrative review of the evidence in East Asian countries. Nutrients. 2021; 13:984.
59. Park YM, Steck SE, Fung TT, Zhang J, Hazlett LJ, Han K, Lee SH, Kwon HS, Merchant AT. Mediterranean diet, Dietary Approaches to Stop Hypertension (DASH) style diet, and metabolic health in U.S. adults. Clin Nutr. 2017; 36:1301-9.
60. Hidayat K, Huang YH, Qian XY, Chen XF, Yu LG, Zhou H, Qin LQ. The association between soy consumption and metabolic syndrome in Chinese adults: A cross-sectional study. Front Nutr. 2025; 12:1637413.
61. Mohammadifard N, Sajjadi F, Haghighatdoost F. Effects of soy consumption on metabolic parameters in patients with metabolic syndrome: A systematic review and meta-analysis. EXCLI J. 2021; 20:665–85.
62. Chinese Center for Disease Control and Prevention. Revision and explanation of Chinese Food Guide Pagoda and Plate (2022). *http://en.chinacdc.cn/health_topics/nutrition_health/202206/t20220622_259773.html* (accessed January 2, 2026).
63. Chen GC, Szeto IM, Chen LH, Han SF, Li YJ, van Hekezen R, Qin LQ. Dairy products consumption and metabolic syndrome in adults: Systematic review and meta-analysis of observational studies. Sci Rep. 2015; 5:14606.
64. Drehmer M, Pereira MA, Schmidt MI, Alvim S, Lotufo PA, Luft VC, Duncan BB. Total and full-fat, but not low-fat, dairy product intakes are inversely associated with metabolic syndrome in adults. J Nutr. 2016; 146:81-9.
65. Unger AL, Torres-Gonzalez M, Kraft J. Dairy Fat Consumption and the Risk of Metabolic Syndrome: An examination of the saturated fatty acids in dairy. Nutrients. 2019; 11:2200.
66. Tulipano G. Role of bioactive peptide sequences in the potential impact of dairy protein intake on metabolic health. Int J Mol Sci. 2020; 21:8881.
67. D'Souza K, Mercer A, Mawhinney H, Pulinilkunnil T, Udenigwe CC, Kienesberger PC. Whey peptides stimulate differentiation and lipid metabolism in adipocytes and ameliorate lipotoxicity-induced insulin resistance in muscle cells. Nutrients. 2020; 12:425.
68. Fardet A, Dupont D, Rioux L-E, Turgeon SL. Influence of food structure on dairy protein, lipid and calcium bioavailability: A narrative review of evidence. Crit Rev Food Sci Nutr. 2019; 59:1987-2010.
69. Karppanen H, Mervaala E. Sodium intake and hypertension. Prog Cardiovasc Dis. 2006; 49:59-75.
70. Huang L, Trieu K, Yoshimura S, Neal B, Woodward M, Campbell NRC, Li Q, Lackland DT, Leung AA, Anderson CAM, MacGregor GA, He FJ. Effect of dose and duration of reduction in dietary sodium on blood pressure levels: Systematic review and meta-analysis of randomised trials. BMJ. 2020; 368:m315.
71. He FJ, Campbell NRC, MacGregor GA. Reducing salt intake to prevent hypertension and cardiovascular disease. Rev Panam Salud Publica. 2012; 32:293-300.
72. He FJ, Tan M, Ma Y, MacGregor GA. Salt reduction to prevent hypertension and cardiovascular disease: JACC State-of-the-Art Review. J Am Coll Cardiol. 2020; 75:632-47.
73. Xiao Z, Sun X, Zhaxi D, Zhang F, Ji Y, Cheng T, Li X, Xu X. Distinct nutrient intake style in inhabitants of ultra-high-altitude areas in North of Tibet, China: A cross-sectional study based on newly developed Tibetan food frequency questionnaires. Front Nutr. 2021; 8:743896.
74. Saeed A, Virani SS, Mulukutla S, Chow CK. Dyslipidemia and cardiovascular disease prevention in South Asians: A review and discussion of causes, challenges and management strategies. Curr Diabetes Rev. 2021; 17:e011221190238.
75. Frank ATH, Zhao B, Jose PO, Azar KMJ, Fortmann SP, Palaniappan LP. Racial/ethnic differences in dyslipidemia patterns. Circulation. 2014; 129:570-9.
76. Kim SM, Han JH, Park HS. Prevalence of low HDL-cholesterol levels and associated factors among Koreans. Circ J. 2006; 70:820-6.
77. Salehi-Abargouei A, Maghsoudi Z, Shirani F, Azadbakht L. Effects of Dietary Approaches to Stop Hypertension (DASH)-style diet on fatal or nonfatal cardiovascular diseases--Incidence: A systematic review and meta-analysis on observational prospective studies. Nutrition. 2013; 29:611-8.
78. Ge P, Dong C, Ren X, Weiderpass E, Zhang C, Fan H, Zhang J, Zhang Y, Xi J. The high prevalence of low HDL-cholesterol levels and dyslipidemia in rural populations in Northwestern China. PLoS One. 2015; 10:e0144104.
79. März W, Kleber ME, Scharnagl H, Speer T, Zewinger S, Ritsch A, Parhofer KG, von Eckardstein A, Landmesser U, Laufs U. HDL cholesterol: Reappraisal of its clinical relevance. Clin Res Cardiol. 2017; 106:663-75.
80. Farrer S. Beyond Statins: Emerging evidence for HDL-increasing therapies and diet in treating cardiovascular disease. Adv Prev Med. 2018; 2018:6024747.
81. Guria S, Hoory A, Das S, Chattopadhyay D, Mukherjee S. Adipose tissue macrophages and their role in obesity-associated insulin resistance: An overview of the complex dynamics at play. Biosci Rep. 2023; 43:BSR20220200.
82. Harford KA, Reynolds CM, McGillicuddy FC, Roche HM. Fats, inflammation and insulin resistance: Insights to the role of macrophage and T-cell accumulation in adipose tissue. Proc Nutr Soc. 2011; 70:408-17.
83. Jeppesen J, Facchini FS, Reaven GM. Individuals with high total cholesterol/HDL cholesterol ratios are insulin resistant. J Intern Med. 1998; 243:293-8.
84. Pantoja-Torres B, Toro-Huamanchumo CJ, Urrunaga-Pastor D, Guarnizo-Poma M, Lazaro-Alcantara H, Paico-Palacios S, Del Carmen Ranilla-Seguin V, Benites-Zapata VA; Insulin Resistance and Metabolic Syndrome Research Group. High triglycerides to HDL-cholesterol ratio is associated with insulin resistance in normal-weight healthy adults. Diabetes Metab Syndr. 2019; 13:382-8.
85. Rizzo AC, Goldberg TB, Silva CC, Kurokawa CS, Nunes HR, Corrente JE. Metabolic syndrome risk factors in overweight, obese, and extremely obese Brazilian

adolescents. Nutr J. 2013; 12:19.
86. Singla P, Bardoloi A, Parkash AA. Metabolic effects of obesity: A review. World J Diabetes. 2010; 1:76-88.
87. Song P, Man Q, Li Y, Jia S, Yu D, Zhang J, Ding G. Association between dietary patterns and low HDL-C among community-dwelling elders in North China. Nutrients. 2021; 13:3308.
88. Wu Y, Sun H, Yi R, Tan F, Zhao X. Anti-obesity effect of Liupao tea extract by modulating lipid metabolism and oxidative stress in high-fat-diet-induced obese mice. J Food Sci. 2021; 86:215-27.
89. Adedeji TG, Jeje SO, Omayone TP, Agbonifo WO. Oxidative stress and inflammatory response to high dietary fat and carbonated soda intake in male and female Wistar rats. Nutrition. 2022; 103-104:111800.
90. Zhan JK, Liu YS. Interpretation of Expert Consensus on Drug Treatment for Metabolic Syndrome in the Elderly in China (2022). Chin J Clin Health Care. 2024; 27:43-46. (in Chinese)
91. Soltani S, Chitsazi MJ, Salehi-Abargouei A. The effect of dietary approaches to stop hypertension (DASH) on serum inflammatory markers: A systematic review and meta-analysis of randomized trials. Clin Nutr. 2018; 37:542-50.
92. Wang M, Liu J, Zhang Z, Zhang H, Wang N, Chen X, Han X, Lu Q, Chi S. Effects of dietary intervention on inflammatory markers in metabolic syndrome: A systematic review and meta-analysis. Front Nutr. 2022; 9:846591.
93. Onu A, Tutu A, Trofin DM, Onu I, Galaction AI, Onita CA, Iordan DA, Matei DV. Diet, Physical exercise, and gut microbiota modulation in metabolic syndrome: A narrative review. Life (Basel). 2026; 16:98.
94. Fan Y, Pedersen O. Gut microbiota in human metabolic health and disease. Nat Rev Microbiol. 2021; 19:55-71.
95. Papaetis GS, Papakyriakou P, Panagiotou TN. Central obesity, type 2 diabetes and insulin: Exploring a pathway full of thorns. Arch Med Sci. 2015; 11:463-82.
96. Li Y, Teng D, Shi X, *et al*. Prevalence of diabetes recorded in mainland China using 2018 diagnostic criteria from the American Diabetes Association: National cross sectional study. BMJ. 2020; 369:m997.
97. Zhang ST, Zhang JG, Jia XF, Jiang HR, Wang LS, Zhang B, Wang HJ, Wang ZH, Ding GG. Association between obesity and the prevalence of type 2 diabetes mellitus among Chinese adults aged 18-65 years in 15 provinces in 2018. Zhonghua Liu Xing Bing Xue Za Zhi. 2022; 43:1596-602.
98. Woolcott OO, Ader M, Bergman RN. Glucose homeostasis during short-term and prolonged exposure to high altitudes. Endocr Rev. 2015; 36:149-73.
99. Holden JE, Stone CK, Clark CM, Brown WD, Nickles RJ, Stanley C, Hochachka PW. Enhanced cardiac metabolism of plasma glucose in high-altitude natives: Adaptation against chronic hypoxia. J Appl Physiol (1985). 1995; 79:222-8.
100. Song K, Zhang Y, Ga Q, Bai Z, Ge R-L. Increased insulin sensitivity by high-altitude hypoxia in mice with high-fat diet-induced obesity is associated with activated AMPK signaling and subsequently enhanced mitochondrial biogenesis in skeletal muscles. Obes Facts. 2020; 13:455-72.
101. Murray AJ. Energy metabolism and the high-altitude environment. Exp Physiol. 2016; 101:23-7.
102. Blauw LL, Aziz NA, Tannemaat MR, Blauw CA, de Craen AJ, Pijl H, Rensen PC. Diabetes incidence and glucose intolerance prevalence increase with higher outdoor temperature. BMJ Open Diabetes Res Care. 2017; 5:e000317.
103. Tyrovolas S, Chalkias C, Morena M, Kalogeropoulos K, Tsakountakis N, Zeimbekis A, Gotsis E, Metallinos G, Bountziouka V, Lionis C, Polychronopoulos E, Panagiotakos D. High relative environmental humidity is associated with diabetes among elders living in Mediterranean islands. J Diabetes Metab Disord. 2014; 13:25.
104. Lopez-Pascual A, Arévalo J, Martínez JA, González-Muniesa P. Inverse association between metabolic syndrome and altitude: A cross-sectional study in an adult population of Ecuador. Front Endocrinol. 2018; 9.
105. Hirschler V. Cardiometabolic risk factors in native populations living at high altitudes. Int J Clin Pract. 2016; 70:113-8.
106. Anderson JD, Honigman B. The effect of altitude-induced hypoxia on heart disease: Do acute, intermittent, and chronic exposures provide cardioprotection? High Alt Med Biol. 2011; 12:45-55.
107. Xiaoyue T, Qichuan Q, Jing G, Pengcuo S, Yu H, Tingxin L. Lipid levels in the Jiarong Tibetan's diet at high altitudes: A cross-sectional survey. Front Nutr. 2023; 10:1207710.
108. Wang X, Bian H, Xu X, Geng D, Chen QH. Dyslipidemia analysis in Tibetan and Han adult populations of Qinghai Province. Clinical Focus. 2017, 32:4. (in Chinese)
109. Guzy RD, Schumacker PT. Oxygen sensing by mitochondria at complex III: The paradox of increased reactive oxygen species during hypoxia. Exp Physiol. 2006; 91:807-19.
110. Lusina S-JC, Kennedy PM, Inglis JT, McKenzie DC, Ayas NT, Sheel AW. Long-term intermittent hypoxia increases sympathetic activity and chemosensitivity during acute hypoxia in humans. J Physiol. 2006; 575:961-70.
111. Wu W, Chen G, Zhang X, Wu H, Wang YE, Li X, Liang Y, Liu D. The effect of long-term exposure to moderate high altitude on adipokines and insulin sensitivity. Cytokine. 2025; 185:156823.
112. Behre CJ. Adiponectin, obesity and atherosclerosis. Scand J Clin Lab Invest. 2007; 67:449-58.
113. Tilg H, Moschen AR. Adipocytokines: Mediators linking adipose tissue, inflammation and immunity. Nat Rev Immunol. 2006; 6:772-83.
114. Ge RL, Simonson TS, Cooksey RC, Tanna U, Qin G, Huff CD, Witherspoon DJ, Xing J, Zhengzhong B, Prchal JT, Jorde LB, McClain DA. Metabolic insight into mechanisms of high-altitude adaptation in Tibetans. Mol Genet Metab. 2012; 106:244-7.
115. Brooks GA, Butterfield GE, Wolfe RR, Groves BM, Mazzeo RS, Sutton JR, *et al*. Increased dependence on blood glucose after acclimatization to 4,300 m. J Appl Physiol (1985). 1991; 70:919-27.
116. Tremblay JC, Ainslie PN. Global and country-level estimates of human population at high altitude. Proc Natl Acad Sci U S A. 2021; 118:e2102463118.
117. Zhang C, Wu Y, Wang S, Li M, Tian H, Li S. Adaptive regulation of glucose metabolism and diseases in high-altitude areas. Sichuan Da Xue Xue Bao Yi Xue Ban. 2024; 55:1460-8.
118. Schulze MB, Martínez-González MA, Fung TT, Lichtenstein AH, Forouhi NG. Food based dietary

patterns and chronic disease prevention. BMJ. 2018; 361:k2396.

Received December 11, 2025; Revised February 2, 2026; Accepted February 18, 2026.

[§]These authors contributed equally to this work.
**Address correspondence to:*
Peipei Song, Center for Clinical Sciences, Japan Institute for Health Security, Tokyo, 1-21-1 Toyama Shinjuku-ku, Tokyo 162-8655, Japan.
E-mail: psong@jihs.go.jp

Yanming Ren, Department of Public Health, Qinghai University Medical College, No. 16 Kunlun Rd, Xining 810008, China.
E-mail: btyqh@126.com

Released online in J-STAGE as advance publication February 25, 2026.

Original Article

DOI: 10.5582/bst.2025.01323

Predicting non-alcoholic fatty liver disease (NAFLD) using machine learning algorithms: Evidence from a large-scale community cohort in Taiwan

Tzu-Chun Lin[1], Yu-Ju Wei[1], Po-Cheng Liang[1], Pei-Chien Tsai[1], Yi-Hung Lin[1], Meng-Hsuan Hsieh[1,2], Tyng-Yuan Jang[1,3], Chih-Wen Wang[1,3], Ming-Yen Hsieh[1,4], Zu-Yau Lin[1,3], Ming-Lun Yeh[1,2,3,5], Jee-Fu Huang[1,3], Chung-Feng Huang[1,3], Wan-Long Chuang[1,3], Ming-Lung Yu[1,2,3], Chia-Yen Dai[1,2,3,4,6,*], Hon-Yi Shi[7,8,9,10,*]

[1] Hepatobiliary Division, Department of Internal Medicine, Center for Liquid Biopsy and Cohort Research, Kaohsiung Medical University Hospital, Kaohsiung Medical University, Kaohsiung, Taiwan;
[2] Health Management Center, Department of Occupational and Environmental Medicine, Kaohsiung Medical University Hospital, Kaohsiung Medical University, Kaohsiung, Taiwan;
[3] College of Medicine, Drug Development and Value Creation Research Center, Center for Metabolic Disorders and Obesity, Kaohsiung Medical University, Kaohsiung, Taiwan;
[4] Department of Internal Medicine, Gangshan Hospital, Kaohsiung Medical University, Kaohsiung, Taiwan.;
[5] School of Medicine and Doctoral Program of Clinical and Experimental Medicine, College of Medicine and Center of Excellence for Metabolic Associated Fatty Liver Disease, National Sun Yat-sen University, Kaohsiung, Taiwan;
[6] College of Professional Studies, National Pingtung University of Science and Technology, Pingtung, Taiwan;
[7] Department of Healthcare Administration and Medical Informatics, Kaohsiung Medical University, Kaohsiung, Taiwan;
[8] Master of Health Care Management, Department of Business Management, National Sun Yat-sen University, Kaohsiung, Taiwan;
[9] Department of Medical Research, Kaohsiung Medical University Hospital, Kaohsiung, Taiwan;
[10] Department of Medical Research, China Medical University Hospital, China Medical University, Taichung, Taiwan.

SUMMARY: Closely associated with metabolic disorders, non-alcoholic fatty liver disease (NAFLD) substantially increases the risk of hepatocellular carcinoma. This study aimed to apply machine learning (ML) algorithms to a community-based cohort in southern Taiwan to identify key risk factors for NAFLD and to develop predictive models with clinical applicability. Data were derived from community health examinations, and eighteen clinical and demographic features were analyzed. Five ML algorithms were evaluated: logistic regression (LR), random forest (RF), K-nearest neighbors (KNN), adaptive boosting (AdaBoost), and extreme gradient boosting (XGBoost). Model performance was assessed using accuracy, precision, recall, F1 score, and area under the receiver operating characteristic curve (AUROC). A total of 7,510 participants were included (38.8% male; mean age 50.9 ± 15.0 years). The dataset was randomly divided into training (80%) and testing (20%) subsets, with no significant differences observed between groups in most independent variables. The Synthetic Minority Over-sampling Technique (SMOTE) was employed to balance NAFLD and non-NAFLD groups in the training dataset. Among all models, XGBoost achieved the highest performance, with an accuracy of 83.48%, precision of 84.31%, recall of 81.21%, F1 score of 82.72%, and AUROC of 92.85%. Feature importance analysis identified low-density lipoprotein cholesterol (LDL-C), body mass index (BMI), waist circumference, fasting plasma glucose (FPG), and triglycerides (TG) as the most influential predictors of NAFLD. ML algorithms, particularly XGBoost, demonstrated high accuracy in predicting NAFLD and effectively identified key clinical predictors. These findings may enhance early diagnosis and facilitate the development of targeted intervention strategies in the management of NAFLD.

Keywords: non-alcoholic fatty liver disease (NAFLD), risk factor, machine learning, prediction

1. Introduction

Non-alcoholic fatty liver disease (NAFLD) represents one of the most prevalent chronic liver conditions globally, with an estimated prevalence of approximately 30.0%, showing an upward trend annually (*1*). Projections indicate that by 2040, the global prevalence of NAFLD will escalate to 55.7%, particularly affecting regions such as Asia and Europe (*2*). In Taiwan, NAFLD affects approximately one-third of the population

(*3*). This condition encompasses a spectrum of liver pathologies, including non-alcoholic fatty liver (NAFL) and non-alcoholic steatohepatitis (NASH), which can progress to liver fibrosis, cirrhosis, and hepatocellular carcinoma (HCC). NAFLD is closely linked with obesity, type 2 diabetes, and metabolic syndrome, and it significantly elevates the risk of non-viral HCC (*4-6*). The increasing incidence and associated mortality of NAFLD present substantial health challenges, highlighting the critical importance of early identification and intervention strategies.

The integration of artificial intelligence into medical research has facilitated the extensive application of machine learning (ML) in predicting liver disease risk and treatment outcomes (*7*). ML algorithms, categorized into supervised and unsupervised learning, utilize large datasets to discern complex patterns, thereby enhancing predictive accuracy and classification efficiency. Supervised learning, which relies on training models with labeled datasets, enables precise analysis and prediction. Prominent supervised methods include Logistic Regression (LR), Random Forest (RF), K-Nearest Neighbors (KNN), Adaptive Boosting (AdaBoost), and eXtreme Gradient Boosting (XGBoost). Compared to traditional approaches, ML optimizes predictive capabilities by refining preprocessing models, thereby supporting more effective and precise decision-making.

The present study leveraged a real-world, multi-regional screening database from southern Taiwan to examine risk factors associated with NAFLD using ML algorithms. Advanced artificial intelligence techniques were employed to construct predictive models, identify the most accurate model, and analyze the relative contributions of key influencing factors.

2. Patients and Methods

2.1. Data source and study population

The study population comprised individuals who underwent community health screenings in southern Taiwan between June 1, 2001, and December 31, 2023. Eligibility criteria included the availability of anthropometric and biochemical data, along with abdominal ultrasound records. Major exclusion criteria encompassed duplicate screenings, age below 18 years, hepatitis B or C infection, and excessive alcohol consumption. As illustrated in Figure 1, a total of 7,510 participants met the inclusion criteria. The study was also approved by the Institutional Review Board of Kaohsiung Medical University Hospital (KMUHIRB-E(I)-20220347). Written informed consent was obtained from all participants, and the study was conducted in accordance with the principles outlined in the Declaration of Helsinki.

2.2. Study variables

All participants underwent standardized assessments within a controlled evaluation setting. Data collection encompassed demographic variables (age, sex), medical history (hypertension, diabetes, hyperlipidemia), and lifestyle factors (smoking, alcohol consumption). Anthropometric measurements included height, weight, waist circumference, systolic blood pressure (SBP), and diastolic blood pressure (DBP). Biochemical analyses were conducted using a multichannel automatic analyzer (Hitachi, Tokyo, Japan) to measure aspartate aminotransferase (AST), alanine aminotransferase (ALT), triglycerides (TG), total cholesterol (TC), high-density lipoprotein cholesterol (HDL-C), and low-density lipoprotein cholesterol (LDL-C). Fasting plasma glucose (FPG) levels were determined *via* radioimmunoassay (Diagnostic Products Co., Los Angeles, CA), and hepatic assessments were performed using ultrasound imaging.

NAFLD is diagnosed through imaging or histological confirmation of significant hepatic steatosis, excluding alternative causes such as Wilson's disease, celiac disease, chronic hepatitis C, chronic hepatitis B, and excessive alcohol consumption (>210 g/week in men, >140 g/week in women), in accordance with the American Association for the Study of Liver Diseases (AASLD) guidelines (*8*). Abdominal ultrasound examinations were conducted by licensed hepatology specialists trained at the same institution to ensure diagnostic consistency and minimize

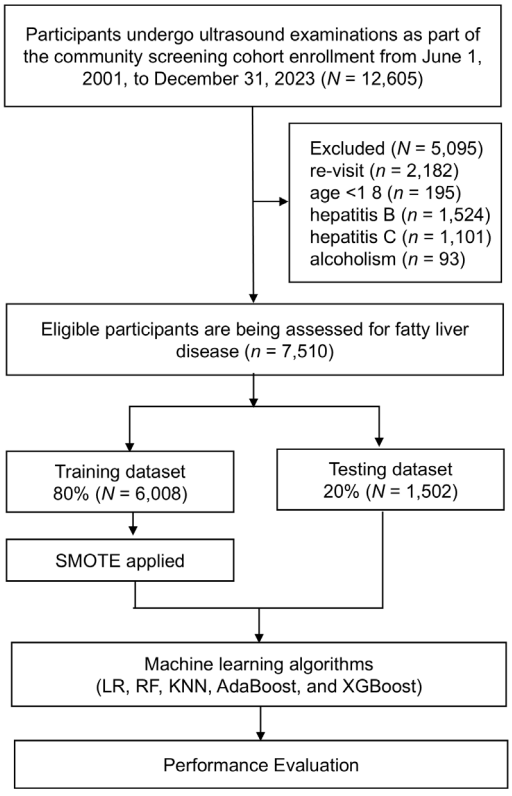

Figure 1. Study flow chart. *Abbreviation*: SMOTE, the synthesized minority oversampling technique. LR, logistic regression; RF, random forest; KNN, k-nearest neighbors; AdaBoost, adaptive boosting; XGBoost, eXtreme Gradient Boosting.

interobserver variability.

2.3. ML algorithms

ML models were constructed using five widely adopted supervised learning algorithms. These included logistic regression (LR), a linear model-based approach, and random forest (RF), an ensemble method utilizing bagging to aggregate multiple decision trees. The k-nearest neighbors (KNN) algorithm predicts outcomes based on feature-space proximity, while adaptive boosting (AdaBoost) iteratively enhances model performance by combining multiple weak learners. Additionally, extreme gradient boosting (XGBoost), an advanced gradient boosting algorithm, integrates bagging and boosting techniques to optimize predictive accuracy and computational efficiency.

2.4. ML algorithms construction and validation

This study included 3,660 individuals in the NAFLD group and 3,850 in the non-NAFLD group, resulting in a data imbalance that could compromise algorithm stability and predictive accuracy. To address this, the synthetic minority oversampling technique (SMOTE) was applied only to the training dataset to balance class distribution during model development (*9*). The dataset was randomly partitioned using the Monte Carlo method into 80% for training and 20% for testing, enabling simultaneous model construction and internal validation. At the same time, the test set retained the original class distribution to provide an unbiased evaluation of model performance. Feature selection was performed through univariate analysis to identify statistically significant predictors for the ML models. Model validation was conducted using 10-fold cross-validation and 1,000 bootstrap resampling iterations.

2.5. Model Interpretability: SHAP Method

When applying ML in medicine, there is often a trade-off between model interpretability and prediction accuracy. Medical decision making relies heavily on understanding the model inference logic to increase the credibility of predictions. To this end, we utilize the Shapley Additive exPlanations (SHAP) method, an additive feature attribution technique based on game-theoretic Shapley values that assesses the relative contribution of each feature to the model output. Through SHAP analysis, we can gain a more transparent understanding of the drivers of model predictions, thereby promoting trust and acceptance in clinical applications (*10,11*).

2.6. Statistical analysis

The unit of analysis was the individual patient who underwent community health screenings in southern Taiwan during the study period. Continuous variables were reported as mean ± standard deviation, while categorical variables were expressed as frequencies and proportions. Comparisons of continuous variables were conducted using Student *t*-test, whereas categorical data were analyzed using the chi-square test. Univariate logistic regression was performed to identify independent risk factors for NAFLD. Mean differences across multiple independent groups were assessed using one-way analysis of variance.

The statistical analysis in this study was conducted in five distinct steps. Initially, The full dataset of 7,510 cases was randomly divided into a training dataset (6,008 cases) for model development and a testing dataset (1,502 cases) for internal validation. Baseline characteristics between the training and testing datasets were compared using Student *t* test for continuous variables and the chi-square test for categorical variables to ensure representativeness and balance. In the second step, univariate logistic regression analyses were performed to identify variables significantly associated with NAFLD. These variables, together with the NAFLD outcome, were used as inputs for ML model development. The third step involved ML model development and performance evaluation. The models were trained using the training dataset, and predictive outputs were generated from the testing dataset. To assess model stability and estimate 95% confidence intervals, 1,000 bootstrap resamples of the datasets were generated. For each resample, model predictions were obtained, and five key performance metrics: accuracy, precision, recall, F1 score, and the area under the receiver operating characteristic curve (AUROC), were calculated. Differences in performance metrics across the models were evaluated using one-way analysis of variance (ANOVA). Confusion matrices were constructed to summarize true positives, true negatives, false positives, and false negatives for each model (*12,13*). The final step involved feature importance analysis to identify the most influential variables for NAFLD. Feature importance was assessed using SHAP, which quantifies the contribution of each feature to the model predictions based on cooperative game theory (*10,11*) SHAP values provide a consistent, model-agnostic measure of feature impact and allow for detailed interpretation of both global and individual level effects, ensuring a robust identification of key predictors.

Statistical analyses were performed using IBM SPSS Statistics v23.0 (IBM Corp., Armonk, NY, USA) and the Python programming language with Anaconda (Spyder v6.1.0). All tests were two-tailed, with statistical significance set at $p < 0.05$.

3. Results

3.1. Distribution of the study variables

This study encompassed a total of 7,510 individuals,

Table 1. Comparisons between the NAFLD and non-NAFLD groups in the screening population were performed

Variables	Total (N = 7,510)	No NAFLD group (n = 3,850, 51.3%)	NAFLD group (n = 3,660, 48.7%)	p-value
Sex, male	2,912 (38.8)	1,388 (36.1)	1,524 (41.6)	< 0.001
Age, years	50.9 ± 15.0	49.1 ± 16.2	52.8 ± 13.4	< 0.001
BMI, kg/m^2	24.9 ± 4.2	23.2 ± 3.5	26.3 ± 4.1	< 0.001
Waist circumference, cm	82.9 ± 10.7	78.5 ± 9.5	87.4 ± 10.0	< 0.001
Smoking	495 (6.6)	221 (5.7)	274 (7.5)	0.002
Alcohol	416 (5.5)	165 (4.3)	251 (6.7)	< 0.001
Hypertension	1,242 (16.5)	461 (12.0)	781 (21.3)	< 0.001
Diabetes	481 (6.4)	150 (3.9)	331 (9.0)	< 0.001
Hyperlipidemia	690 (9.2)	238 (6.2)	452 (12.4)	< 0.001
SBP, mmHg	129.4 ± 19.2	125.6 ± 19.2	133.4 ± 18.5	< 0.001
DBP, mmHg	79.9 ± 11.6	77.7 ± 11.3	82.1 ± 11.6	< 0.001
AST, U/L	26.0 ± 18.9	24.2 ± 16.6	28.0 ± 20.9	< 0.001
ALT, U/L	23.6 ± 17.6	19.7 ± 14.1	27.8 ± 19.7	< 0.001
Triglyceride, mg/dL	133.8 ± 104.5	108.8 ± 86.7	160.1 ± 114.7	< 0.001
Total cholesterol, mg/dL	203.7 ± 36.9	200.8 ± 37.0	206.8 ± 36.5	< 0.001
HDL-C, mg/dL	56.9 ± 13.5	60.5 ± 14.0	53.2 ± 12.0	< 0.001
LDL-C, mg/dL	121.6 ± 28.4	118.0 ± 28.0	125.4 ± 28.3	< 0.001
FPG, mg/dL	94.0 ± 29.3	88.9 ± 24.2	99.4 ± 33.1	< 0.001

Values are presented as mean ± standard deviation or n (%). *Abbreviations*: NAFLD, non-alcoholic fatty liver disease; BMI, body mass index; SBP, systolic blood pressure; DBP, diastolic blood pressure; AST, aspartate aminotransferase; ALT, alanine aminotransferase; HDL-C, high-density lipoprotein cholesterol; LDL-C, low-density lipoprotein cholesterol; FPG, fasting plasma glucose.

including 2,912 males (38.8%) and 4,598 females (61.2%), with a mean age of 50.9 ± 15.0 years (Table 1). The non-NAFLD and NAFLD groups included 3,850 and 3,660 individuals, respectively, accounting for 51.3% and 48.7% of the total population. The distributions of independent variables are presented in Table 1. Univariate statistical analysis identified significant independent variables, which were subsequently included as predictors in the ML models (Table 2).

Table 2. Univariate analysis of NAFLD associated variables in the training dataset (N = 6,008)

Variables	OR (95% CI)	p-value
Sex, male *vs*. female	1.30 (1.17-1.44)	< 0.001
Age, years	1.02 (1.01-1.02)	< 0.001
BMI, kg/m^2	1.30 (1.27-1.32)	< 0.001
Waist circumference, cm	1.10 (1.09-1.11)	< 0.001
Smoking, yes *vs*. no	1.27 (1.04-1.56)	0.020
Alcohol, yes *vs*. no	1.58 (1.26-1.98)	< 0.001
Hypertension, yes *vs*. no	1.96 (1.71-2.26)	< 0.001
Diabetes, yes *vs*. no	2.36 (1.89-2.96)	< 0.001
Hyperlipidemia, yes *vs*. no	2.05 (1.71-2.46)	< 0.001
SBP, mmHg	1.02 (1.02-1.03)	< 0.001
DBP, mmHg	1.03 (1.03-1.04)	< 0.001
AST, U/L	1.02 (1.01-1.02)	< 0.001
ALT, U/L	1.04 (1.03-1.04)	< 0.001
Triglyceride, mg/dL	1.01 (1.01-1.01)	< 0.001
Total cholesterol, mg/dL	1.00 (1.00-1.01)	<0.001
HDL-C, mg/dL	0.96 (0.95-0.96)	<0.001
LDL-C, mg/dL	1.01 (1.01-1.01)	< 0.001
FPG, mg/dL	1.02 (1.02-1.02)	< 0.001

Abbreviations: NAFLD, non-alcoholic fatty liver disease; OR, odds ratio; BMI, body mass index; SBP, systolic blood pressure; DBP, diastolic blood pressure; AST, aspartate aminotransferase; ALT, alanine aminotransferase; HDL-C, high-density lipoprotein cholesterol; LDL-C, low-density lipoprotein cholesterol; FPG, fasting plasma glucose.

3.2. Comparison of the ML models

The dataset was stratified into training and testing subsets, with a division ratio of 80:20. The training subset comprised 6,008 individuals, while the testing subset included 1,502 individuals (Supplementary Table S1, *https://www.biosciencetrends.com/action/getSupplementalData.php?ID=289*). Statistical analyses revealed no significant differences in most independent variables between the two datasets, indicating that both were derived from a relatively homogeneous population. Moreover, optimal hyperparameters and model architectures for the ML models were determined through grid search during the hyperparameter tuning process. The number of training epochs was fine-tuned through the procedure detailed in Supplementary Table S2 (*https://www.biosciencetrends.com/action/getSupplementalData.php?ID=289*).

Supplementary Figure S1 (*https://www.biosciencetrends.com/action/getSupplementalData.php?ID=289*) presents the confusion matrices for all ML models applied to the SMOTE resampled training (80%) and testing (20%) datasets. The performance metrics for LR, RF, KNN, AdaBoost, and XGBoost on the testing dataset were as follows: accuracy (0.72, 0.80, 0.66, 0.81, 0.84), precision (0.71, 0.82, 0.74, 0.81, 0.84), recall (0.72, 0.76, 0.47, 0.80, 0.83), F1 score (0.72, 0.79, 0.57, 0.80, 0.83), and AUROC (0.80, 0.88, 0.72, 0.90, 0.93) (Supplementary Table S3, *https://www.biosciencetrends.com/action/getSupplementalData.php?ID=289*). To enhance model robustness and mitigate overfitting, 10-fold cross-validation was conducted on both datasets (*data*

Table 3. Comparison of the machine learning (ML) model performance metrics following bootstrapping (*N* = 7,510)

Training dataset (*n* = 6,008)					
Model	Accuracy (95% CI)	Precision (95% CI)	Recall (95% CI)	F1 score (95% CI)	AUROC (95% CI)
LR	72.55% (71.39-73.81%)	72.25% (70.50-74.01%)	70.89% (69.12-72.67%)	71.56% (70.12-73.04%)	79.09% (77.89-80.36%)
RF	80.59% (79.55-81.65%)	81.75% (80.21-83.26%)	77.47% (75.87-79.09%)	79.55% (78.30-80.77%)	88.59% (87.71-89.47%)
KNN	82.85% (81.78-83.84%)	100.00% (100.00-100.00%)	64.81% (62.89-66.57%)	78.64% (77.22-79.93%)	93.89% (93.40-94.32%)
AdaBoost	82.18% (81.14-83.13%)	81.93% (80.40-83.37%)	81.36% (79.85-82.84%)	81.64% (80.49-82.77%)	90.70% (89.95-91.40%)
XGBoost	89.03% (88.16-89.88%)	89.21% (87.96-90.38%)	88.17% (86.94-89.50%)	88.68% (87.75-89.59%)	96.51% (96.13-96.88%)
p-value	< 0.001	< 0.001	< 0.001	< 0.001	< 0.001
Testing dataset (*n* = 1,502)					
Model	Accuracy (95% CI)	Precision (95% CI)	Recall (95% CI)	F1 score (95% CI)	AUROC (95% CI)
LR	73.41% (71.21-75.80%)	73.68% (70.44-76.98%)	70.72% (67.07-74.14%)	72.15% (69.46-74.89%)	79.79% (77.55-82.04%)
RF	79.22% (76.91-81.42%)	81.36% (78.09-84.38%)	74.44% (70.95-77.60%)	77.73% (74.98-80.13%)	88.04% (86.13-89.71%)
KNN	65.38% (62.92-67.80%)	73.51% (68.95-77.75%)	45.29% (41.38-49.08%)	56.02% (52.33-59.28%)	71.29% (68.61-73.83%)
AdaBoost	81.74% (79.50-83.79%)	83.03% (79.94-85.83%)	78.64% (75.27-81.71%)	80.76% (78.24-83.13%)	91.02% (89.49-92.36%)
XGBoost	83.48% (81.50-85.42%)	84.31% (81.48-87.18%)	81.21% (78.24-84.17%)	82.72% (80.46-85.00%)	92.85% (91.55-94.13%)
p-value	< 0.001	< 0.001	< 0.001	< 0.001	< 0.001

P values were calculated using one-way analysis of variance (ANOVA) to assess whether differences in performance metrics were statistically significant across ML models. *Abbreviations*: AUROC, area under the receiver operating characteristic curve; LR, logistic regression; RF, random forest; KNN, K-nearest neighbors; AdaBoost, adaptive boosting; XGBoost, eXtreme gradient boosting.

not shown). Furthermore, model stability was assessed through 1,000 bootstrap resampling iterations, followed by ANOVA, which demonstrated statistically significant differences among the models ($p < 0.05$) (Table 3). Among the models evaluated, XGBoost exhibited the highest predictive performance for NAFLD in both the training and testing datasets, with a test set accuracy of 83.48% (95% CI 81.50-85.42%), precision of 84.31% (95% CI 81.48-87.18%), recall of 81.21% (95% CI 78.24-84.17%), F1 score of 82.72% (95% CI 80.46-85.00%), and AUROC of 92.85% (95% CI 91.55-94.13%).

3.3. Results of feature importance analysis

The analysis demonstrated that among the five ML models evaluated, XGBoost achieved the highest classification performance across all key metrics, establishing it as the most effective model for predicting NAFLD. To further elucidate the relative contribution of individual predictors, a feature importance analysis was performed using the SHAP framework. SHAP values quantify the impact of each independent variable on model predictions, with higher absolute values indicating a stronger contribution to NAFLD risk. As illustrated in Figure 2, the five most influential variables of NAFLD were LDL-C, BMI, waist circumference, FPG, and TG. While XGBoost internal feature importance provided similar trends (Figure 3), SHAP analysis was used as the primary interpretability tool due to its model agnostic transparency and stability against correlated variables.

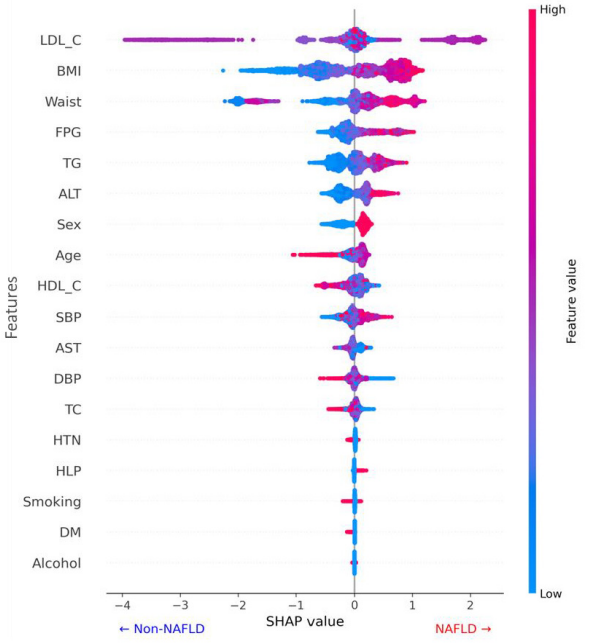

Figure 2. SHAP summary plot. The SHAP summary plot combined the feature importance and effects on non-alcoholic fatty liver. *Abbreviation*: SHAP, Shapley additive explanations; LDL-C, low-density lipoprotein cholesterol; BMI, body mass index; FPG, fasting plasma glucose; TG, triglyceride; ALT, alanine aminotransferase; HDL-C, high-density lipoprotein cholesterol; SBP, systolic blood pressure; AST, aspartate aminotransferase; DBP, diastolic blood pressure; TC, Total Cholesterol; HTN, hypertension; HLP, hyperlipidemia; DM, diabetes mellitus.

4. Discussion

4.1. Major findings

Given the absence of effective pharmacological interventions for NAFLD, early detection and prevention are paramount in improving patient outcomes. The increasing integration of AI and ML in healthcare has enhanced clinicians' ability to analyze the epidemiology,

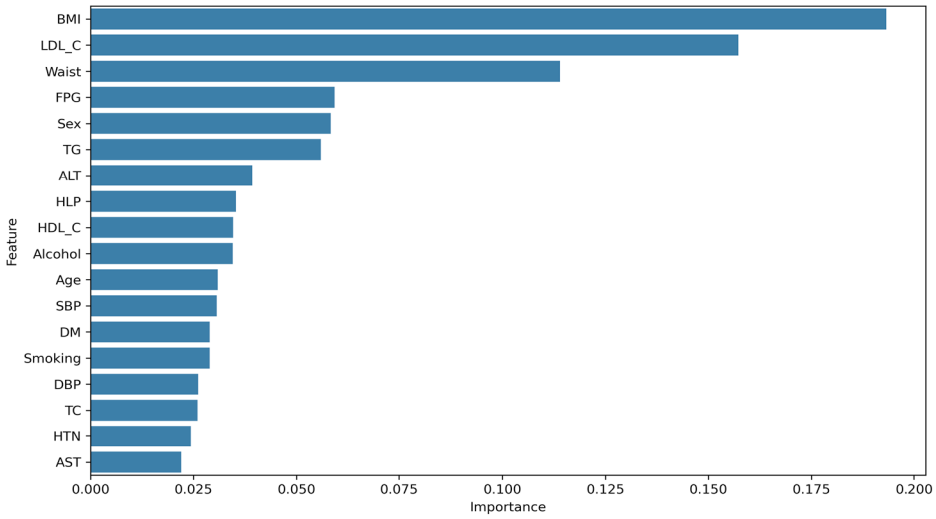

Figure 3. Analysis of feature importance for the occurrence of non-alcoholic fatty liver disease using the XGBoost model. *Abbreviation*: XGBoost, eXtreme Gradient Boosting; BMI, body mass index; LDL-C, low-density lipoprotein cholesterol; FPG, fasting plasma glucose; TG, triglyceride; ALT, alanine aminotransferase; HLP, hyperlipidemia; HDL-C, high-density lipoprotein cholesterol; SBP, systolic blood pressure; DM, diabetes mellitus; DBP, diastolic blood pressure; TC, Total Cholesterol; HTN, hypertension; AST, aspartate aminotransferase.

etiology, and management of diseases. Leveraging AI-driven analysis of healthcare big data enables the precise identification of at-risk individuals, facilitating targeted interventions and optimizing patient care strategies (*14-16*).

4.2. Comparison of ML-based NAFLD prediction with previous literatures

This study assessed five ML models for predicting fatty liver disease in a Taiwanese community cohort. Using data from 7,510 individuals and 18 anthropometric and biochemical variables, XGBoost demonstrated superior predictive performance (AUROC: 96.51% training, 92.85% validation). By integrating gradient boosting and regularization, XGBoost effectively addresses multicollinearity and overfitting, enhancing classification performance (*17*). A review of global studies highlights XGBoost superior accuracy in liver disease prediction, particularly in early NAFLD detection (*18-27*). Table 4 summarizes related studies on ML-based NAFLD prediction (*18-27*). Its robustness is enhanced by optimizing max depth and colsample bytree, while the application of multiple imputation by chained equations (MICE) for missing data and SMOTE for class balancing mitigates bias and overfitting. XGBoost has demonstrated excellence in diagnosing and staging MASLD. In our previous study, we have compared five ML models for predicting direct-acting antiviral drugs treatment failure in hepatitis C, with XGBoost outperforming others through iterative gradient boosting (*20*). Similarly, in a liver cancer risk model using epigenomic data, XGBoost achieved the highest accuracy (99.67%) and AUROC (100%) (*24*). This study assessed LR, RF, KNN, AdaBoost, and XGBoost using accuracy, precision, recall, F1 score, and AUROC. XGBoost consistently outperformed other models, underscoring its potential for precise NAFLD prediction and its clinical utility in personalized medicine.

4.3. Comparison of risk factors of NAFLD with previous literatures

Feature contributions assessed *via* SHAP values in the XGBoost model identified LDL-C, BMI, waist circumference, FPG, and TG as the five most significant predictors of NAFLD. NAFLD, defined by hepatic lipid accumulation exceeding 5%, is strongly associated with metabolic dysfunction, including obesity, insulin resistance, and hypertension (*28*). Hepatic lipid accumulation arises from dysregulated lipid metabolism, characterized by excessive hepatic de novo lipogenesis (DNL), impaired fatty acid oxidation, and altered lipid export *via* very low-density lipoproteins (VLDL-C) (*29*). These metabolic disturbances contribute to atherogenic dyslipidemia, marked by elevated TG, small dense LDL-C (sdLDL-C), and decreased high-density lipoprotein cholesterol (HDL-C) (*30,31*). The accumulation of LDL-C promotes vascular plaque formation, thereby increasing the risk of cardiovascular disease (CVD) and potentially exacerbating hepatic steatosis and progression to steatohepatitis, underscoring its significant association with NAFLD.

Notably, the SHAP summary plot demonstrated that the contribution of LDL-C to NAFLD prediction was not strictly monotonic, as both positive and negative SHAP values were observed across comparable LDL-C levels. This distribution indicates that the influence of LDL-C on NAFLD risk is dependent and likely modified by coexisting metabolic characteristics, including BMI,

Table 4. Summary of related studies on machine learning (ML) algorithms in individuals with non-alcoholic fatty liver disease (NAFLD)

Author (Country)	No. of subjects	Major findings
Lin *et al*., 2026 (Taiwan)	A total of 7,510 subjects participated in community health and abdominal ultrasound examinations	In predicting NAFLD using logistic regression (LR), random forest (RF), k-nearest neighbors (KNN), adaptive boosting (AdaBoost), and extreme gradient boosting (XGBoost), XGBoost exhibited the highest accuracy, emerging as the superior predictive model.
Cao *et al*., 2024 (China) (*18*)	22,140 health checkup participants	XGBoost outperformed LR, naive bayes (NB), and decision tree (DT) models in the early prediction of NAFLD.
McTeer *et al*., 2024 (UK) (*19*)	European non-alcoholic fatty liver disease (NAFLD) database	Using XGBoost to diagnose and stage patients with metabolic dysfunction-associated steatotic liver disease (MASLD), the AUROC reached 99%.
Lu *et al*., 2024 (Taiwan) (*20*)	34,301 hepatitis patients received direct-acting antiviral (DAA) therapy	Among five machine learning models: LR, DT, RF, XGBoost, and artificial neural network (ANN), used to predict factors leading to treatment failure in hepatitis C patients receiving direct-acting antiviral (DAA) therapy, XGBoost exhibited the highest predictive capability.
Peng *et al*., 2023 (China) (*21*)	578 physical examination subjects	Using machine learning algorithms such as LR, RF, XGBoost, gradient boosting machine (GBM), and support vector machine (SVM), the development and validation of models for NAFLD were performed, with XGBoost showing the best performance.
Zeng *et al.*, 2023 (China) (*22*)	6,648 patients with decompensated cirrhosis (DC)	The overall performance of the XGBoost model surpasses that of the traditional LR model and accurately predicts the risk of developing decompensated cirrhosis.
Suárez *et al*., 2023 (Mexico) (*23*)	215 patients with non-alcoholic steatohepatitis (NASH)	XGBoost outperformed SVM, DT, GBM, and KNN in predicting liver fibrosis progression in NASH patients.
Vekariya *et al*., 2022 (Canada) (*24*)	The Cancer Genome Atlas (TCGA)	Using epigenomic data, a predictive model for hepatocellular carcinoma risk was developed by applying XGBoost, RF, NB, KNN, multilayer perceptron (MLP), DT, and SVM. XGBoost emerged as the best model.
Ghandian *et al*., 2022 (U.S.A) (*25*)	141,293 patients with NAFLD	XGBoost outperformed LR and MLP models in assessing the risk of progression from NAFLD to NASH or fibrosis in patients.
Liu e*t al*., 2021 (China) (*26*)	15,315 adults underwent health check-ups	Compared to LR, SVM, stochastic gradient descent (SGD), MLP, convolutional neural network (CNN), and long short-term memory (LSTM) models, XGBoost exhibits superior predictive capability for NAFLD.
Agarwal *et al*., 2021 (India) (*27*)	828 patients with chronic liver disease	The application of XGBoost models has enhanced the accuracy of predicting esophageal variceal bleeding in patients with compensated advanced chronic liver disease.

waist circumference, triglyceride concentrations, and glycaemic status, all of which ranked highly in feature importance. Such non-linear and interaction patterns are intrinsic to tree-based ML algorithms and reflect complex multivariable dependencies rather than independent linear associations. However, formal interaction analyses, such as SHAP interaction values or stratified modeling approaches, were not undertaken in the present study. Further research incorporating explicit interaction modeling is warranted to elucidate these metabolic interrelationships and to enhance interpretability of model risk estimates. Previous research has demonstrated that elevated LDL-C levels, even within the normal range, constitute a significant risk factor for NAFLD (*32*). A retrospective study conducted in Japan by Tomizawa *et al*. identified a strong correlation between triglyceride levels and NAFLD within the context of dyslipidemia (*33*). Furthermore, a meta-analysis confirmed obesity as an independent risk factor, indicating that obese individuals have a 3.5-fold increased risk of developing NAFLD (*34*). The same analysis revealed a dose-dependent association between BMI and NAFLD risk, with each unit increase in BMI corresponding to a 1.20-fold elevation in risk. Additionally, a meta-analysis of 20 studies demonstrated that abdominal obesity, as measured by waist circumference, poses a greater risk for NAFLD than general obesity, as assessed by BMI (*35*). Elevated FPG levels may indicate an increased risk

Table 5. Selected studies on risk factors influencing non-alcoholic fatty liver disease (NAFLD)

Author (Country)	No of subjects	Major findings
Lin *et al.*, 2026 (Taiwan)	7,510 subjects participated in community health examinations and abdominal ultrasound screenings	The primary risk factor for NAFLD is low-density lipoprotein cholesterol (LDL-C), followed by body mass index (BMI), waist circumference (WC), fasting plasma glucose (FPG), and triglycerides (TG).
Alnimer & Alnimer, 2023 (U.S.A) (*37*)	2017-2018 national health and nutrition examination survey (NHANES) dataset	TG, age, BMI, and glycated hemoglobin (HbA1c) are the primary factors influencing the prediction of hepatic steatosis.
Wang *et al*., 2023 (China) (*38*)	31,718 adults undergoing medical examinations	The prevalence of NAFLD is 53.5%. key risk factors include age, BMI, systolic blood pressure (SBP), diastolic blood pressure (DBP), alanine aminotransferase (ALT), aspartate aminotransferase (AST), FPG, total bilirubin, TG, and LDL-C.
Noureddin *et al.*, 2022 (U.S.A) (*39*)	2017-2018 NHANES dataset	Risk factors influencing NAFLD include gender, HbA1c, BMI, WC, and AST.
Huang *et al*., 2022 (Taiwan) (*40*)	2,483 subjects who underwent community health examinations	The prevalence of NAFLD and metabolic syndrome was 44.5% and 15.8%, respectively. Increasing age, higher BMI (obesity), and elevated insulin resistance (IR) were identified as major risk factors for NAFLD, with high IR serving as a significant independent predictor in both obese and non-obese individuals.
Chen *et al*., 2022 (Taiwan) (*41*)	31,930 adults aged 20 and older underwent health screenings and ultrasounds.	ALT, BMI, WC, and TG are important risk factors influencing NAFLD.
Long *et al*., 2018 (U.S.A) (*42*)	685 participants in the Framingham Heart Study	Significant associated factors include age, female sex, BMI, alcohol consumption, and TG.
Sun *et al*., 2016 (Korea) (*32*)	20,433 subjects who underwent liver ultrasound	Elevated LDL-C levels are a risk factor for NAFLD.
Li *et al*., 2016 (China) (*43*)	21 studies were selected for this study (381,655 participants)	Obesity increases the risk of NAFLD by 3.5 times, demonstrating a clear dose-response relationship between BMI and NAFLD.
Pang *et al*., 2015 (China) (*35*)	20 studies were selected from PubMed, EMBASE, and the ISI Web of Science for this analysis	Abdominal obesity, measured by WC, is associated with a higher risk of developing NAFLD compared to general obesity assessed by BMI.
Tomizawa *et al*., 2014 (Japan) (*33*)	293 subjects underwent abdominal ultrasound	Among lipid abnormalities, TG are closely correlated with NAFLD, and elevated TG levels serve as an important marker for the condition.
Eguchi *et al*., 2012 (Japan) (*44*)	5,075 subjects who underwent health examinations	The prevalence of NAFLD is 29.7%, with males (41.0%) showing a three-fold higher rate than females (17.7%). Significant relationship exists between NAFLD prevalence and metabolic indices, including BMI, TG, and LDL-C ($p < 0.001$).

of NAFLD, and this association is more pronounced in shorter individuals (*36*). The important influencing factors related to NAFLD are summarized in Table 5 (*32,33,35,37-44*). Collectively, these findings highlight LDL-C, BMI, waist circumference, FPG, and TG as major contributors to metabolic dysfunction underlying NAFLD. Given that NAFLD is now encompassed under the concept of metabolic dysfunction–associated steatotic liver disease (MASLD) (*45*), these factors reflect underlying metabolic derangements, including dyslipidemia, insulin resistance, and central obesity, that contribute to both hepatic steatosis and cardiometabolic risk. Consequently, monitoring and managing these variables may provide critical opportunities for early identification and intervention in individuals at risk of MASLD.

4.4. Strengths and limitations

This study has several notable strengths. First, unlike prior research primarily based on single-institution datasets or interdisciplinary studies, this study utilizes community health check-up data from multiple counties and cities in southern Taiwan, thereby enhancing its generalizability and applicability to the broader Taiwanese population. Second, rather than incorporating all variables into the ML model without distinction, this study employed univariate analysis to identify

significant predictors of NAFLD, thereby mitigating the risk of confounding effects and improving model interpretability. Furthermore, the application of SMOTE to balance the sample sizes of NAFLD and non-NAFLD groups effectively addresses class imbalance, minimizing selection bias across variables. In contrast to previous studies that relied solely on absolute performance metrics for model comparison, this study adopted a more rigorous approach by implementing the bootstrap method with Monte Carlo simulations, conducting 1,000 resampling iterations. ANOVA testing was subsequently performed to assess the statistical significance of performance differences among models. Finally, feature importance analysis of the optimal model identified key predictors of NAFLD risk, ensuring that the predictive accuracy is robust and reflective of the relative contribution of each variable.

This study has several limitations. First, the absence of diagnostic evaluations for drug-induced, acquired metabolic, and genetic liver diseases, including autoimmune hepatitis, primary biliary cholangitis, and hemochromatosis, precludes the precise exclusion of these conditions, thereby limiting the accuracy of NAFLD classification. Second, key clinical variables, such as lifestyle and dietary factors, were not incorporated into the analysis, potentially introducing unaccounted confounding effects and affecting the performance metrics of the models. Third, the study was restricted to five commonly used ML algorithms. Future research should explore a broader spectrum of predictive models to enhance the methodological rigor, predictive accuracy, and generalizability of the findings. Fourth, although SHAP analysis enhances model interpretability, the present study did not conduct formal interaction or non-linear effect modeling to quantify dependencies among metabolic predictors. The observed SHAP patterns should be interpreted as reflecting complex multivariable relationships rather than isolated independent effects. Future investigations incorporating explicit interaction terms or causal models may further elucidate these underlying mechanisms. Finally, the lack of external validation represents an important limitation, as the models were evaluated only within the internal dataset. This may limit their applicability in real-world settings, where population characteristics and clinical practices may differ, underscoring the need for external validation before clinical implementation.

In conclusion, ML algorithms facilitate the development of highly accurate predictive models and the identification of key determinants of disease risk, providing critical insights for diagnosis and intervention. Among the five models analyzed, XGBoost exhibited the highest predictive performance for NAFLD, identifying LDL-C, BMI, waist circumference, FPG, and TG as significant risk factors. This model enhances the understanding of NAFLD pathophysiology and supports early detection and targeted prevention strategies, thereby contributing to improved public health outcomes and healthcare quality.

Funding: This study was supported by the Ministry of Health and Welfare and National Sun Yat-sen University and National Pingtung University of Science and Technology and Kaohsiung Medical University and Kaohsiung Medical University Hospital by grants from the National Science Council of Taiwan (grant number NSTC 112-2314-B-037-076-MY3), and Kaohsiung Medical University (114CM-KMU-04, NYCUKMU-115-I004, MOHW115-TDU-B-222-114011), and Kaohsiung Medical University Hospital (S11413, KMUH114-4R07). We appreciate the support from the staff of the Taiwan Liver Research Foundation.

Conflict of Interest: The authors have no conflicts of interest to disclose.

References

1. Younossi ZM, Golabi P, Paik JM, Henry A, Dongen CV, Henry L. The global epidemiology of nonalcoholic fatty liver disease (NAFLD) and nonalcoholic steatohepatitis (NASH): A systematic review. Hepatology. 2023; 77:1335-1347.
2. Le MH, Yeo YH, Zou B, Barnet S, Henry L, Cheung R, Nguyen MH. Forecasted 2040 global prevalence of nonalcoholic fatty liver disease using hierarchical bayesian approach. Clin Mol Hepatol. 2022; 28:841-850.
3. Li J, Zou B, Yeo YH, *et al*. Prevalence, incidence, and outcome of non-alcoholic fatty liver disease in Asia, 1999-2019: a systematic review and meta-analysis. Lancet Gastroenterol Hepatol. 2019; 4:389-398.
4. Le MH, Le DM, Baez TC, Dang H, Nguyen VH, Lee K, Stave CD, Ito T, Wu Y, Yeo YH, Ji F, Cheung R, Nguyen MH. Global incidence of adverse clinical events in non-alcoholic fatty liver disease: A systematic review and meta-analysis. Clin Mol Hepatol. 2024; 30:235-246.
5. Petroni ML, Brodosi L, Bugianesi E, Marchesini G. Management of non-alcoholic fatty liver disease. BMJ. 2021; 372:m4747.
6. Huang YC, Huang JC, Chien HH, Lin CI, Chuang YS, Cheng HY, Lin WT, Lin YY, Chuang HY, Ho CK, Wang CL, Dai CY. Performance of nonalcoholic fatty liver fibrosis score in estimating atherosclerotic cardiovascular disease risk. Nutr Metab Cardiovasc Dis. 2023; 33:2479-2487.
7. Hur MH, Yip TC, Kim SU, *et al*. A machine learning model to predict liver-related outcomes after the functional cure of chronic hepatitis B. J Hepatol. 2025; 82:235-244.
8. Rinella ME, Neuschwander-Tetri BA, Siddiqui MS, Abdelmalek MF, Caldwell S, Barb D, Kleiner DE, Loomba R. AASLD Practice Guidance on the clinical assessment and management of nonalcoholic fatty liver disease. Hepatology. 2023; 77:1797-1835.
9. Mathew J, Pang CK, Luo M, Leong WH. Classification of Imbalanced Data by Oversampling in Kernel Space of Support Vector Machines. IEEE Trans Neural Netw Learn Syst. 2018; 29:4065-4076.
10. Thomson W, Roth AE. The Shapley value: Essays in honor of Lloyd S. Shapley. Economica 1991; 58:123.

11. Belle V, Papantonis I. Principles and Practice of Explainable Machine Learning. Front Big Data. 2021; 4:688969.
12. Hinterreiter A, Ruch P, Stitz H, Ennemoser M, Bernard J, Strobelt H, Streit M. ConfusionFlow: A Model-Agnostic Visualization for Temporal Analysis of Classifier Confusion. IEEE Trans Vis Comput Graph. 2022; 28:1222-1236.
13. Garnavi R, Aldeen M. Optimized weighted performance index for objective evaluation of border-detection methods in dermoscopy images. IEEE Trans Inf Technol Biomed. 2011; 15:908-917.
14. Hamlet P, Tremblay J. Artificial intelligence in medicine. Metabolism 2017;69:S36-S40.
15. Ahn JC, Connell A, Simonetto DA, Hughes C, Shah VH. Application of Artificial Intelligence for the Diagnosis and Treatment of Liver Diseases. Hepatology. 2021; 73:2546-2563.
16. Le Berre C, Sandborn WJ, Aridhi S, Devignes MD, Fournier L, Smaïl-Tabbone M, Danese S, Peyrin-Biroulet L. Application of Artificial Intelligence to Gastroenterology and Hepatology. Gastroenterology 2020; 158:76-94.
17. Liu P, Fu B, Yang SX, Deng L, Zhong X, Zheng H. Optimizing Survival Analysis of XGBoost for Ties to Predict Disease Progression of Breast Cancer. IEEE Trans Biomed Eng. 2021; 68:148-160.
18. Cao T, Zhu Q, Tong C, Halengbieke A, Ni X, Tang J, Han Y, Li Q, Yang X. Establishment of a machine learning predictive model for non-alcoholic fatty liver disease: A longitudinal cohort study. Nutr Metab Cardiovasc Dis. 2024; 34:1456-1466.
19. McTeer M, Applegate D, Mesenbrink P, *et al*. Machine learning approaches to enhance diagnosis and staging of patients with MASLD using routinely available clinical information. PLoS One. 2024; 19:e0299487.
20. Lu MY, Huang CF, Hung CH, *et al.* Artificial intelligence predicts direct-acting antivirals failure among hepatitis C virus patients: A nationwide hepatitis C virus registry program. Clin Mol Hepatol. 2024; 30:64-79.
21. Peng HY, Duan SJ, Pan L, Wang MY, Chen JL, Wang YC, Yao SK. Development and validation of machine learning models for nonalcoholic fatty liver disease. Hepatobiliary Pancreat Dis Int. 2023; 22:615-621.
22. Zheng J, Li J, Zhang Z, Yu Y, Tan J, Liu Y, Gong J, Wang T, Wu X, Guo Z. Clinical Data based XGBoost Algorithm for infection risk prediction of patients with decompensated cirrhosis: A 10-year (2012-2021) Multicenter Retrospective Case-control study. BMC Gastroenterol. 2023; 23:310.
23. Suárez M, Martínez R, Torres AM, Torres B, Mateo J. A Machine Learning Method to Identify the Risk Factors for Liver Fibrosis Progression in Nonalcoholic Steatohepatitis. Dig Dis Sci. 2023; 68:3801-3809.
24. Vekariya V, Passi K, Jain CK. Predicting liver cancer on epigenomics data using machine learning. Front Bioinform. 2022; 2:954529.
25. Ghandian S, Thapa R, Garikipati A, Barnes G, Green-Saxena A, Calvert J, Mao Q, Das R. Machine learning to predict progression of non-alcoholic fatty liver to non-alcoholic steatohepatitis or fibrosis. JGH Open. 2022; 6:196-204.
26. Liu YX, Liu X, Cen C, Li X, Liu JM, Ming ZY, Yu SF, Tang XF, Zhou L, Yu J, Huang KJ, Zheng SS. Comparison and development of advanced machine learning tools to predict nonalcoholic fatty liver disease: An extended study. Hepatobiliary Pancreat Dis Int. 2021; 20:409-415.
27. Agarwal S, Sharma S, Kumar M, Venishetty S, Bhardwaj A, Kaushal K, Gopi S, Mohta S, Gunjan D, Saraya A, Sarin SK. Development of a machine learning model to predict bleed in esophageal varices in compensated advanced chronic liver disease: A proof of concept. J Gastroenterol Hepatol. 2021; 36:2935-2942.
28. de Alwis NMW, Day CP. Non-alcoholic fatty liver disease: the mist gradually clears. J Hepatol. 2008; 48:S104-S112.
29. Martin A, Lang S, Goeser T, Demir M, Steffen HM, Kasper P. Management of Dyslipidemia in Patients with Non-Alcoholic Fatty Liver Disease. Curr Atheroscler Rep. 2022; 24:533-546.
30. Deprince A, Haas JT, Staels B. Dysregulated lipid metabolism links NAFLD to cardiovascular disease. Mol Metab. 2020; 42:101092.
31. Chatrath H, Vuppalanchi R, Chalasani N. Dyslipidemia in patients with nonalcoholic fatty liver disease. Semin Liver Dis. 2012; 32:22-29.
32. Sun DQ, Liu WY, Wu SJ, Zhu GQ, Braddock M, Zhang DC, Shi KQ, Song D, Zheng MH. Increased levels of low-density lipoprotein cholesterol within the normal range as a risk factor for nonalcoholic fatty liver disease. Oncotarget. 2016; 7:5728-5737.
33. Tomizawa M, Kawanabe Y, Shinozaki F, Sato S, Motoyoshi Y, Sugiyama T, Yamamoto S, Sueishi M. Triglyceride is strongly associated with nonalcoholic fatty liver disease among markers of hyperlipidemia and diabetes. Biomed Rep. 2014; 2:633-636.
34. Li L, Liu DW, Yan HY, Wang ZY, Zhao SH, Wang B. Obesity is an independent risk factor for non-alcoholic fatty liver disease: evidence from a meta-analysis of 21 cohort studies. Obes Rev. 2016; 17:510-519.
35. Pang Q, Zhang JY, Song SD, Qu K, Xu XS, Liu SS, Liu C. Central obesity and nonalcoholic fatty liver disease risk after adjusting for body mass index. World J Gastroenterol. 2015; 21:1650-1662.
36. Zou Y, Yu M, Sheng G. Association between fasting plasma glucose and nonalcoholic fatty liver disease in a nonobese Chinese population with normal blood lipid levels: a prospective cohort study. Lipids Health Dis 2020; 19:145.
37. Alnimer Y, Alnimer T. Prediction of Liver Steatosis and Fibrosis Based on Clinical Variables Using a Large National Survey Database. Can J Gastroenterol Hepatol. 2023; 1791500.
38. Wang G, Shen X, Wang Y, Lu H, He H, Wang X. Analysis of risk factors related to nonalcoholic fatty liver disease: a retrospective study based on 31,718 adult Chinese individuals. Front Med. 2023; 10:1168499.
39. Noureddin M, Ntanios F, Malhotra D, Hoover K, Emir B, McLeod E, Alkhouri N. Predicting NAFLD prevalence in the United States using National Health and Nutrition Examination Survey 2017-2018 transient elastography data and application of machine learning. Hepatol Commun. 2022; 6:1537-1548.
40. Huang JF, Tsai PC, Yeh ML, Huang CF, Huang CI, Hsieh MH, Dai CY, Yang JF, Chen SC, Yu ML, Chuang WL, Chang WY. Risk stratification of non-alcoholic fatty liver disease across body mass index in a community basis. J Formos Med Assoc. 2020; 119:89-96.
41. Chen YY, Lin CY, Yen HH, Su PY, Zeng YH, Huang SP,

Liu IL. Machine-Learning Algorithm for Predicting Fatty Liver Disease in a Taiwanese Population. J Pers Med. 2022; 12:1026.42.
42. Long MT, Pedley A, Massaro JM, Hoffmann U, Ma J, Loomba R, Chung RT, Benjamin EJ. A simple clinical model predicts incident hepatic steatosis in a community-based cohort: The Framingham Heart Study. Liver Int. 2018; 38:1495-1503.
43. Li L, Liu DW, Yan HY, Wang ZY, Zhao SH, Wang B. Obesity is an independent risk factor for non-alcoholic fatty liver disease: evidence from a meta-analysis of 21 cohort studies. Obes Rev. 2016; 17:510-519.
44. Eguchi Y, Hyogo H, Ono M, Mizuta T, Ono N, Fujimoto K, Chayama K, Saibara T; JSG-NAFLD. Prevalence and associated metabolic factors of nonalcoholic fatty liver disease in the general population from 2009 to 2010 in Japan: A multicenter large retrospective study. J Gastroenterol. 2012; 47:586-595.
45. Hagström H, Vessby J, Ekstedt M, Shang Y. 99% of patients with NAFLD meet MASLD criteria and natural history is therefore identical. J Hepatol. 2024; 80:e76-e77.

Received October 30, 2025; Revised February 7, 2026; Accepted February 20, 2026

*Address correspondence to:
Hon-Yi Shi, Department of Healthcare Administration and Medical Informatics, Kaohsiung Medical University, 100, Zihyou 1st Road, Kaohsiung 80708, Taiwan.
E-mail: hshi@kmu.edu.tw

Chia-Yen Dai, Hepatobiliary Division, Department of Internal Medicine, Kaohsiung Medical University Hospital, Kaohsiung Medical University, 100, Zihyou 1st Road, Kaohsiung 80708, Taiwan.
E-mail: daichiayen@gmail.com

Released online in J-STAGE as advance publication February 27, 2026.

Original Article

DOI: 10.5582/bst.2025.01302

The dual role of TRPA1 in dextran sulfate sodium (DSS)-induced murine colitis: Suppression alleviates acute inflammation but exacerbates subacute disease

Fangzhou Dou[1,§], Jing Li[1,§], Daoran Lu[1], Yueyi Sun[1], Shasha Hu[2,*], Jianjun Gao[1,*]

[1] Department of Pharmacology, School of Pharmacy, Qingdao Medical College, Qingdao University, Qingdao, Shandong, China;
[2] Department of Pathology, The Affiliated Hospital of Qingdao University, Qingdao, Shandong, China.

SUMMARY: Ulcerative colitis (UC) is a chronic inflammatory bowel disease with limited treatment options. Transient receptor potential ankyrin 1 (TRPA1) has been implicated in inflammation and pain, but its role in UC remains a subject of debate. The current study investigated the effects of TRPA1 inhibition in both acute and subacute murine models of dextran sulfate sodium (DSS)-induced colitis. Genetic knockout of *Trpa1* or pharmacological inhibition with A967079 significantly ameliorated inflammation in the acute model, reducing the disease activity index (DAI), colon shortening, histopathological damage, and TNF-α secretion from macrophages. In contrast, TRPA1 suppression exacerbated subacute colitis and worsened weight loss, DAI, colon shortening, and histopathology. Mechanistically, *Trpa1* deletion promoted $CD4^+$ T cell polarization toward the Th1 subtype in subacute colitis, increasing IFN-γ levels. These findings reveal a dual role for TRPA1 in colonic inflammation: it mediates pro-inflammatory effects primarily *via* innate immune cells in the acute phase but has anti-inflammatory effects by modulating adaptive immunity in the subacute phase. These findings provide new insights into the context-dependent roles of TRPA1 and suggest that TRPA1 may represent a context-specific and stage-dependent therapeutic target in UC.

Keywords: TRPA1, inflammatory bowel disease, ulcerative colitis, animal model

1. Introduction

Ulcerative colitis (UC) is a chronic, idiopathic inflammatory bowel disease characterized by continuous inflammation of the colonic mucosa and submucosa, clinically presenting with recurrent diarrhea, bloody and mucopurulent stools, and abdominal pain (*1*). Global epidemiological data indicate a rising incidence and prevalence, particularly in industrialized nations, imposing a substantial disease burden and significantly diminishing patients' quality of life (*2-5*).

Current pharmacotherapeutic strategies primarily encompass 5-aminosalicylic acid (5-ASA) compounds (for inducing and maintaining remission in mild-to-moderate disease), corticosteroids (for inducing remission in moderate-to-severe disease), immunosuppressants (*e.g.*, azathioprine for maintenance therapy), and biological agents (*e.g.*, anti-TNF-α monoclonal antibodies) (*2,6-8*). However, existing therapies have notable limitations, as a substantial proportion of patients exhibit primary non-response or experience a loss of therapeutic efficacy over time (*9*). Consequently, there is a pressing clinical need to develop innovative therapeutics with novel mechanisms of action, sustained efficacy, and improved safety profiles in order to achieve deep and durable remission in a greater proportion of patients and to improve long-term clinical outcomes.

Transient receptor potential ankyrin 1 (TRPA1) is a member of the TRP ion channel family and is predominantly expressed in sensory neurons, epithelial cells, and immune cells (*10,11*). Functioning as a polymodal nocisensor, it is activated by environmental stimuli (*e.g.*, cold and mechanical force), endogenous inflammatory mediators (*e.g.*, reactive oxygen species and prostaglandins), and exogenous compounds (*e.g.*, mustard oil), mediating Ca^{2+} influx (*12,13*). Under pathological conditions, TRPA1 activation directly contributes to nociceptive signaling and the initiation of neurogenic inflammation (*14*). By promoting the release of neuropeptides such as substance P and calcitonin gene-related peptide (CGRP), it amplifies local vasodilation, plasma extravasation, and immune cell infiltration, playing a pivotal role in chronic pain conditions (*e.g.*, neuropathic pain and visceral pain) and inflammatory diseases (*e.g.*, asthma and dermatitis) (*15,16*). Its potential as an anti-inflammatory and analgesic target has been

substantiated by preclinical studies, demonstrating that targeted inhibition significantly alleviates inflammatory responses and pain hypersensitivity (*17*). However, the role of TRPA1 inhibition in UC—whether it has an anti-inflammatory or pro-inflammatory effect—remains a subject of debate (*18,19*). The role of TRPA1 activation in intestinal immune cells in modulating innate and adaptive immune responses needs to be further elucidated.

The current study used both acute and subacute murine colitis models to investigate the role of TRPA1 across distinct inflammatory milieus. The acute model reflects an inflammatory environment predominantly driven by innate immune responses, whereas the subacute model additionally engages adaptive immunity. Results revealed a dual role for TRPA1 in colonic inflammation: inhibition of TRPA1 had anti-inflammatory effects in the acute inflammatory milieu, while TRPA1 inhibition promoted pro-inflammatory responses in the subacute inflammatory milieu. This dichotomous behavior of TRPA1 may be attributable to its distinct functions in macrophages and $CD4^+$ T cells. Collectively, these findings provide new insights into the context-dependent roles of TRPA1 and suggest that TRPA1 may represent a context-specific and stage-dependent therapeutic target in UC.

2. Materials and Methods

2.1. Reagents and animals

Reagents and materials were sourced as follows: dextran sulfate sodium (DSS) (MW 40,000) and 5-aminosalicylic acid (5-ASA) were purchased from Shanghai Aladdin Biochemical Technology Co., Ltd. (Shanghai, China). A967079 and lipopolysaccharide (LPS) were obtained from Sigma-Aldrich (St. Louis, MO, USA). A hematoxylin and eosin (H&E) staining kit, Alcian blue staining kit, and periodic acid-Schiff (PAS) staining kit were acquired from Beijing Solarbio Science & Technology Co., Ltd. (Beijing, China). A Cell Counting Kit-8 (CCK-8) assay kit was supplied by Shanghai Topscience Co., Ltd. (Shanghai, China). Ficoll-Paque PREMIUM 1.084 was obtained from Cytiva (Marlborough, MA, USA). Fixable Viability Stain 780, Mouse BD Fc Block, BD™ CompBeads Anti-Rat Ig, κ/Negative Control Compensation Particles Set, and BB700 Rat Anti-Mouse CD4 (RM4-5) were sourced from BD Biosciences (Franklin Lakes, NJ, USA). The following antibodies were from BioLegend (San Diego, CA, USA): FITC anti-mouse CD3, APC anti-mouse CD25, Brilliant Violet 421™ anti-mouse IL-17A, PE anti-mouse FOXP3, Brilliant Violet 650™ anti-mouse IFN-γ, and PE/Cyanine7 anti-mouse IL-4. A Mouse IL-17A ELISA Kit and Mouse TNF-α ELISA Kit were purchased from Wuhan ABclonal Biotechnology Co., Ltd. (Wuhan, China). A Mouse IFN-γ ELISA Kit was acquired from Shanghai Absin Bioscience Inc. (Shanghai, China). An Intracellular Fixation/Permeabilization Buffer Kit was obtained from Wuhan Elabscience Biotechnology Co., Ltd. (Wuhan, China).

Wild-type (WT) C57BL/6N mice were purchased from Beijing Vital River Laboratory Animal Technology Co., Ltd. (Beijing, China). *Trpa1*$^{+/-}$ C57BL/6N mice were purchased from Cyagen Biosciences Co., Ltd. (Jiangsu, China). The *Trpa1*$^{-/-}$ mice and WT mice that were used to compare the effects of gene knockout were bred from the aforementioned heterozygous mice. All experimental animals were housed in a specific pathogen-free environment, and the mice had free access to water and food. All experimental procedures strictly adhered to international guidelines for the care and use of laboratory animals, and the protocols were approved by the Ethics Committee of the Medical College of Qingdao University (20230324C5719220250105064).

2.2. Protocol for the effect that suppressing TRPA1 had on acute colitis in mice

Impact of Trpa1 knockout on acute colitis in mice. Female C57BL/6N WT and *Trpa1*$^{-/-}$ mice, age 8-10 weeks, were selected. After a one-week acclimatization period, WT mice were randomly divided into: a normal control (NC) group and a DSS treatment group (WT+DSS). Concurrently, *Trpa1*$^{-/-}$ mice were assigned to a DSS treatment group (*Trpa1*$^{-/-}$+DSS). Each group consisted of 5-8 mice. From days 1 to 7, the WT+DSS and *Trpa1*$^{-/-}$+DSS groups had access to a 2.5% DSS solution *ad libitum*, while the NC group received sterile drinking water. Throughout the experiment, body weight, general condition, fecal consistency, and intestinal bleeding were monitored daily. The disease activity index (DAI) was calculated according to the criteria outlined in Table S1 (*https://www.biosciencetrends.com/action/getSupplementalData.php?ID=282*). On day 7, mice were euthanized. The colon and spleen were collected, and colon length and spleen weight were measured and recorded. Colon tissue sections were prepared for histological analysis, including hematoxylin and eosin (HE) staining, Alcian blue staining, and periodic acid-Schiff (PAS) staining. Remaining tissue samples were stored at -80°C.

Impact of a TRPA1 inhibitor on acute colitis in mice. Female C57BL/6N WT mice (8-10 weeks old) were acclimatized for 1-2 weeks and subsequently randomized into four experimental groups (n = 5-7 per group): an NC group, a colitis model (DSS+vehicle) group, an A967079 intervention (DSS+A967079) group, and a positive control (DSS+5-ASA) group. During the modeling phase (days 1-7), all groups except the NC group had access to a 2.5% DSS solution *ad libitum*, while the NC group received sterile drinking water. Pharmacological interventions commenced on the first day of modeling: the DSS+A967079 group received 10 mg/kg A967079 *via* oral gavage twice

daily (BID), the DSS+5-ASA group received 200 mg/kg 5-ASA *via* gavage BID, and the DSS+vehicle group received the drug formulation vehicle *via* gavage BID. Daily monitoring included body weight measurement, assessment of general condition, fecal consistency, and intestinal bleeding, with the DAI calculated according to the criteria in Table S1 (*https://www.biosciencetrends.com/action/getSupplementalData.php?ID=282*). On day 7, mice were euthanized for tissue collection; colon length was measured, spleen weight was recorded, and colon tissues were processed for HE histological analysis. Residual tissues were cryopreserved at -80°C.

2.3. Protocol for the effect that suppressing TRPA1 had on subacute colitis in mice

Impact of Trpa1 knockout on subacute colitis in mice. Female C57BL/6N WT and *Trpa1*$^{-/-}$ mice, age 8-10 weeks, were selected. After a one-week acclimatization period, WT mice were randomly divided into: an NC group (n = 8) and a DSS treatment group (WT+DSS, n = 8). *Trpa1*$^{-/-}$ mice were assigned to the DSS treatment group (*Trpa1*$^{-/-}$+DSS, n = 8). From day 0 to 30, both the WT+DSS group and the *Trpa1*$^{-/-}$+DSS group mice had access to a 1.0% DSS solution *ad libitum*. From day 31 to 45, these groups had access to a 1.5% DSS solution *ad libitum*. Mice in the NC group had access to water *ad libitum* from Day 1-45. During the experimental period, body weight was recorded every 3 days. The mouse's status, fecal consistency, and intestinal bleeding were observed, and the DAI was calculated according to the criteria detailed in Table S1 (*https://www.biosciencetrends.com/action/getSupplementalData.php?ID=282*). On day 45, mice were euthanized, and the colon and spleen were harvested. Colon length and spleen weight were measured. Colon tissues were subjected to histological analysis including H&E staining, Alcian blue staining, and PAS staining. The remaining tissues were stored at -80°C.

Impact of a TRPA1 inhibitor on subacute colitis in mice. Female C57BL/6N WT mice (age 8-10 weeks) were acclimatized for one week. Three mice were then randomly assigned to the NC group and given access to water *ad libitum*. The remaining 18 mice had access to a 1% DSS solution *ad libitum* for 30 days. On day 31, the mice treated with DSS were randomly divided into three groups (n = 6/group): a model group (DSS+vehicle), an A967079 intervention group (DSS+A967079), and a positive control group (DSS+5-ASA). From day 31 onward, the DSS concentration was increased to 1.5% for all groups except the NC group, which continued receiving water. Concurrent with the increase to 1.5% DSS, drug intervention was initiated. Mice in the DSS+A967079 group received A967079 (10 mg/kg) *via* oral gavage BID. Mice in the DSS+5-ASA group received 5-ASA (200 mg/kg) *via* oral gavage BID. Mice in the DSS+vehicle group received the corresponding vehicle *via* oral gavage BID. This treatment regimen was maintained for 10-15 days. Throughout the modeling period, body weight and symptoms (diarrhea and fecal blood) were recorded every 3 days. At the experimental endpoint, the DAI was calculated. Mice were then euthanized, tissues were harvested, and colon length was measured.

2.4. H&E, Alcian blue, and PAS staining

Fresh colon tissues were fixed in 4% paraformaldehyde for 24 h, followed by dehydration, embedding in paraffin, and sectioning using standard histological protocols. Sections were dried overnight at 37°C. After deparaffinization in xylene and rehydration through a graded ethanol series, staining procedures were performed. For H&E staining, sections were stained with hematoxylin for 5 min, differentiated in 0.5% acid alcohol for 2-5 s, rinsed in running water for 20 min for blue development, counterstained with eosin for 1 min, and rinsed with water. For Alcian blue staining, sections were treated with an acidification solution for 3 min, incubated with Alcian blue stain in a humid chamber for 30 min at room temperature (RT), rinsed with water (3×1 min), counterstained with Nuclear Fast Red (5 min), and rinsed (1 min). For PAS staining, sections were oxidized with periodic acid (5-8 min, RT), rinsed with water (2-3 min), washed with distilled water (2×3 min), incubated in Schiff's reagent (15 min, dark), rinsed with water (10 min), stained with hematoxylin (1-2 min), differentiated in an acid solution (2-5 s), and rinsed for blue development (10-15 min). All sections were dehydrated in graded ethanol, cleared in xylene, and mounted with neutral balsam. After fume hood drying, whole-slide scanning was performed. Histopathological scoring of H&E-stained sections followed the criteria in Table S2 (*https://www.biosciencetrends.com/action/getSupplementalData.php?ID=282*).

2.5. CCK-8 assay

Cells were cultured in T25 flasks until reaching ~90% confluency and then trypsinized and resuspended in fresh medium to achieve an appropriate density. The cell suspension (100 µL/well) was seeded onto a 96-well plate. After incubation at 37°C overnight in a 5% CO_2 humidified incubator to allow cell attachment, test compounds were added and incubated for 24 h. Following removal of compound-containing medium, 150 µL of CCK-8 working solution (prepared by mixing 1 mL CCK-8 stock with 9 mL PBS) was added to each well. The plate was returned to the incubator for 1 h, after which absorbance at 450 nm was measured using a microplate reader.

2.6. RAW264.7 cell culture and tumor necrosis factor-α (TNF-α) detection

Mouse RAW 264.7 cells were cultured to 80-90% confluency, after which the spent medium was aspirated and monolayers were gently washed with 2 mL of pre-warmed PBS. Following PBS removal, adherent cells were detached by gentle pipetting with fresh medium to generate a single-cell suspension. The suspension was adjusted to a density of 2.5×10^5 cells/mL with additional medium, and 2-mL aliquots were seeded per well on 6-well plates. Plates were gently agitated for uniform distribution and incubated overnight in a humidified 37°C/5% CO_2 incubator. The following day, after confirming cell attachment, the medium was aspirated and replaced with 2 mL of compound-containing medium at specified concentrations per experimental design, followed by incubation for 2 h. Subsequently, 2 μL of LPS (1 mg/mL stock) was added to each well depending on the experimental group, plates were gently swirled, and incubation continued for 22 h. Post-incubation, culture supernatants were collected, centrifuged at 1,000× *g* for 20 min at 4°C, and the clarified supernatants were harvested for subsequent quantification of TNF-α levels using enzyme-linked immunosorbent assay (ELISA) according to the manufacturer's instructions.

2.7. Lymphocyte extraction

Mice were euthanized by cervical dislocation, sterilized in 75% ethanol for ~2 min, and dissected to isolate the spleen. The spleen was rinsed in ice-cold PBS and mechanically dissociated in a petri dish containing 1 mL of medium until only fibrous tissue remained. The homogenate was filtered through a 40-μm nylon mesh into a 50-mL conical tube. The dish and mesh were rinsed with additional medium (2-3 washes), with filtrates pooled. The cell suspension was transferred to a 15-mL conical tube and centrifuged at 1,000 × *g* for 10 min at RT. After supernatant removal, the pellet was resuspended in 2 mL of medium and adjusted to 0.25–0.5 × 10^8 cells/mL. For density gradient separation, 3 mL of Ficoll-Paque Plus was layered under 2 mL of cell suspension in a 15-mL tube, followed by centrifugation at 400× *g* for 30 min (RT). The lymphocyte-rich interface layer was carefully collected and transferred to a new 15-mL tube containing 6 mL of medium. After centrifugation (1000× *g*, 10 min, RT), the pelleted lymphocytes were washed once by resuspension in 3 mL of medium and recentrifuged. Finally, cells were resuspended in 1 mL of medium to generate splenic lymphocyte suspensions, with 50 μL aliquoted for cell counting.

2.8. Flow cytometry

Isolated splenic lymphocytes were resuspended in PBS and stained with Fixable Viability Stain 780 under light-protected conditions for 10-15 min. Cells were washed and centrifuged (350× *g*, 5 min) and then blocked with mouse BD Fc Block™ at 4°C for 5 min. Subsequently, cells were stained with fluorochrome-conjugated anti-CD3, anti-CD4, and anti-CD25 antibodies (optimally titrated) for 30 min at 4°C in darkness. Following another wash cycle, cells were resuspended in 200 μL of stain buffer and fixed with 200 μL of Fixation Buffer for 45 min at RT protected from light. After permeabilization using 1 mL of 1× Permeabilization Working Solution and centrifugation (600× *g*, 5 min, RT), intracellular staining was performed with anti-interferon (IFN)-γ, anti-interleukin (IL)-4, anti-IL-17A, and Treg markers separately per staining panel during incubation for 30 min (RT, dark). Cells were washed with 1.5 mL of stain buffer, centrifuged (600× *g*, 5 min, RT), and finally resuspended in 500 μL of stain buffer. The suspension was filtered through a 300-mesh sieve before acquisition on a flow cytometer pre-calibrated with compensation microspheres.

2.9. Detection of colonic cytokines

Colon tissue segments were excised, thoroughly rinsed in ice-cold PBS, and blotted dry on filter paper. After weighing (typically 30-40 mg per sample), tissues were transferred to microcentrifuge tubes. Samples were homogenized by adding 360 μL of PBS per 40 mg tissue weight along with a grinding bead, followed by mechanical disruption in a high-throughput tissue homogenizer (60 Hz, 150-180 seconds). The resulting homogenates were centrifuged at 12,000× *g* for 15 min at 4°C. Supernatants were collected and stored at -20°C until subsequent quantification of TNF-α, IL-17A, and IFN-γ levels using ELISA according to the manufacturer's protocols.

2.10. Statistical analyses

Data are expressed as the mean ± standard error of the mean (Mean ± SEM). Graphical representations were generated using GraphPad Prism 8.0. Histopathological images were acquired *via* whole-slide scanning, processed with the software SlideViewer, and exported as representative micrographs. Flow cytometry data were acquired and analyzed using the software CytExpert 2.5. Statistical analyses were performed in SPSS (IBM) using either one-way ANOVA or a Student's *t*-test as appropriate, with significance denoted as $*p < 0.05$, $**p < 0.01$, and $***p < 0.001$.

3. Results

3.1. *Trpa1* gene knockout does not alter the macroscopic structure or morphology of the mouse colon

To determine whether *Trpa1* knockout causes physiological structural changes in the mouse colon, the colon of euthanized *Trpa1*$^{-/-}$ and WT mice was dissected for comparative analysis. There were no significant

differences in colon length between WT mice (7.66 ± 0.19 cm) and *Trpa1*$^{-/-}$ mice (7.50 ± 0.24 cm) (Figure 1A). Colonic tissue segments from both groups were further fixed in 4% paraformaldehyde and paraffin sections were prepared. H&E, Alcian blue, and PAS staining were performed to compare colonic architecture and the number of goblet cells. As shown in Figure 1B, there were no discernible structural differences between the two groups. Crypts were tightly arranged in both, with no evidence of mucous layer disruption or inflammatory cell infiltration. Alcian blue and PAS staining further revealed no significant differences in the number of goblet cells in the colon of *Trpa1*$^{-/-}$ and WT mice (Figure 1C). Collectively, these findings indicate that *Trpa1* gene knockout does not induce alterations in the macroscopic structure or morphology of the mouse colon.

3.2. *Trpa1* knockout attenuates DSS-induced acute colitis in mice

The model of DSS-induced acute colitis in mice was used in this study to investigate the role of the TRPA1 channel in the pathogenesis of UC. Mice in the WT+DSS and *Trpa1*$^{-/-}$+DSS groups received 2.5% DSS in drinking water *ad libitum* for 7 days, while the NC group received sterile water throughout the modeling period.

Mice in both DSS-treated groups developed soft stools between days 2-4, with diarrhea appearing by day 5. By day 6, severe hematochezia and significant weight loss were prominent in most WT+DSS mice, whereas these symptoms were markedly milder in the *Trpa1*$^{-/-}$+DSS group. Both DSS-treated groups exhibited significant weight loss starting on day 6, with a significant difference in body weight between the WT+DSS and *Trpa1*$^{-/-}$+DSS groups emerging by day 7 (Figure 2A). The average daily DSS intake did not differ significantly between the two DSS-treated groups (Figure 2B), although the *Trpa1*$^{-/-}$+DSS group tended to have higher DSS intake compared to the WT+DSS group. The DAI increased abruptly from day 5 onwards in all DSS-treated groups. On day 7, the DAI was significantly higher in WT+DSS mice compared to that in *Trpa1*$^{-/-}$+DSS mice (Figure 2C). Spleen index analysis revealed significant differences between both DSS-treated groups and the NC group. While the *Trpa1*$^{-/-}$+DSS group tended to have a lower spleen index compared to the WT+DSS group, this difference was not significant. Upon necropsy, no enlargement of mesenteric lymph nodes was observed in DSS-treated groups compared to the NC group, suggesting that the colonic inflammation is mainly mediated by the innate immune response (Figure 2D). DSS-induced colitis resulted in significant colon shortening. Notably, *Trpa1*$^{-/-}$+DSS mice had a significantly greater colon length compared to that in WT+DSS mice (Figure 2E).

Histopathological examination of colon tissue *via* H&E staining revealed substantial structural damage in mice with DSS-induced UC, characterized by epithelial loss, crypt distortion with irregular architecture, and inflammatory cell infiltration into the submucosa.

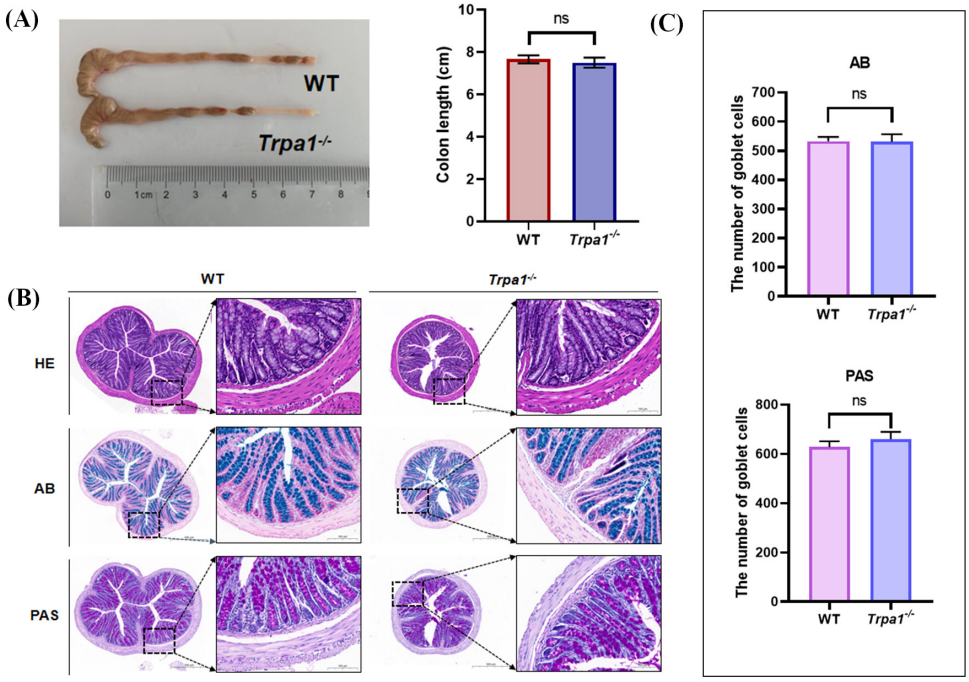

Figure 1. Comparison of colon morphology between *Trpa1*$^{-/-}$ and WT mice. (**A**) Representative images and statistical comparison of colon length between WT and *Trpa1*-knockout mice. (**B**) Representative cross-sectional images of colon tissue from WT and *Trpa1*-knockout mice stained with H&E, Alcian blue, and PAS; from left to right, magnifications are 100× and 400×. (**C**) Goblet cell counts corresponding to Alcian blue and PAS staining for each group in panel B.

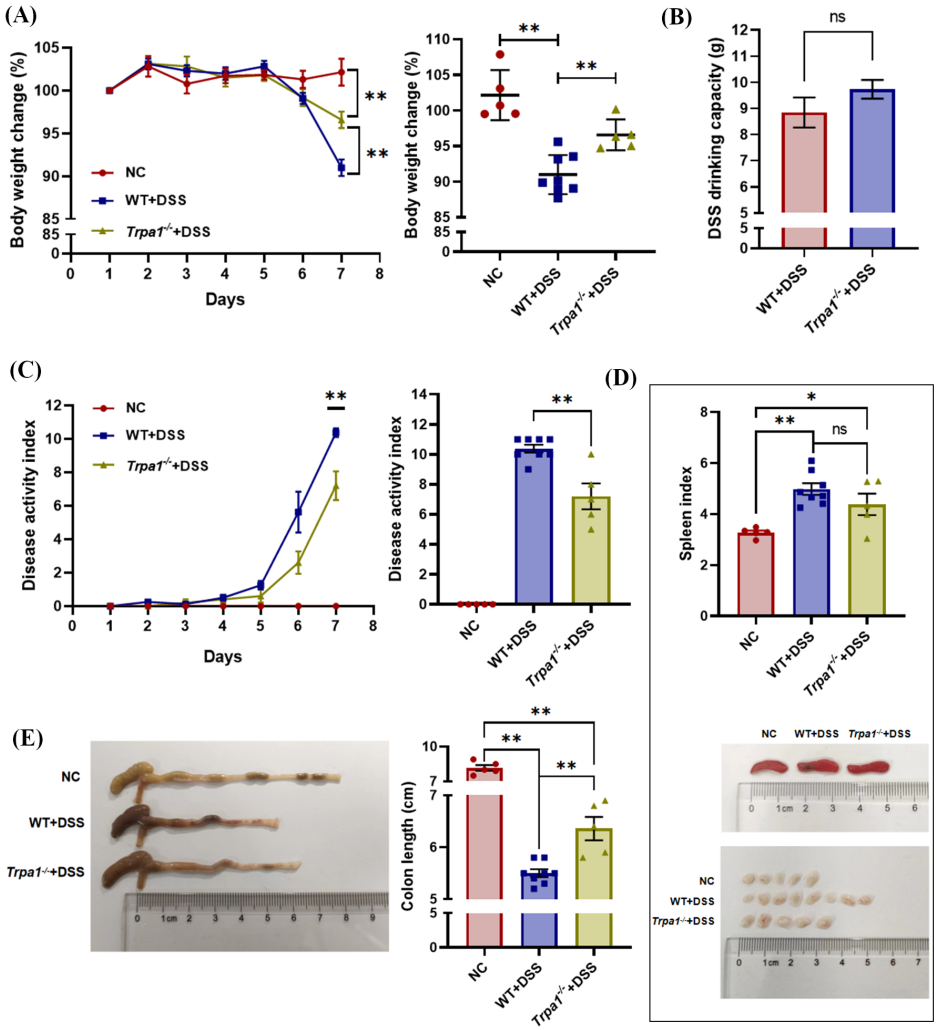

Figure 2. *Trpa1* knockout alleviates DSS-induced acute colitis in mice. (**A**) Time course of body weight loss (%) and comparison of body weight loss (%) on the final day among groups. (**B**) Average daily DSS consumption per mouse during modeling in WT+DSS and *Trpa1*$^{-/-}$+DSS groups. (**C**) DAI over the modeling period and DAI comparison among groups on the final day. (**D**) Spleen index (spleen weight [mg] / body weight [g]) and macroscopic comparison of spleen and mesenteric lymph nodes among groups. (**E**) Representative images and quantification of colon length among groups. *$p < 0.05$, **$p < 0.01$.

Compared to WT+DSS mice, the *Trpa1*$^{-/-}$+DSS group exhibited milder colon structural disruption and less epithelial loss. Consequently, the *Trpa1*$^{-/-}$+DSS group had significantly lower histopathological scores (Figure 3A). To further investigate the effect of *Trpa1* knockout on goblet cells in DSS-induced acute colitis, Alcian blue staining and PAS staining were performed to quantify goblet cells. Results indicated a significantly higher number of goblet cells in the colon of *Trpa1*$^{-/-}$ mice compared to that in the colon of WT mice, suggesting that *Trpa1* knockout may mitigate DSS-induced destruction of goblet cells (Figures 3B and 3C). Collectively, these findings indicate that genetic deletion of *Trpa1* significantly attenuates the symptoms of DSS-induced acute colitis in mice.

3.3. TRPA1 inhibitor attenuates DSS-induced acute colitis in mice

To further delineate the role of TRPA1 channels in acute colitis pathogenesis, the TRPA1-specific inhibitor A967079 was administered in a model of DSS-induced acute colitis, with 5-ASA serving as a positive control. Following 5 days of exposure to DSS, mice in the DSS+vehicle, DSS+A967079, and DSS+5-ASA groups all exhibited varying degrees of diarrhea and hematochezia. Compared to the DSS+vehicle group, mice treated with A967079 or 5-ASA had milder diarrhea and less pronounced weight loss (Figure 4A). By day 7, the DSS+A967079 group had a 8.4% reduction in weight loss relative to the DSS+vehicle group (11.1% *vs.* 19.5%, Figure 4B). Both the DSS+A967079 and DSS+5-ASA groups had significantly lower DAI scores than the DSS+vehicle group (Figures 4C and 4D). Post-mortem analysis revealed substantial attenuation of DSS-induced colon shortening in the DSS+A967079 and DSS+5-ASA groups compared to that in the DSS+vehicle group

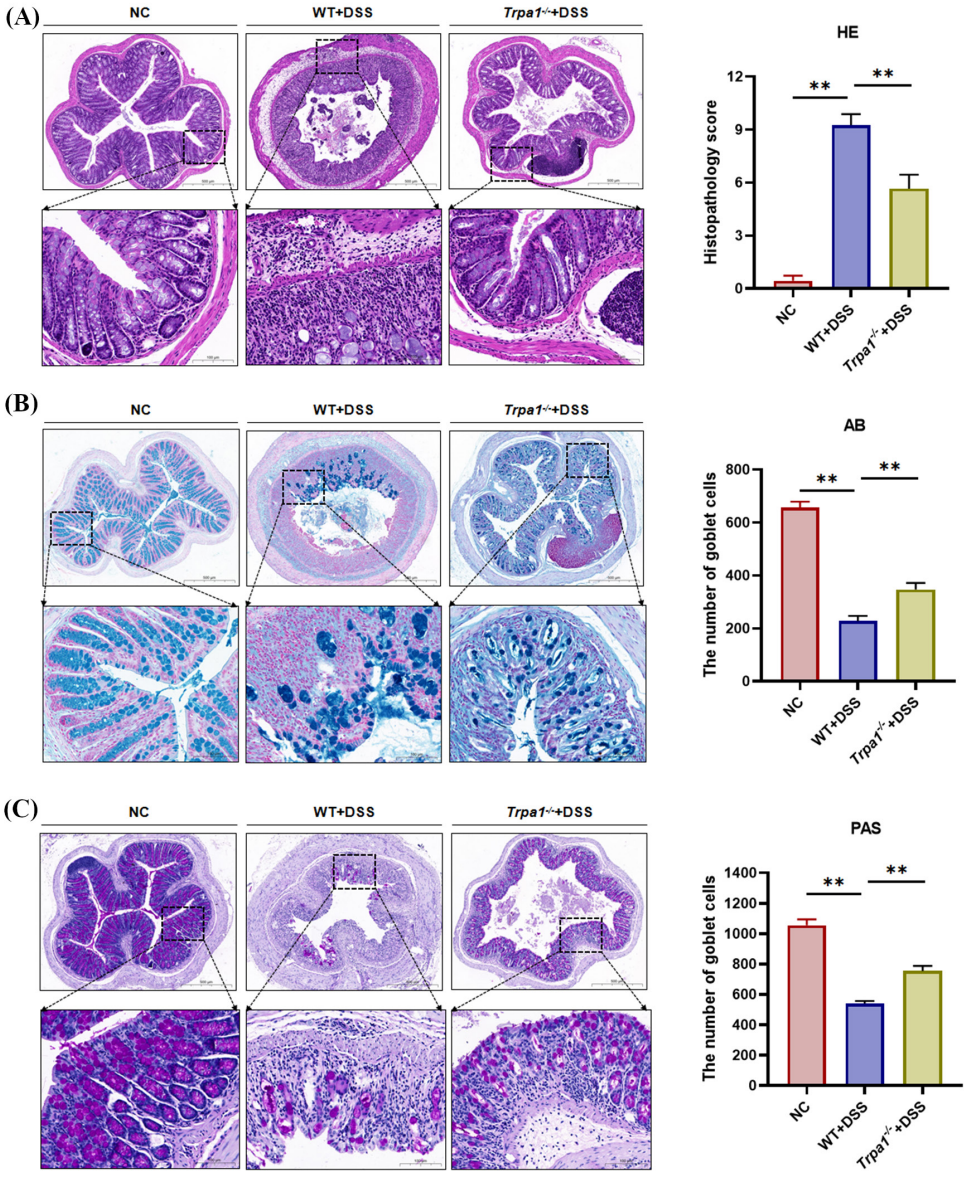

Figure 3. *Trpa1* knockout reduces colonic histopathological scores and goblet cells loss in mice with DSS-induced acute colitis. (**A**) Cross-sectional H&E staining of colon from DSS-induced acute colitis mice, with images shown at 100× (top) and 400× (bottom) magnification, followed by colonic histopathological scoring. Representative Alcian blue–stained (**B**) and PAS-stained (**C**) cross-sections of colon from DSS-induced acute colitis mice (top: 100×, bottom: 400× magnification) and quantification of goblet cells. $^{**}p < 0.01$.

(Figures 4E and 4F). Histopathological examination *via* H&E staining further confirmed reduced colonic damage in mice treated with the inhibitor (Figures 4G and 4H). Collectively, these results indicate that pharmacological inhibition of TRPA1 significantly ameliorates DSS-induced acute colitis in mice.

3.4. Inhibition of TRPA1 downregulates TNF-α secretion in RAW264.7 cells

Macrophages play a critical role in innate immune responses. As TRPA1 is expressed in macrophages (*19*), an LPS-induced RAW264.7 cell inflammation model was used to assess the impact of a TRPA1 inhibitor on cytokine secretion. To determine an appropriate drug concentration, RAW264.7 cells were co-incubated with varying concentrations of A967079 for 24 h. Cell proliferation was then assessed using a CCK-8 assay. As shown in Figure 5A, 30 μM A967079 had a mild inhibitory effect on RAW264.7 cell proliferation. Based on these results, A967079 concentrations of 1 μM, 3 μM, and 10 μM, which had no significant impact on cell proliferation, were selected for subsequent experiments. ELISA indicated that intervention with the TRPA1 inhibitor A967079 significantly reduced TNF-α secretion by RAW264.7 cells in a concentration-dependent manner (Figure 5B). This indicates that the TRPA1 inhibitor may have anti-inflammatory effects by suppressing the secretion of the macrophage-derived inflammatory cytokine TNF-α.

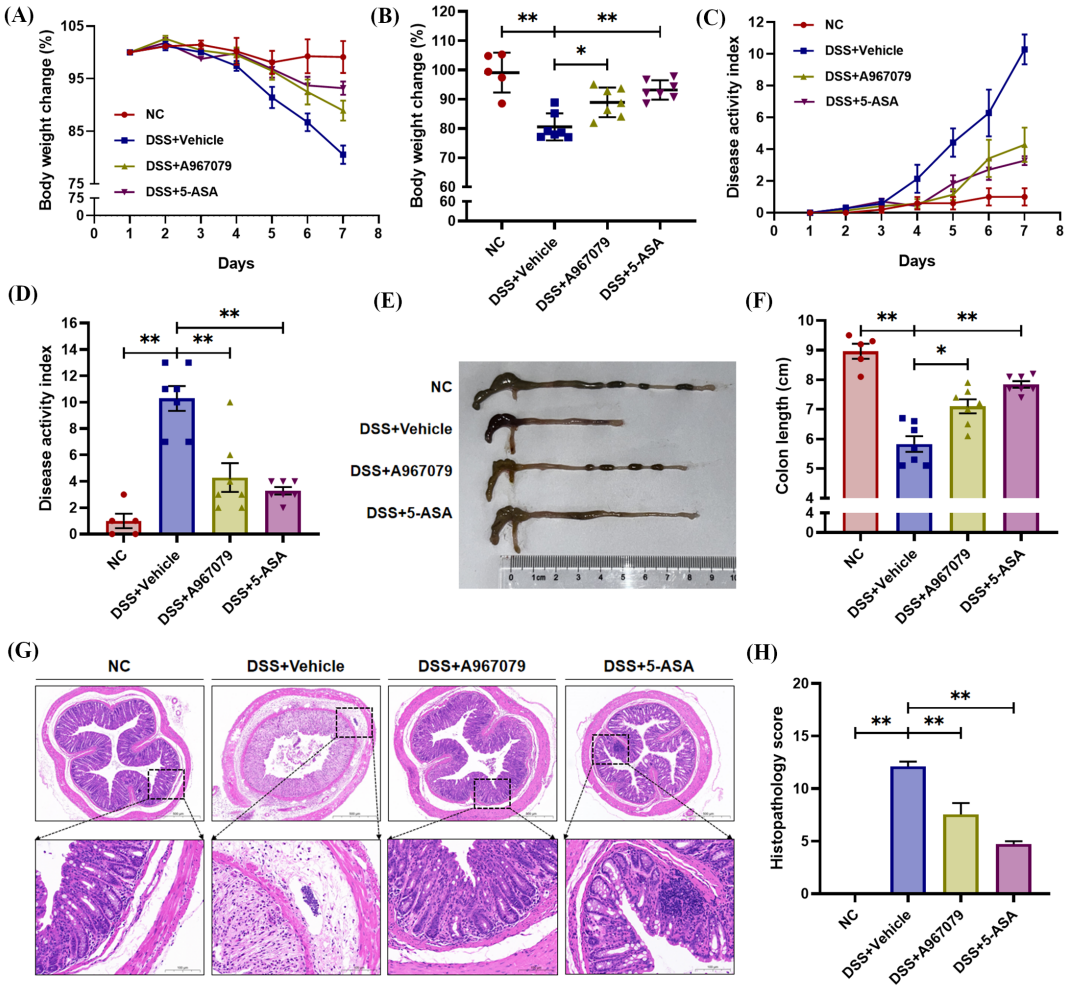

Figure 4. TRPA1 inhibitor alleviates DSS-induced acute colitis in mice. (A) Time course of body weight loss (%) in each group. (**B**) Comparison of body weight loss (%) among groups on the final day of modeling. (**C**) DAI over the modeling period in each group. (**D**) Comparison of DAI among groups on the final day. (**E**) Representative images of colon length from each group. (**F**) Quantitative analysis of colon length among groups. (**G**) Cross-sectional H&E staining of the colon in each group; images are shown at 100× (top) and 400× (bottom) magnification. (**H**) Colonic tissues from each group were scored according to the histopathological scoring criteria after H&E staining, and the results were statistically analyzed. $*p < 0.05$, $**p < 0.01$.

3.5. *Trpa1* knockout exacerbates DSS-induced subacute colitis in mice

UC is a chronic inflammatory disease that often presents with sudden and severe symptoms during acute flare-ups. To better model the characteristics of human UC, the authors previously established a DSS-induced murine model of subacute colitis (*20*). This model features prolonged colonic inflammation involving adaptive immunity, closely resembling the pathological features of UC. In this model, mice in both WT+DSS and *Trpa1*$^{-/-}$+DSS groups received 1% DSS in drinking water *ad libitum* for 30 days, followed by 1.5% DSS until modeling ended. Both DSS-treated groups developed diarrhea starting around day 15. Body weight in *Trpa1*$^{-/-}$+DSS mice began to decline significantly around day 33, whereas WT+DSS mice exhibited weight fluctuations without significant loss of weight (Figure 6A). DSS consumption did not differ significantly between the two groups throughout the experiment (Figure 6B). Compared to WT+DSS mice, *Trpa1*$^{-/-}$+DSS mice had significantly greater colon shortening, a higher DAI, and an increased spleen index, indicating a more severe inflammatory response (Figures 6C-6G).

Histopathological evaluation of colon tissue using H&E staining revealed severe colonic structural damage in mice with DSS-induced colitis, characterized by epithelial loss, crypt destruction with irregular arrangement, and lymphocyte infiltration into the submucosa (Figure 7A). Colonic damage was markedly more severe in *Trpa1*$^{-/-}$+DSS mice compared to that in WT+DSS mice, characterized by extensive epithelial loss and pronounced inflammatory cell infiltration. The knockout group had significantly higher histopathological scores. Alcian blue and PAS staining revealed a significantly greater reduction in the number of goblet cells in *Trpa1* knockout mice compared to that in WT mice (Figures 7B and 7C). Collectively, these findings

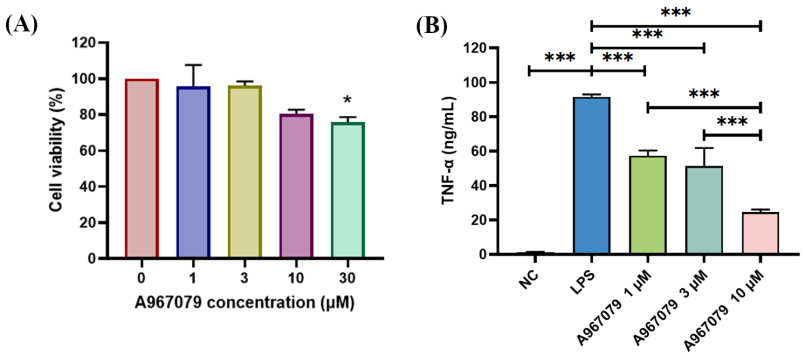

Figure 5. Inhibition of TRPA1 downregulates TNF-α secretion in RAW264.7 cells. (**A**) Effect of A967079 on RAW264.7 cell viability, assessed with a CCK-8 assay after 24 h of exposure to different concentrations of A967079. (**B**) Determination of the effect of a TRPA1 inhibitor on TNF-α secretion in LPS-stimulated RAW264.7 cells using ELISA. *$p < 0.05$, ***$p < 0.001$.

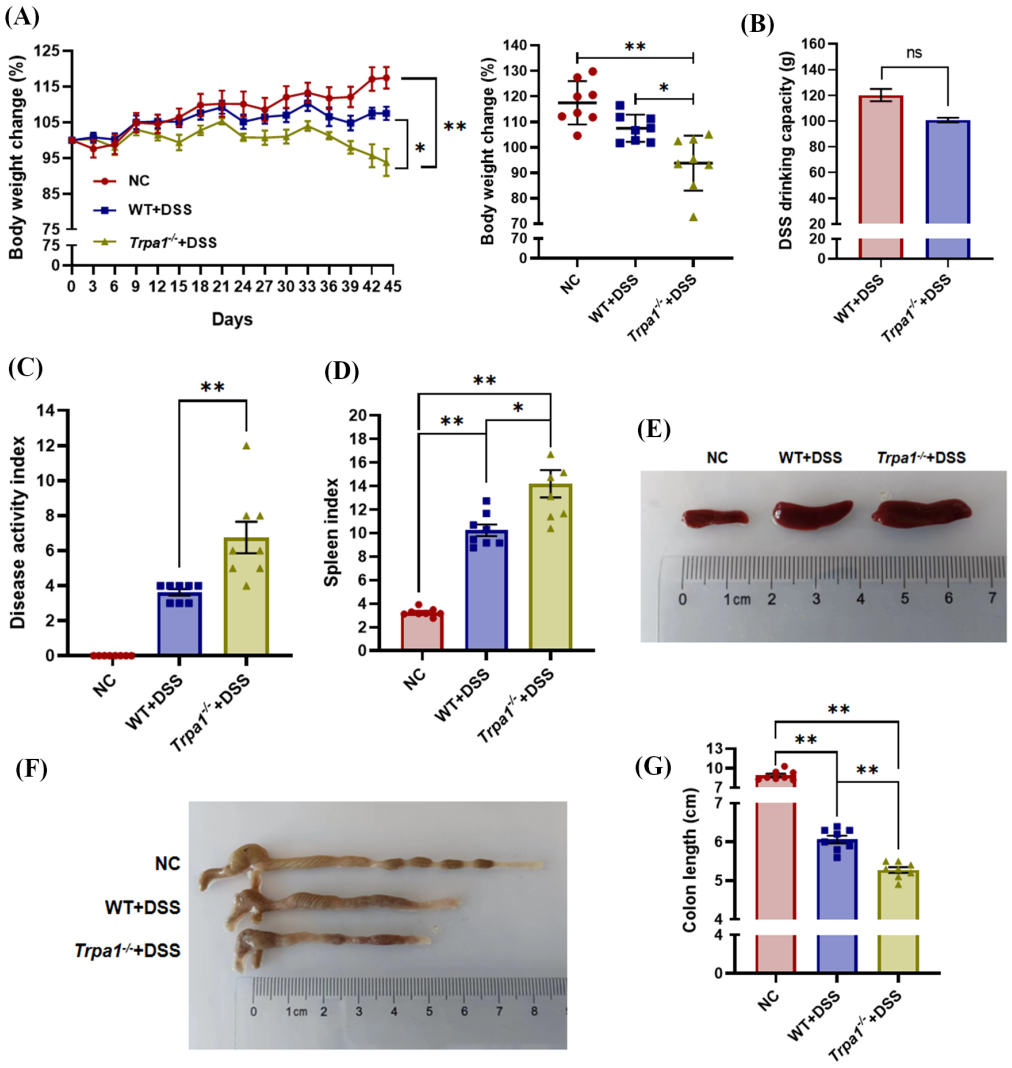

Figure 6. *Trpa1* knockout exacerbates DSS-induced subacute colitis in mice. (**A**) Time course of body weight loss (%) and comparison of body weight loss (%) among groups before tissue collection. (**B**) Water intake during modeling in the WT+DSS and *Trpa1*$^{-/-}$+DSS groups. (**C**) Comparison of DAI on the final day. (**D**) Comparison of the spleen index among groups (spleen index = spleen weight [mg] / body weight [g]). (**E**) Representative images of the spleen from each group. (**F**) Representative images of the colon from each group. (**G**) Quantitative analysis of colon length among groups. *$p < 0.05$, **$p < 0.01$.

indicate that *Trpa1* deletion has pro-inflammatory effects in subacute colitis in mice.

3.6. TRPA1 inhibitor exacerbates DSS-induced subacute colitis in mice

To further validate TRPA1's role in murine subacute colitis, mice were treated with the TRPA1 inhibitor A967079 (10 mg/kg, orally). Mice treated with A967079 exhibited exacerbated symptoms, including more severe weight loss, diarrhea with bloody stools, and colon shortening (Figures 8A-8E). Histopathological examination of colonic tissue using H&E staining was performed to assess pathological changes. As shown in Figure 8F, groups with DSS-induced subacute colitis displayed varying degrees of colonic mucosal damage, including disruption of the epithelium, destruction of crypts in the mucosal layer, and lymphocyte infiltration. Compared to the DSS+vehicle group, the DSS+A967079 group exhibited more severe colonic damage, aggravated inflammation, and had significantly higher histopathological scores (Figure 8G). Collectively, these results indicate that pharmacological inhibition of TRPA1 exacerbates DSS-induced subacute colitis in mice.

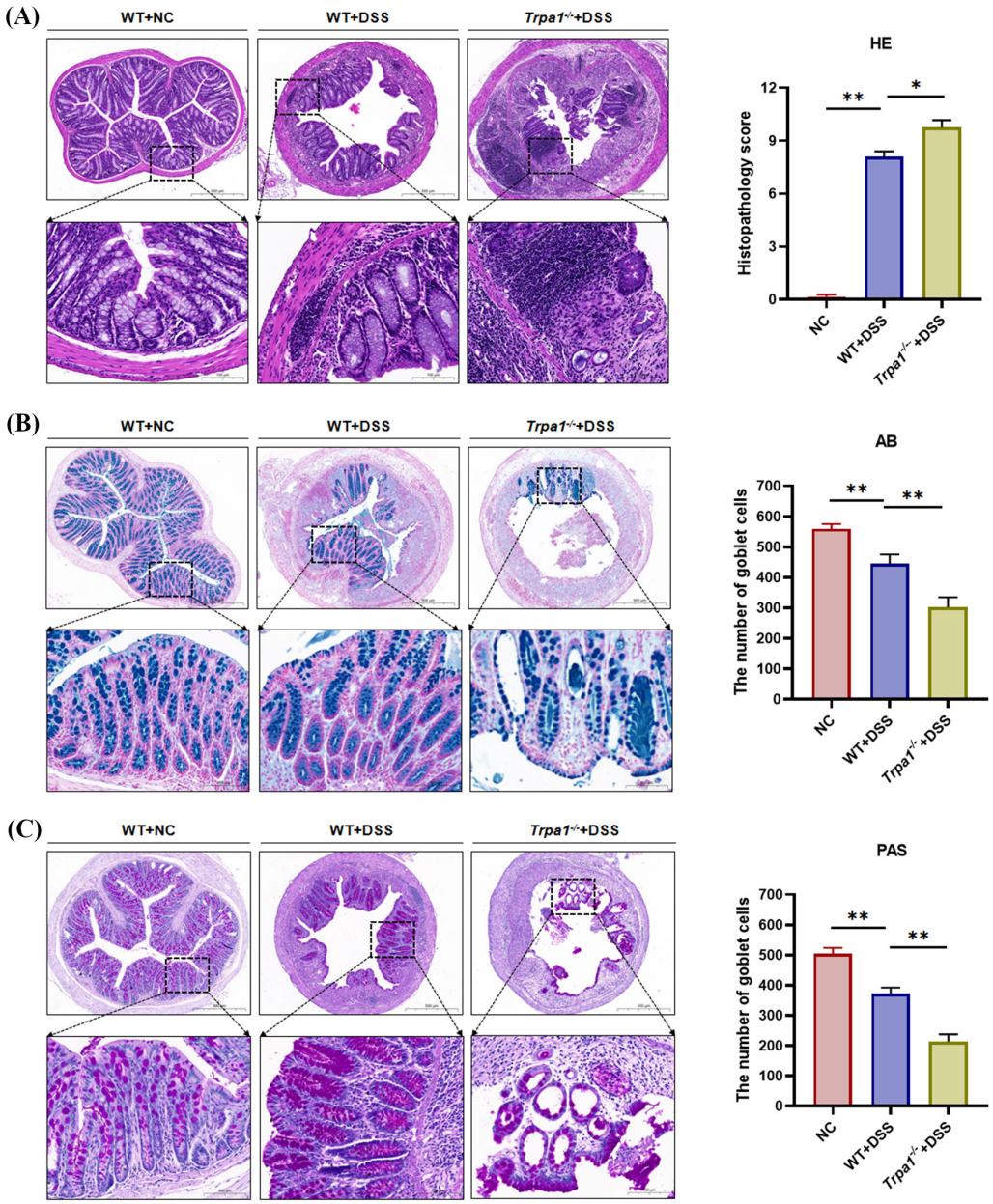

Figure 7. *Trpa1* knockout promotes inflammatory progression and goblet cell depletion in subacute colitis. (**A**) Cross-sectional H&E staining of the colon from mice with DSS-induced subacute colitis (from top to bottom, images are at 100× and 400× magnification) and histopathological scoring of colonic tissue. Representative images of cross-sectional Alcian blue (**B**) and PAS (**C**) staining of the colon from mice with DSS-induced subacute colitis (from top to bottom, images are at 100× and 400× magnification) and quantification of goblet cells. *$p < 0.05$, **$p < 0.01$.

3.7. *Trpa1* knockout promotes CD4+ T cell polarization towards the Th1 subtype

Our previous study indicated an elevated proportion of Th1 cells in a DSS-induced murine model of subacute colitis (*20*). Given that TRPA1 is expressed in CD4+ T cells (*19*), we hypothesized that TRPA1 might regulate CD4+ T cell polarization towards the Th1 subtype, thereby influencing DSS-induced subacute colitis. To verify this hypothesis, lymphocytes isolated from mice with colitis were analyzed using flow cytometry. Results indicated a significantly higher proportion of Th1 cells within the CD4+ T cell population in *Trpa1*$^{-/-}$+DSS mice (Figure 9A) compared to that in WT+DSS mice. There were no significant differences in the proportions of other CD4+ T cell subsets (Th2, Th17, and Treg).

To further confirm changes in CD4+ T cell subsets within the colonic tissue, colon segments from each group were homogenized, and cytokine levels (IFN-γ, IL-17A, TNF-α) were measured using ELISA. IFN-γ, a signature cytokine secreted by Th1 cells, and IL-17A, a specific cytokine produced by Th17 cells, play pivotal roles in the pathogenesis of colitis (*21*). TNF-α, a key inflammatory mediator, is secreted not only by macrophages but also by Th1 cells. ELISA revealed that colonic tissues from *Trpa1*$^{-/-}$+DSS mice contained significantly higher levels of IFN-γ compared to tissues from WT+DSS mice (Figure 9B), while TNF-α levels

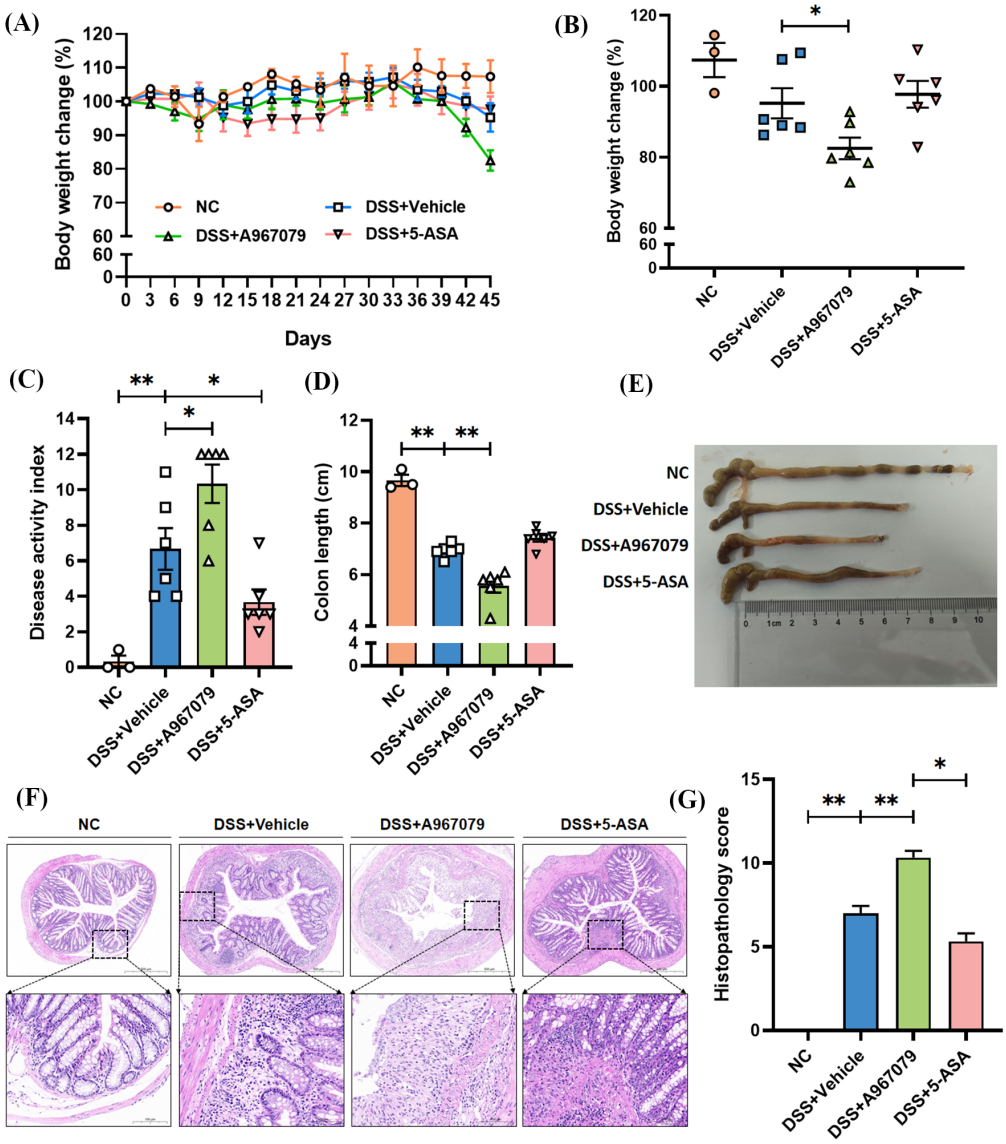

Figure 8. TRPA1 inhibitor exacerbates DSS-induced subacute colitis in mice. (**A**) Time course of body weight loss (%) in each group. (**B**) Comparison of body weight loss (%) among groups before tissue collection. (**C**) Comparison of DAI on the final day of the experiment. (**D**) Quantitative analysis of colon length among groups. (**E**) Representative images of colon length from each group. (**F**) Cross-sectional H&E staining of colon from each group; images are shown at 100× (top) and 400× (bottom) magnification. (**G**) Quantitative analysis of histopathological scores for colonic tissues from each group, assessed according to the histopathological scoring criteria after H&E staining. *$p < 0.05$, **$p < 0.01$.

tended to increase (Figure 9C). There were no significant differences in IL-17A levels between the two groups (Figure 9D). Collectively, these findings suggest that *Trpa1* deletion may facilitate CD4$^+$ T cell polarization towards the Th1 subtype, leading to increased secretion of pro-inflammatory cytokines and exacerbating colonic inflammation in a model of subacute colitis.

4. Discussion

The mouse model of DSS-induced acute colitis is currently the most commonly used animal model for UC. However, this model has several limitations, including a short modeling period, minimal involvement of the adaptive immune response, rapid progression of acute

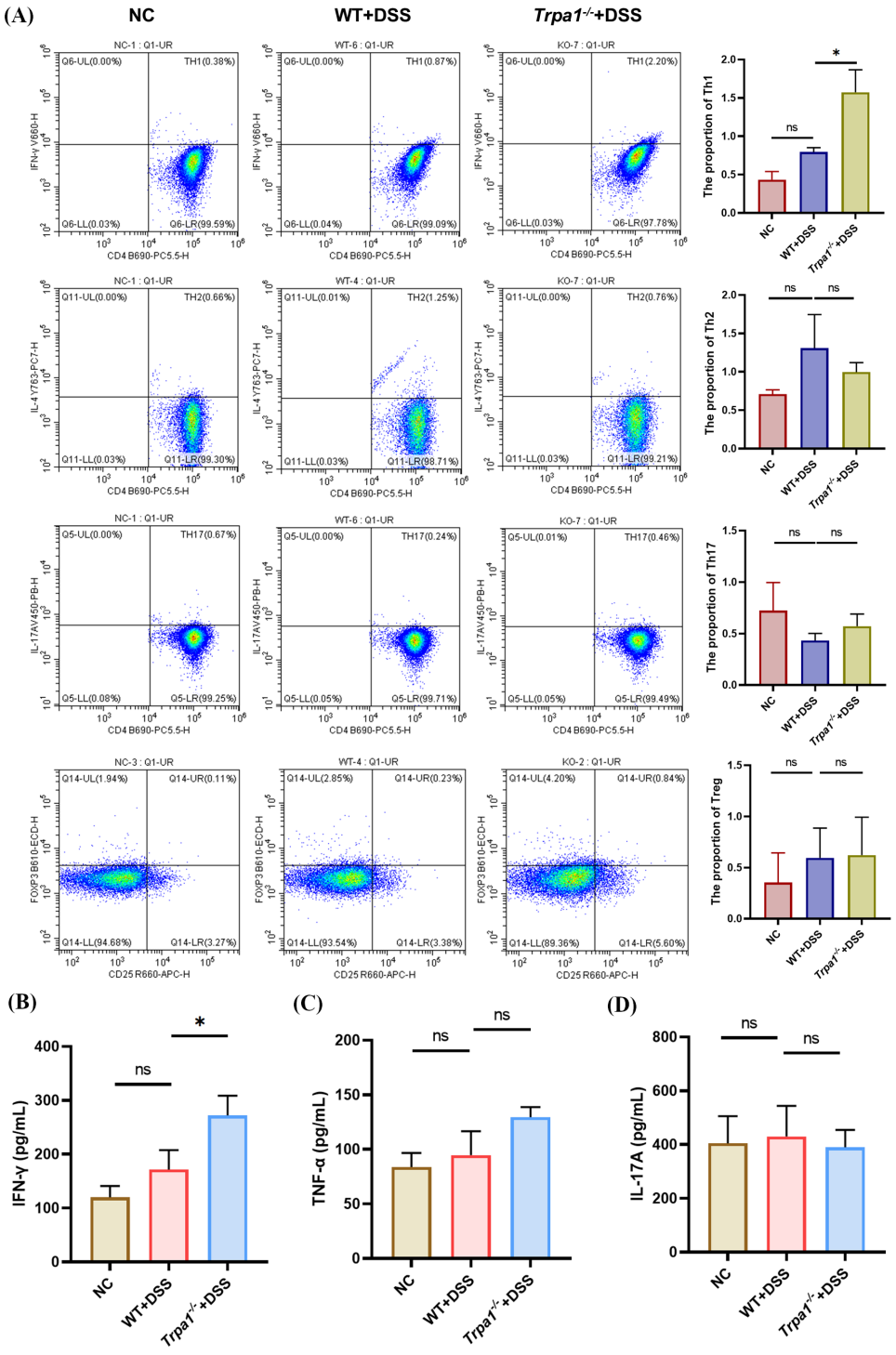

Figure 9. *Trpa1* knockout promotes CD4$^+$ T cell polarization towards the Th1 subtype. (**A**) Flow cytometry analysis of splenic lymphocytes after extraction. Mice were euthanized on day 45, and the spleen was removed to isolate lymphocytes for flow cytometry analysis. (**B-D**) Detection of IFN-γ, TNF-α, and IL-17A levels in colonic tissues using ELISA. *$p < 0.05$.

inflammation, and significant mouse mortality. To better recreate the pathological mechanisms of human UC, we created a novel murine model of DSS-induced subacute colitis in a previous study (*20*). This model features inflammation persisting for approximately 4 weeks, with a significantly increased proportion of adaptive immune cells, particularly Th1 cells, in the colonic mucosa, closely resembling the pathological characteristics of chronic inflammation.

The current study found that TRPA1 plays opposing roles in acute and subacute DSS-induced murine colitis. During the acute phase dominated by macrophages and neutrophils, TRPA1 inhibition attenuated colitis by suppressing the release of pro-inflammatory cytokines like TNF-α from macrophages. Conversely, during the subacute phase in which Th1-type $CD4^+$ T cells increased markedly alongside innate immune cells, TRPA1 inhibition exacerbated colonic inflammation, possibly by further increasing the proportion of Th1 cells. This aligns with the findings of Bertin *et al.*, which indicated that TRPA1 knockout worsened spontaneous colitis in IL-10-deficient mice and significantly upregulated Th1 proportions in lymphocytes (*19*). *In vitro*, TRPA1 knockout promoted the differentiation of naïve $CD4^+$ T cells into Th1 cells (*19*), which is consistent with our observations in a model of subacute colitis. The divergent functions of TRPA1 in different immune cell types likely underlie its dual role in colitis pathogenesis.

Results confirmed that TRPA1 inhibitors can ameliorate symptoms in an acute colitis model, which is consistent with prior studies. Engel *et al*. found that the TRPA1 inhibitor HC-030031 alleviated symptoms, reduced inflammatory markers, and improved histopathological damage in acute colitis (*18*). Our finding that TRPA1 inhibition exacerbates subacute colitis raises potential concerns regarding TRPA1 inhibition as a therapeutic strategy for human UC. However, human UC is primarily mediated by Th2 and Th17 cells within the adaptive immune compartment, unlike the Th1-driven pathology in our murine model of subacute colitis (*22*). Given the mutually inhibitory relationship between Th1 and Th2 differentiation, does TRPA1 inhibition-mediated Th1 promotion imply a corresponding reduction in Th2 cells, potentially offering a therapeutic benefit? Preliminary evidence supports this hypothesis. Cannabidivarin is a safe, non-psychoactive phytocannabinoid that acts as a TRPA1 desensitizing agent (*23*), and cannabis use that specifically involves this compound has been reported to alleviate symptoms in patients with UC (*23*). Moreover, a clinical study found that curcumin, which desensitizes and inhibits the TRPA1 channel, significantly reduced relapse rates in UC patients (*24,25*). Whether targeting TRPA1 inhibition in human UC could therapeutically reduce macrophage activity and lower Th2 cell proportions requires further investigation.

In summary, *Trpa1* gene knockout or pharmacological inhibition significantly ameliorates DSS-induced acute UC in a murine model but it exacerbates DSS-induced subacute UC. This dichotomy likely stems from the distinct functions of TRPA1 in macrophages versus $CD4^+$ T cells. Our findings provide new insights into the context-dependent roles of TRPA1 and suggest that TRPA1 may represent a context-specific and stage-dependent therapeutic target in UC.

Funding: None.

Conflict of Interest: The authors have no conflicts of interest to disclose.

References

1. Attauabi M, Madsen GR, Bendtsen F, Burisch J, Seidelin JB. The role of environmental factors prior to diagnosis on the activity and severity of inflammatory bowel diseases-Results from the prospective population-based Copenhagen Inflammatory Bowel Disease Inception Cohort. United European Gastroenterol J. 2025; 13:697-709.
2. Kobayashi T, Siegmund B, Le Berre C, Wei SC, Ferrante M, Shen B, Bernstein CN, Danese S, Peyrin-Biroulet L, Hibi T. Ulcerative colitis. Nat Rev Dis Primers. 2020; 6:74.
3. Ng SC, Shi HY, Hamidi N, Underwood FE, Tang W, Benchimol EI, Panaccione R, Ghosh S, Wu JCY, Chan FKL, Sung JJY, Kaplan GG. Worldwide incidence and prevalence of inflammatory bowel disease in the 21st century: A systematic review of population-based studies. Lancet. 2017; 390:2769-2778.
4. Bisgaard TH, Allin KH, Keefer L, Ananthakrishnan AN, Jess T. Depression and anxiety in inflammatory bowel disease: Epidemiology, mechanisms and treatment. Nat Rev Gastroenterol Hepatol. 2022; 19:717-726.
5. Sun Q, Jiang Z, Yang L, Liu H, Song P, Yuan L. Towards an Asian paradigm of inflammatory bowel disease management: A comparative review of China and Japan. Intractable Rare Dis Res. 2025; 14:192-202.
6. Mantzaris GJ. Thiopurines and methotrexate use in IBD patients in a biologic era. Curr Treat Options Gastroenterol. 2017; 15:84-104.
7. Kucharzik T, Koletzko S, Kannengiesser K, Dignass A. Ulcerative colitis-diagnostic and therapeutic algorithms. Dtsch Arztebl Int. 2020; 117:564-574.
8. Wehkamp J, Stange EF. Recent advances and emerging therapies in the non-surgical management of ulcerative colitis. F1000Res. 2018; 7:F1000.
9. Singh S, George J, Boland BS, Vande Casteele N, Sandborn WJ. Primary non-response to tumor necrosis factor antagonists is associated with inferior response to second-line biologics in patients with inflammatory bowel diseases: A systematic review and meta-analysis. J Crohns Colitis. 2018; 12:635-643.
10. Zhang M, Ma Y, Ye X, Zhang N, Pan L, Wang B. TRP (transient receptor potential) ion channel family: Structures, biological functions and therapeutic interventions for diseases. Signal Transduct Target Ther. 2023; 8:261.
11. Naert R, López-Requena A, Talavera K. TRPA1 Expression and pathophysiology in immune cells. Int J Mol Sci. 2021; 22:11460.

12. Lapointe TK, Altier C. The role of TRPA1 in visceral inflammation and pain. Channels (Austin). 2011; 5:525-529.
13. Nilius B, Owsianik G. The transient receptor potential family of ion channels. Genome Biol. 2011; 12:218.
14. Cheah EY, Burcham PC, Mann TS, Henry PJ. Acrolein relaxes mouse isolated tracheal smooth muscle *via* a TRPA1-dependent mechanism. Biochem Pharmacol. 2014; 89:148-156.
15. Bautista DM, Pellegrino M, Tsunozaki M. TRPA1: A gatekeeper for inflammation. Annu Rev Physiol. 2013; 75:181-200.
16. Russell FA, King R, Smillie SJ, Kodji X, Brain SD. Calcitonin gene-related peptide: Physiology and pathophysiology. Physiol Rev. 2014; 94:1099-1142.
17. Iannone LF, Nassini R, Patacchini R, Geppetti P, De Logu F. Neuronal and non-neuronal TRPA1 as therapeutic targets for pain and headache relief. Temperature (Austin). 2023; 10:50-66.
18. Engel MA, Leffler A, Niedermirtl F, *et al.* TRPA1 and substance P mediate colitis in mice. Gastroenterology. 2011; 141:1346-1358.
19. Bertin S, Aoki-Nonaka Y, Lee J, *et al*. The TRPA1 ion channel is expressed in $CD4^+$ T cells and restrains T-cell-mediated colitis through inhibition of TRPV1. Gut. 2017; 66:1584-1596.
20. Li J, Dou F, Hu S, Gao J. Involvement of adaptive immune responses in a model of subacute colitis induced with dextran sulfate sodium in C57BL/6 mice. Drug Discov Ther. 2023; 17:294-298.
21. Harbour SN, Maynard CL, Zindl CL, Schoeb TR, Weaver CT. Th17 cells give rise to Th1 cells that are required for the pathogenesis of colitis. Proc Natl Acad Sci U S A. 2015; 112:7061-7066.
22. Kałużna A, Olczyk P, Komosińska-Vassev K. The role of innate and adaptive immune cells in the pathogenesis and development of the inflammatory response in ulcerative colitis. J Clin Med. 2022; 11:400.
23. Pagano E, Romano B, Iannotti FA, *et al*. The non-euphoric phytocannabinoid cannabidivarin counteracts intestinal inflammation in mice and cytokine expression in biopsies from UC pediatric patients. Pharmacol Res. 2019; 149:104464.
24. Hanai H, Iida T, Takeuchi K, *et al*. Curcumin maintenance therapy for ulcerative colitis: Randomized, multicenter, double-blind, placebo-controlled trial. Clin Gastroenterol Hepatol. 2006; 4:1502-1506.
25. Csekő K, Beckers B, Keszthelyi D, Helyes Z. Role of TRPV1 and TRPA1 ion channels in inflammatory bowel diseases: Potential therapeutic targets? Pharmaceuticals (Basel). 2019; 12:48.

Received October 14, 2025; Revised January 10, 2026; Accepted January 15, 2026.

[§]These authors contributed equally to this work.

**Address correspondence to:*
Jianjun Gao, Department of Pharmacology, School of Pharmacy, Qingdao Medical College, Qingdao University, Qingdao, Shandong, China.
E-mail: gaojj@qdu.edu.cn

Shasha Hu, Department of Pathology, The Affiliated Hospital of Qingdao University, Qingdao, Shandong, China.
E-mail: huss0501@qdu.edu.cn

Released online in J-STAGE as advance publication January 23, 2026.

Original Article

DOI: 10.5582/bst.2025.01327

Elevated alpha-fetoprotein affects the long-term prognosis after hepatectomy in patients with hepatitis B-related intrahepatic cholangiocarcinoma

Yizhe Dai[1,§], Shilei Bai[2,§], Pinghua Yang[3,§], Huifeng Wang[4], Xiaoying Li[5], Feng Shen[1,*], Kui Wang[2,*]

[1] Department of Hepatic Surgery IV, the Eastern Hepatobiliary Surgery Hospital, Second Military Medical University (Naval Medical University), Shanghai, China;
[2] Department of Hepatic Surgery II, the Eastern Hepatobiliary Surgery Hospital, Second Military Medical University (Naval Medical University), Shanghai,China;
[3] Department of Biliary Surgery IV, the Eastern Hepatobiliary Surgery Hospital, Second Military Medical University (Naval Medical University), Shanghai, China;
[4] Department of Hepatic Surgery, the Fifth Clinical Medical College of Henan University of Chinese Medicine, Zhengzhou,China;
[5] College of Basic Medical Sciences, Second Military Medical University (Naval Medical University), Shanghai, China.

SUMMARY: This study investigates the prognostic significance of alpha-fetoprotein (AFP) in hepatitis B virus-related intrahepatic cholangiocarcinoma (HBV-ICC), given that AFP — though commonly used for hepatocellular carcinoma — is sometimes elevated in HBV-ICC, yet its clinical relevance remains unclear. The research retrospectively analyzed 839 HBV-ICC patients who underwent curative hepatectomy, categorizing them into AFP-positive (≥ 20 ng/mL) and AFP-negative groups. Using propensity score matching and inverse probability of treatment weighting to reduce bias, the study compared overall survival (OS) and time to recurrence (TTR). Results showed that AFP-positive patients had poorer liver function and more aggressive tumor characteristics, including higher rates of cirrhosis, microvascular invasion, and satellite nodules. Across both unadjusted and adjusted cohorts, elevated AFP was significantly associated with worse OS and earlier recurrence. Multivariate Cox analysis identified AFP as an independent predictor of poor prognosis. While CA19-9 alone demonstrated limited predictive value, its combination with AFP improved prognostic accuracy. The study concludes that elevated serum AFP independently predicts adverse survival and recurrence outcomes in HBV-ICC patients after curative resection, and combining AFP with CA19-9 enhances prognostic stratification, supporting AFP as a practical biomarker for postoperative risk assessment.

Keywords: alpha-fetoprotein (AFP), CA19-9, Intrahepatic cholangiocarcinoma (ICC), hepatitis B virus (HBV), hepatectomy

1. Introduction

Intrahepatic cholangiocarcinoma (ICC) originates from the intrahepatic secondary bile ducts and their branches, accounting for approximately 10–15% of primary liver cancers, and is the second most common primary malignant tumor of the liver (*1,2*). In recent years, both the incidence and mortality of ICC have been rapidly increasing worldwide (*1,3*). Radical hepatectomy remains the preferred curative treatment for patients with early- and intermediate-stage ICC; however, the 5-year postoperative survival rate remains below 40% (*4*). In Asia, particularly in China, hepatitis B virus (HBV) infection is an important etiological factor for ICC, it has been reported that HBV-related ICC accounts for about 27.7–77.2% of cases (*5,6*). Compared with non-HBV-related ICC, HBV-related ICC exhibits poorer prognosis and distinct heterogeneity (*7-9*). Song *et al*. suggested that patients with HBV-related ICC have shorter recurrence-free survival than those without HBV infection, and that HBV-related ICC may originate from hepatocytes (*9*). Therefore, HBV-related ICC may share certain biological characteristics with hepatocellular carcinoma (HCC).

Alpha-fetoprotein (AFP) is another important tumor marker for liver cancer and has been widely used to assess treatment efficacy, particularly in HBV-related HCC (*10,11*). In addition, AFP is also associated with germ cell tumors, gastric cancer, and colorectal cancer (*12*). For example, compared with AFP-negative gastric

cancer, AFP-positive gastric cancer demonstrates stronger invasiveness and worse prognosis (*13,14*). In Asia, a considerable proportion of ICC cases are associated with HBV infection (*8*). A previous study reported that approximately 25% of HBV-related ICC patients present with elevated AFP (*8*). However, the clinicopathological differences between AFP-positive and AFP-negative subgroups in HBV-related ICC, as well as the prognostic significance of AFP, remain unclear.

Based on a large clinical cohort, the present study aims to explore the clinicopathological characteristics of HBV-related ICC patients with different AFP levels, analyze the role of AFP in long-term prognosis and tumor recurrence, and evaluate the prognostic predictive value of combining AFP with CA19-9.

2. Materials and Methods

2.1. Study design

A total of 839 patients with HBV-related ICC who underwent hepatectomy at the Third Affiliated Hospital of Naval Medical University between January 2016 and December 2020 were retrospectively analyzed. Patients were stratified into AFP-positive and AFP-negative groups based on a serum AFP cutoff value of 20 ng/mL, comprising 237 and 602 patients, respectively. Eligibility criteria included: (1) Postoperative histopathological confirmation of ICC; (2) All patients were classified as Child–Pugh class A; (3) No prior antitumor therapy and no history of other malignancies; (4) All surgeries were performed as radical hepatectomies (R0); (5) Absence of major vascular or bile duct invasion, including bile duct, hepatic vein, or portal vein tumor thrombus; and (6) Eastern Cooperative Oncology Group (ECOG) performance status of ≤ 2. Exclusion criteria were: (1) Non-hepatitis B virus-related ICC; (2) Recurrence ICC; (3) Microscopic positive margins; (4) Tumor recurrence within 1 month postoperatively; (5) History of previous anticancer therapy; (6) Failure to recover within 1 month owing to severe postoperative complications; (7) Missing clinicopathological data or loss to follow-up withen 90 days after resection. The study was conducted in accordance with the Declaration of Helsinki, approved by the institutional ethics committee, and written informed consent was obtained from all participants.

2.2. Surgical procedures and pathological assessment

R0 resection was defined as complete macroscopic removal of the tumor with histologically negative margins (*15*). Major hepatectomy was defined as resection of three or more hepatic segments, while minor hepatectomy referred to resection of fewer than three segments (*16*). Surgical margin width was classified as wide (≥ 1 cm) and narrow (< 1 cm) according to the minimum distance from the tumor edge to the resection plane (*17*). The extent of lymph node dissection was standardized according to previously published criteria (*18*). Microvascular invasion (MVI) was defined as the presence of tumor cell nests within vascular spaces lined by endothelial cells, including the portal vein, hepatic vein, or capsular vessels (*19*).

2.3. Pathological criteria for ICC

All tumor specimens were sampled using a 7-point baseline sampling method (*20*). According to the 4th and 5th edition of the World Health Organization classification of liver tumors, ICC was defined as a tumor arising proximal to the second-order bile ducts and showing strong positivity for at least one cholangiocytic marker, such as cytokeratin 19 or mucin core protein 1. Patients diagnosed with hepatocellular carcinoma or combined hepatocellular-cholangiocarcinoma, characterized by the presence of distinct HCC and ICC components-regardless of whether transitional or transformation zones were present-or tumors with separate cells or regions expressing hepatocytic and cholangiocytic markers were excluded.

2.4. Postoperative surveillance

Patients were monitored every 2 months during the first 6 months after surgery, and every 6 months thereafter. Follow-up evaluations consisted of serum tumor marker (AFP, CEA, CA19-9), abdominal ultrasonography, and contrast-enhanced computed tomography (CT) or magnetic resonance imaging (MRI). In cases of suspected recurrence or metastasis, repeat enhanced CT or MRI of the upper abdomen was performed. Positron emission tomography–CT (PET-CT) or bone scintigraphy was conducted when clinically indicated. The primary endpoints were overall survival (OS) and time to recurrence (TTR). OS was defined as the interval from hepatectomy to death from any cause or last follow-up, while TTR was defined as the interval from hepatectomy to the first documented recurrence or last follow-up.

2.5. Statistical analysis

Statistical analyses were performed using R software, version 4.3.2 (*http://www.r-project.org*). Categorical variables were expressed as counts (*n*) or percentages (%) and compared using the χ^2 test or Fisher's exact test, as appropriate. To minimize baseline imbalances between groups, propensity score matching (PSM) with nearest-neighbor matching (1:1 ratio) and inverse probability of treatment weighting (IPTW) were applied. OS and TTR were estimated using the Kaplan–Meier method and compared by the log-rank test. Prognostic factors for OS and TTR were identified using univariate and multivariate Cox proportional hazards regression analyses. Variables with a p value < 0.05 in univariate

analysis were entered into multivariate analysis to determine independent predictors. A two-tailed p value < 0.05 was considered statistically significant.

3. Patient characteristics

The inclusion and exclusion process is shown in Figure 1. Among the 839 patients with HBV-related ICC, 237 were classified as AFP-positive and 602 as AFP-negative. Compared with AFP-negative patients, those in the AFP-positive group were more likely to be male (82.7% *vs*. 73.9%, $p = 0.009$), have concomitant cirrhosis (51.5% *vs*. 34.7%, $p < 0.001$), present with ascites (51.5% *vs*. 34.7%, $p < 0.001$), exhibit higher serum ALT levels (33.3% *vs*. 25.6%, $p = 0.030$), demonstrate poorer liver function (49.8% *vs*. 40.4%, $p = 0.016$), and have a higher proportion of elevated HBV-DNA load (54.0% *vs*. 40.0%, $p < 0.001$) (Table 1). To minimize bias due to baseline imbalances, propensity score matching (PSM) and inverse probability of treatment weighting (IPTW) were performed. In the PSM cohort, 222 AFP-positive patients were matched to 222 AFP-negative patients, while in the IPTW cohort, 238.2 AFP-positive and 600.3 AFP-negative patients were included (Table 2).

3.2. Survival analysis

The median follow-up time for all patients was 35.1 months (95% CI: 30.9-39.2). In the primary cohort, the 1-, 3-, and 5-year recurrence rates were 53.0%, 64.2%, and 68.2% in the AFP-positive group, compared with 40.2%, 56.3%, and 60.8% in the AFP-negative group ($p < 0.001$, Figure 2A). Correspondingly, the 1-, 3-, and 5-year OS rates were 65.1%, 43.1%, and 37.1% in the AFP-positive group, and 78.1%, 54.8%, and 47.5% in the AFP-negative group ($p < 0.001$, Figure 2B). In the PSM cohort, recurrence rates at 1, 3, and 5 years were 52.4%, 63.4%, and 66.7% in the AFP-positive group, compared with 40.7%, 50.5%, and 59.5% in the AFP-negative group ($p = 0.005$, Figure 3A). OS rates were 67.4%, 44.2%, and 37.8% in the AFP-positive group, compared with 75.0%, 55.5%, and 47.9% in the AFP-negative group ($p = 0.008$, Figure 3B). In the IPTW cohort, the 1-, 3-, and 5-year recurrence rates were 50.3%, 63.0%, and 66.3% in the AFP-positive group, compared with 40.7%, 56.2%, and 61.1% in the AFP-negative group ($p = 0.004$). OS rates were 67.4%, 44.2%, and 37.8% in the AFP-positive group, compared with 77.6%, 55.5%, and 47.9% in the AFP-negative group ($p < 0.001$, Figure 4A and 4B).

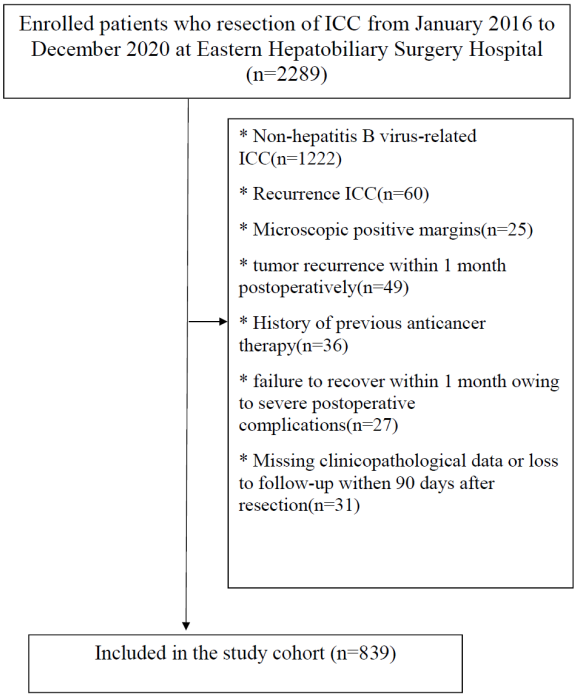

Figure 1. The flow chart of the study.

3.3. Independent risk Factors for tumor recurrence and OS

Results of univariate analysis are summarized in Tables 3–5. In the multivariate analysis of the primary cohort, independent predictors of OS included Cirrhosis (yes *vs*. no, HR = 1.471, 95%CI 1.174-1.842, $p < 0.001$), AFP level (> 20 *vs*. ≤ 20 ng/mL, HR = 1.294, 95%CI 1.037-1.615, $p = 0.023$), CA19-9 level (> 37 *vs*. ≤ 37 U/mL, HR = 1.570, 95%CI 1.239-1.990, $p < 0.001$), lymphadenectomy (yes *vs*. no, HR = 1.514, 95%CI 1.150-1.992, $p = 0.003$), tumor size (> 5 *vs*. ≤ 5 cm, HR = 1.577, 95%CI 1.246-1.995, $p < 0.001$), MVI (present *vs*. absent, HR = 1.433, 95%CI 1.106-1.857, $p = 0.007$), and satellite lesions (yes *vs*. no, HR = 1.329, 95%CI 1.056-1.673, $p = 0.016$). Independent predictors of recurrence were AFP level (> 20 *vs*. ≤ 20 ng/mL, HR = 1.363, 95%CI 1.113-1.670, $p = 0.003$), CA19-9 level (> 37 *vs*. ≤ 37 U/mL, HR = 1.376, 95%CI 1.103-1.716, $p = 0.005$), tumor size (> 5 *vs*. ≤ 5 cm, HR = 1.268, 95%CI 1.029-1.563, $p = 0.026$), MVI (present *vs*. absent, HR = 1.484, 95%CI 1.162-1.895, $p = 0.002$), satellite lesions (yes *vs*. no, HR = 1.381, 95%CI 1.112-1.716, $p = 0.004$), and lymph node metastasis (yes *vs*. no, HR = 1.492, 95%CI 1.063-2.094, $p = 0.021$). In the PSM cohort, independent predictors of OS included AFP level (> 20 *vs*. ≤ 20 ng/mL, HR = 1.589, 95%CI 1.188-2.216, $p = 0.002$), CA19-9 level (> 37 *vs*. ≤ 37 U/mL, HR = 1.520, 95%CI 1.077-2.145, $p = 0.017$), lymphadenectomy (yes *vs*. no, HR = 1.571, 95%CI 1.097-2.249, $p = 0.014$), tumor size (> 5 *vs*. ≤ 5 cm, HR = 1.566, 95%CI 1.154-2.216, $p = 0.004$), MVI (present *vs*. absent, HR = 1.689, 95%CI 1.217-2.345, $p = 0.002$), and satellite lesions (yes *vs*. no, HR = 1.491, 95%CI 1.102-2.017, $p = 0.010$). Independent predictors of recurrence were sex (male *vs*. female, HR = 1.502, 95%CI 1.036-2.177, $p = 0.032$), AFP level (> 20 *vs*. ≤ 20 ng/mL, HR = 1.471, 95%CI 1.144-1.890, $p = 0.003$), CA19-9 level (> 37 *vs*. ≤ 37 U/mL, HR = 1.373,

Table 1. Basal clinicopathological characteristics of ICC patients before propensity score analysis

Variables	AFP ≤ 20 ng/mL (*n* = 602)	AFP > 20 ng/mL (*n* = 237)	*p*-value	*SMD*
Sex			0.009	0.214
Female	157 (26.1)	41 (17.3)		
Male	445 (73.9)	196 (82.7)		
Age, years			0.165	0.117
≤ 60	484 (80.4)	201 (84.8)		
> 60	118 (19.6)	36 (15.2)		
BMI			1.000	0.006
≤ 22	194 (32.2)	77 (32.5)		
> 22	408 (67.8)	160 (67.5)		
Diabetes			0.359	0.088
No	571 (94.8)	229 (96.6)		
Yes	31 (5.2)	8 (3.4)		
Antivirus			0.649	0.045
No	530 (88.0)	212 (89.5)		
Yes	72 (12.0)	25 (10.5)		
Cirrhosis			0.001	0.270
No	387 (64.3)	121 (51.1)		
Yes	215 (35.7)	116 (48.9)		
Gastroesophageal Varices			0.739	0.034
No	535 (88.9)	208 (87.8)		
Yes	67 (11.1)	29 (12.2)		
Ascites			< 0.001	0.292
No	581 (96.5)	211 (89.0)		
Yes	21 (3.5)	26 (14.0)		
ALT, U/L			0.030	0.171
≤ 44	448 (74.4)	158 (66.7)		
> 44	154 (25.6)	79 (33.3)		
PLT, $*10^9$/mL			0.032	0.167
≤ 100	82 (13.6)	47 (19.831%)		
> 100	520 (86.4)	190 (80.169%)		
NLR			0.242	0.096
≤ 2.5	336 (55.8)	121 (51.1)		
> 2.5	266 (44.2)	116 (48.9)		
INR			0.176	0.110
≤ 1.1	542 (90.0)	205 (86.5)		
> 1.1	60 (10.0)	32 (13.5)		
ALBI Grade			0.016	0.063
Grade I	359 (59.6)	119 (50.2)		
Grade II	243 (40.4)	118 (49.8)		
HBV-DNA, IU/mL			< 0.001	0.283
≤ 2,000	361 (60.0)	109 (46.0)		
> 2,000	241 (40.0)	128 (54.0)		
CEA, ng/mL			0.184	0.109
≤ 10	555 (92.0)	211 (89.0)		
> 10	47 (7.8)	26 (11.0%)		
CA19-9, U/mL			0.065	0.151
≤ 37	436 (72.4)	187 (78.9)		
> 37	166 (27.6)	50 (21.2)		
ASA grade			0.311	0.086
II	146 (24.3)	49 (20.7)		
III	456 (75.7)	188 (79.3)		
Major Hepatectomy			0.138	0.112
No	460 (76.4)	193 (81.435%)		
Yes	142 (23.6)	44 (18.565%)		
Hilar Clamping, min			0.687	0.037
≤ 15	293 (48.7)	111 (46.8)		
> 15	309 (51.3)	126 (53.2)		
Surgical Margin, cm			0.187	0.039
≤ 1	502 (83.4)	207 (87.3)		
> 1	100 (16.6)	30 (12.7)		
Lymphadenectomy			0.691	0.178
No	432 (71.8)	174 (73.4)		
Yes	170 (28.2)	63 (26.6)		

Bold values indicate statistical significance ($p < 0.05$). PLT, platelet; AST, Aspartate transaminase; AFP, alpha fetoprotein; NLR, neutrophil-to-lymphocyte ratio; ALBI, Albumin-bilirubin; HBsAg, Hepatitis B surface antigen; HBV-DNA, hepatitis B virus-deoxyribonucleic acid; ASA, American society of Aneshesiologists.

Table 1. Basal clinicopathological characteristics of ICC patients before propensity score analysis (continued)

Variables	AFP ≤ 20 ng/mL (*n* = 602)	AFP > 20 ng/mL (*n* = 237)	*p*-value	*SMD*
Blood loss,mL	200.0 [150.0;400.0]	210.0 [200.0;400.0]	0.216	0.047
Transfusion			0.601	0.049
No	521 (86.5)	209 (88.2)		
Yes	81 (13.5)	28 (11.8)		
Tumor Size, cm			0.012	0.201
≤ 5	296 (49.2)	93 (39.2)		
> 5	306 (50.8)	144 (60.8)		
Tumor Number			0.176	0.105
Single	564 (93.7)	215 (90.7)		
Multiple	38 (6.3)	22 (9.3)		
Microvascular Invasion			0.029	0.024
Absent	525 (87.2)	192 (81.0)		
Present	77 (12.8)	45 (19.0)		
Satellite			0.042	0.160
No	464 (77.1)	166 (70.0)		
Yes	138 (22.9)	71 (30.0)		
Capsule			0.099	0.119
Incomplete	526 (87.4)	196 (82.7)		
Complete	76 (12.6)	41 (17.3)		
Differentiation			0.180	0.116
Poor	69 (11.5)	19 (8.0)		
Moderate/Well	533 (88.5)	218 (92.0)		
Lymph node metastasis			0.643	0.044
No	532 (88.4)	206 (86.9)		
Yes	70 (11.6)	31 (13.1)		
Adjuvant Therapy			0.101	0.131
No	447 (74.3)	162 (68.4)		
Yes	155 (25.7)	75 (31.6)		

Bold values indicate statistical significance ($p < 0.05$). PLT, platelet; AST, Aspartate transaminase; AFP, alpha fetoprotein; NLR, neutrophil-to-lymphocyte ratio; ALBI, Albumin-bilirubin; HBsAg, Hepatitis B surface antigen; HBV-DNA, hepatitis B virus-deoxyribonucleic acid; ASA, American society of Aneshesiologists.

95%CI 1.011-1.865, $p = 0.042$), MVI (present *vs*. absent, HR = 1.674, 95%CI 1.231-2.276, $p = 0.001$), and satellite lesions (yes *vs*. no, HR = 1.476, 95%CI 1.103-1.976, $p = 0.009$). In the IPTW cohort, independent predictors of OS were ALBI grade (II *vs*. I, HR = 1.293, 95%CI 1.030-1.624, $p = 0.027$), AFP level (> 20 *vs*. ≤ 20 ng/mL, HR = 1.314, 95%CI 1.038-1.663, $p = 0.023$), CA19-9 level (> 37 *vs*. ≤ 37 U/mL, HR = 1.570, 95%CI 1.193-2.064, $p = 0.001$), lymphadenectomy (yes *vs*. no, HR = 1.574, 95%CI 1.185-2.091, $p = 0.011$), tumor size (> 5 *vs*. ≤ 5 cm, HR = 1.469, 95%CI 1.162-1.857, $p = 0.001$), MVI (present *vs*. absent, HR = 1.387, 95%CI 1.028-1.870, $p = 0.032$), and satellite lesions (yes *vs*. no, HR = 1.351, 95%CI 1.056-1.729, $p = 0.017$). Independent predictors of recurrence were AFP level (> 20 *vs*. ≤ 20 ng/mL, HR = 1.360, 95%CI 1.090-1.696, $p = 0.006$), CA19-9 level (> 37 *vs*. ≤ 37 U/mL, HR = 1.459, 95%CI 1.148-1.853, $p = 0.002$), MVI (present *vs*. absent, HR = 1.482, 95%CI 1.147-1.915, $p = 0.003$), and satellite lesions (yes *vs*. no, HR = 1.386, 95%CI 1.106-1.736, $p = 0.004$).

3.4. Prognostic prediction of AFP and CA19-9

Receiver operating characteristic (ROC) analysis showed that CA19-9 alone yielded 1-, 3-, and 5-year areas under the curve (AUCs) of 0.604, 0.589, and 0.583 for OS prediction, which improved to 0.658, 0.623, and 0.620 when combined with AFP. For recurrence prediction, CA19-9 alone yielded AUCs of 0.570, 0.543, and 0.593, which improved to 0.658, 0.623, and 0.619 when combined with AFP (Figure 5A and 5B).

4. Discussion

Elevated AFP predicts poor prognosis in HCC patients, but there are relatively few studies evaluating the prognostic impact of marked AFP elevation in ICC patients, particularly in those with HBV-related ICC. Huang *et al*. enrolled 119 HBV-ICC patients and reported an AFP > 20 ng/mL prevalence of 25.2% (30/119) (*8*). Their multivariable Cox analysis indicated that elevated AFP was an independent risk factor for poor prognosis in HBV-related ICC, but a similar association was not observed in non-HBV-related ICC; however, that retrospective study had a small sample size and did not perform an in-depth analysis of AFP (*8*).

In the present study we evaluated the prognostic significance of AFP in a substantially larger HBV-ICC cohort. We first observed that patients with different AFP levels differed with respect to sex, cirrhosis, ascites, ALT, platelet count, ALBI grade, HBV-DNA load, tumor diameter, MVI, and satellite nodules. These findings

Table 2. Basal clinicopathological characteristics of ICC patients after propensity score analysis

Variables	PSM Cohort				Stable IPTW Cohort			
	AFP ≤ 20 ng/mL (*n* = 222)	AFP > 20 ng/mL (*n* = 222)	*p*-value	*SMD*	AFP ≤ 20 ng/mL (*n* = 600.3)	AFP > 20 ng/mL (*n* = 238.3)	*p*-value	*SMD*
Sex			0.612	0.060			0.990	0.001
Female	35 (15.8)	40 (18.0)			142.1 (23.7)	56.5 (23.47)		
Male	187 (84.2)	182 (82.0)			458.2 (76.3)	181.8 (76.3)		
Age, years			0.442	0.085			0.262	0.101
≤ 60	182 (82.0)	189 (85.1)			486.1 (81.0)	202.0 (84.8)		
> 60	40 (18.0)	33 (14.9)			114.2 (19.0)	36.3 (15.2)		
BMI			0.919	0.019			0.703	0.032
≤ 22	70 (31.5)	72 (32.4)			195.4 (32.5)	81.2 (34.1)		
> 22	152 (68.5)	150 (67.6)			404.9 (7.5)	157.1 (65.9)		
Diabetes			0.371	0.106			0.578	0.050
No	209 (94.1)	214 (96.4)			571.0 (95.1)	229.1 (96.2)		
Yes	13 (5.9)	8 (3.6)			29.3 (4.9)	9.2 (3.8)		
Antivirus			0.640	0.059			0.669	0.037
No	201 (90.5)	197 (88.7)			530.6 (88.4)	207.7 (87.2)		
Yes	21 (9.5)	25 (11.3)			69.7 (11.6)	30.5 (12.8)		
Cirrhosis			0.084	0.174			0.746	0.026
No	136 (61.3)	117 (52.7)			363.6 (60.6)	141.2 (59.3)		
Yes	86 (38.7)	105 (47.3)			236.7 (39.4)	97.0 (40.7)		
Gastroesophageal Varices			0.317	0.109			0.099	0.129
No	190 (85.6)	198 (89.2)			523.2 (87.2)	217.2 (91.2)		
Yes	32 (14.4)	24 (10.8)			77.1 (12.8)	21.0 (8.8)		
Ascites			0.582	0.070			0.981	0.002
No	204 (91.9)	208 (93.7)			568.7 (94.7)	225.8 (94.8)		
Yes	18 (8.1)	14 (6.3)			31.6 (5.3)	12.4 (5.2)		
ALT,U/L			0.143	0.149			0.908	0.010
≤ 44	165 (74.3)	150 (67.6)			435.4 (72.5)	171.8 (72.1)		
> 44	57 (25.7)	72 (32.4)			164.9 (27.5)	66.5 (27.9)		
PLT, $*10^9$/mL			0.804	0.035			0.728	0.028
≤ 100	38 (17.1)	41 (18.5)			91.9 (15.3)	38.9 (16.3)		
> 100	184 (82.9)	181 (81.5)			508.4 (84.7)	199.4 (83.7)		
NLR			0.776	0.036			0.865	0.014
≤ 2.5	118 (53.2)	114 (51.4)			333.0 (55.5)	130.5 (54.8)		
> 2.5	104 (46.8)	108 (48.6)			267.3 (44.5)	107.8 (45.2)		
INR			0.773	0.041			0.571	0.043
≤ 1.1	196 (88.3)	193 (86.9)			532.6 (88.7)	214.6 (90.1)		
> 1.1	26 (11.7)	29 (13.1)			67.7 (11.3)	23.7 (9.9)		

Bold values indicate statistical significance ($p < 0.05$). AFP, alpha fetoprotein; BMI, body mass index; ALT, alanine aminotransferase; PLT, platelet; NLR, neutrophil-to-lymphocyte ratio; INR, international normalized ratio; ALBI, Albumin-bilirubin; HBV-DNA, hepatitis B virus-deoxyribonucleic acid; CEA, carcinoembryonic antigen; CA19-9, Carbohydrate antigen19-9; ASA, American society of Aneshesiologists.

Table 2. Basal clinicopathological characteristics of ICC patients after propensity score analysis (continued)

Variables	PSM Cohort				Stable IPTW Cohort			
	AFP ≤ 20 ng/mL (*n* = 222)	AFP > 20 ng/mL (*n* = 222)	*p*-value	*SMD*	AFP ≤ 20 ng/mL (*n* = 600.3)	AFP > 20 ng/mL (*n* = 238.3)	*p*-value	*SMD*
ALBI Grade			0.569	0.063			0.733	0.028
Grade I	109 (49.1)	116 (52.3)			343.0 (57.1)	139.4 (58.5)		
Grade II	113 (50.9)	106 (47.7)			257.3 (42.9)	98.8 (41.5)		
HBV-DNA, IU/mL			0.776	0.036			0.825	0.018
≤ 2,000	110 (49.550)	106 (47.748)			339.4 (56.5)	136.8 (57.4)		
> 2,000	112 (50.450)	116 (52.252)			260.9 (43.5)	101.4 (42.6)		
CEA, ng/mL			0.180	0.144			0.056	0.165
≤ 10	207 (93.2)	198 (89.2)			554.1 (92.3)	208.1 (87.3)		
> 10	15 (6.8)	24 (10.8)			46.2 (7.7)	30.2 (12.7)		
CA19-9, U/mL			0.177	0.139			0.877	0.014
≤ 37	164 (73.9)	177 (79.7)			445.5 (74.2)	178.2 (74.8)		
> 37	58 (26.1)	45 (20.3)			154.8 (25.8)	60.0 (25.2)		
ASA grade			0.145	0.149			0.903	0.010
II	59 (26.6)	45 (20.3)			139.7 (23.3)	54.4 (22.8)		
III	163 (73.4)	177 (79.7)			460.6 (76.7)	183.9 (77.2)		
Major Hepatectomy			0.158	0.145			0.144	0.122
No	170 (76.6)	183 (82.4)			459.6 (76.6)	194.2 (81.5)		
Yes	52 (23.4)	39 (17.6)			140.7 (23.4)	44.0 (18.5)		
Hilar Clamping, min			0.634	0.054			0.766	0.025
≤ 15	100 (45.0)	106 (47.7)			290.2 (48.3)	112.2 (47.1)		
> 15	122 (55.0)	116 (52.3)			310.1 (51.7)	126.1 (52.9)		
Surgical Margin, cm			0.786	0.039			0.332	0.082
≤ 1	189 (85.1)	192 (86.5)			504.9 (84.1)	207.3 (87.0)		
> 1	33 (14.9)	30 (13.5)			95.3 (15.9)	31.0 (13.0)		
Lymphadenectomy			0.078	0.178			0.584	0.047
No	147 (66.2)	165 (74.3)			434.8 (72.4)	177.5 (74.5)		
Yes	75 (33.8)	57 (25.7)			165.5 (27.6)	60.8 (25.5)		
Blood loss, mL	250.000 [150.0;400.0]	200.000 [150.0;400.0]	0.902	0.098	405.05 ± 1864.78	334.26 ± 323.70	0.329	0.053
Transfusion			0.668	0.054				
No	192 (86.5)	196 (88.3)			521.4 (86.9)	207.8 (87.2)	0.904	0.011
Yes	30 (13.5)	26 (11.7)			78.9 (13.1)	30.5 (12.8)		
Tumor Size, cm			0.441	0.082			0.734	0.029
≤ 5	97 (43.7)	88 (39.6)			278.3 (46.4)	113.9 (47.8)		
> 5	125 (56.3)	134 (60.4)			321.9 (53.6)	124.4 (52.2)		
Tumor Number			0.359	0.105			0.358	0.070
Single	209 (94.1)	203 (91.4)			561.5 (93.5)	218.5 (91.7)		
Multiple	13 (5.9)	19 (8.6)			38.8 (6.5)	19.7 (8.3)		

Bold values indicate statistical significance ($p < 0.05$). AFP, alpha fetoprotein; BMI, body mass index; ALT, alanine aminotransferase; PLT, platelet; NLR, neutrophil-to-lymphocyte ratio; INR, international normalized ratio; ALBI, Albumin-bilirubin; HBV-DNA, hepatitis B virus-deoxyribonucleic acid; CEA, carcinoembryonic antigen; CA19-9, Carbohydrate antigen19-9; ASA, American society of Aneshesiologists.

Table 2. Basal clinicopathological characteristics of ICC patients after propensity score analysis (continued)

Variables	PSM Cohort				Stable IPTW Cohort			
	AFP ≤ 20 ng/mL (n = 222)	AFP > 20 ng/mL (n = 222)	p-value	*SMD*	AFP ≤ 20 ng/mL (n = 600.3)	AFP > 20 ng/mL (n = 238.3)	p-value	*SMD*
Microvascular Invasion			0.900	0.024			0.989	0.001
Absent	183 (82.4)	185 (83.3)			513.2 (85.5)	203.6 (85.5)		
Present	39 (17.6)	37 (16.7)			87.1 (14.5)	34.6 (14.5)		
Satellite			1.000	0.010			0.680	0.032
No	161 (72.5)	162 (73.0)			452.5 (75.4)	182.9 (76.8)		
Yes	61 (27.5)	60 (27.0)			147.8 (24.6)	55.4 (23.2)		
Capsule			0.356	0.100			0.467	0.059
Incomplete	192 (86.5)	184 (82.9)			522.2 (87.0)	202.4 (85.0)		
Complete	30 (13.5)	38 (17.2)			78.1 (13.0)	35.9 (15.0)		
Edmondson-Steiner Grade			0.512	0.078			0.014	0.201
I-II	23 (10.4)	18 (8.1)			73.0 (12.2)	15.1 (6.4)		
III-VI	199 (89.6)	204 (91.9)			527.3 (87.8)	223.1 (93.6)		
Lymph node metastasis			0.581	0.065			0.938	0.006
No	189 (85.1)	194 (87.4)			532.7 (88.7)	211.0 (88.5)		
Yes	33 (14.9)	28 (12.6)			67.6 (11.3)	27.3 (11.5)		
Adjuvant Therapy			0.681	0.049			0.099	0.139
No	151 (68.0)	156 (70.3)			446.8 (74.4)	162.4 (68.2)		
Yes	71 (32.0)	66 (29.3)			153.5 (25.6)	31.8 (31.8)		

Bold values indicate statistical significance ($p < 0.05$). AFP, alpha fetoprotein; BMI, body mass index; ALT, alanine aminotransferase; PLT, platelet; NLR, neutrophil-to-lymphocyte ratio; INR, international normalized ratio; ALBI, Albumin-bilirubin; HBV-DNA, hepatitis B virus-deoxyribonucleic acid; CEA, carcinoembryonic antigen; CA19-9, Carbohydrate antigen19-9; ASA, American society of Aneshesiologists.

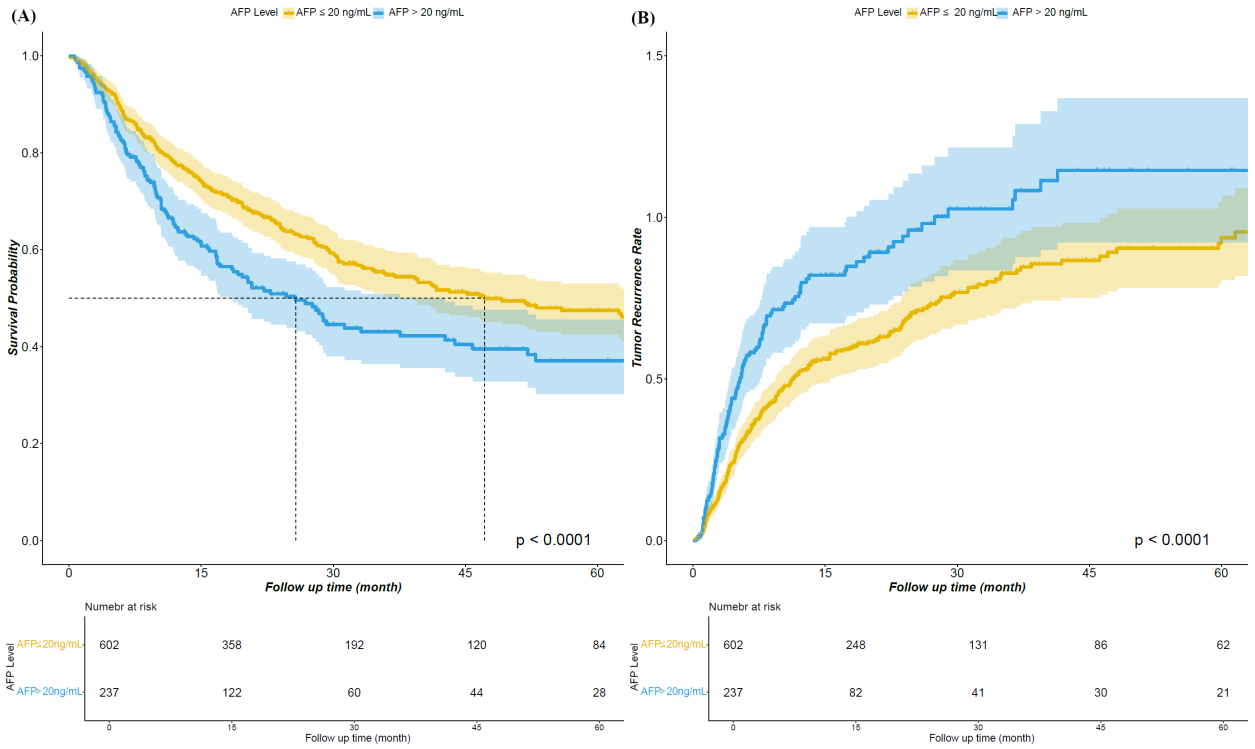

Figure 2. Kaplan-Meier analysis for OS in HBV-ICC patients with different alpha-fetoprotein levels in primary cohort. (A) Overall Survival; **(B)** Time to recurrence.

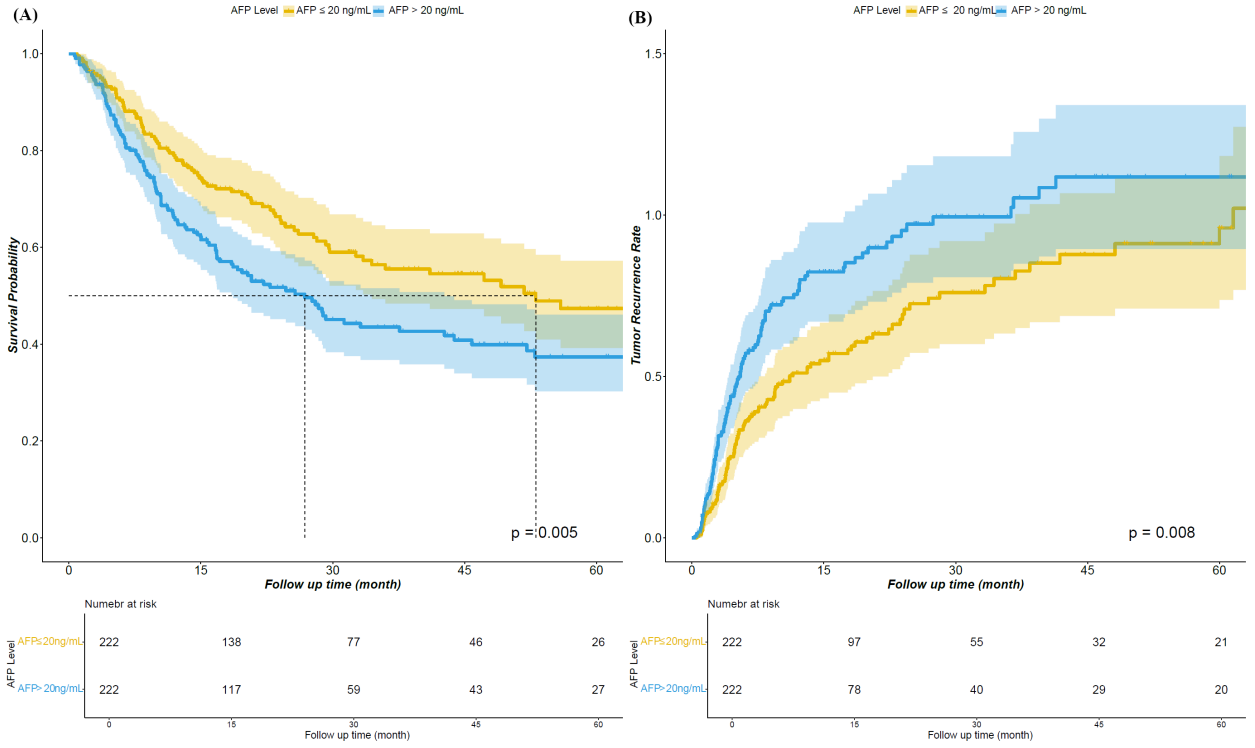

Figure 3. Kaplan-Meier analysis for OS in HBV-ICC patients with different alpha-fetoprotein levels in PSM cohort. (A) Overall Survival; **(B)** Time to recurrence.

suggest that AFP-positive patients have worse liver function and more aggressive tumor features. In the unmatched cohort, the 1-, 3-, and 5-year OS rates and recurrence rates in the AFP-positive group were 65.1%, 43.1%, 37.1% and 53.0%, 64.2%, 68.2%, respectively. The AFP-positive group exhibited poorer overall survival and higher recurrence compared with the AFP-negative group. After adjustment for potential confounders, both

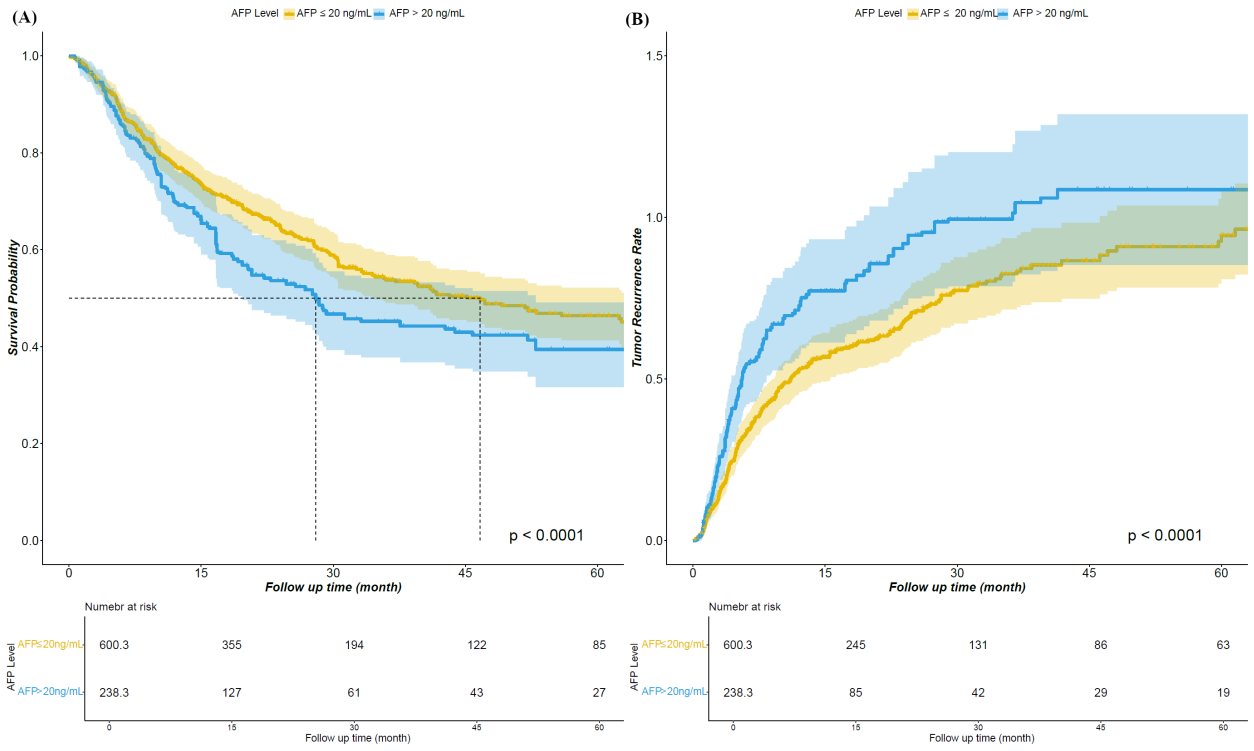

Figure 4. Kaplan-Meier analysis for OS in HBV-ICC patients with different alpha-fetoprotein levels in IPTW cohort. (A) Overall Survival; **(B)** Time to recurrence.

the PSM and IPTW cohorts produced concordant results. Subsequent Cox regression analyses demonstrated that serum AFP level was an independent prognostic factor in the original, PSM, and IPTW cohorts. Additionally, we found that CA19-9 alone had limited prognostic performance (OS AUCs at 1, 3, 5 years: 0.604, 0.589, 0.583; recurrence AUCs: 0.570, 0.543, 0.593), whereas combining CA19-9 with AFP improved predictive accuracy.

The association between AFP and ICC tumor biology has been explored previously. Prior studies reported correlations between higher AFP and cirrhosis and worse liver function (*21*). A multicenter retrospective study found that higher AFP was strongly associated with formation of massive tumor nodules (OR 25.000, $p < 0.001$) (*22*). At the molecular level, AFP expression in cholangiocarcinoma has been reported to correlate positively with eIF3C expression, which may promote ICC progression by enhancing cholangiocyte proliferation (*23*). Established independent prognostic factors for recurrence and survival-such as CA19-9 level, MVI, and tumor size-were also confirmed in our study, consistent with previous reports (*24*). The lower discriminatory power of CA19-9 for ICC prognosis is in part due to its elevation in various benign and malignant biliary disorders, which reduces specificity. Given this limitation, several investigators have proposed combining CA19-9 with other circulating markers; for example, Wang *et al*. combined CA19-9 with circulating cell-free DNA (cfDNA) for prognostic assessment (*25*). AFP is routinely measured in clinical practice, is inexpensive, and readily available. Until other serum biomarkers are validated at scale, combining AFP with CA19-9 may offer a pragmatic improvement in prognostic stratification for HBV-ICC.

Regarding potential biological mechanisms linking HBV, AFP, and ICC: the canonical "inflammation-to-carcinoma" pathway explains HBV-driven hepatocarcinogenesis and the associated AFP elevation in HCC (*26,27*). HBV is a hepatotropic virus that primarily infects hepatocytes and does not readily persist in cholangiocytes (*28*). The mechanism by which HBV contributes to ICC remains unclear. Stem/progenitor-cell theories of cholangiocarcinogenesis may reconcile the observed relationships among HBV, HCC-like biology, and AFP. Hepatic progenitor cells located in the Hering canal can, under injurious or oncogenic stimuli, differentiate along hepatocytic or cholangiocytic lineages (*29*). HBV can integrate fragments of its genome (*e.g.*, HBx) into the genomes of adult hepatic progenitor cells, potentially driving transformation toward malignant hepatocytic or cholangiocytic phenotypes (*30*). AFP is a marker of cellular dedifferentiation and immaturity and is expressed in hepatic progenitor cells. ICCs that synthesize and secrete substantial AFP may therefore retain progenitor-like or hepatocytic features (*31*). Beyond effects on progenitor cells, Song *et al*. reported that HBV can induce transdifferentiation of mature hepatocytes into ICC-like cells, which in hepatocyte-origin ICCs continue to proliferate and

Table 3. Univariate cox regression analysis of OS and recurrence in HBV-related ICC patients before propensity score analysis

Variable	OS		Recurrence	
	HR (95% CI)	*p*	HR (95% CI)	*p*
Sex		0.597		0.131
Male *vs*. Female	1.068 (0.837 - 1.362)		1.191 (0.949 - 1.495)	
Age, years		0.133		0.453
> 60 *vs*. ≤ 60	1.215 (0.943 - 1.565)		0.910 (0.712 - 1.164)	
BMI		0.182		0.545
> 22 *vs*. ≤ 22	0.863 (0.696 - 1.071)		0.940 (0.770 - 1.148)	
Diabetes		0.551		0.168
Yes *vs*. No	1.155 (0.719 - 1.855)		1.343 (0.883 - 2.045)	
Antivirus		0.160		0.174
Yes *vs*. No	0.771 (0.536 - 1.108)		0.806 (0.590 - 1.101)	
Cirrhosis		0.035		0.998
Yes *vs*. No	1.247 (1.015 - 1.532)		1.000 (0.826- 1.211)	
Gastroesophageal Varices		0.725		0.235
Yes *vs*. No	1.058 (0.772 - 1.450)		0.826 (0.603 - 1.132)	
Ascites		0.133		0.720
Yes *vs*. No	1.374 (0.908 - 2.079)		0.923 (0.595 - 1.431)	
ALT,U/L		0.262		0.106
> 44 *vs*. ≤ 44	1.135 (0.910 - 1.415)		1.183 (0.965 - 1.450)	
PLT, $*10^9$/mL		0.408		0.554
> 100 *vs*. ≤ 100	0.892 (0.680 - 1.170)		1.082 (0.834 - 1.403)	
NLR		< 0.001		0.040
> 2.5 *vs*. ≤ 2.5	1.466 (1.195 - 1.798)		1.127 (0.798 - 1.593)	
INR		0.024		0.712
> 1.1 *vs*. ≤ 1.1	1.397 (1.044 - 1.869)		0.944 (0.694 - 1.283)	
ALBI Grade		< 0.001		0.351
II *vs*. I	1.449 (1.181 - 1.777)		1.094 (0.906 - 1.322)	
HBV-DNA, IU/mL		0.588		0.861
> 2,000 *vs*. ≤ 2,000	1.058 (0.862 - 1.300)		1.017 (0.842 - 1.228)	
AFP, ng/mL		0.001		< 0.001
> 20 *vs*. ≤ 20	1.449 (1.1681 -1.798)		1.430 (1.171 - 1.746)	
CEA, ng/mL		0.086		0.925
> 10 *vs*. ≤ 10	1.362 (0.957 - 1.940)		0.983 (0.689 - 1.402)	
CA19-9, U/mL		< 0.001		< 0.001
> 37 *vs*. ≤ 37	1.981 (1.588 - 2.471)		1.599 (1.296 - 1.971)	
ASA grade		0.188		0.766
III *vs*. II	0.852 (0.670 - 1.0816)		0.967 (0.775 - 1.207)	
Major Hepatectomy		0.218		0.036
Yes *vs*. No	1.164 (0.914 - 1.482)		1.264 (1.015 - 1.575)	
Hilar Clamping, min		0.556		0.045
> 15 *vs*. ≤ 15	1.063 (0.867 - 1.305)		1.213 (1.005 - 1.464)	
Surgical Margin, cm		0.054		0.089
> 1 *vs*. ≤ 1	0.744 (0.551 - 1.006)		0.796 (0.613 - 1.035)	
Lymphadenectomy		< 0.001		< 0.001
Yes *vs*. No	1.892 (1.529 - 2.341)		1.551 (1.268 - 1.898)	
Blood loss,mL	1.000 (0.999 - 1.000)	0.931	1.000 (0.999 - 1.000)	0.637
Transfusion		0.021		0.685
Yes *vs*. No	1.389 (1.052 - 1.835)		1.060 (0.800 - 1.403)	
Tumor Size, cm		< 0.001		< 0.001
> 5 *vs*. ≤ 5	1.913 (1.547 - 2.366)		1.545 (1.278 - 1.868)	
Tumor Number		0.319		0.496
Multiple *vs*. Single	1.200 (0.839 - 1.715)		1.217 (1.009 - 1.469)	
Microvascular Invasion		< 0.001		< 0.001
Present *vs*. Absent	1.754 (1.362 - 2.257)		1.780 (1.404 - 2.256)	
Satellite		< 0.001		< 0.001
Yes *vs*. No	1.764 (1.417 - 2.195)		1.686 (1.374 - 2.069)	
Capsule		0.039		0.923
Complete *vs*. Incomplete	0.719 (0.526 - 0.983)		1.013 (0.780 - 1.315)	
Diferentiation		0.243		0.153
Moderate/Well *vs*. Poor	0.834 (0.615 - 1.131)		0.815 (0.615 - 1.079)	
Lymph node metastasis		< 0.001		< 0.001
Yes *vs*. No	2.062 (1.572 - 2.704)		1.950 (1.504 - 2.529)	
Adjuvant Therapy		0.140		0.804
Yes *vs*. No	0.838 (0.662 - 1.060)		0.974 (0.792 - 1.198)	

Table 4. Univariate cox regression analysis of OS and recurrence in HBV-related ICC patients after PSM

Variable	OS		Recurrence	
	HR (95% CI)	*p*	HR (95% CI)	*p*
Sex		0.056		0.020
Male *vs*. Female	1.450 (0.990 - 2.122)		1.528 (1.070 - 2.183)	
Age, years		0.863		0.297
> 60 *vs*. ≤ 60	1.032 (0.723 - 1.473)		0.833 (0.590 - 1.175)	
BMI		0.139		0.423
> 22 *vs*. ≤ 22	0.808 (0.610 - 1.072)		0.897 (0.688 - 1.170)	
Diabetes		0.383		0.722
Yes *vs*. No	0.692 (0.303 - 1.583)		0.885 (0.453 - 1.731)	
Antivirus		0.232		0.176
Yes *vs*. No	0.743 (0.457 - 1.209)		0.752 (0.498 - 1.136)	
Cirrhosis		0.115		0.642
Yes *vs*. No	1.254 (0.946 - 1.662)		1.060 (0.828 - 1.358)	
Gastroesophageal Varices		0.594		0.222
Yes *vs*. No	0.884 (0.561 - 1.392)		0.771 (0.508 - 1.170)	
Ascites		0.487		0.287
Yes *vs*. No	1.198 (0.720 - 1.992)		0.702 (0.366 - 1.346)	
ALT,U/L		0.713		0.757
> 44 *vs*. ≤ 44	0.947 (0.707 - 1.268)		1.044 (0.796 - 1.368)	
PLT, $*10^9$/mL		0.512		0.988
> 100 *vs*. ≤ 100	0.890 (0.628 - 1.261)		0.988 (0.718 - 1.360)	
NLR		0.016		0.027
> 2.5 *vs*. ≤ 2.5	1.414 (1.066 - 1.877)		1.330 (1.034 - 1.711)	
INR		0.322		0.686
> 1.1 *vs*. ≤ 1.1	1.226 (0.819 - 1.834)		0.914 (0.591 - 1.414)	
ALBI Grade		0.116		0.540
II *vs*. I	1.241 (0.948 - 1.623)		1.081 (0.843 - 1.386)	
HBV-DNA, IU/mL		0.931		0.488
> 2,000 *vs*. ≤ 2,000	1.012 (0.765 - 1.339)		0.914 (0.710 - 1.177)	
AFP, ng/mL		0.006		0.008
> 20 *vs*. ≤ 20	1.477 (1.120 - 1.948)		1.404 (1.094 - 1.802)	
CEA, ng/mL		0.146		0.760
> 10 *vs*. ≤ 10	1.465 (0.875 - 2.452)		1.081 (0.656 - 1.781)	
CA19-9, U/mL		< 0.001		0.003
> 37 *vs*. ≤ 37	1.840 (1.326 - 2.553)		1.576 (1.167 - 2.128)	
ASA grade		0.205		0.727
III *vs*. II	0.813 (0.590 - 1.120)		0.950 (0.712 - 1.268)	
Major Hepatectomy		0.212		0.041
Yes *vs*. No	1.223 (0.892 - 1.678)		1.370 (1.012 - 1.855)	
Hilar Clamping, min		0.734		0.328
> 15 *vs*. ≤ 15	1.045 (0.811 - 1.347)		1.126 (0.888 - 1.430)	
Surgical Margin, cm		0.744		0.516
> 1 *vs*. ≤ 1	1.062 (0.739 - 1.528)		0.896 (0.644 - 1.248)	
Lymphadenectomy		< 0.001		< 0.001
Yes *vs*. No	2.117 (1.559 - 2.877)		1.667 (1.254 - 2.217)	
Blood loss,mL	1.000 (0.999 - 1.000)	0.606	1.000 (0.999 - 1.000)	0.340
Transfusion		0.235		0.399
Yes *vs*. No	1.316 (0.837 - 2.070)		1.204 (0.782 - 1.855)	
Tumor Size, cm		< 0.001		0.002
> 5 *vs*. ≤ 5	1.942 (1.467 - 2.570)		1.463 (1.144 - 1.870)	
Tumor Number		0.773		0.961
Multiple *vs*. Single	0.931 (0.571 - 1.516)		1.011 (0.660 - 1.548)	
Microvascular Invasion		< 0.001		< 0.001
Present *vs*. Absent	1.892 (1.395 - 2.568)		1.925 (1.457 - 2.544)	
Satellite		< 0.001		< 0.001
Yes *vs*. No	1.763 (1.314 - 2.366)		1.638 (1.249 - 2.148)	
Capsule		0.160		0.656
Complete *vs*. Incomplete	0.752 (0.505 - 1.119)		1.072 (0.789 - 1.457)	
Diferentiation		0.503		0.221
Moderate/Well *vs*. Poor	0.851 (0.530 - 1.365)		0.774 (0.513 - 1.166)	
Lymph node metastasis		< 0.001		< 0.001
Yes *vs*. No	2.303 (1.610 - 3.2957)		1.757 (1.254 - 2.460)	
Adjuvant Therapy		0.161		0.458
Yes *vs*. No	0.798 (0.582 - 1.094)		0.903 (0.690 - 1.182)	

Table 5. Univariate cox regression analysis of OS and recurrence in HBV-related ICC patients after IPTW

Variable	OS		Recurrence	
	HR (95% CI)	*p*	HR (95% CI)	*p*
Sex		0.729		0.335
Male *vs*. female	1.046 (0.813 - 1.345)		1.125 (0.886 - 1.429)	
Age, years		0.047		0.836
> 60 *vs*. ≤ 60	1.292 (1.004 - 1.663)		0.974 (0.756 - 1.253)	
BMI		0.246		0.889
> 22 *vs*. ≤ 22	0.876 (0.701 - 1.095)		0.985 (0.795 - 1.219)	
Diabetes		0.994		0.605
Yes *vs*. No	0.998 (0.581 - 1.713)		1.140 (0.693 - 1.876)	
Antivirus		0.180		0.264
Yes *vs*. No	0.785 (0.551 - 1.118)		0.840 (0.618 - 1.141)	
Cirrhosis		0.156		0.522
Yes *vs*. No	1.169 (0.942 - 1.452)		0.936 (0.765 - 1.146)	
Gastroesophageal Varices		0.893		0.270
Yes *vs*. No	1.025 (0.718 - 1.463)		0.823 (0.582 - 1.163)	
Ascites		0.424		0.405
Yes *vs*. No	1.206 (0.762 - 1.910)		0.779 (0.433 - 1.402)	
ALT,U/L		0.373		0.166
> 44 *vs*. ≤ 44	1.111 (0.881 - 1.401)		1.162 (0.940 - 1.436)	
PLT, $*10^9$/mL		0.654		0.470
> 100 *vs*. ≤ 100	0.937 (0.705 - 1.246)		1.106 (0.842 - 1.451)	
NLR		0.001		0.058
> 2.5 *vs*. ≤ 2.5	1.428 (1.153 - 1.769)		1.213 (0.994 - 1.480)	
INR		0.048		0.403
> 1.1 *vs*. ≤ 1.1	1.366 (1.003 - 1.862)		0.866 (0.619 - 1.213)	
ALBI Grade		0.001		0.529
II *vs*. I	1.434 (1.159 - 1.775)		1.066 (0.873 - 1.303)	
HBV-DNA, IU/mL		0.979		0.893
> 2,000 *vs*. ≤ 2,000	1.003 (0.808 - 1.244)		0.986 (0.809 - 1.202)	
AFP, ng/mL		0.044		0.010
> 20 *vs*. ≤ 20	1.275 (1.006 - 1.616)		1.342 (1.073 - 1.678)	
CEA, ng/mL		0.024		0.528
> 10 *vs*. ≤ 10	1.536 (1.057 - 2.232)		1.137 (0.764 - 1.691)	
CA19-9, U/mL		< 0.001		< 0.001
> 37 *vs*. ≤ 37	2.028 (1.599 - 2.573)		1.703 (1.354 - 2.142)	
ASA grade		0.105		0.628
III *vs*. II	0.815 (0.637 - 1.044)		0.945 (0.752 - 1.188)	
Major Hepatectomy		0.229		0.053
Yes *vs*. No	1.166 (0.908 - 1.498)		1.261 (0.997 - 1.596)	
Hilar Clamping, min		0.712		0.070
> 15 *vs*. ≤ 15	1.041 (0.841 - 1.288)		1.201 (0.985 - 1.464)	
Surgical Margin, cm		0.104		0.106
> 1 *vs*. ≤ 1	0.774 (0.568 - 1.054)		0.809 (0.626 - 1.046)	
Lymphadenectomy		< 0.001		< 0.001
Yes *vs*. No	2.038 (1.640 - 2.532)		1.663 (1.351 - 2.047)	
Blood loss, mL	1.000 (0.999 - 1.000)	0.925	1.000 (0.999 - 1.000)	0.682
Transfusion		0.023		0.270
Yes *vs*. No	1.430 (1.050 - 1.948)		1.188 (0.874 - 1.614)	
Tumor Size, cm		< 0.001		< 0.001
> 5 *vs*. ≤ 5	1.858 (1.492 - 2.314)		1.516 (1.243 - 1.849)	
Tumor Number		0.398		0.460
Multiple *vs*. Single	1.160 (0.823 - 1.636)		1.141 (0.804 - 1.619)	
Microvascular Invasion		< 0.001		< 0.001
Present *vs*. Absent	1.647 (1.244 - 2.180)		1.732 (1.350 - 2.221)	
Satellite		< 0.001		< 0.001
Yes *vs*. No	1.725 (1.370 - 2.172)		1.653 (1.325 - 2.063)	
Capsule		0.023		0.789
Complete *vs*. Incomplete	0.676 (0.482 - 0.948)		1.038 (0.790 - 1.364)	
Diferentiation		0.723		0.292
Moderate/Well *vs*. Poor	0.939 (0.662 - 1.331)		0.856 (0.640 - 1.143)	
Lymph node metastasis		< 0.001		< 0.001
Yes *vs*. No	2.157 (1.635 - 2.846)		1.963 (1.510 - 2.553)	
Adjuvant Therapy		0.171		0.657
Yes *vs*. No	0.842 (0.658 - 1.077)		1.051 (0.844 - 1.308)	

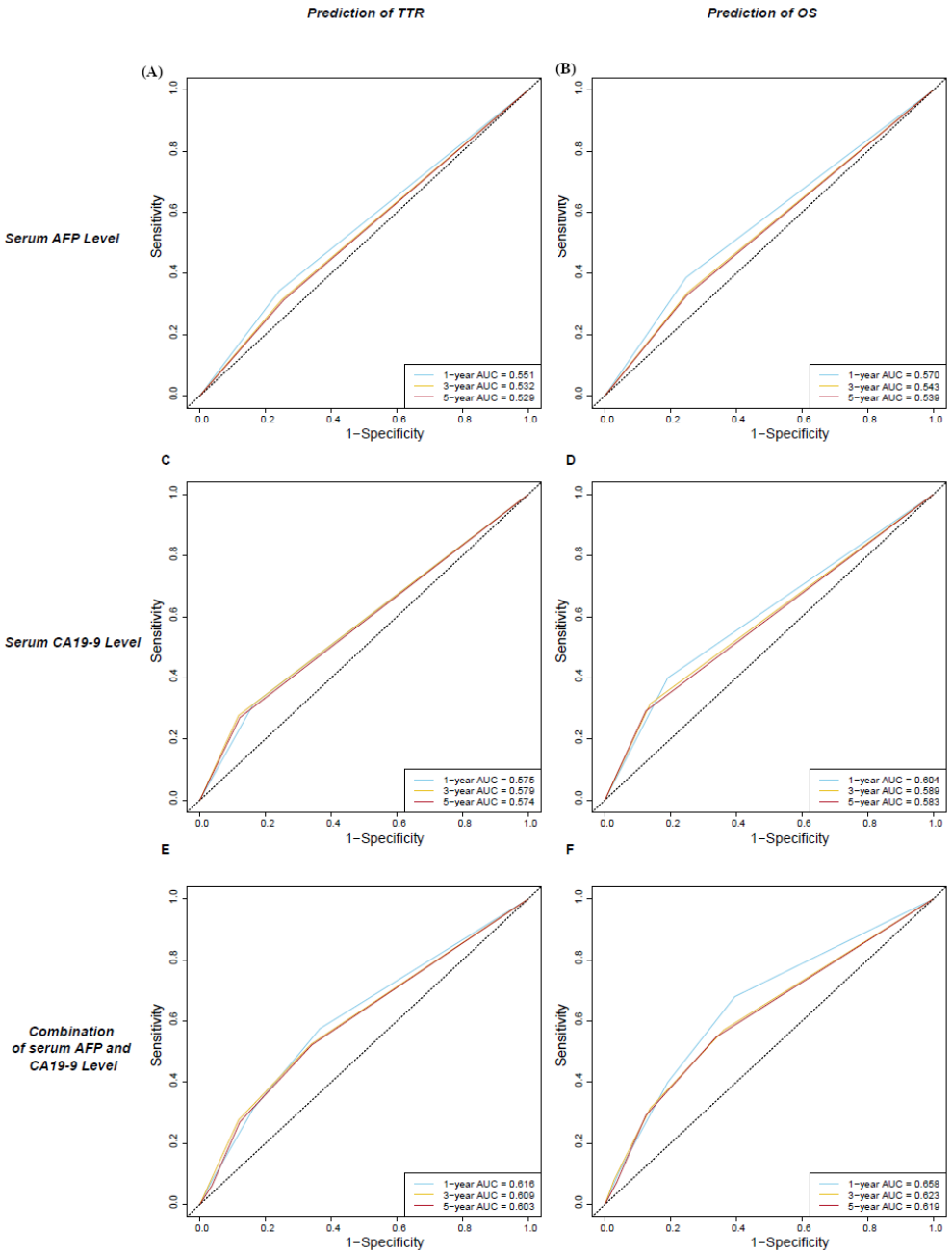

Figure 5. Receiver operating characteristic curve for prediction of TTR and OS. (A) Predition of TTR; **(B)** Predition of OS.

produce alterations in tumor markers and hematologic indices (*32*). Taken together, these findings support the hypothesis that AFP may act as an independent prognostic marker in HBV-ICC because HBV promotes cell-type reprogramming and preserves progenitor-like characteristics in tumors (*9*). Nevertheless, this proposed mechanism requires further tumor-biological investigation.

In conclusion. This retrospective single-center study of a large HBV-related ICC cohort, we demonstrated that elevated serum AFP was independently associated with worse overall survival and higher recurrence across the original, PSM, and IPTW cohorts. Lymph node dissection was identified as a risk factor irrespective of AFP level. Combining AFP with CA19-9 improved prognostic assessment for HBV-ICC. These results suggest that AFP, a routine and accessible biomarker, may help refine risk stratification and guide postoperative surveillance and management in HBV-related ICC; however, multicenter prospective studies and mechanistic research are needed to cnfoirm and further elucidate these observations.

This study has limitations. It is a single-center, retrospective analysis; therefore, our findings require external validation in multicenter cohorts. Residual confounding that was not accounted for in propensity-score methods may still exist.

Table 6. Multivariate cox regression analysis of recurrence and OS in HBV-related ICC patients

Variable	OS		Recurrence	
	HR (95% CI)	*p*	HR (95% CI)	*p*
Primary Cohort				
NLR		0.240		0.870
> 2.5 *vs*. ≤ 2.5	1.140 (0.916 - 1.417)		1.017 (0.833 - 1.241)	
INR		0.306		-
> 1.1 *vs*. ≤ 1.1	1.175 (0.863 - 1.600)		-	
ALBI Grade		0.074		-
II *vs*. I	1.218 (0.981 - 1.512)		-	
Cirrhosis		< 0.001		-
Yes *vs*. No	1.471 (1.174 - 1.842)		-	
AFP, ng/mL		0.023		0.003
> 20 *vs*. ≤ 20	1.294 (1.037 - 1.615)		1.363 (1.113 - 1.670)	
CA19-9, U/mL		< 0.001		0.005
> 37 *vs*. ≤ 37	1.570 (1.239 - 1.990)		1.376 (1.103 - 1.716)	
Lymphadenectomy		0.003		0.424
Yes *vs*. No	1.514 (1.150 - 1.992)		1.114 (0.855 - 1.451)	
Transfusion		0.955		-
Yes *vs*. No	0.992 (0.738 - 1.333)		-	
Tumor Size, cm		< 0.001		0.026
> 5 *vs*. ≤ 5	1.577 (1.246 - 1.995)		1.268 (1.029 - 1.563)	
Microvascular Invasion		0.007		0.002
Present *vs*. Absent	1.433 (1.106 - 1.857)		1.484 (1.162 - 1.895)	
Satellite		0.016		0.004
Yes *vs*. No	1.329 (1.056 - 1.673)		1.381 (1.112 - 1.716)	
Capsule		0.050		-
Complete *vs*. Incomplete	0.727 (0.528 - 0.999)		-	
Lymph node metastasis		0.246		0.021
Yes *vs*. No	1.227 (0.869 - 1.733)		1.492 (1.063 - 2.094)	
PSM Cohort				
Sex		-		0.032
Male *vs*. female	-		1.502 (1.036 - 2.177)	
NLR		0.947		0.533
> 2.5 *vs*. ≤ 2.5	1.010 (0.750 - 1.361)		1.091 (0.829 - 1.436)	
AFP, ng/mL		0.002		0.003
> 20 *vs*. ≤ 20	1.589 (1.188 - 2.126)		1.471 (1.144 - 1.890)	
CA19-9, U/mL		0.017		0.042
> 37 *vs*. ≤ 37	1.520 (1.077 - 2.145)		1.373 (1.011 - 1.865)	
Major Hepatectomy		-		0.874
Yes *vs*. No	-		1.026 (0.744 - 1.417)	
Lymphadenectomy		0.014		0.077
Yes *vs*. No	1.571 (1.097 - 2.249)		1.387 (0.965 - 1.993)	
Tumor Size, cm		0.004		0.150
> 5 *vs*. ≤ 5	1.566 (1.154 - 2.126)		1.231 (0.928 - 1.633)	
Microvascular Invasion		0.002		0.001
Present *vs*. Absent	1.689 (1.217 - 2.345)		1.674 (1.231 - 2.276)	
Satellite		0.010		0.009
Yes *vs*. No	1.491 (1.102 - 2.017)		1.476 (1.103 - 1.976)	
Lymph node metastasis		0.180		0.587
Yes *vs*. No	1.350 (0.871 - 2.094)		1.125 (0.736 - 1.719)	
IPTW Cohort				
Age,years		0.148		-
> 60 *vs*. ≤ 60	1.222 (0.932 - 1.602)		-	
NLR		0.489		-
> 2.5 *vs*. ≤ 2.5	1.084 (0.863 - 1.360)		-	
INR		0.131		-
> 1.1 *vs*. ≤ 1.1	1.299 (0.925 - 1.824)		-	
ALBI Grade		0.027		-
II *vs*. I	1.293 (1.030 - 1.624)		-	
AFP, ng/mL		0.023		0.006
> 20 *vs*. ≤ 20	1.314 (1.038 - 1.663)		1.360 (1.090 - 1.696)	
CEA, ng/mL		0.996		-
> 10 *vs*. ≤ 10	1.001 (0.672 - 1.492)		-	
CA19-9, U/mL		0.001		0.002
> 37 *vs*. ≤ 37	1.570 (1.193 - 2.064)		1.459 (1.148 - 1.853)	
Lymphadenectomy		0.002		0.074
Yes *vs*. No	1.574 (1.185 - 2.091)		1.281 (0.976 - 1.680)	

Table 6. Multivariate cox regression analysis of recurrence and OS in HBV-related ICC patients (continued)

Variable	OS		Recurrence	
	HR (95% CI)	*p*	HR (95% CI)	*p*
Transfusion		0.982		-
Yes *vs*. No	0.996 (0.705 - 1.406)		-	
Tumor Size, cm		0.001		0.024
> 5 *vs*. ≤ 5	1.469 (1.162 - 1.857)		1.272 (1.032 - 1.566)	
Microvascular Invasion		0.032		0.003
Present *vs*. Absent	1.387 (1.028 - 1.870)		1.482 (1.147 - 1.915)	
Satellite		0.017		0.004
Yes *vs*. No	1.351 (1.056 - 1.729)		1.386 (1.106 - 1.736)	
Capsule		0.119		-
Complete *vs*. Incomplete	0.740 (0.507 - 1.081)		-	
Lymph node metastasis		0.485		0.143
Yes *vs*. No	1.144 (0.785 - 1.666)		1.298 (0.916 - 1.839)	

Acknowledgements

We thank the patients who participated in this study.

Funding: The Tengfei Project of the Third Affiliated Hospital of Naval Medical University (TF2024YZZY01 and TF2024XSYJ03). Research Cultivation Project of the Third Affiliated Hospital of Naval Medical University (2023QN001).

Conflict of Interest: The authors have no conflicts of interest to disclose.

Availability of data and materials: The datasets analysed during the current study are available from the corresponding author on reasonable request.

References

1. Moris D, Palta M, Kim C, Allen PJ, Morse MA, Lidsky ME. Advances in the treatment of intrahepatic cholangiocarcinoma: An overview of the current and future therapeutic landscape for clinicians. CA Cancer J Clin. 2023; 73:198-222.
2. EASL-ILCA Clinical Practice Guidelines on the management of intrahepatic cholangiocarcinoma. J Hepatol. 2023; 79:181-208.
3. Bray F, Laversanne M, Sung H, Ferlay J, Siegel RL, Soerjomataram I, Jemal A. Global cancer statistics 2022: GLOBOCAN estimates of incidence and mortality worldwide for 36 cancers in 185 countries. CA: a cancer journal for clinicians. 2024; 74:229-263.
4. Mazzaferro V, Gorgen A, Roayaie S, Droz Dit Busset M, Sapisochin G. Liver resection and transplantation for intrahepatic cholangiocarcinoma. Journal of hepatology. 2020; 72:364-377.
5. Clements O, Eliahoo J, Kim JU, Taylor-Robinson SD, Khan SA. Risk factors for intrahepatic and extrahepatic cholangiocarcinoma: A systematic review and meta-analysis. J Hepatol. 2020; 72:95-103.
6. Li M, Li J, Li P, Li H, Su T, Zhu R, Gong J. Hepatitis B virus infection increases the risk of cholangiocarcinoma: a meta-analysis and systematic review. J Gastroenterol Hepatol. 2012; 27:1561-1568.
7. Wang Z, Sheng YY, Dong QZ, Qin LX. Hepatitis B virus and hepatitis C virus play different prognostic roles in intrahepatic cholangiocarcinoma: A meta-analysis. World J Gastroenterol. 2016; 22:3038-3051.
8. Huang J, Wang X, Zhu Y, Wang Z, Li J, Xu D, Wang S, Li TE, Lu L. Specific prognostic factors in hepatitis B virus-related and non-hepatitis B virus-related intrahepatic cholangiocarcinoma after macroscopic curative resection. J Surg Oncol. 2019; 119:40-46.
9. Song Z, Lin S, Wu X, *et al*. Hepatitis B virus-related intrahepatic cholangiocarcinoma originates from hepatocytes. Hepatol Int. 2023; 17:1300-1317.
10. Galle PR, Foerster F, Kudo M, Chan SL, Llovet JM, Qin S, Schelman WR, Chintharlapalli S, Abada PB, Sherman M, Zhu AX. Biology and significance of alpha-fetoprotein in hepatocellular carcinoma. Liver Int. 2019; 39:2214-2229.
11. Sun J, Zhao Y, Qin L, Li K, Zhao Y, Sun H, Zhang T, Zhang Y. Metabolomic Profiles for HBV Related Hepatocellular Carcinoma Including Alpha-Fetoproteins Positive and Negative Subtypes. Front Oncol. 2019; 9:1069.
12. Yeo YH, Lee YT, Tseng HR, Zhu Y, You S, Agopian VG, Yang JD. Alpha-fetoprotein: Past, present, and future. Hepatol Commun. 2024; 8:e0422.
13. Ding Y, Chen Y, Zhang J, *et al*. Blood Biomarker-Based Predictive Indicator for Liver Metastasis in Alpha-Fetoprotein-Producing Gastric Cancer and Multi-Omics Tumor Microenvironment Insights. Ad*vs*ci (Weinh). 2025; 12:e03499.
14. Li Y, Lin Y, Zhao L, Yang C, Wang B, Gao Z, Ye Y, Wang S, Shen Z. Characteristics of alpha-fetoprotein-positive gastric cancer revealed by analysis of cancer databases and transcriptome sequencing data. Transl Oncol. 2023; 36:101737.
15. Görgec B, Benedetti Cacciaguerra A, Lanari J, *et al*. Assessment of Textbook Outcome in Laparoscopic and Open Liver Surgery. JAMA Surg. 2021; 156:e212064.
16. Lin NC, Nitta H, Wakabayashi G. Laparoscopic major hepatectomy: a systematic literature review and comparison of 3 techniques. Ann Surg. 2013; 257:205-213.
17. Bai S, Yang P, Liu J, Xue H, Xia Y, Liu F, Yang Z, Zhang L, Wu Y, Shen F, Wang K. Surgical Margin Affects the Long-Term Prognosis of Patients With Hepatocellular Carcinoma Undergoing Radical Hepatectomy Followed by Adjuvant TACE. Oncologist. 2023; 28:e633-e644.

18. Sha M, Jeong S, Xia Q. Antiviral therapy improves survival in patients with HBV infection and intrahepatic cholangiocarcinoma undergoing liver resection: Novel concerns. J Hepatol. 2018; 68:1315-1316.
19. Xu X, Zhang HL, Liu QP, Sun SW, Zhang J, Zhu FP, Yang G, Yan X, Zhang YD, Liu XS. Radiomic analysis of contrast-enhanced CT predicts microvascular invasion and outcome in hepatocellular carcinoma. Journal of hepatology. 2019; 70:1133-1144.
20. Zhou J, Sun H, Wang Z, *et al*. Guidelines for the Diagnosis and Treatment of Primary Liver Cancer (2022 Edition). Liver cancer. 2023; 12:405-444.
21. Zhou YM, Yang JM, Li B, Yin ZF, Xu F, Wang B, Liu P, Li ZM. Clinicopathologic characteristics of intrahepatic cholangiocarcinoma in patients with positive serum a-fetoprotein. World J Gastroenterol. 2008; 14:2251-2254.
22. Sheng R, Zhang Y, Wang H, Zhang W, Jin K, Sun W, Dai Y, Zhou J, Zeng M. A multi-center diagnostic system for intrahepatic mass-forming cholangiocarcinoma based on preoperative MRI and clinical features. Eur Radiol. 2024; 34:548-559.
23. Xu YP, Dong ZN, Zhou YQ, Zhao YJ, Zhao Y, Wang F, Huang XY, Guo CY. Role of eIF3C Overexpression in Predicting Prognosis of Intrahepatic Cholangiocarcinoma. Digestive diseases and sciences. 2022; 67:559-568.
24. Izquierdo-Sanchez L, Lamarca A, La Casta A, *et al*. Cholangiocarcinoma landscape in Europe: Diagnostic, prognostic and therapeutic insights from the ENSCCA Registry. Journal of hepatology. 2022; 76:1109-1121.
25. Bagante F, Spolverato G, Merath K, *et al*. Intrahepatic cholangiocarcinoma tumor burden: A classification and regression tree model to define prognostic groups after resection. Surgery. 2019; 166:983-990.
26. Luedde T, Kaplowitz N, Schwabe RF. Cell death and cell death responses in liver disease: Mechanisms and clinical relevance. Gastroenterology. 2014; 147:765-783.e764.
27. Dhar D, Antonucci L, Nakagawa H, *et al*. Liver Cancer Initiation Requires p53 Inhibition by CD44-Enhanced Growth Factor Signaling. Cancer Cell. 2018; 33:1061-1077.e1066.
28. Kojima K, Takata A, Vadnais C, *et al*. MicroRNA122 is a key regulator of α-fetoprotein expression and influences the aggressiveness of hepatocellular carcinoma. Nat Commun. 2011; 2:338.
29. Karayiannis P. Hepatitis B virus: virology, molecular biology, life cycle and intrahepatic spread. Hepatol Int. 2017; 11:500-508.
30. Nomoto K, Tsuneyama K, Cheng C, Takahashi H, Hori R, Murai Y, Takano Y. Intrahepatic cholangiocarcinoma arising in cirrhotic liver frequently expressed p63-positive basal/stem-cell phenotype. Pathol Res Pract. 2006; 202:71-76.
31. Ishii T, Yasuchika K, Suemori H, Nakatsuji N, Ikai I, Uemoto S. Alpha-fetoprotein producing cells act as cancer progenitor cells in human cholangiocarcinoma. Cancer Lett. 2010; 294:25-34.
32. Takahashi H, Oyamada M, Fujimoto Y, Satoh MI, Hattori A, Dempo K, Mori M, Tanaka T, Watabe H, Masuda R, Yoshida M. Elevation of serum alpha-fetoprotein and proliferation of oval cells in the livers of LEC rats. Jpn J Cancer Res. 1988; 79:821-827.

Received November 3, 2025; Revised January 18, 2026; Accepted January 27, 2026.

[§]These authors contributed equally to this work.

**Address correspondence to:*
Kui Wang, Department of Hepatic Surgery II, the Eastern Hepatobiliary Surgery Hospital, Naval Medical University, Shanghai, China, No. 225, Changhai Road, Yangpu District, Shanghai 200438, China.
E-mail: wangkuiykl@163.com

Feng Shen, Department of Hepatic Surgery IV and Clinical Research Institute, the Eastern Hepatobiliary Surgery Hospital, Naval Medical University, 225 Changhai Road, Shanghai 200433, China.
E-mail: shenfengehbh@sina.com

Released online in J-STAGE as advance publication February 6, 2026.

Original Article

DOI: 10.5582/bst.2025.01354

Long-term effects of multidisciplinary team recommendations on adult patients with acute myeloid leukemia

Jingtao Huang[1,2,§], Yiwen Wu[3,§], Yunxiang Zhang[1,§], Chuanhe Jiang[1,§], Min Wu[1], Zengkai Pan[1], Qiusheng Chen[1], Huijin Zhao[1], Yu Zheng[1], Yang Shen[1], Yang He[1,*], Jiong Hu[1,*], Junmin Li[1,*], Xiaoxia Hu[1,*]

[1] Shanghai Institute of Hematology, State Key Laboratory of Medical Genomics, National Research Center for Translational Medicine at Shanghai, Ruijin Hospital, Shanghai Jiao Tong University School of Medicine, Shanghai, China;
[2] State Key Laboratory of Experimental Hematology, National Clinical Research Center for Blood Diseases, Haihe Laboratory of Cell Ecosystem, Institute of Hematology and Blood Diseases Hospital, Chinese Academy of Medical Sciences and Peking Union Medical College, Tianjin, China;
[3] Haihe Laboratory of Cell Ecosystem, Tianjin Medical University, Tianjin, China.

SUMMARY: Optimal post-remission therapy is crucial for long-term survival in patients with acute myeloid leukemia (AML). Multidisciplinary team (MDT) conferences address this challenge by providing comprehensive, patient-centered consultations that support individualized treatment decision-making. We evaluated the effectiveness of MDT conferences in guiding post-remission treatment decisions in adults with de novo AML. We enrolled 653 adult patients with de novo AML who were treated at our center between January 2017 and December 2022. Of the 591 eligible patients (90.5%), 501 (84.8%) attended a scheduled MDT evaluation. Allogeneic hematopoietic cell transplantation (allo-HCT) was recommended for 315 patients (62.9%), of whom 251 (79.7%) subsequently underwent transplantation. Survival analyses showed that MDT attendees had superior 3-year overall survival (68.9% *vs.* 53.5%, $p < 0.0001$) and a lower 3-year cumulative incidence of relapse (30.7% *vs.* 44.9%; $p < 0.0001$) compared with patients who did not attend MDT conferences. Patients most likely to benefit from allo-HCT following MDT recommendations included those with intermediate- or adverse-risk disease according to the European LeukemiaNet 2017 classification, and those with favorable-risk disease who showed a suboptimal response to induction therapy. The main barriers to allo-HCT were persistent or relapsed disease and patient preference. Overall, MDT conferences effectively identified patients who were most likely to benefit from allo-HCT and were associated with higher transplantation rates within a modern healthcare system.

Keywords: acute myeloid leukemia, multidisciplinary team, allogeneic hematopoietic stem cell transplantation, long-term outcomes

1. Introduction

Allogeneic hematopoietic stem cell transplantation (allo-HCT) is a potentially curative treatment for several hematologic malignancies, with acute myeloid leukemia (AML) representing the most common indication for allo-HCT in adult patients (*1-4*). AML accounts for approximately 37% of allo-HCT procedures, a proportion that continues to increase in China (*5*). Current consensus guidelines recommend allo-HCT as standard post-remission therapy for patients with AML who are at high risk of relapse (*6-9*). Results from previous studies, however, have shown that only a minority of patients who are likely to benefit from allo-HCT ultimately undergo transplantation (*10-14*). Delays in human leukocyte antigen (HLA) typing and referral to an allo-HCT program represent major barriers, even within academic centers, and these challenges may be exacerbated when eligible patients receive induction therapy at institutions without an established allo-HCT program (*6,15,16*).

Multidisciplinary team (MDT) conferences provide comprehensive, patient-centered consultations by integrating expertise across specialties, facilitating collaborative decision-making, and supporting individualized treatment strategies. MDT-based care has been shown to influence patient management practices and has been increasingly adopted across cancer centers in developed countries(*17,18*), where it has contributed to higher rates of allo-HCT in patients with AML (*11,19,20*).

In China, MDT evaluation remains at a relatively early stage, owing to the substantial time, effort, and human resources required, as well as existing disciplinary boundaries (*21*). At our center, MDT conferences are used to assess the suitability of individual patients with AML for allo-HCT; however, their impact on long-term survival among transplant-eligible patients remains unclear (*19*).

In this single-center, retrospective study, we enrolled patients with newly diagnosed AML at the time of diagnosis and followed them throughout their treatment course to assess the rate of allo-HCT among patients who did and did not undergo MDT evaluation. We evaluated the effectiveness of MDT conferences in guiding consolidation decisions, particularly recommendations regarding transplantation.

2. Methods

2.1. Study design and patient enrollment

This single-center, retrospective study screened patients with newly diagnosed AML who were admitted as inpatients between January 2017 and December 2022. Patients aged ≥ 14 to ≤ 65 years with non–acute promyelocytic leukemia (APL) AML, diagnosed according to the fourth edition of the WHO Classification of Tumours of Haematopoietic and Lymphoid Tissues (*22*), were eligible. Patients with incomplete medical information or a diagnosis of APL were excluded.

AML risk stratification (favorable, intermediate, or adverse) was performed according to the European LeukemiaNet (ELN) 2017 classification (*23*). Clinical data were retrospectively extracted from the institutional AML and transplant database. In total, 653 patients with complete follow-up information were screened; 62 patients (9.5%) were excluded due to early death (within 3 months of diagnosis), leaving 591 patients available for analysis. The last follow-up date was December 31, 2024.

The primary objective was to determine the rate of allo-HCT among patients with newly diagnosed AML. Secondary objectives were to assess the concordance between post-remission therapies initially recommended and those ultimately administered, and to evaluate survival outcomes in patients who attended MDT conferences compared with those who did not.

This study was approved by the institutional review board of Shanghai Ruijin Hospital (RJ-2024-08) and was conducted in accordance with the Declaration of Helsinki. The requirement for written informed consent was waived because of the retrospective, non-interventional study design.

2.2. Measurable residual disease detection and relapse definition

Measurable residual disease (MRD) detection using multiparameter flow cytometry (MFC) and/or real-time quantitative polymerase chain reaction (qRT-PCR) was performed as previously described (*24*). Leukemia-associated aberrant immunophenotypes and/or "different-from-normal" approaches were applied for MRD assessment by MFC, with a threshold of 0.01% used to define MRD positivity (*25*). Complete remission (CR) in AML was defined as < 5% bone marrow blasts, recovery of peripheral blood counts (absolute neutrophil count ≥ 1.0 × 10^9/L and platelet count ≥ 100 × 10^9/L), absence of circulating blasts, no extramedullary disease, and transfusion independence. Relapse was defined as the recurrence of bone marrow blasts > 5%, reappearance of blasts in peripheral blood, development of extramedullary disease, or recurrence of pre-transplantation chromosomal abnormalities.

2.3. Inclusion and exclusion criteria for allo-HCT recommendation

(I). *Allo-HCT recommendation criteria*:

a) AML in first CR(CR1):

(i). Patients who achieved CR1 after > 2 cycles of induction (*7,8*);

(ii). Intermediate- or adverse-risk AML according to the ELN 2017 risk stratification (*23*);

(iii). Myelodysplasia-related AML or therapy-related AML (*7,8*);

(iv). Favorable-risk AML with any of the following features (*6*): failure to attain major molecular remission (MMR; *RUNX1::RUNX1T1* decrease < 3 log units) after two consolidation cycles, or loss of MMR within 6 months; recurrence of *CBFβ::MYH11*/*ABL* transcript levels > 0.1% at any time after two consolidation cycles; presence of the *KIT* D816 mutation in *CBF*-AML (*26*); biallelic mutated *CEBPA* (*CEBPA*$^{bi+}$) AML with positive MFC-MRD after two consolidation cycles (*27*); AML with an *NPM1* mutation and positive MFC-MRD or detectable *NPM1* transcripts by qRT-PCR (Ct < 40 in at least 2 of 3 replicates) after two consolidation cycles (*24*);

b) ≥ CR2 (*7,8*);

c) Relapsed or refractory AML, or AML with extramedullary disease (*7,8*).

(II). *Allo-HCT exclusion criteria*:

a) Patients aged > 70 years and/or with overt contraindications to transplantation;

b) No available donor;

c) Severe comorbidities, including active central nervous system leukemia, severe cardiovascular disease, or active uncontrolled infection.

2.4. MDT process

Each patient underwent MDT evaluation at two separate visits. The MDT was required to include at least

two adult leukemia specialists, two HCT specialists, one psychologist, one dietitian, and two full-time coordinators from the leukemia/HCT program.

The first MDT visit was scheduled after one or two cycles of induction therapy. Treatment recommendations were based on baseline disease characteristics and the patient's physical condition. During this visit, post-remission treatment strategies were discussed and evaluated. Allo-HCT was recommended for patients with intermediate- to adverse-risk AML, whereas chemotherapy and/or targeted therapy was reserved for patients with favorable-risk disease. For patients with intermediate- to adverse-risk AML, HLA typing of patients and eligible immediate relatives was performed, and a preliminary unrelated donor search was initiated to identify potential donor sources in advance.

The second MDT visit was scheduled after two cycles of consolidation therapy. At this visit, a comprehensive assessment of treatment response and optimal timing of allo-HCT was performed, and individualized recommendations were made. Patients with intermediate- to adverse-risk AML were recommended to proceed to allo-HCT within the subsequent few weeks. Recommendations for allo-HCT in patients with favorable-risk AML were limited to those who met the allo-HCT recommendation criteria described above.

For patients who agreed to the recommended allo-HCT plan, an HCT coordinator organized and coordinated the transplant procedure. Follow-up was conducted by MDT coordinators within 3 months after the second MDT visit to determine whether patients proceeded with the planned allo-HCT. Reasons for failure to proceed to transplantation were documented.

2.5. Best available therapy

Best available therapy (BAT) was provided for all transplant-ineligible patients and included chemotherapy, targeted therapy, immunotherapy, traditional Chinese medicine therapy, and palliative care (*28,29*).

2.6. Statistical analysis

Continuous variables were compared using unpaired, two-tailed Student's *t* test for between-group comparisons. Categorical variables were compared using the chi-square test or Fisher's exact test, as appropriate.

Propensity score weighting (PSW) with overlap weighting was applied to minimize confounding and improve covariate balance between MDT and non-MDT groups, based on propensity scores estimated from a logistic regression model. Covariate balance before and after weighting was assessed using standardized mean differences (SMDs).

For MDT-related outcome analyses, a landmark time point of 3 months after diagnosis was defined to evaluate whether MDT involvement was associated with a reduced risk of mortality, as this corresponds to the period during which patients would have attended MDT evaluation and received treatment recommendations. In the overlap-weighted cohort, overall survival (OS) was estimated using the Kaplan–Meier method and compared using the log-rank test. The cumulative incidence of relapse (CIR) was estimated using the Fine–Gray subdistribution hazard model, with death treated as a competing event.

Logistic regression analyses were performed to identify factors associated with MDT transplant recommendations. Cox proportional hazards regression models were used to evaluate the association between MDT evaluation and survival outcomes. All analyses were performed using R software version 4.3.1. Statistical significance was defined as a two-sided P value < 0.05.

To evaluate the robustness of OS estimates to loss to follow-up, sensitivity analyses were conducted under extreme assumptions. Specifically, best-case and worst-case scenarios were considered, in which all patients lost to follow-up were assumed to be alive until the end of follow-up or to have died at the time of last contact, respectively. Overlap weighting was applied consistently across all sensitivity analyses.

All analyses were performed in a blinded manner, such that investigators conducting the data analyses were unaware of ELN risk classification and treatment assignments.

3. Results

3.1. Patients

In total, 653 patients met the eligibility criteria and consented to participate in this study. Of these, 62 patients (9.5%) died within 3 months of diagnosis and were thus excluded from further analysis. The remaining 591 patients were considered eligible for MDT evaluation to support individualized treatment planning. Among them, 501 patients (84.8%) attended at least one MDT visit following the recommendation of their attending physicians (Figure 1), and 372 patients (74.3%) attended two MDT evaluations (Table 1).

The median age of the entire cohort was 45 years (range, 15–65 years). According to the ELN 2017 risk stratification, 48.2% of patients had favorable-risk disease (n = 258), 24.7% had intermediate-risk disease (n = 146), and 27.1% had adverse-risk disease (n = 160). The most common AML subtype was AML with *NPM1* mutation (20.5%), followed by AML with *CEBPA* mutation (20.1%), AML with other defined genetic lesions (16.6%), and AML with myelodysplasia-related changes (10.7%).

The distribution of ELN risk categories did not significantly differ between patients who attended MDT evaluation and those who did not (favorable: 48.70% *vs.* 45.55%; intermediate: 25.35% *vs.* 21.11%;

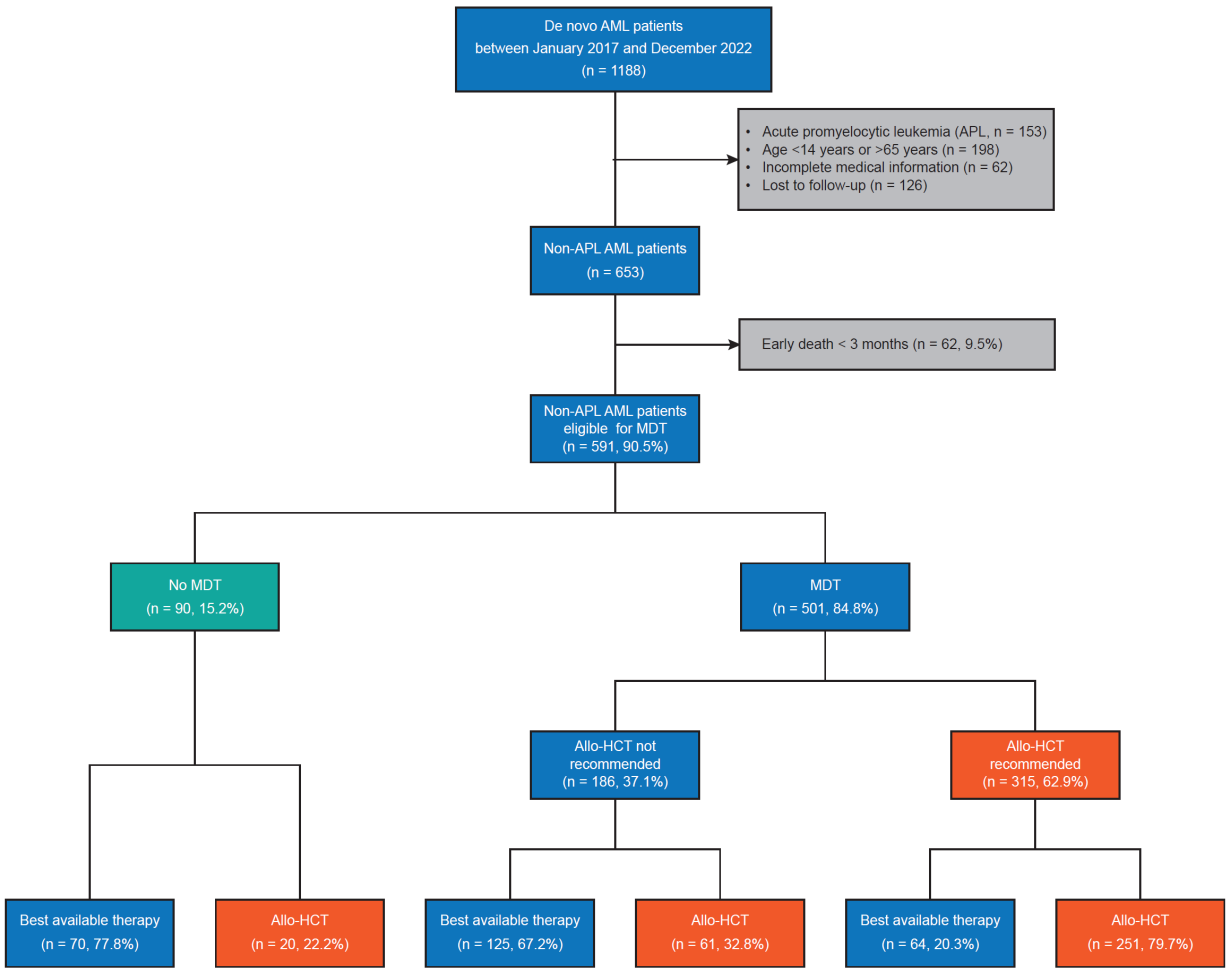

Figure 1. Flowchart of MDT consultation and transplant utilization. *Abbreviations*: APL, acute promyelocytic leukemia; allo-HCT, allogeneic hematopoietic cell transplantation; AML, acute myeloid leukemia; MDT, multidisciplinary team.

adverse: 25.95% *vs.* 33.34%; $p = 0.3373$; Figure 2A). Compared with non-MDT patients, MDT attendees had a higher CR rate after one cycle of induction therapy ($p < 0.001$), whereas rates of MRD negativity were comparable between the two groups (55.1% *vs.* 45.5%). After application of PSW with overlap weighting, all covariates included in the model (age, sex, ELN 2017 risk stratification, AML subtype, and MRD status after induction therapy) were well balanced, with standardized mean differences < 0.01. Outcome analyses demonstrated that MDT attendees had superior 3-year OS compared with non-MDT patients (68.9% *vs.* 53.5%; $p < 0.0001$; Figure 2B), as well as a lower 3-year CIR (30.7% *vs.* 44.9%; $p = 0.001$; Figure 2C).

3.2. MDT and transplantation recommendation

The number of patients who participated in MDT evaluation was higher in 2020–2022 ($n = 354$) than in 2017–2019 ($n = 147$). Baseline characteristics of patients who attended MDT evaluation are summarized in Supplementary Table S1 (*https://www.biosciencetrends.com/action/getSupplementalData.php?ID=285*). The median age of MDT attendees was 44 years (range, 15–65 years), with a significant increase observed in 2020–2022 compared with 2017–2019 (45.5 years [range, 15–59] *vs.* 42 years [range, 15–65]; $p = 0.015$).

In the overlap-weighted cohort, allo-HCT was associated with superior 3-year OS compared with BAT (73.8% *vs.* 51.9%, $p < 0.0001$; Supplementary Figure S1A, *https://www.biosciencetrends.com/action/getSupplementalData.php?ID=285*) and a lower 3-year CIR (28.0% *vs.* 45.5%; $p < 0.0001$; Supplementary Figure S1B, *https://www.biosciencetrends.com/action/getSupplementalData.php?ID=285*). Among the 501 patients who attended MDT evaluation, 315 (62.9%) were recommended for allo-HCT, of whom 251 (79.4%) proceeded to transplantation (Figure 1). This transplantation rate was significantly higher than that observed in the non-MDT group (22.2%, $p < 0.001$). Among patients recommended for allo-HCT, transplantation rates were higher in those aged < 55 years (82.4%; $n = 250$) than in those aged ≥ 55 years (69.2%; $n = 65$) ($p = 0.0243$). Of the 186 patients (37.1%) who were

Table 1. Comparison of MDT and non-MDT patients

	Before weighting					After weighting				
	Total (n = 591)	MDT (n = 501)	Non-MDT (n = 90)	p value	SMD	Total (n = 138.76)	MDT (n = 69.38)	Non-MDT (n = 69.38)	p value	SMD
Diagnosis year				0.831	0.039				1	< 0.001
2017-2019	175 (29.6%)	147 (29.3%)	28 (31.1%)			40.20 (29.0%)	20.10 (29.0%)	20.10 (29.0%)		
2020-2022	416 (70.4%)	354 (70.7%)	62 (68.9%)			98.56 (71.0%)	49.28 (71.0%)	49.28 (71.0%)		
Age, n (%)				0.435	0.148				1	< 0.001
15-39 years	229 (38.8%)	199 (39.7%)	30 (33.3%)			49.27 (35.5%)	24.64 (35.5%)	24.64 (35.5%)		
40-54 years	229 (38.8%)	193 (38.5%)	36 (40.0%)			54.66 (39.4%)	27.33 (39.4%)	27.33 (39.4%)		
55-65 years	133 (22.4%)	109 (21.8%)	24 (26.7%)			34.83 (25.1%)	17.42 (25.1%)	17.42 (25.1%)		
Sex, n (%)				0.166	0.173				1	< 0.001
Male	305 (51.6%)	252 (50.3%)	53 (58.9%)							
Female	286 (48.4%)	249 (49.7%)	37 (41.1%)			58.93 (42.5%)	29.46 (42.5%)	29.46 (42.5%)		
ELN 2017 stratification, n (%)				0.325	0.169				1	< 0.001
Favorable risk	285 (48.2%)	244 (48.7%)	41 (45.6%)			66.35 (47.8%)	33.18 (47.8%)	33.18 (47.8%)		
Intermediate risk	146 (24.7%)	127 (25.3%)	19 (21.1%)			30.18 (21.8%)	15.09 (21.8%)	15.09 (21.8%)		
Adverse risk	160 (27.1%)	130 (26.0%)	30 (33.3%)			42.23 (30.4%)	21.11 (30.4%)	21.11 (30.4%)		
AML subtype, n (%)				0.143	0.465				1	< 0.001
AML with defining genetic abnormalities										
AML with *RUNX1::RUNX1T1* fusion	46 (7.8%)	37 (7.4%)	9 (10.0%)			13.35 (9.6%)	6.68 (9.6%)	6.68 (9.6%)		
AML with *CBFB::MYH11* fusion	56 (9.5%)	51 (10.1%)	5 (5.6%)			9.08 (6.5%)	4.54 (6.5%)	4.54 (6.5%)		
AML with *BCR::ABL1* fusion	4 (0.7%)	4 (0.8%)	0 (0.0%)			0 (0.0%)	0 (0.0%)	0 (0.0%)		
AML with *KMT2A* rearrangement	48 (8.1%)	44 (8.8%)	4 (4.4%)			7.47 (5.4%)	3.74 (5.4%)	3.74 (5.4%)		
AML with *NUP98* rearrangement	6 (1.0%)	6 (1.2%)	0 (0.0%)			0 (0.0%)	0 (0.0%)	0 (0.0%)		
AML with *NPM1* mutation	121 (20.4%)	97 (19.7%)	24 (26.7%)			34.95 (25.2%)	17.47 (25.2%)	17.47 (25.2%)		
AML with *CEBPA* mutation	119 (20.1%)	105 (20.9%)	14 (15.6%)			24.77 (17.9%)	12.38 (17.9%)	12.38 (17.9%)		
AML, myelodysplasia-related	63 (10.7%)	51 (10.1%)	12 (13.3%)			17.32 (12.5%)	8.66 (12.5%)	8.66 (12.5%)		
AML with other defined genetic alterations	98 (16.6%)	84 (16.7%)	14 (15.6%)			21.10 (15.2%)	10.55 (15.2%)	10.55 (15.2%)		
AML, defined by differentiation	27 (4.6%)	19 (3.8%)	8 (8.9%)			10.72 (7.7%)	5.36 (7.7%)	5.36 (7.7%)		
Myeloid sarcoma	3 (0.5%)	3 (0.6%)	0 (0.0%)			0 (0.0%)	0 (0.0%)	0 (0.0%)		
MRD status after induction therapy, n (%)				< 0.001	0.467				1	< 0.001
CR after one cycle of induction										
Negative MRD	317 (53.6%)	276 (55.1%)	41 (45.6%)			68.91 (49.7%)	34.45 (49.7%)	34.45 (49.66%)		
Positive MRD	145 (24.5%)	127 (25.4%)	18 (20.0%)			30.88 (22.3%)	15.44 (22.3%)	15.44 (22.25%)		
CR after two cycles of induction										
Negative MRD	15 (2.5%)	12 (2.4%)	3 (3.3%)			4.44 (3.2%)	2.22 (3.2%)	2.22 (3.20%)		
Positive MRD	44 (7.5%)	39 (7.8%)	5 (5.6%)			8.66 (6.2%)	4.33 (6.2%)	4.33 (6.24%)		
NR	54 (9.1%)	39 (7.8%)	15 (16.7%)			20.36 (14.7%)	10.18 (14.7%)	10.18 (14.67%)		
NA	16 (2.7%)	8 (1.6%)	8 (8.9%)			5.52 (4.0%)	2.76 (4.0%)	2.76 (3.98%)		

Abbreviations: allo-HCT, allogeneic hematopoietic cell transplantation; AML, acute myeloid leukemia; CR: complete response; ELN 2017 European LeukemiaNet 2017; MDT, multidisciplinary team; MRD: measurable residual disease; NA, not available; NR: non-remission; SMD, standardized mean difference.

Table 1. Comparison of MDT and non-MDT patients (continued)

	Before weighting					After weighting				
	Total (n = 591)	MDT (n = 501)	Non-MDT (n = 90)	p value	SMD	Total (n = 138.76)	MDT (n = 69.38)	Non-MDT (n = 69.38)	p value	SMD
Allo-HCT, n (%)				< 0.001	0.887				< 0.001	0.768
No	259 (43.8%)	189 (37.7%)	70 (77.8%)			83.01 (59.8%)	29.31 (42.3%)	53.70 (77.41%)		
Yes	332 (56.2%)	312 (62.3%)	20 (22.2%)			55.75 (40.2%)	40.07 (57.7%)	15.68 (22.59%)	0.029	0.254
Relapse, n (%)	175 (29.6%)	139 (27.7%)	36 (40.0%)	0.026	0.261	45.95 (33.1%)	18.85 (27.2%)	27.09 (39.05%)		
Death, n (%)	175 (29.6%)	132 (26.4%)	43 (47.8%)	< 0.001	0.455	52.73 (38.0%)	22.21 (32.0%)	30.52 (43.98%)	0.038	0.248

Abbreviations: allo-HCT, allogeneic hematopoietic cell transplantation; AML, acute myeloid leukemia; CR: complete response; ELN 2017 European LeukemiaNet 2017; MDT, multidisciplinary team; MRD: measurable residual disease; NA, not available; NR: non-remission; SMD, standardized mean difference.

not recommended for allo-HCT, 61 (32.8%) nevertheless underwent transplantation.

3.3. Long-term impact of MDT on survival

Within the MDT program, 79.7% of patients (n = 251) received allo-HCT as recommended, and 67.2% of patients (n = 125) received BAT as recommended. Among patients who adhered to MDT recommendations, outcome analyses showed comparable 3-year OS (78.5% *vs.* 67.8%; p = 0.26; Supplementary Figure S2A, *https://www.biosciencetrends.com/action/getSupplementalData.php?ID=285*) and CIR (20.2% *vs.* 33.0%; p = 0.61; Supplementary Figure S2B, *https://www.biosciencetrends.com/action/getSupplementalData.php?ID=285*) between those receiving allo-HCT and those receiving BAT.

Among patients who were recommended for allo-HCT, those who proceeded to transplantation had significantly improved 3-year OS (78.6% *vs.* 34.8%; p < 0.0001; Figure 3A) and lower 3-year CIR (20.2% *vs.* 62.0%; p = 0.0011; Figure 3D) compared with those who did not undergo allo-HCT. By contrast, among patients who were not recommended for allo-HCT, allo-HCT and BAT were associated with similar 3-year OS (77.6% *vs.* 67.8%; p = 0.21; Figure 3B), while allo-HCT was associated with a higher 3-year CIR compared with BAT (41.7% *vs.* 33.0%; p = 0.025; Figure 3E).

Among non-MDT attendees, neither allo-HCT nor BAT was associated with significant differences in clinical outcomes (3-year OS: 61.6% *vs.* 49.2%, p = 0.38; three-year CIR: 37.5% *vs.* 47.8%, p = 0.32) (Figure 3C and 3F). Notably, 95.1% of patients who underwent allo-HCT contrary to MDT recommendations were classified as favorable-risk according to the ELN 2017 criteria (Supplementary Figure S3A, *https://www.biosciencetrends.com/action/getSupplementalData.php?ID=285*).

Among transplant recipients in the non-MDT, MDT-not-recommended, and MDT-recommended groups, patients in the non-MDT group had the lowest 3-year OS (61.6% *vs.* 77.6% *vs.* 78.6%, p = 0.02) (Supplementary Figure S3B, *https://www.biosciencetrends.com/action/getSupplementalData.php?ID=285*), whereas patients in the MDT-recommended group had the lowest 3-year CIR (37.5% *vs.* 41.7% *vs.* 20.2%, p = 0.01) (Supplementary Figure S3C, *https://www.biosciencetrends.com/action/getSupplementalData.php?ID=285*).

3.4. Identification of transplant beneficiaries by MDT evaluation

During MDT evaluation, experts assessed the potential benefit of allo-HCT based on ELN risk stratification and response to induction therapy. Logistic regression analysis revealed that intermediate-risk (OR [95% CI], 63.252 [5.758–3385.266]; p = 0.006) and adverse-risk disease (OR [95% CI], 28.128 [3.222–768.62];

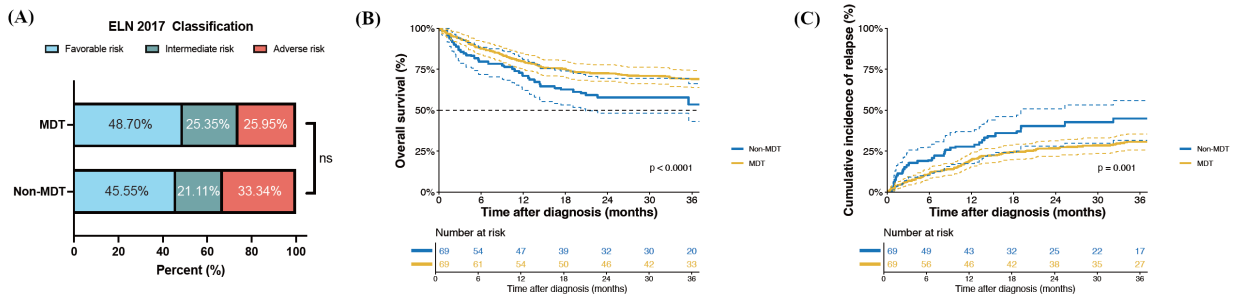

Figure 2. Overall survival (OS) of patients who attended multidisciplinary team (MDT) conferences and those who did not. Distribution of ELN 2017 risk stratification **(A),** and comparison of OS **(B)** and cumulative incidence of relapse (CIR) **(C)** between MDT attendees and non-attendees.

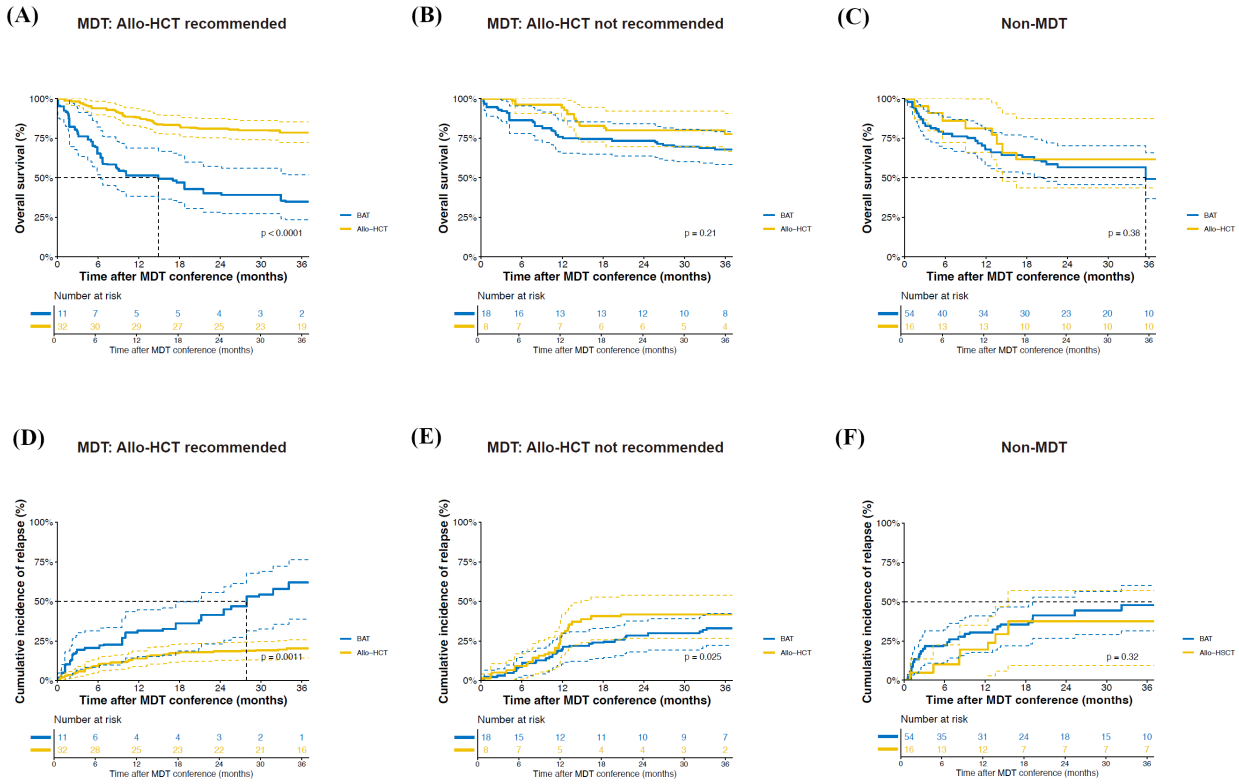

Figure 3. Impact of multidisciplinary team (MDT) recommendations on survival outcomes in patients with acute myeloid leukemia (AML). Comparison of overall survival (OS) among patients who were recommended for allogeneic hematopoietic cell transplantation (allo-HCT) **(A)**, not recommended for allo-HCT **(B)**, or who declined MDT evaluation **(C)** and underwent different treatment modalities. Comparison of cumulative incidence of relapse (CIR) for patients with AML who were recommended for allo-HCT **(D)**, who were not recommended for allo-HCT **(E)**, and who refused MDT **(F)**, and underwent different treatment modalities.

p = 0.011) were the main factors associated with MDT recommendations for transplantation (Table 2). Among patients who were recommended for allo-HCT, transplantation was associated with improved 3-year OS compared with BAT in those with intermediate- or adverse-risk disease (favorable risk: 81.3% *vs.* 61.6%, p = 0.16; intermediate risk: 78.5% *vs.* 25.5%, $p < 0.0001$; adverse risk: 76.8% *vs.* 32.6%, $p < 0.0001$; Figures 4A-C). Allo-HCT was also associated with a lower 3-year CIR across all ELN risk categories (favorable risk: 20.0% *vs.* 60.9%, p = 0.022; intermediate risk: 17.8% *vs.* 64.5%, p = 0.00012; adverse risk: 22.8% *vs.* 58.6%, $p < 0.0001$; Figures 4D-F). By contrast, we found no significant differences in outcomes between allo-HCT and BAT among patients who were recommended for BAT across different risk stratifications (Supplementary Figure S4, *https://www.biosciencetrends.com/action/getSupplementalData.php?ID=285*) or among patients who declined MDT evaluation (Supplementary Figure S5, *https://www.biosciencetrends.com/action/getSupplementalData.php?ID=285*).

Factors associated with survival outcomes were further examined using Cox proportional hazards regression analysis (Table 3). MDT involvement (HR

Table 2. Logistic regression analysis of transplantation recommendation by MDT

Variable	Univariate			Multivariable		
	OR	95%CI	*p* value	OR	95%CI	*p* value
Diagnosis year						
2017-2019	1.0	Ref		1.0	Ref	
2020-2022	3.342	0.952-12.472	0.063	3.342	0.952-12.472	0.063
Sex						
Male	1.0	Ref		1.0	Ref	
Female	2.037	0.658-6.598	0.223	2.037	0.658-6.598	0.223
Age						
15-39	1.0	Ref		1.0	Ref	
40-54	0.621	0.150-2.377	0.492	0.621	0.150-2.377	0.492
55-65	0.403	0.084-1.794	0.237	0.403	0.084-1.794	0.237
ELN 2017 stratification						
Favorable	1.0	Ref		1.0	Ref	
Intermediate	29.249	4.317-795.899	0.005	29.249	4.317-795.899	0.005
Adverse	18.610	3.296-244.077	0.004	18.610	3.296-244.077	0.004
MRD status after induction therapy						
CR after one cycle of induction						
Negative MRD	1.0	Ref		1.0	Ref	
Positive MRD	1.748	0.453-7.678	0.430	1.748	0.453-7.678	0.430
CR after two cycles of induction						
Negative MRD	3.104	0.088-6138.122	0.587	3.104	0.088-6138.122	0.587
Positive MRD	9.017	0.680-4981.675	0.212	9.017	0.680-4981.675	0.212
NR	1.047	0.095-14.548	0.969	1.047	0.095-14.548	0.969
NA	3.445	0.026-Inf	0.662	3.445	0.026-Inf	0.662

Abbreviations: AML, acute myeloid leukemia; CI: confidence interval; CR: complete response; ELN 2017 European LeukemiaNet 2017; MDT, multidisciplinary team; MRD: measurable residual disease; NA, not available; NR: non-remission, OR: odds ratio.

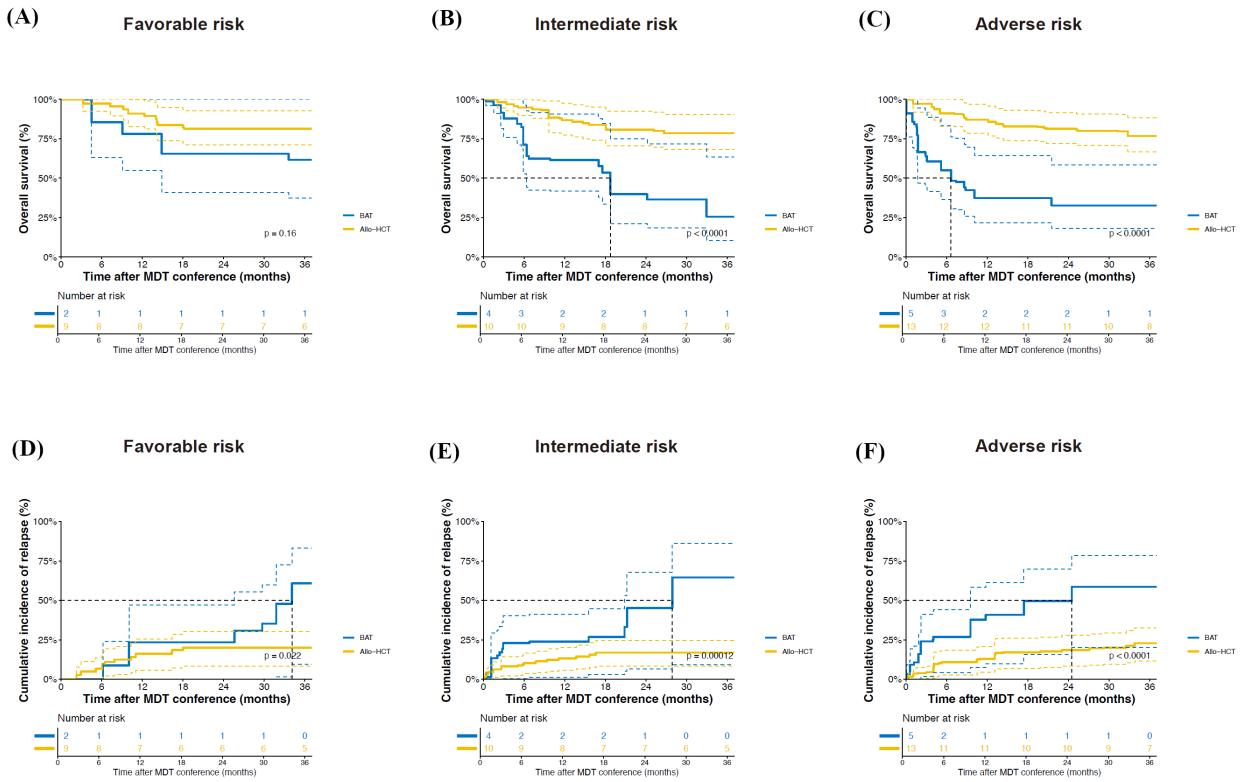

Figure 4. Long-term outcomes of multidisciplinary team (MDT) consultation attendees who were recommended for allogenic hematopoietic cell transplantation (allo-HCT) and received different consolidation strategies. Comparison of overall survival (OS) in patients with favorable-risk acute myeloid leukemia (AML) **(A)** and intermediate- or adverse-risk AML **(B–C)** who underwent allo-HCT or best available therapy (BAT). Comparison of cumulative incidence of relapse (CIR) in patients with favorable-risk AML **(D)** and intermediate- or adverse-risk AML **(E–F)** who underwent allo-HCT or BAT. ****$p < 0.0001$.

[95% CI], 0.647 [0.450–1.008]; $p = 0.055$) and allo-HCT (HR [95% CI], 0.425 [0.269–0.672]; $p < 0.001$) were associated with improved long-term survival. Among MDT attendees, the distribution of ELN risk differed markedly between patients who were recommended for allo-HCT (favorable risk, 23.49%; intermediate risk, 37.78%; adverse risk, 38.73%) and those who were not (favorable risk, 91.40%; intermediate risk, 4.30%; adverse risk, 4.30%; $p < 0.0001$; Supplementary Table S2, *https://www.biosciencetrends.com/action/getSupplementalData.php?ID=285*). Among MDT attendees, ELN risk category was not independently associated with survival after accounting for treatment allocation (intermediate risk: HR [95% CI], 1.408 [0.780–2.542], $p = 0.257$; adverse risk: HR [95% CI], 1.340 [0.754–2.382], $p = 0.318$).

3.5. Post-induction MRD and MDT transplant recommendations

Logistic regression analysis did not identify post-induction MRD as a significant factor influencing transplant recommendations made by the MDT (Table 2). Cox analysis revealed that achieving CR beyond one cycle of induction and non-remission (NR) status were associated with poorer long-term survival outcomes in the overall cohort (Table 3). These findings suggest that post-induction MRD status warrants closer consideration in MDT decision-making.

Among MDT attendees with favorable-risk disease, the effectiveness of BAT declined progressively in patients who achieved CR after one cycle of induction, after two cycles of induction, or who remained in NR status (3-year OS: 74.1% vs. 38.3% vs. 0%, $p < 0.0001$; 3-year CIR: 29.6% *vs*. 61.7% *vs*. 38.8%, $p = 0.00021$) (Supplementary Figures S6A and S6C, *https://www.biosciencetrends.com/action/getSupplementalData.php?ID=285*). By contrast, allo-HCT was associated with relatively stable outcomes across different post-induction response categories in favorable-risk patients (3-year OS: 79.2% *vs*. 69.4% *vs*. 100%, $p = 0.58$; 3-year CIR: 30.7% *vs*. 30.6% *vs*. 0%, $p = 0.70$) (Supplementary Figures S6B and S6D, *https://www.biosciencetrends.com/action/getSupplementalData.php?ID=285*).

Among MDT attendees with intermediate- or adverse-risk disease, allo-HCT was associated with higher 3-year OS compared with BAT across all response categories (CR after one cycle of induction: 80.1% *vs*. 52.6%, $p < 0.0001$; CR after two cycles of induction: 87.7% *vs*. 25.6%, $p < 0.0001$; NR: 64.4% *vs*. 0%, $p <$

Table 3. Cox analysis of survival following initial diagnosis in our patients

Variable	Univariate			Multivariable		
	HR	95%CI	*p* value	HR	95%CI	*p* value
Diagnosis year						
2017-2019	1.0	Ref		1.0	Ref	
2020-2022	0.921	0.616-1.377	0.689	1.080	0.704-1.657	0.724
Sex						
Male	1.0	Ref		1.0	Ref	
Female	0.785	0.529-1.165	0.229	0.778	0.507-1.192	0.249
Age						
15-39	1.0	Ref		1.0	Ref	
40-54	1.579	0.953-2.618	0.076	1.412	0.831-2.400	0.202
55-65	2.340	1.388-3.946	0.001	1.340	0.754-2.382	0.318
ELN 2017 stratification						
Favorable	1.0	Ref		1.0	Ref	
Intermediate	2.128	1.299-3.487	0.003	1.408	0.780-2.542	0.257
Adverse	2.728	1.732-4.298	< 0.001	1.567	0.890-2.756	0.119
MRD status after induction therapy						
CR after one cycle of induction						
Negative MRD	1.0	Ref		1.0	Ref	
Positive MRD	1.334	0.738-2.411	0.340	1.436	0.778-2.649	0.247
CR after two cycles of induction						
Negative MRD	3.303	1.256-8.688	0.015	3.150	1.263-7.859	0.014
Positive MRD	3.346	1.882-5.947	< 0.001	3.420	2.051-5.701	< 0.001
NR	9.249	5.714-14.971	< 0.001	10.045	5.305-19.019	< 0.001
NA	3.560	1.599-7.925	0.002	3.478	1.444-8.376	0.005
MDT						
No	1.0	Ref		1.0	Ref	
Yes	0.635	0.438-0.920	0.017	0.674	0.450-1.008	0.055
Treatment						
BAT	1.0	Ref		1.0	Ref	
Allo-HCT	0.491	0.330-0.730	< 0.001	0.425	0.269-0.672	< 0.001

Abbreviations: allo-HCT, allogeneic hematopoietic cell transplantation; AML, acute myeloid leukemia; BAT, best available therapy; CI: confidence interval; CR: complete response; ELN 2017 European LeukemiaNet 2017; HR: hazard ratio; MDT, multidisciplinary team; MRD: measurable residual disease; NA, not available; NR: non-remission.

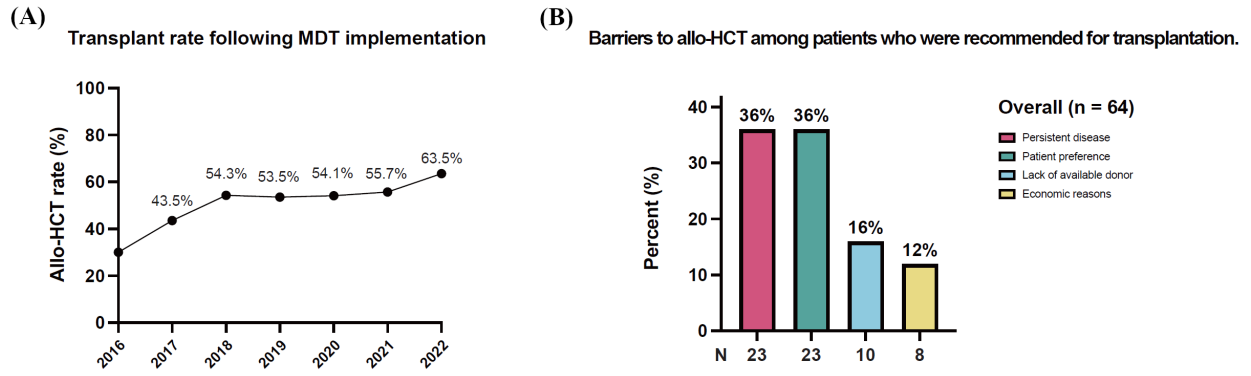

Figure 5. Transplantation practice in the multidisciplinary team (MDT) era. (A) Increase in allogenic hematopoietic cell transplantation (allo-HCT) rates following MDT implementation. **(B)** Barriers to allo-HCT among patients who were recommended for, but did not undergo, allo-HCT.

0.0001) and with lower 3-year CIR (CR after one cycle of induction: 20.7% *vs*. 55.3%, $p < 0.0001$; CR after two cycles of induction: 27.2% *vs*. 100%, $p = 0.0028$; non-remission: 19.5% *vs*. 100%, $p = 0.022$) (Supplementary Figures S7, *https://www.biosciencetrends.com/action/getSupplementalData.php?ID=285*).

3.6. MDT increases allo-HCT availability

The allo-HCT rate in the overall cohort showed a sustained annual increase, reaching 63.5% of all non-APL AML patients by 2022 and 79.4% among patients enrolled in the MDT program (Figure 5A). The most common reasons for failure to proceed to allo-HCT were persistent or relapsed disease (36%) and patient preference (36%), followed by lack of available donors (16%) and economic factors (12%) (Figure 5B).

Comparison of baseline characteristics between patients who were recommended for and underwent allo-HCT ($n = 251$) and those who were recommended for but did not undergo allo-HCT ($n = 64$) showed no significant differences in age, sex, or ELN 2017 risk stratification between the two groups (Supplementary Table S3, *https://www.biosciencetrends.com/action/getSupplementalData.php?ID=285*). These findings indicate that baseline clinical characteristics were broadly comparable between patients who did and did not proceed to transplantation following MDT recommendation.

4. Discussion

In this retrospective study, we evaluated the effectiveness of MDT evaluation in guiding optimal post-remission therapy for 653 patients with non-APL AML. Patients who attended MDT conferences had superior 3-year OS (68.9% *vs.* 53.5%, $p < 0.0001$) and a lower 3-year CIR (30.7% *vs.* 44.9%; $p < 0.0001$) compared with those who did not attend MDT. The higher rate of allo-HCT among MDT attendees is likely a key contributor to this survival difference. Among patients who were initially recommended for allo-HCT following MDT evaluation, the transplantation rate reached 79%, and remained high at 66.9% among those with intermediate- to adverse-risk AML. The most common reason for failure to proceed to transplantation was persistent or relapsed disease, consistent with findings from prior studies (*11,19*).

Previous reports have highlighted substantial attrition between eligibility for allo-HCT and actual transplantation. In a prospective analysis conducted between 2001 and 2003, 38% of patients achieved CR after induction therapy, of whom 54% were referred for transplant consultation; however, only 26% of those referred ultimately underwent allo-HCT (*10*). Similarly, a retrospective analysis from the Fred Hutchinson Cancer Research Center conducted in 2013 reported that 67% of newly diagnosed patients with intermediate- to adverse-risk AML in first CR underwent allo-HCT(*11*). When accounting for patients who did not proceed to transplantation because of early death, failure to achieve remission, or loss to follow-up, the overall transplant rate declined to 48% (*11*). More recent studies have reported utilization rates of approximately 57–66% among patients with acute leukemia who were recommended for allo-HCT (*19,20*).

An important factor contributing to the higher allo-HCT rate observed in our study may be the widespread use of haploidentical donors (HIDs), which accounted for up to approximately 80% of transplants in our cohort. Routine use of HIDs was not reported in a comparable study by Pagel *et al*. (*11*) and most earlier reports (*10,19*). However, because HID transplantation is not yet widely implemented in many primary hospitals, increasing timely referral of eligible patients with AML to transplant-capable centers might further improve cure rates. Consistent with the growing availability of HLA-mismatched donor sources, including HIDs, only 16% of patients in our study cited lack of a suitable donor as a barrier to allo-HCT. Recent data from the Chinese Blood and Marrow Transplantation Registry Group show that the number of haploidentical transplants has increased steadily since 2008 and that HID transplantation has

become the predominant transplant modality for AML across major transplant centers in China (*31*). In this context, further improvements in induction regimens (particularly through the incorporation of targeted agents and immunotherapy) might increase the proportion of patients who are able to proceed to allo-HCT. Patient preference was the second most common reason for not undergoing transplantation. We expect that enhancing patient education and confidence regarding the safety and benefits of allo-HCT would help increase transplant utilization and, ultimately, improve long-term outcomes for patients with AML.

Many factors can hinder the implementation of MDT programs, including not only material and resource limitations but also less visible barriers to intra- and inter-professional collaboration (*21*). In our MDT process, recommendations regarding patient suitability for allo-HCT as consolidation therapy were comprehensively discussed during two MDT visits within a 4-month period, taking into account disease characteristics, donor availability, performance status, and response to therapy.

An important observation from the present study was that MDT attendees experienced better survival outcomes than non-attendees. Several factors might contribute to this difference. First, patients who attended MDT evaluation may have demonstrated better treatment adherence, which could translate into improved survival. Second, the utilization rate of allo-HCT was substantially higher in the MDT group (79.7%) than in the non-MDT group (22.2%). As shown in our analyses, allo-HCT was associated with favorable outcomes across risk stratifications, with a 3-year OS of up to 78.6% and a 3-year CIR as low as 20.2% among patients who underwent transplantation following MDT recommendation. These findings might explain, in part, the survival advantage observed among MDT attendees. Taken together, our experience suggests that patients with intermediate- or high-risk AML should be prioritized for allo-HCT during consolidation therapy, whereas in patients with favorable-risk disease, transplantation should be considered primarily for those with suboptimal responses to induction therapy.

This study has several limitations to consider. First, owing to its retrospective design, 16.1% of patients (126/779) were lost to follow-up, primarily because of missing or incorrect contact information. Sensitivity analyses using best-case and worst-case assumptions for patients lost to follow-up yielded results consistent with the primary analysis, with no material change in the direction or significance of the estimated treatment effects (Supplementary Table S4, *https://www.biosciencetrends.com/action/getSupplementalData.php?ID=285*). Second, MRD data during induction or consolidation therapy and before allo-HCT were insufficient to allow a detailed analysis of the impact of MRD on MDT decision-making. Third, as a referral center, our cohort included a higher proportion of patients with intermediate- and adverse-risk disease, resulting in an ELN risk distribution that differs from those reported in other AML cohorts (*32-34*), which may introduce selection bias. Fourth, only patients admitted to our center for induction therapy were enrolled, whereas patients initially treated at community centers were referred to our institution primarily for allo-HCT evaluation. This referral pattern may limit the generalizability of our findings and highlights the need to further develop coordinated strategies and partnerships with community centers. In addition, although approximately 7.2% of patients with AML harbor *NUP98* rearrangements (*35*), only six such cases were identified in our cohort. This finding likely reflects the fact that RNA sequencing for genetic abnormalities was implemented at our center only in 2019, indicating incomplete molecular characterization in earlier years. Accordingly, MDT-based recommendations for patients with AML may benefit from further refinement as more comprehensive molecular profiling becomes available.

5. Conclusions

In summary, we demonstrate that MDT evaluation can support optimized treatment decision-making, particularly with respect to allo-HCT recommendations for patients with intermediate- and adverse-risk AML. Early disease progression and patient preference remained major barriers to transplantation. Our findings suggest that further improvements in allo-HCT utilization in China may depend on expanding MDT implementation to facilitate earlier and more efficient transplant workup, broader use of HLA-mismatched donors, continued refinement of induction regimens, and optimization of allo-HCT strategies for patients with AML who do not achieve remission.

Funding: This work was supported by the National Natural Science Foundation of China (82170206, 82470213), Shanghai Municipal Health Commission Project of Disciplines of Excellence (20234Z0002) and National Research Center for Translational Medicine under grant number (NRCTM(SH)-2023-11).

Conflict of Interest: The authors have no conflicts of interest to disclose.

Availability of data and materials: The datasets generated during and analyzed during the current study are available from the corresponding author (hu_xiaoxia@126.com) on reasonable request.

References

1. Xu L, Chen H, Chen J, *et al*. The consensus on indications, conditioning regimen, and donor selection of allogeneic hematopoietic cell transplantation for hematological diseases in China-recommendations from the Chinese

Society of Hematology. J Hematol Oncol. 2018; 11:33.
2. Chang YJ, Pei XY, Huang XJ. Haematopoietic stem-cell transplantation in China in the era of targeted therapies: current advances, challenges, and future directions. Lancet Haematol. 2022; 9:e919-e929.
3. Cornelissen JJ, Blaise D. Hematopoietic stem cell transplantation for patients with AML in first complete remission. Blood. 2016; 127:62-70.
4. Fu W, Chen J, Hu X. Immune reconstitution following allogeneic hematopoietic cell transplantation and CAR-T therapy: dynamics, determinants, and directions. Best Practice & Research Clinical Haematology. 2025; 38:101634.
5. Xu LP, Lu PH, Wu DP, *et al*. Hematopoietic stem cell transplantation activity in China 2019: a report from the Chinese Blood and Marrow Transplantation Registry Group. Bone Marrow Transplant. 2021; 56:2940-2947.
6. Zhang XH, Chen J, Han MZ, *et al*. The consensus from The Chinese Society of Hematology on indications, conditioning regimens and donor selection for allogeneic hematopoietic stem cell transplantation: 2021 update. J Hematol Oncol. 2021; 14:145.
7. Duarte RF, Labopin M, Bader P, *et al*. Indications for haematopoietic stem cell transplantation for haematological diseases, solid tumours and immune disorders: current practice in Europe, 2019. Bone Marrow Transplant. 2019; 54:1525-1552.
8. Kanate AS, Majhail NS, Savani BN, *et al*. Indications for Hematopoietic Cell Transplantation and Immune Effector Cell Therapy: Guidelines from the American Society for Transplantation and Cellular Therapy. Biol Blood Marrow Transplant. 2020; 26:1247-1256.
9. Huang J, Wu X, Wang G, Cao Y, Hu X, Behalf Of Trophy Working Group O. Allogeneic transplantation in adverse-risk acute myeloid leukemia: Challenges, strategies, and future directions. Chin J Cancer Res. 2025; 37:718-736.
10. Estey E, de Lima M, Tibes R, Pierce S, Kantarjian H, Champlin R, Giralt S. Prospective feasibility analysis of reduced-intensity conditioning (RIC) regimens for hematopoietic stem cell transplantation (HSCT) in elderly patients with acute myeloid leukemia (AML) and high-risk myelodysplastic syndrome (MDS). Blood. 2007; 109:1395-1400.
11. Mawad R, Gooley TA, Sandhu V, *et al*. Frequency of allogeneic hematopoietic cell transplantation among patients with high- or intermediate-risk acute myeloid leukemia in first complete remission. J Clin Oncol. 2013; 31:3883-3888.
12. Medeiros BC, Satram-Hoang S, Hurst D, Hoang KQ, Momin F, Reyes C. Big data analysis of treatment patterns and outcomes among elderly acute myeloid leukemia patients in the United States. Ann Hematol. 2015; 94:1127-1138.
13. Ostgard LSG, Lund JL, Norgaard JM, Norgaard M, Medeiros BC, Nielsen B, Nielsen OJ, Overgaard UM, Kallenbach M, Marcher CW, Riis AH, Sengelov H. Impact of Allogeneic Stem Cell Transplantation in First Complete Remission in Acute Myeloid Leukemia: A National Population-Based Cohort Study. Biol Blood Marrow Transplant. 2018; 24:314-323.
14. Stelljes M, Beelen DW, Braess J, *et al*. Allogeneic transplantation as post-remission therapy for cytogenetically high-risk acute myeloid leukemia: landmark analysis from a single prospective multicenter trial. Haematologica. 2011; 96:972-979.
15. Crivello P, Arrieta-Bolaños E, He M, Wang T, Fingerson S, Gadalla SM, Paczesny S, Marsh SGE, Lee SJ, Spellman SR, Bolon Y-T, Fleischhauer K. Impact of the HLA Immunopeptidome on Survival of Leukemia Patients After Unrelated Donor Transplantation. J Clin Oncol. 2023; 41:2416-2427.
16. Döhner H, Wei AH, Appelbaum FR, *et al*. Diagnosis and management of AML in adults: 2022 recommendations from an international expert panel on behalf of the ELN. Blood. 2022; 140:1345-1377.
17. Pillay B, Wootten AC, Crowe H, Corcoran N, Tran B, Bowden P, Crowe J, Costello AJ. The impact of multidisciplinary team meetings on patient assessment, management and outcomes in oncology settings: A systematic review of the literature. Cancer Treat Rev. 2016; 42:56-72.
18. Taylor C, Munro AJ, Glynne-Jones R, Griffith C, Trevatt P, Richards M, Ramirez AJ. Multidisciplinary team working in cancer: what is the evidence? BMJ. 2010; 340:c951.
19. Nath K, Lee J, Elko TA, *et al*. Prospective analysis to determine barriers to allogeneic hematopoietic cell transplantation in patients with acute leukemia. Am J Hematol. 2023; 98:1869-1876.
20. Bashey A, Zhang X, Morris LE, Holland HK, Bachier-Rodriguez L, Solomon SR, Solh M. Improved access to HCT with reduced racial disparities through integration with leukemia care and haploidentical donors. Blood Advances. 2023; 7:3816-3823.
21. Liberati EG, Gorli M, Scaratti G. Invisible walls within multidisciplinary teams: Disciplinary boundaries and their effects on integrated care. Soc Sci Med. 2016; 150:31-39.
22. Khoury JD, Solary E, Abla O, *et al*. The 5th edition of the World Health Organization Classification of Haematolymphoid Tumours: Myeloid and Histiocytic/Dendritic Neoplasms. Leukemia. 2022; 36:1703-1719.
23. Döhner H, Estey E, Grimwade D, *et al*. Diagnosis and management of AML in adults: 2017 ELN recommendations from an international expert panel. Blood. 2017; 129:424-447.
24. Gao MG, Ruan GR, Chang YJ, Liu YR, Qin YZ, Jiang Q, Jiang H, Huang XJ, Zhao XS. The predictive value of minimal residual disease when facing the inconsistent results detected by real-time quantitative PCR and flow cytometry in NPM1-mutated acute myeloid leukemia. Ann Hematol. 2020; 99:73-82.
25. Chang YJ, Wang Y, Liu YR, *et al*. Haploidentical allograft is superior to matched sibling donor allograft in eradicating pre-transplantation minimal residual disease of AML patients as determined by multiparameter flow cytometry: a retrospective and prospective analysis. J Hematol Oncol. 2017; 10:134.
26. Yui S, Kurosawa S, Yamaguchi H, *et al*. D816 mutation of the KIT gene in core binding factor acute myeloid leukemia is associated with poorer prognosis than other KIT gene mutations. Annals of Hematology. 2017; 96:1641-1652.
27. Wang J, Lu R, Wu Y, *et al*. Detection of measurable residual disease may better predict outcomes than mutations based on next-generation sequencing in acute myeloid leukaemia with biallelic mutations of CEBPA. Br J Haematol. 2020; 190:533-544.
28. De Kouchkovsky I, Abdul-Hay M. 'Acute myeloid leukemia: a comprehensive review and 2016 update'. Blood Cancer J. 2016; 6:e441.

29. Liu H. Emerging agents and regimens for AML. J Hematol Oncol. 2021; 14:49.
30. Hilgendorf I, Greinix H, Halter JP, Lawitschka A, Bertz H, Wolff D. Long-term follow-up after allogeneic stem cell transplantation. Dtsch Arztebl Int. 2015; 112:51-58.
31. Xu LP, Lu PH, Wu DP, *et al*. Hematopoietic stem cell transplantation activity in China 2022-2023. The proportions of peripheral blood for stem cell source continue to grow: a report from the Chinese Blood and Marrow Transplantation Registry Group. Bone Marrow Transplant. 2024; 59:17261734.
32. Grimm J, Jentzsch M, Bill M, Goldmann K, Schulz J, Niederwieser D, Platzbecker U, Schwind S. Prognostic impact of the ELN2017 risk classification in patients with AML receiving allogeneic transplantation. Blood Advances. 2020; 4:3864-3874.
33. Buccisano F, Palmieri R, Piciocchi A, *et al*. ELN2017 risk stratification improves outcome prediction when applied to the prospective GIMEMA AML1310 protocol. Blood Advances. 2022; 6:2510-2516.
34. Zhang H, Zheng X, Guo W, *et al*. Outcomes of acute myeloid leukemia patients undergoing allogeneic hematopoietic stem cell transplantation: validation, comparison and improvement of 2022 ELN genetic risk system. Exp Hematol Oncol. 2024; 13:16.
35. Bertrums EJM, Smith JL, Harmon L, *et al*. Comprehensive molecular and clinical characterization of NUP98 fusions in pediatric acute myeloid leukemia. Haematologica. 2023; 108:2044-2058.

Received November 28, 2025; Revised January 9, 2026; Accepted January 29, 2026.

[§]These authors contributed equally to this work.
**Address correspondence to:*
Xiaoxia Hu, Junmin Li, Jiong Hu, and Yang He, Shanghai Institute of Hematology, State Key Laboratory of Medical Genomics, National Research Center for Translational Medicine at Shanghai, Ruijin Hospital, Shanghai Jiao Tong University School of Medicine, 197 Ruijin Er Road, Shanghai 200025, China.
E-mail: hu_xiaoxia@126.com (HX), lijunmin@medmail.com.cn (LJ), hj10709@rjh.com.cn (HJ), hy21369@rjh.com.cn (HY)

Released online in J-STAGE as advance publication February 6, 2026.

BST
BioScience Trends

Guide for Authors

1. Scope of Articles

BioScience Trends (Print ISSN 1881-7815, Online ISSN 1881-7823) is an international peer-reviewed journal. *BioScience Trends* devotes to publishing the latest and most exciting advances in scientific research. Articles cover fields of life science such as biochemistry, molecular biology, clinical research, public health, medical care system, and social science in order to encourage cooperation and exchange among scientists and clinical researchers.

2. Submission Types

Original Articles should be well-documented, novel, and significant to the field as a whole. An Original Article should be arranged into the following sections: Title page, Abstract, Introduction, Materials and Methods, Results, Discussion, Acknowledgments, and References. Original articles should not exceed 5,000 words in length (excluding references) and should be limited to a maximum of 50 references. Articles may contain a maximum of 10 figures and/or tables. Supplementary Data are permitted but should be limited to information that is not essential to the general understanding of the research presented in the main text, such as unaltered blots and source data as well as other file types.

Brief Reports definitively documenting either experimental results or informative clinical observations will be considered for publication in this category. Brief Reports are not intended for publication of incomplete or preliminary findings. Brief Reports should not exceed 3,000 words in length (excluding references) and should be limited to a maximum of 4 figures and/or tables and 30 references. A Brief Report contains the same sections as an Original Article, but the Results and Discussion sections should be combined.

Reviews should present a full and up-to-date account of recent developments within an area of research. Normally, reviews should not exceed 8,000 words in length (excluding references) and should be limited to a maximum of 10 figures and/or tables and 100 references. Mini reviews are also accepted, which should not exceed 4,000 words in length (excluding references) and should be limited to a maximum of 5 figures and/or tables and 50 references.

Policy Forum articles discuss research and policy issues in areas related to life science such as public health, the medical care system, and social science and may address governmental issues at district, national, and international levels of discourse. Policy Forum articles should not exceed 3,000 words in length (excluding references) and should be limited to a maximum of 5 figures and/or tables and 30 references.

Communications are short, timely pieces that spotlight new research findings or policy issues of interest to the field of global health and medical practice that are of immediate importance. Depending on their content, Communications will be published as "Comments" or "Correspondence". Communications should not exceed 1,500 words in length (excluding references) and should be limited to a maximum of 2 figures and/or tables and 20 references.

Editorials are short, invited opinion pieces that discuss an issue of immediate importance to the fields of global health, medical practice, and basic science oriented for clinical application. Editorials should not exceed 1,000 words in length (excluding references) and should be limited to a maximum of 10 references. Editorials may contain one figure or table.

News articles should report the latest events in health sciences and medical research from around the world. News should not exceed 500 words in length.

Letters should present considered opinions in response to articles published in *BioScience Trends* in the last 6 months or issues of general interest. Letters should not exceed 800 words in length and may contain a maximum of 10 references. Letters may contain one figure or table.

3. Editorial Policies

For publishing and ethical standards, *BioScience Trends* follows the Recommendations for the Conduct, Reporting, Editing, and Publication of Scholarly Work in Medical Journals issued by the International Committee of Medical Journal Editors (ICMJE, *https://icmje.org/recommendations*), and the Principles of Transparency and Best Practice in Scholarly Publishing jointly issued by the Committee on Publication Ethics (COPE, *https://publicationethics.org/resources/guidelines-new/principles-transparency-and-best-practice-scholarly-publishing*), the Directory of Open Access Journals (DOAJ, *https://doaj.org/apply/transparency*), the Open Access Scholarly Publishers Association (OASPA, *https://oaspa.org/principles-of-transparency-and-best-practice-in-scholarly-publishing-4*), and the World Association of Medical Editors (WAME, *https://wame.org/principles-of-transparency-and-best-practice-in-scholarly-publishing*).

BioScience Trends will perform an especially prompt review to encourage innovative work. All original research will be subjected to a rigorous standard of peer review and will be edited by experienced copy editors to the highest standards.

Ethical Approval of Studies and Informed Consent: For all manuscripts reporting data from studies involving human participants or animals, formal review and approval, or formal review and waiver, by an appropriate institutional review board or ethics committee is required and should be described in the Methods section. When your manuscript contains any case details, personal information and/or images of patients or other individuals, authors must obtain appropriate written consent, permission and release in order to comply with all applicable laws and regulations concerning privacy and/or security of personal information. The consent form needs to comply with the relevant legal requirements of your particular jurisdiction, and please do not send signed consent form to *BioScience Trends* to respect your patient's and any other individual's privacy. Please instead describe the information clearly in the Methods (patient consent) section of your manuscript while retaining copies of the signed forms in the event they should be needed. Authors should also state that the study conformed to the provisions of the Declaration of Helsinki (as revised in 2013, *https://wma.net/what-we-do/medical-ethics/declaration-of-helsinki*). When reporting experiments on animals, authors should indicate whether the institutional and national guide for the care and use of laboratory animals was followed.

Reporting Clinical Trials: The ICMJE (*https:// icmje.org/recommendations/browse/publishing-and-editorial-issues/clinical-trial-registration.html*) defines a clinical trial as any research project that prospectively assigns people or a group of people to an intervention, with or without concurrent comparison or control groups, to study the relationship between a health-related intervention and a health outcome. Registration of clinical trials in a public trial registry at or before the time of first patient enrollment is a condition of consideration for publication in *BioScience Trends*, and the trial registration number will be published at the end of the Abstract. The registry must be independent of for-profit interest and publicly accessible. Reports of trials must conform to CONSORT 2010 guidelines (*https://consort-statement.org/consort-2010*). Articles reporting the results of randomized trials must include the CONSORT flow diagram showing the progress of patients throughout the trial.

Conflict of Interest: All authors are required to disclose any actual or potential conflict of interest including financial interests or relationships with other people or organizations that might raise questions of bias

in the work reported. If no conflict of interest exists for each author, please state "There is no conflict of interest to disclose".

Submission Declaration: When a manuscript is considered for submission to *BioScience Trends*, the authors should confirm that 1) no part of this manuscript is currently under consideration for publication elsewhere; 2) this manuscript does not contain the same information in whole or in part as manuscripts that have been published, accepted, or are under review elsewhere, except in the form of an abstract, a letter to the editor, or part of a published lecture or academic thesis; 3) authorization for publication has been obtained from the authors' employer or institution; and 4) all contributing authors have agreed to submit this manuscript.

Initial Editorial Check: Immediately after submission, the journal's managing editor will perform an initial check of the manuscript. A suitable academic editor will be notified of the submission and invited to check the manuscript and recommend reviewers. Academic editors will check for plagiarism and duplicate publication at this stage. The journal has a formal recusal process in place to help manage potential conflicts of interest of editors. In the event that an editor has a conflict of interest with a submitted manuscript or with the authors, the manuscript, review, and editorial decisions are managed by another designated editor without a conflict of interest related to the manuscript.

Peer Review: *BioScience Trends* operates a single-anonymized review process, which means that reviewers know the names of the authors, but the authors do not know who reviewed their manuscript. All articles are evaluated objectively based on academic content. External peer review of research articles is performed by at least two reviewers, and sometimes the opinions of more reviewers are sought. Peer reviewers are selected based on their expertise and ability to provide quality, constructive, and fair reviews. For research manuscripts, the editors may, in addition, seek the opinion of a statistical reviewer. Every reviewer is expected to evaluate the manuscript in a timely, transparent, and ethical manner, following the COPE guidelines (*https://publicationethics.org/files/cope-ethical-guidelines-peer-reviewers-v2_0.pdf*). We ask authors for sufficient revisions (with a second round of peer review, when necessary) before a final decision is made. Consideration for publication is based on the article's originality, novelty, and scientific soundness, and the appropriateness of its analysis.

Suggested Reviewers: A list of up to 3 reviewers who are qualified to assess the scientific merit of the study is welcomed. Reviewer information including names, affiliations, addresses, and e-mail should be provided at the same time the manuscript is submitted online. Please do not suggest reviewers with known conflicts of interest, including participants or anyone with a stake in the proposed research; anyone from the same institution; former students, advisors, or research collaborators (within the last three years); or close personal contacts. Please note that the Editor-in-Chief may accept one or more of the proposed reviewers or may request a review by other qualified persons.

Language Editing: Manuscripts prepared by authors whose native language is not English should have their work proofread by a native English speaker before submission. If not, this might delay the publication of your manuscript in *BioScience Trends*.

The Editing Support Organization can provide English proofreading, Japanese-English translation, and Chinese-English translation services to authors who want to publish in *BioScience Trends* and need assistance before submitting a manuscript. Authors can visit this organization directly at *https://www.iacmhr.com/iac-eso/support.php?lang=en*. IAC-ESO was established to facilitate manuscript preparation by researchers whose native language is not English and to help edit works intended for international academic journals.

Copyright and Reuse: Before a manuscript is accepted for publication in *BioScience Trends*, authors will be asked to sign a transfer of copyright agreement, which recognizes the common interest that both the journal and author(s) have in the protection of copyright. We accept that some authors (*e.g.*, government employees in some countries) are unable to transfer copyright. A JOURNAL PUBLISHING AGREEMENT (JPA) form will be e-mailed to the authors by the Editorial Office and must be returned by the authors by mail, fax, or as a scan. Only forms with a hand-written signature from the corresponding author are accepted. This copyright will ensure the widest possible dissemination of information. Please note that the manuscript will not proceed to the next step in publication until the JPA Form is received. In addition, if excerpts from other copyrighted works are included, the author(s) must obtain written permission from the copyright owners and credit the source(s) in the article.

4. Cover Letter

The manuscript must be accompanied by a cover letter prepared by the corresponding author on behalf of all authors. The letter should indicate the basic findings of the work and their significance. The letter should also include a statement affirming that all authors concur with the submission and that the material submitted for publication has not been published previously or is not under consideration for publication elsewhere. The cover letter should be submitted in PDF format. For an example of Cover Letter, please visit: *https://www.biosciencetrends.com/downcentre* (Download Centre).

5. Submission Checklist

The Submission Checklist should be submitted when submitting a manuscript through the Online Submission System. Please visit Download Centre (*https://www.biosciencetrends.com/downcentre*) and download the Submission Checklist file. We recommend that authors use this checklist when preparing your manuscript to check that all the necessary information is included in your article (if applicable), especially with regard to Ethics Statements.

6. Manuscript Preparation

Manuscripts are suggested to be prepared in accordance with the "Recommendations for the Conduct, Reporting, Editing, and Publication of Scholarly Work in Medical Journals", as presented at *https://www.ICMJE.org*.

Manuscripts should be written in clear, grammatically correct English and submitted as a Microsoft Word file in a single-column format. Manuscripts must be paginated and typed in 12-point Times New Roman font with 24-point line spacing. Please do not embed figures in the text. Abbreviations should be used as little as possible and should be explained at first mention unless the term is a well-known abbreviation (*e.g.* DNA). Single words should not be abbreviated.

Title page: The title page must include 1) the title of the paper (Please note the title should be short, informative, and contain the major key words); 2) full name(s) and affiliation(s) of the author(s), 3) abbreviated names of the author(s), 4) full name, mailing address, telephone/fax numbers, and e-mail address of the corresponding author; 5) author contribution statements to specify the individual contributions of all authors to this manuscript, and 6) conflicts of interest (if you have an actual or potential conflict of interest to disclose, it must be included as a footnote on the title page of the manuscript; if no conflict of interest exists for each author, please state "There is no conflict of interest to disclose").

Abstract: The abstract should briefly state the purpose of the study, methods, main findings, and conclusions. For articles that are Original Articles, Brief Reports, Reviews, or Policy Forum articles, a one-paragraph abstract consisting of no more than 250 words must be included in the manuscript. For Communications, Editorials, News, or Letters, a brief summary of main content in 150 words or fewer should be included in the manuscript. For articles reporting clinical trials, the trial registration number should be stated at the end of the Abstract. Abbreviations must be kept to a minimum and non-standard

abbreviations explained in brackets at first mention. References should be avoided in the abstract. Three to six key words or phrases that do not occur in the title should be included in the Abstract page.

Introduction: The introduction should provide sufficient background information to make the article intelligible to readers in other disciplines and sufficient context clarifying the significance of the experimental findings

Materials/Patients and Methods: The description should be brief but with sufficient detail to enable others to reproduce the experiments. Procedures that have been published previously should not be described in detail but appropriate references should simply be cited. Only new and significant modifications of previously published procedures require complete description. Names of products and manufacturers with their locations (city and state/country) should be given and sources of animals and cell lines should always be indicated. All clinical investigations must have been conducted in accordance Materials/ Patients and Methods.

Results: The description of the experimental results should be succinct but in sufficient detail to allow the experiments to be analyzed and interpreted by an independent reader. If necessary, subheadings may be used for an orderly presentation. All Figures and Tables should be referred to in the text in order, including those in the Supplementary Data.

Discussion: The data should be interpreted concisely without repeating material already presented in the Results section. Speculation is permissible, but it must be well-founded, and discussion of the wider implications of the findings is encouraged. Conclusions derived from the study should be included in this section.

Acknowledgments: All funding sources (including grant identification) should be credited in the Acknowledgments section. Authors should also describe the role of the study sponsor(s), if any, in study design; in the collection, analysis, and interpretation of data; in the writing of the report; and in the decision to submit the paper for publication. If the funding source had no such involvement, the authors should so state.

In addition, people who contributed to the work but who do not meet the criteria for authors should be listed along with their contributions.

References: References should be numbered in the order in which they appear in the text. Citing of unpublished results, personal communications, conference abstracts, and theses in the reference list is not recommended but these sources may be mentioned in the text. In the reference list, cite the names of all authors when there are fifteen or fewer authors; if there are sixteen or more authors, list the first three followed by *et al*. Names of journals should be abbreviated in the style used in PubMed. Authors are responsible for the accuracy of the references. The EndNote Style of *BioScience Trends* could be downloaded at **EndNote** (*https://ircabssagroup.com/examples/ BioScience_Trends.ens*).

Examples are given below:

Example 1 (Sample journal reference):

Inagaki Y, Tang W, Zhang L, Du GH, Xu WF, Kokudo N. Novel aminopeptidase N (APN/CD13) inhibitor 24F can suppress invasion of hepatocellular carcinoma cells as well as angiogenesis. Biosci Trends. 2010; 4:56-60.

Example 2 (Sample journal reference with more than 15 authors):

Darby S, Hill D, Auvinen A, *et al*. Radon in homes and risk of lung cancer: Collaborative analysis of individual data from 13 European case-control studies. BMJ. 2005; 330:223.

Example 3 (Sample book reference):

Shalev AY. Post-traumatic stress disorder: Diagnosis, history and life course. In: Post-traumatic Stress Disorder, Diagnosis, Management and Treatment (Nutt DJ, Davidson JR, Zohar J, eds.). Martin Dunitz, London, UK, 2000; pp. 1-15.

Example 4 (Sample web page reference):

World Health Organization. The World Health Report 2008 – primary health care: Now more than ever. *http://www.who.int/whr/2008/whr08_ en.pdf* (accessed September 23, 2022).

Tables: All tables should be prepared in Microsoft Word or Excel and should be arranged at the end of the manuscript after the References section. Please note that tables should not in image format. All tables should have a concise title and should be numbered consecutively with Arabic numerals. If necessary, additional information should be given below the table.

Figure Legend: The figure legend should be typed on a separate page of the main manuscript and should include a short title and explanation. The legend should be concise but comprehensive and should be understood without referring to the text. Symbols used in figures must be explained. Any individually labeled figure parts or panels (A, B, *etc*.) should be specifically described by part name within the legend.

Figure Preparation: All figures should be clear and cited in numerical order in the text. Figures must fit a one- or two-column format on the journal page: 8.3 cm (3.3 in.) wide for a single column, 17.3 cm (6.8 in.) wide for a double column; maximum height: 24.0 cm (9.5 in.). Please make sure that the symbols and numbers appeared in the figures should be clear. Please make sure that artwork files are in an acceptable format (TIFF or JPEG) at minimum resolution (600 dpi for illustrations, graphs, and annotated artwork, and 300 dpi for micrographs and photographs). Please provide all figures as separate files. Please note that low-resolution images are one of the leading causes of article resubmission and schedule delays.

Units and Symbols: Units and symbols conforming to the International System of Units (SI) should be used for physicochemical quantities. Solidus notation (*e.g.* mg/kg, mg/mL, mol/mm^2/min) should be used. Please refer to the SI Guide *www.bipm.org/en/si/* for standard units.

Supplemental data: Supplemental data might be useful for supporting and enhancing your scientific research and *BioScience Trends* accepts the submission of these materials which will be only published online alongside the electronic version of your article. Supplemental files (figures, tables, and other text materials) should be prepared according to the above guidelines, numbered in Arabic numerals (*e.g.*, Figure S1, Figure S2, and Table S1, Table S2) and referred to in the text. All figures and tables should have titles and legends. All figure legends, tables and supplemental text materials should be placed at the end of the paper. Please note all of these supplemental data should be provided at the time of initial submission and note that the editors reserve the right to limit the size and length of Supplemental Data.

5. Submission Checklist

The Submission Checklist will be useful during the final checking of a manuscript prior to sending it to *BioScience Trends* for review. Please visit Download Centre and download the Submission Checklist file.

6. Online Submission

Manuscripts should be submitted to *BioScience Trends* online at *https://www.biosciencetrends.com/login*. Receipt of your manuscripts submitted online will be acknowledged by an e-mail from Editorial Office containing a reference number, which should be used in all future communications. If for any reason you are unable to submit a file online, please contact the Editorial Office by e-mail at *office@ biosciencetrends.com*

8. Accepted Manuscripts

Page Charge: Page charges will be levied on all manuscripts accepted for publication in *BioScience Trends* (Original Articles / Brief Reports / Reviews / Policy Forum / Communications: $140 per page for black white pages, $340 per page for color pages; News / Letters: a total cost of $600). Under exceptional circumstances, the author(s) may apply to the editorial office for a waiver of the publication charges by stating the reason in the Cover Letter when the manuscript online.

Misconduct: *BioScience Trends* takes seriously all allegations of potential misconduct and adhere to the ICMJE Guideline (*https://icmje.org/recommendations*) and COPE Guideline (*https://publicationethics.org/files/Code_of_conduct_for_journal_editors.pdf*). In cases of suspected research or publication misconduct, it may be necessary for the Editor or Publisher to contact and share submission details with third parties including authors' institutions and ethics committees. The corrections, retractions, or editorial expressions of concern will be performed in line with above guidelines.

(As of December 2022)

BioScience Trends
Editorial and Head Office
Pearl City Koishikawa 603,
2-4-5 Kasuga, Bunkyo-ku,
Tokyo 112-0003, Japan.
E-mail: office@biosciencetrends.com